The Role of Surface Sodium Species in Electrochemical Promotion of Catalysis

By

NAIMAH IBRAHIM

A Thesis Submitted for the Degree of Doctor of Philosophy
at Newcastle University, United Kingdom

School of Chemical Engineering and Advanced Materials

April 2013

Abstract

Electrochemical Promotion of Catalysis (EPOC) studies the promotion of catalytic activity and selectivity by supplying promoting species from the electrolyte support to the catalyst surface via the application of an external electrical potential between the catalyst-electrode and a counter electrode also supported on the electrolyte. The effect has been observed for a wide range of catalytic systems, however, very little work exists on the role of impurities in EPOC, although their presence may affect the catalytic and electrocatalytic properties of a catalyst or may in fact is necessary for the promotion to occur. In order to systematically study the role of impurities in EPOC, a known type and amount of an impurity can be deposited in increasing concentration on a nominally 'clean' catalyst surface. In this work, the role of sodium addition to a platinum catalyst-film interfaced with an yttria-stabilised-zirconia (YSZ) dense membrane was studied under non-reactive conditions (oxygen charge transfer) and reactive conditions (ethylene oxidation and NO reduction by propene). It was found that sodium addition on the catalyst surface can significantly affect the oxygen charge transfer, catalytic and electrocatalytic properties of the Pt/YSZ system, however, there is no clear evidence that such species are necessary for the observation of EPOC. Electrical polarisation and sodium addition seem to a first approximation to have an additive effect as electronic promoter on the electrochemical promotion when there is low lateral interaction between the surface ions and insignificant sodium interaction with the reaction components. Ethylene oxidation reaction changed in behaviour from electrophilic at low sodium coverage (0.11%) and low to intermediate oxygen partial pressure ($p_{O2} \leq 3$kPa) to electrophobic at high sodium coverage (65%) and under high oxygen partial pressures ($p_{O2} = 8$ kPa). In between the two sets of conditions, the reaction showed volcano-type behaviour depending on the coverage of sodium and gas phase oxygen partial pressure. The behavioural changes are more complicated for the NO reduction system as more reaction components are involved especially under high oxygen partial pressures.

Acknowledgements

I would like to thank all the people that helped me throughout the research course

Nomenclature

List of acronyms

AFR	Air to fuel ratio
CE	Counter electrode
CV	Cyclic voltammetry
EDX	Energy dispersive x-ray spectroscopy
EP	Electrochemical promotion
EPOC	Electrochemical promotion of catalysis
ICP-OES	Inductively coupled plasma-optical emission spectroscopy
MFC	Mass flow controller
MS	Mass spectrometer
NaOH	Sodium hydroxide
NASICON	Sodium super-ionic conductor
NEMCA	Non-faradaic electrochemical modification of catalytic activity
NSR	NO_x storage-reduction
OC	Open-circuit conditions
PLD	Pulse laser deposition
RE	Reference electrode
SCR	Selective catalytic reduction
SEM	Scanning electron microscopy
SOFC	Solid oxide fuel cell
STP	Standard temperature and pressure
tpb	Three-phase boundaries
TWC	Three-way catalyst
WE	Working electrode
XPS	X-ray photoelectron spectroscopy
YSZ	Yttria stabilised zirconia

List of symbols

A	Area (cm^2)
A_{Pt}	Area occupied by platinum atom (cm^2)
e	electron charge (1.60×10^{19} C)
E_p	Peak position or peak potential (V)
F	Faraday's constant (96485 C mol^{-1})
H	Enthalpy (J mol^{-1})

G	Gibbs free energy (J mol^{-1})
I	Current (A)
i	Current density (A cm^{-2})
i_o	Exchange current density (A cm^{-2})
i_p	Peak height or peak current density (A cm^{-2})
IR_u	Ohmic drop
k	Rate constant
l	length (cm)
n	Number of electron or charge transferred
N_{AV}	Avogadro constant (atom mol^{-1})
N_G	Surface area of platinum (mol or cm^2)
N_O	Number of oxygen adsorbed on the catalyst surface (mol)
p_A	Partial pressure of A (kPa)
PI	Promotional index
Q	Charge (C)
r	Reaction rate (mol s^{-1})
R	Ideal gas constant (8.314 J K^{-1} mol^{-1})
r_{Pt}	Atomic radius of platinum atom (m)
S	Entropy (J K^{-1} mol^{-1})
t	time (s)
T	Temperature (^{o}C)
V	Potential or voltage (V)
V_{WR}	Potential between working and reference electrodes (V)
V_{WC}	Potential between working and counter electrodes (V)
W	Work (J)
η	Overpotential (V)
α	Transfer coefficient
Λ	Rate enhancement factor
t_H	Holding time, s
ν	Scan rate, mV s^{-1}
$\Delta\Phi$	Change in the work function, eV
$\Delta\Phi_{el}$	Change in the work function caused by electrical polarisation
$\Delta\Phi_{Na}$	Change in the work function caused by sodium addition
ρ	Rate enhancement ratio
Λ	Faradaic efficiency
U	Internal energy (J mol^{-1})
$V_O^{\cdot\cdot}$	Oxygen vacancy site in the solid electrolyte (YSZ)

Table of Contents

List of Figures

List of Tables

Introduction

1.1.   Background of the research

The subject of this research is electrochemical promotion of catalysis (EPOC). EPOC or NEMCA for non-Faradaic electrochemical modification of catalytic activity studies the changes in the activity and selectivity of a conductive catalyst deposited on a solid electrolyte by application of low potentials or currents between the catalyst and a reference electrode also deposited on the solid electrolyte [1-3]. It has been found [2, 4] that the origin of EPOC lies in the backspillover (from the support to the catalyst) of ionic promoting species that form (together with their compensating charge) an overall neutral double layer on the catalyst surface changing the work function of the catalyst thus modifying its activity and selectivity. The effect has been shown in almost 100 different catalytic systems. In the recent years, EPOC studies focused mainly on reactions of environmental importance, mechanistic and fundamental studies, scaling up of EPOC reactors for potential commercialization and its emerging application in fuel cell devices [5-8]. While extensive studies were done to predict and investigate the behaviour of catalytic systems under controlled spillover (EPOC) conditions, where the supply of promoting species is dictated by the imposed electrical overpotential or current, very little work has been carried out to investigate the effect of pre-existing species (that can be found on the catalyst surface in the form of uncharacterised impurities) such as metal cations. Such species often have promoting properties and are often (as in the case of alkali metals) used as additives during catalyst preparation in order to enhance the catalytic activity [9-10]. In other cases pre-existing impurities (such as silicon) may block the catalyst active sites thus poisoning the catalyst [11]. In fact, the question whether pre-existing impurities on the catalyst surface may be responsible for the observed rate modification, via some interaction with the spillover species (oxygen or other) has not been successfully addressed to date.

1.2.   Scope of the research

In this research we aimed to clarify the issues regarding the role of impurities in electrochemical promotion by investigating the non-reactive and reactive properties of a nominally 'clean' catalyst system deposited with known type and amount of a foreign species. The term nominally 'clean' is used here as it is possible that a certain level of unknown and uncharacterised impurities may exist on any catalyst surface (due to the method of preparation, the purity of raw materials etc). By gradually increasing a species concentration on the catalyst, we can systematically investigate the difference between the 'clean' and the contaminated systems while eliminating the effects of variation in electrode characteristics due to inconsistencies in the electrode preparation. The catalyst system consists of a porous polycrystalline platinum film interfaced with yttria stabilised zirconia solid electrolyte (Pt/YSZ system) and modified with variable-coverage sodium (by depositing sodium hydroxide (NaOH) solutions of different concentrations ranging from 10^{-12} to 10^{-1} M). The Pt/YSZ system was chosen as it is a well-studied system and often used as a model system in both solid state electrochemistry and EPOC studies [2, 12-15]. Sodium was chosen in this study due to the promoting properties it has been found to have in heterogeneous catalysis [16-20]. Additionally, sodium ions supplied electrochemically through the use of sodium-ion conducting supports also act as promoter in many EPOC studies [21-23], particularly to enhance the rate of NO_x reduction [6, 24]. Experiments conducted on the 'clean' and sodium-modified systems were mainly focused to:

i.   Investigate the catalyst surface characteristics i.e. physical morphology, surface chemical state and composition, surface area and work function, and their dependence on sodium coverage

ii.   Propose a conceptual model that describes the role of sodium under non-reactive and reactive conditions

iii. Investigate sodium modification of the catalyst electrochemical properties under non-reactive conditions, mainly the effect of variable-coverage sodium on oxygen charge transfer

iv. Investigate sodium modification of the catalytic and electrocatalytic properties using a model reaction, i.e. ethylene oxidation.

- The combined effect of *ex situ* (sodium) and *in situ* (electrochemically supplied oxygen ions) promoters, in order to assess the possible interactions between them and their combined effect on promotion.

- The dependence of the reaction promotional behaviour on sodium coverage

v. Verify the findings from (iv) with a case study of NO reduction by propene which is an environmentally important reaction as well as investigate sodium modification of:

- The catalyst selectivity for NO reduction to N_2 and other product gases

- The effect of temperature on the catalytic activity

The effect of sodium addition on the catalyst system was characterised using scanning electron microscopy-energy-dispersive x-ray (SEM-EDX), Kelvin Probe work function measurements, x-ray pohotoelectron spectroscopy (XPS) analysis and isothermal oxygen surface titration. Under non-reactive conditions, sodium modification of the kinetics of oxygen charge transfer was investigated using cyclic and linear sweep voltammetry techniques. Using a chronoamperometry technique, the role of variable coverage sodium on the catalytic and electrocatalytic properties of the platinum catalyst was investigated using two different reactions; i.e. ethylene oxidation and NO reduction by propene. Ethylene oxidation was selected as a probe reaction because a total oxidation leading to one carbon product (CO_2) can be achieved. Moreover it has been used in many EPOC studies [2, 25-27].

NO reduction was chosen as a case study since it is an environmentally important reaction particularly in automotive exhaust catalysis.

1.3.   Thesis outline

The thesis is divided into ten chapters discussing the different aspects of the research. The current chapter (Chapter 1) contains general introduction to the research, the aim of the research as well as the outline of the thesis. In Chapter 2 a brief literature review is given. Initially the principles of electrochemistry that are relevant to the work presented in the thesis are discussed. These are followed by an introduction to the use of promoters in heterogeneous catalysis, the fundamentals and practical application of EPOC, $Pt(O_2)$/YSZ and ethylene oxidation as model systems and an environmentally significant reaction, NO reduction. Finally the subject of impurities is also discussed.

Chapter 3 describes the materials used and the experimental procedures followed for materials preparation, characterisation and data acquisition during the course of project. The design of the electrode system, reactor and experimental rig was also described. Also included are the procedure of sodium deposition on the catalyst film and the calculation of sodium coverage. Finally, the technique used and procedure for each specific experiment are described as well. Chapter 4 discusses the characterisation of the Pt/YSZ catalyst system. The techniques used include scanning electron microscopy in combination with energy-dispersive X-ray microscopy (SEM-EDX) for morphology and elemental analysis, X-ray photoelectron spectroscopy (XPS) for surface chemical state and composition analysis, isothermal surface titration technique for surface area analysis as well as Kelvin probe for work function measurements.

Based on the findings from the surface characterisation of the Pt/YSZ system and the literature, an experimental hypothesis is given in Chapter 5. In this chapter, we attempt to predict the change in the electrochemical, catalytic and electropromoted properties of the

system due to sodium addition under both non-reactive and reactive conditions. The experimental results obtained on samples with varying sodium coverage under non-reactive conditions (with a flow of 20 kPa oxygen at 400°C) mainly using cyclic and linear sweep voltammetry are presented and discussed in Chapter 6. Chapter 7 and 8 discuss the results obtained under reactive conditions, i.e. ethylene oxidation and NO reduction by propene respectively. Cyclic voltammetry and chronoamperometry (potentiostatic transient) techniques were used to investigate the role of sodium addition on the kinetics of ethylene oxidation and NO reduction by propene under open-circuit and polarised conditions. The studies were also conducted under varying oxygen partial pressures and for NO reduction under varying temperature as well. The results from both non-reactive and reactive studies are discussed with respect to the proposed hypothesis discussed in Chapter 5. Chapter 9 concludes the overall results and discusses the role of sodium in electrochemical promotion of catalysis and suggests some useful future work.

Literature Review

1.4.   Introduction

This chapter reviews the principles of electrochemistry and the studies of electrochemical promotion of catalysis (EPOC) that are relevant to the work presented in the thesis. Initially a theoretical background on electrochemistry is given; this includes Faraday's Law, thermodynamics, electrode kinetics charge and mass transfer limitations. This is followed by an introduction to promotion in heterogeneous catalysis, EPOC phenomena, solid electrolytes and catalysts used in EPOC, solid electrolyte cell, three-phase boundary, origin of EPOC, promotional rules, practical application of EPOC, $Pt(O_2)/YSZ$ and ethylene oxidation as model systems and an environmentally significant reaction, NO reduction. Finally the subject of impurities is also discussed.

1.5.   Principles of electrochemistry

1.5.1.   Faraday's Law for electrochemical reaction

In a typical electrochemical experiment, the potential difference between the electrodes can be varied by an external power source to produce a current flow in the external circuit because the electrons cross electrode/electrolyte interfaces as reactions occur [28]. Consider the following reduction reaction, where O is the oxidised species, R is the reduced species and n is the number of electrons exchanged between O and R.

$$O + ne^- \rightarrow R \tag{2.1}$$

The rate of the electrochemical reaction according to Faraday's first law of electrolysis [29], assuming the reaction involves one-step electron transfer (reaction 2.1), can be expressed as,

"*The amount of materials (reactant or product) undergoing electrochemical change, m is proportional to the amount of electrical energy, Q, involved*":

$$m = Q/nF \qquad (2.2)$$

where n is the number of electron involved, F is Faraday constant which is equivalent to the charge associated with a unit amount of electron (96485 C mol^{-1}). Therefore F equals to:

$$F = N_{AV}\, Q_e \qquad (2.3)$$

where N_{AV} is the Avogadro number and Q_e is the (fundamental) charge on a single electron. Q in Equation 2.2 is defined as the integral of the cell current, I with respect to time, t:

$$Q = \int I\, dt \qquad (2.4)$$

In the case of constant current operation, Q equals to the product of I and t:

$$Q = It \qquad (2.5)$$

Therefore Equation 2.2 becomes

$$m = It/nF \qquad (2.6)$$

Differentiating Equation 2.6 with respect to time gives the rate of reaction 2.1. The unit is mol s^{-1}.

$$dm/dt = I/nF \qquad (2.7)$$

Equation 2.7 represents a homogeneous reaction (in a single phase) whereby the rate is uniform everywhere in the volume where it occurs. Heterogeneous reactions on the other hand occur at the electrode-solution interface; therefore the reaction rate depends upon the area of the electrode, A (cm^2), or the area of the three-phase boundary where the reaction occurs:

$$\frac{1}{A}\frac{dm}{dt} = \frac{I}{AnF} = \frac{i}{nF} \qquad (2.8)$$

where I/A is the current density, i (A cm^{-2}). The unit of the reaction rate is mol cm^{-2} s^{-1}. Equation 2.8 represents a balance at the electrode/electrolyte interface between the flux of material and the electrode flux. The flux is [29]:

$$j = i/nF \tag{2.9}$$

Ideally, Equations 2.7 and 2.8 represents the rate of the loss of reactant, which for reaction 2.1 is equal to the formation of R. The actual reaction 2.1 in reality is however, a complex multistep process which may be dependent on the rate of processes such as [30]:

i) Mass transfer, which is the transport of reactants to, or products from, the electrode surface

ii) Chemical reactions preceding or following electron transfer, which might be homogeneous or heterogeneous ones on the electrode surface

iii) Other surface reactions, such as adsorption, desorption, or crystallisation.

Some of these processes (e.g. electron transfer at the electrode surface or adsorption) are in turn controlled by the electrode potential.

1.5.2. *Thermodynamics*

Considering the reduction reaction in Equation 2.1, the relationship between the reduced and oxidised species concentration, C_R and C_O and Gibb's free energy, ΔG, is given by [31]:

$$\Delta G = \Delta G^o + RT \ln \frac{C_R}{C_O} \tag{2.10}$$

where R is the gas constant (8.3145 J mol^{-1} K^{-1}), T (K) is the temperature and ΔG^o is the standard Gibbs energy for the reaction. In Equation 2.10, we can see the relation between the ratio of reduced to oxidised species and the Gibbs free energy change, ΔG, from which the potential, E (V), can be derived. To derive E from ΔG, the electrochemical cell is treated as a

closed system (i.e. no transport material between the system and surroundings) operating at a constant temperature and pressure [32]. The total change in internal energy, ΔU of a closed system equals the heat, q, added to the system minus the work, w, done by the system:

$$\Delta U = q - w \tag{2.11}$$

For a reversible system at constant temperature and pressure, the mechanical contribution due to the volume change is

$$w_p = P\Delta V \tag{2.12}$$

while the total work done by the system is

$$w = w_p + w_{el} \tag{2.13}$$

where w_{el} is electrical work. For a reversible change at constant temperature, the heat transferred is related to the change in entropy, ΔS, by:

$$q = T\Delta S \tag{2.14}$$

The change in Gibbs free energy at constant temperature and pressure is:

$$\Delta G = \Delta H - T\Delta S \tag{2.15}$$

while the enthalpy change is given by:

$$\Delta H = \Delta U + P\Delta V \tag{2.16}$$

Combining Equations 2.11 to 2.14 we get:

$$\Delta U = T\Delta S - P\Delta V - w_{el} \tag{2.17}$$

Substituting Equations 2.16 and 2.17 into Equation 2.15 gives:

$$\Delta G = -w_{el} \tag{2.18}$$

This means that the electrical work obtained from a closed system at constant temperature and pressure, operating reversibly, is equal to the change in Gibbs free energy [32]. The maximum electrical energy available in an external circuit is equal to the number of charges multiplied by the maximum potential difference, which is the reversible cell potential. Since $Q = nF$, from Equations 2.18, we get

$$\Delta G = -nFE \tag{2.19}$$

Here E is the maximum potential between two electrodes or the open-circuit potential (OCP) or the equilibrium potential, which is present when no current is flowing through the cell. If the reactant and product have unit activity, and E is given for the reduction reaction (Equation 2.1), Equation 2.20 can be written as

$$\Delta G^o = -nFE^o \tag{2.20}$$

where the potential, E^o (V) is known as the standard electrode potential and it relates to the standard Gibbs free energy change, ΔG^o (J mol^{-1}). Combining Equations 2.10 and Equations 2.19-2.20 results in the mathematical expression describing the relation between potential and concentration for a cell reaction, the Nernst equation [31]:

$$E = E^o + \frac{RT}{nF} \ln \frac{C_O}{C_R} \tag{2.21}$$

Note that the Nernst equation solves the potential of an electrochemical cell containing a reversible system (Nernstian system) with fast kinetics and it is valid only at equilibrium (open-circuit) and at the surface of the electrode. It also possible to report the reaction potentials with the convention of electromotive force (emf) [31]. For a reduction reaction, the standard potential and the emf have the same value, while for an oxidation (the reverse reaction), their signs are opposite.

1.5.3. *Electrode kinetics*

1.5.3.1. Overpotential

To investigate an electrode reaction, the current is always determined as a function of the electrode potential. The deviation of the electrode potential (or cell potential) from the equilibrium value upon flow of faradaic current is termed polarisation. The extent of polarisation is measured by the overpotential [28]:

$$\eta = E - E_{eq} \tag{2.22}$$

The overpotential, η, here is due to the slow charge transfer reactions at the electrode electrolyte interface. Other overpotentials such as concentration overpotential, η_{conc}, due to slow mass transfer and Ohmic overpotential, η_{ohmic}, due to the electrolyte can also contribute to the total η of an electrode. In a solid electrolyte cell, mass transfer in the gas phase is fast, and consequently gaseous concentration overpotential is usually negligible. In addition only small currents are usually involved in EPOC [2], so the Ohmic overpotential may not be as important as in high current cells. The Ohmic overpotential can be determined via a current interruption technique. The technique in conjunction with a recording oscilloscope measures the ohmic component that decays to zero very quickly once a current flow is stopped or interrupted, and the remaining is the charge transfer overpotential. This charge transfer overpotential is of interest and is related to current via the Butler-Volmer equation.

1.5.3.2. Butler-Volmer model

For a simple reduction reaction (number of electron, $n = 1$), the Butler-Volmer equation can be derived as follows:

$$O + ne^- \underset{k_b}{\overset{k_f}{\rightleftharpoons}} R \tag{2.23}$$

where k_f and k_b (cm s^{-1}) are the heterogeneous rate constants for forward reduction and backward oxidation electrode reactions. The rate of the reaction is given by:

$$\upsilon_f = k_f C_O \tag{2.24}$$

$$\upsilon_b = k_b C_R \tag{2.25}$$

where C_O and C_R are the concentration of oxidised and reduced species at the electrode surface. Assume that the rate constants k_f and k_b have an Arrhenius form [32]:

$$k_f = A_f\, e^{(-\Delta G_c/RT)} \tag{2.26}$$

$$k_b = A_b\, e^{(-\Delta G_a/RT)} \tag{2.27}$$

where ΔG_a and ΔG_c are the anodic and cathodic free energy of activation respectively, while A_f and A_b are constants. If the cell potential, E^o, is changed by ΔE to a new value, E, the relative energy of the electron resident on the electrode changes by $-F\Delta E = -F(E-E^o)$. The energy barrier for oxidation, ΔG_a, will become less than ΔG_a^o by a fraction $(1-\alpha)$ of the total energy change, where α, the transfer coefficient can vary between 0 to 1 (typically ~0.5) assuming one-electron transfer at the interface without being involved in any other chemical step [28],

$$\Delta G_a = \Delta G_a^o - (1-\alpha)F(E - E^o) \tag{2.28}$$

and at potential E, the cathodic energy barrier, ΔG_c, is higher than the ΔG_c^o by $\alpha F(E-E^o)$:

$$\Delta G_c = \Delta G_c^o + \alpha F(E - E^o) \tag{2.29}$$

Combining Equations 2.26-2.29 we get:

$$k_f = A_f\, e^{(-\Delta G_c^o/RT)} e^{-\alpha F(E-E^o)/RT} \tag{2.30}$$

$$k_b = A_b\, e^{(-\Delta G_a^o/RT)} e^{(1-\alpha)F(E-E^o)/RT} \tag{2.31}$$

and

$$k_f = k_f^o \, e^{-\alpha F(E-E^o)/RT} \tag{2.32}$$

$$k_b = k_b^o \, e^{(1-\alpha)F(E-E^o)/RT} \tag{2.33}$$

where

$$k_f^o = A_f \, e^{(-\Delta G_c^o/RT)} \tag{2.34}$$

$$k_b^o = A_b \, e^{(-\Delta G_a^o/RT)} \tag{2.35}$$

The overall current (or current density) can be viewed as the sum of the cathodic (reduction), i_c, and the anodic (oxidation), i_a, components [28]:

$$i = i_c + i_a \tag{2.36}$$

From Equations 2.8, 2.24-2.27, 2.32-2.33, we get the current-potential characteristic known as the Butler-Volmer equation:

$$i = Fk^o\left[C_O e^{-\alpha F(E-E^o)/RT} - C_R e^{(1-\alpha)F(E-E^o)/RT}\right] \tag{2.37}$$

At equilibrium, $E = E_{eq}$, there is no net current flow and the fluxes must be balanced, $i = i_a = -i_c = i_o$, Equation 2.37 becomes:

$$Fk^o C_O e^{-\alpha F(E_{eq}-E^o)/RT} = Fk^o C_R e^{(1-\alpha)F(E_{eq}-E^o)/RT} \tag{2.38}$$

At equilibrium, bulk concentrations of O (C_O^*) and R (C_R^*) are also found at the surface, hence:

$$e^{F(E_{eq}-E^o)/RT} = C_O^*/C_R^* \tag{2.39}$$

From Equation 2.39, an exponential form of Nernst relation can be obtained.

$$E_{eq} = E^o + \frac{RT}{F} ln\frac{C_O^*}{C_R^*} \tag{2.40}$$

13

At equilibrium, the exchange current density, i_o, which is an important factor of the charge transfer overpotential has a magnitude equal to either i_c or i_a.

$$i_o = Fk^o C_O e^{-\alpha F(E_{eq}-E^o)/RT} \tag{2.41}$$

If both sides of Equation 2.39 are raised to the -α power,

$$e^{-\alpha F(E_{eq}-E^o)/RT} = [C_O^*/C_R^*]^{-\alpha} \tag{2.42}$$

Substituting Equation 2.42 into Equation 2.41 produces

$$i_o = Fk^o C_O^{*(1-\alpha)} C_R^{*\alpha} \tag{2.43}$$

and dividing Equation 2.37 by 2.43 gives

$$\frac{i}{i_o} = \left[\frac{C_O e^{-\alpha F(E-E^o)/RT}}{C_O^{*(1-\alpha)} C_R^{*\alpha}} - \frac{C_R e^{(1-\alpha)F(E-E^o)/RT}}{C_O^{*(1-\alpha)} C_R^{*\alpha}} \right] \tag{2.44}$$

or

$$\frac{i}{i_o} = \left[\frac{C_O}{C_O^*} e^{-\alpha F(E-E^o)/RT} \left(\frac{C_O^*}{C_R^*} \right)^{\alpha} - \frac{C_R}{C_R^*} e^{(1-\alpha)F(E-E^o)/RT} \left(\frac{C_O^*}{C_R^*} \right)^{-(1-\alpha)} \right] \tag{2.45}$$

Equation 2.45 is simplified to

$$\frac{i}{i_o} = \left[\frac{C_O}{C_O^*} e^{-\alpha F(E-E^o)/RT} - \frac{C_R}{C_R^*} e^{(1-\alpha)F(E-E^o)/RT} \right] \tag{2.46}$$

The current density can be described in terms of the overpotential, η (Equation 2.22),

$$i = i_o \left[\frac{C_O}{C_O^*} e^{-\alpha F\eta/RT} - \frac{C_R}{C_R^*} e^{(1-\alpha)F\eta/RT} \right] \tag{2.47}$$

Equation 2.47 is the current-overpotential equation that predicts the behaviour shown in Figure 0.1. The solid curve is total current density, which is the sum of cathodic and anodic components, i_c and i_a (dashed curves). At large positive or negative overpotentials, either anodic or cathodic component is negligible respectively, therefore the total current density

merges with that for i_c or i_a. At both extreme η values, the current densities may level off due to mass transfer limitations. The limiting current (density), i_l, is reached when the concentration of the reactant at the surface (e.g. C_O) is depleted (i.e. all reactant transported to the electrode has been converted to product [33]) at a rate faster than the reactant being replenished. The limiting current imposed by the reactant supply is manifested by the $\frac{c_O}{c_O^*}$ and $\frac{c_R}{c_R^*}$ factors in Equation 2.47.
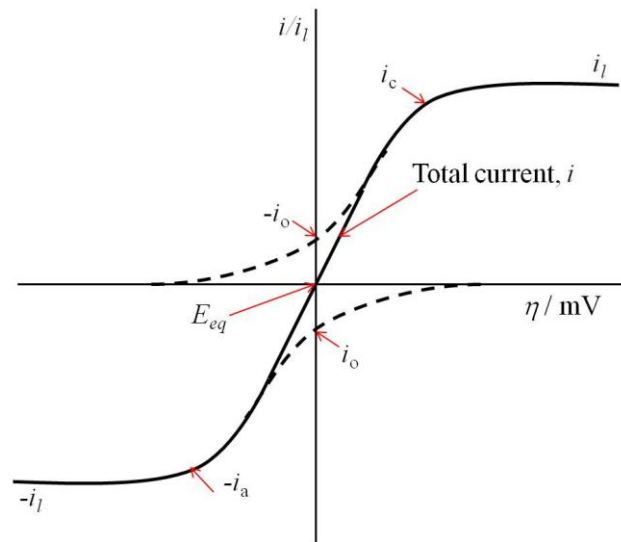
Figure 0.1. Current-overpotential curves for $O + ne^- \rightleftharpoons R$. $T = 298$ K, $\alpha = 0.5$. $i_{l,c} = -i_{l,a} = i_l$ and $i_o/i_l = 0.2$. Adapted from [28].

1.5.3.3. Butler-Volmer approximations

When there is no mass transfer effect, the reactant surface concentration is similar to their bulk values, Equation 2.47 becomes

$$i = i_o \left(e^{\frac{-\alpha F \eta}{RT}} - e^{\frac{(1-\alpha)F\eta}{RT}} \right) \tag{2.48}$$

This form of Butler-Volmer equation is applicable for an electrochemical system where the reaction rate is controlled by charge transfer. For large values of η (either positive or

15

negative), one of the reactions becomes negligible as the system is too far from the equilibrium and Equation 2.48 becomes [29]:

$$i = i_{red} = i_\mathrm{o} e^{-\alpha F \eta / RT} \qquad (2.49)$$

or

$$\log|i_{red}| = \log|i_\mathrm{o}| - \frac{\alpha F \eta_{red}}{2.3RT} \qquad (2.50)$$

or

$$\eta = a_c + b_c \log|i_{red}| \qquad (2.51)$$

where

$$a_c = \frac{2.3RT}{\alpha F} \log i_\mathrm{o} \qquad \text{and} \qquad b_c = -\frac{2.3RT}{\alpha F} \qquad (2.52), (2.53)$$

Equation 2.51 is Tafel equation and a_c and b_c are constants. A typical Tafel plot is shown in Figure 0.2. The Tafel equation links the applied overpotential to the current that passes through the circuit. The plots deviate from log-linear behaviour as η approaches zero (near equilibrium), as the back reactions is no longer negligible.
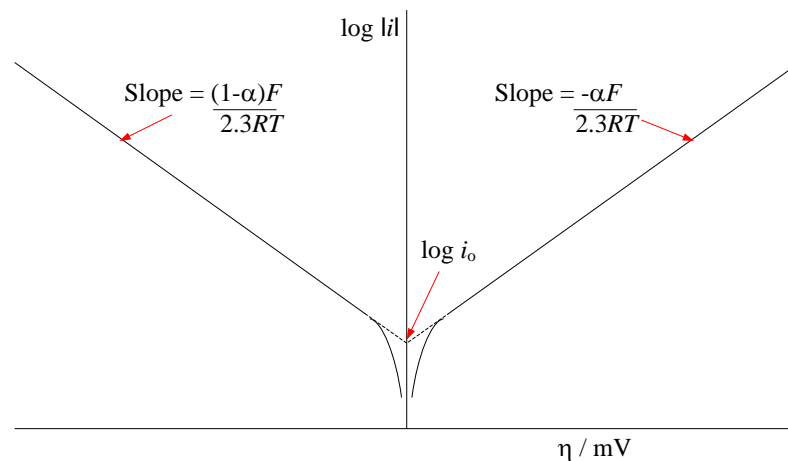
Figure 0.2. A typical Tafel plot for current-overpotential curve with $\alpha = 0.5$. Adapted from [28].

16

For small values of x, the exponential e^x can be approximated as $1 + x$. When the overpotentials are sufficiently small ($\eta < 50$ mV), it is assumed that Fη $<<$ RT, thus Equation 2.48 can be expressed as:

$$i = i_o \left[1 + \frac{-\alpha F \eta}{RT} - 1 + \frac{(1-\alpha) F \eta}{RT} \right] \tag{2.54}$$

or

$$i = i_o \frac{F \eta}{RT} \tag{2.55}$$

This means that the net current (density) is linearly related to the overpotential in a narrow potential range near E_{eq}. The ratio $-\eta/i$ is known as charge-transfer resistance, $R_{ct} = RT/Fi_o$.

1.5.3.4. Mass transfer limitations

In order for an electrochemical reaction to proceed, the reactant species must be transported from the bulk to the electrode surface (or to the three-phase boundary), and the product formed must then be able to diffuse away for a new cycle to take place. Therefore, there is a high possibility that a reaction is controlled by the rate at which material is brought to (or from) the electrode through mass transport (e.g. through diffusion). Fick's first law describes the rate of diffusion through a plane parallel to the electrode at a distance x from the surface, where the concentration varies with distance from the surface [34]:

$$j_O = -D_O \frac{dc_O}{dx} \tag{2.56}$$

where dC_O/dx is the concentration gradient (the driving force of diffusion) and D_O (cm^2 s^{-1}) is the diffusion coefficient of species O. The minus sign indicates that the species move from concentrated to dilute solution. For an electrode reaction $O + ne^- \rightleftharpoons R$, the fluxes of reactant and product at the surface must be equal to satisfy the law of mass conversion on the electrode surface, thus we can equate the fluxes in solution to the flux of electrons to the surface [28]:

$$-D_O \left(\frac{dC_O}{dx}\right)_{x=0} = D_O \left(\frac{dC_R}{dx}\right)_{x=0} = i/nF \tag{2.57}$$

where C_O and C_R are the concentrations of O and R, while D_O and D_R are the diffusion coefficients respectively.

1.6.   Promotion in heterogeneous catalysis

In heterogeneous catalysis, the nature of the interface is crucial for the efficiency of the catalysed processes. Small amount of additives on the top layer of atoms can enhance (promote) or reduce (poison) the catalytic reactions [35]. The use of promoters in heterogeneous catalysis is particularly important as they can improve the catalytic activity, selectivity and/or stability [9]. There are two types of promoters; structural and electronic. The former enhance and stabilise the dispersion of the active phase on the catalyst support, whereas the latter enhance the catalytic properties of the active phase itself [2]. An example is the promotion of ammonia synthesis over iron-based catalysts by Al_2O_3 and K_2O [9]. The alumina as a structural promoter improves the catalyst stability, by preventing the sintering of iron particles. On the other hand the potassium oxide (electronic promoter) promotes the dissociative chemisorption of molecules such as nitrogen on the surface of the transition metals through electron donation. Although an alkali promoter like potassium activates the surrounding sites, the alkali itself is not an active catalyst, thus the site it is sitting on is effectively blocked. In addition, as alkalis have lower surface energy than the transition metals they tend to segregate to the upper layer of the catalyst, resulting in high surface concentration. The use of electrical polarisation to supply a controlled amount of promoter species to a catalyst surface can be realised through electrochemical promotion of catalysis [2] which will be discussed in Section 2.4.

1.6.1. *Alkali metals adsorption on transition metals*

The presence of alkali on transition metal surfaces is known to decrease the metal work function. Generally, at low alkali metal coverages, a strong initial decrease in the metal work function can be observed, followed by a work function minimum and by an increase to a work function value corresponding to near bulk alkali metal work function around a monolayer coverage [36]. The presence of alkali such as sodium on transition metals may also influence the adsorption rate and the maximum uptake of the surface, the stability of the adsorbed species, the strength of intramolecular bonds, the strength of bonds formed between the adsorbed species and the substrate and the propensity for dissociative adsorption [2]. For example, in the case of oxygen adsorption, increasing the alkali coverage was found to increase the dissociative oxygen chemisorption rate (initial sticking coefficient) and the saturation oxygen coverage (adsorptive capacity of the surface) up to a value of unity at alkali coverage corresponding to the work function minimum. The beneficial effect of alkali modification can be explained by the stabilisation of adsorbed oxygen atoms on the alkali-modified sites due to direct interaction between alkali and oxygen, as well as the stabilisation of the molecular oxygen (precursor) and the decrease of the activation barrier for oxygen dissociation due to enhanced backdonation of electron density into the $1\pi^*$ antibonding orbitals of oxygen molecule. Depending on the metal substrate, a stable alkali-oxygen surface complex may be formed above some critical oxygen and alkali coverage, when the interactions between adsorbed oxygen species and alkali become dominant [2].

1.7. Electrochemical promotion of catalysis

Electrochemical promotion of catalysis (EPOC) also known as NEMCA for non-Faradaic electrochemical modification of catalytic activity was first discovered in the 1980's by Vayenas and his group [1, 3, 37]. It was found that by applying electrical currents or

potentials (up to ±2 V) between a conductive catalyst supported on a solid electrolyte and a counter electrode also deposited on the solid electrolyte, the catalytic activity and the selectivity of the catalyst can be altered in a very pronounced, reversible and to some extent predictable manner [2]. As a result, an increase in the catalytic rates up to 1350 times larger than the initial catalytic rates without current application was observed [38]. The electrochemically-induced increase in the catalytic rates was also found to be larger than the rate of electrochemical supply of ions via the solid electrolyte to the catalyst (typically between a factor of 10 up to 10^5 [26, 39]), higher than that expected by Faraday's law of electrolysis. This is the reason why the phenomenon was termed as NEMCA in the first place.

1.7.1. *Solid electrolytes and catalyst/electrodes*

The first observation of EPOC was on ethylene epoxidation over Ag catalyst in early 1980's. It became apparent in 1990's that EPOC is a general phenomenon and not limited to any particular type of catalytic reaction, catalyst or solid electrolyte [40-41]. EPOC has been demonstrated in almost 100 different catalytic systems in the presence of various metal catalysts in contact with a solid electrolyte[1] [2, 6]. So far a variety of solid electrolytes has been employed in EPOC studies, they are characterised based on the conducting ions such as oxygen ion conductors e.g yttria stabilised zirconia (Y_2O_3 ZrO_2) [26, 37, 42-43], alkali ion conductors e.g. Na^+ (NASICON and β''-Al_2O_3) [41, 44] and K^+ (β''-Al_2O_3) [45-47], F^- conductor e.g. CaF_2 [48], proton conductors e.g. Nafion [49] and $Ba_3Ca_{1.18}Nb_{1.82}O_9$-$\alpha$ [50], mixed ionic electronic conductors such as TiO_2 [25] and in a few cases molten salts (V_2O_5-$K_2S_2O_7$) [51] and aqueous alkaline solution [52]. The conductivity of a solid electrolyte is

---

[1] Solid electrolytes are solid-state materials that exhibit significant ionic conductivity at elevated temperatures; the conductivity gained depends on their compositions [C.G. Vayenas, Bebelis, S., Pliangos, C., Brosda, S. and Tsiplakides, D., Electrochemical Activation of Catalysis: Promotion, Electrochemical Promotion, and Metal-Support Interactions, Kluwer Academic/Plenum Publishers, New York, 2001]. The solid electrolytes find commercial application mainly in gas sensors [W. Göpel, Sensors and Actuators B: Chemical, 18 (1994) 1-21] and in the field of solid oxide fuel cells [K. Eguchi, T. Setoguchi, H. Arai, Vacuum, 42 (1991) 1061].

mainly due to ionic displacement [2, 53]. Yttria stabilised zirconia (YSZ) is the most often used solid electrolyte in EPOC studies [2, 27, 37] especially for catalytic oxidations. The oxygen ion conductivity of YSZ relies on the oxygen ion vacancies created in the lattice of ZrO_2, which is a tetravalent metal oxide when doped with the oxide of a divalent or a trivalent material like Y_2O_3, normally to a composition around 6-8 mol% Y_2O_3 in ZrO_2 [53]. In EPOC studies, among the metal catalysts used are platinum [2, 10, 26-27, 37], palladium [2, 54], silver [55-56], rhodium [57-58], gold [59] and nickel [60]. In some cases metal oxides (e.g. oxides of ruthenium and iridium) are also utilised [61-62]. Various methods of catalyst preparation were used such as the classical painting of metal pastes followed by sintering [2] which has produced effective catalyst films for many EPOC studies. Other methods include wet impregnation [7, 63], thermal decomposition [64], electrostatic spray deposition [65] and sputtering [7, 66]. In addition, the last few years have also seen the use of laser deposition technique to produce reproducible and relatively well-defined model catalysts on a single crystal support [67-69], in both dense and porous microstructure. The dense film however showed microstructural changes once being polarised.

1.7.2. Solid electrolyte cells and electrocatalytic operations

A solid electrolyte interfaced with at least two electronically conducting films (e.g. metal electrodes) forms a solid electrolyte galvanic cell. A galvanic cell refers to an electrochemical system whose reactions are spontaneous ($\Delta G < 0$) and if electricity production is desired, the chemical energy can be converted directly to electrical energy. To electrochemically produce a compound, an external power source has to be used to supply currents and drive e.g. an oxygen flux (for an oxygen ion conductor) through the cell in the desired direction, regardless of the spontaneous direction of the flow [53]. The solid electrolyte cell may consist of a dense solid electrolyte membrane and two or three porous electrodes; i.e. the working electrode (WE) and the counter electrode (CE) as well as an additional electrode as the reference electrode (RE). An example shown in Figure 0.3a is a

three-electrode system normally used in the electrochemical promotion studies. The cell can either be operated using the fuel-cell type configuration or the single-chamber type configuration as shown in Figure 0.3b and c respectively, depending on whether the two electrodes are exposed to the same or different gaseous mixture.
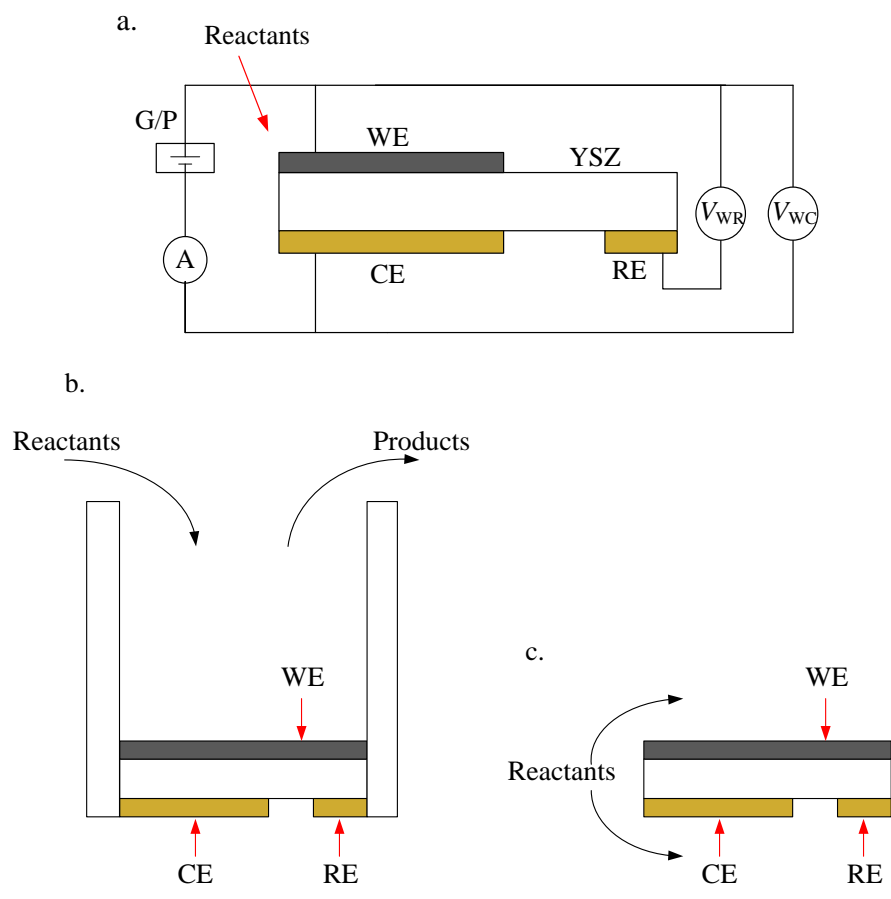
Figure 0.3. Solid electrolyte cell configuration. Adapted from [2].

In the fuel-cell type reactor, the catalyst-working electrode is exposed to the catalytic reactants and products, but the counter and reference electrodes are in a separate chamber [2]. The single-chamber type cell is easier to apply to existing catalytic processes as it does not require the anode and cathode sides to be separated [53]. However, in such case, the counter and reference electrodes must be catalytically inert (e.g. Au), and the reference electrode is only a monitoring (pseudoreference) electrode [2, 63, 70]. As shown in Figure 0.3a, a galvanostat or potentiostat (G/P) can be used to apply constant currents between the

catalyst-working electrode and the counter electrode or constant potentials, V_{WR}, between the catalyst-working electrode and the reference electrode respectively [70]. In the case of YSZ (an oxygen ion conducting membrane), the oxygen ions are supplied from (or to) the solid electrolyte to (or from) the catalyst-electrode surface when the current/potential is applied [70].

1.7.3.   *Three phase boundary*

The application of current/potential on the solid electrolyte cell supplies ions to the catalyst-electrode surface at a rate I/nF where I equals to the applied current, n is the number of electrons involved and F is Faraday's constant (C mol^{-1}). Depending upon the materials involved, this may happen via e.g. the three-phase boundary (tpb); an interface where the solid electrolyte, metal catalyst and the gas reactant meets. It is useful to note that in solid state electrochemistry only a fraction of metal surface (catalyst) which is in the vicinity of the tpb is electrocatalytically active (although the catalytically active area is not confined to the tpb), whereas the entire metal surface is usually electrocatalytically active in aqueous electrochemistry, thus a charge transfer reaction can occur over the whole metal surface [71]. EPOC phenomena showed that the promoter ions supplied through the tpb may be spread out over the entire catalyst surface due to repulsive lateral interactions between the ions [2], thus affecting the catalytic activity of the co-adsorbed species on the catalyst surface as well.

1.7.4.   *Origin of EPOC*

1.7.4.1. *Spillover-backspillover effect*

Spillover effect is described in [2] as the mobility of sorbed species from one phase on which they easily adsorbed (donor) to another phase where they do not directly adsorbed

(acceptor). By convention, spillover is the migration of promoter species from the catalyst to the support, and backspillover denotes the migration from the support to the catalyst. Spillover (and backpillover) of a promoter species from (and to) the catalyst surface may improve the catalytic activity and selectivity of a catalyst as well as increase the lifetime and regenerability of the catalysts. The electrochemical promotion theory is attributed the non-Faradaic effect of a controlled migration (backspillover) of promoting species from the solid electrolyte via the solid electrolyte-catalyst-gas three-phase-boundaries (tpb) to the catalytically active electrode surface upon current/potential application. The evidence for this has been provided through numerous studies such as using catalytic rate transient analysis [72], cyclic and linear sweep voltammetry [73], work function measurements [74-76], X-ray photoelectron spectroscopy (XPS) [77], temperature-programmed desorption (TPD) [74, 78], scanning tunnelling microscopy (STM) [79], photoemission electron spectroscopy and scanning photoelectron microscopy (PEEM and SPEM) [80] and electrochemical impedance spectroscopy (EIS) [54]. The ionic promoting species (e.g. $O^{\delta-}$) accompanied by the image (screening) charge in the metal form surface dipoles and establish an overall neutral dipole layer (termed as 'effective' electrochemical double layer) on the gas exposed catalytically active electrode surface as shown in Figure 0.4 and changes its work function [2, 81]. The backspillover species occupy primarily the strongly bonded chemisorption state, forcing the gas phase oxygen to populate mainly the weakly bonded state, which is highly reactive, thus enhancing the catalytic rates (e.g. CO oxidation), while also acting as a sacrificial promoter by reacting with other reactive molecules such as CO or C_2H_4 at a slower rate than the weakly bonded atomic oxygen [2, 70]. Similar electrochemical double layer can also be formed without current/potential application by e.g. evaporating sodium on platinum electrodes deposited on β''-Al_2O_3 [2].
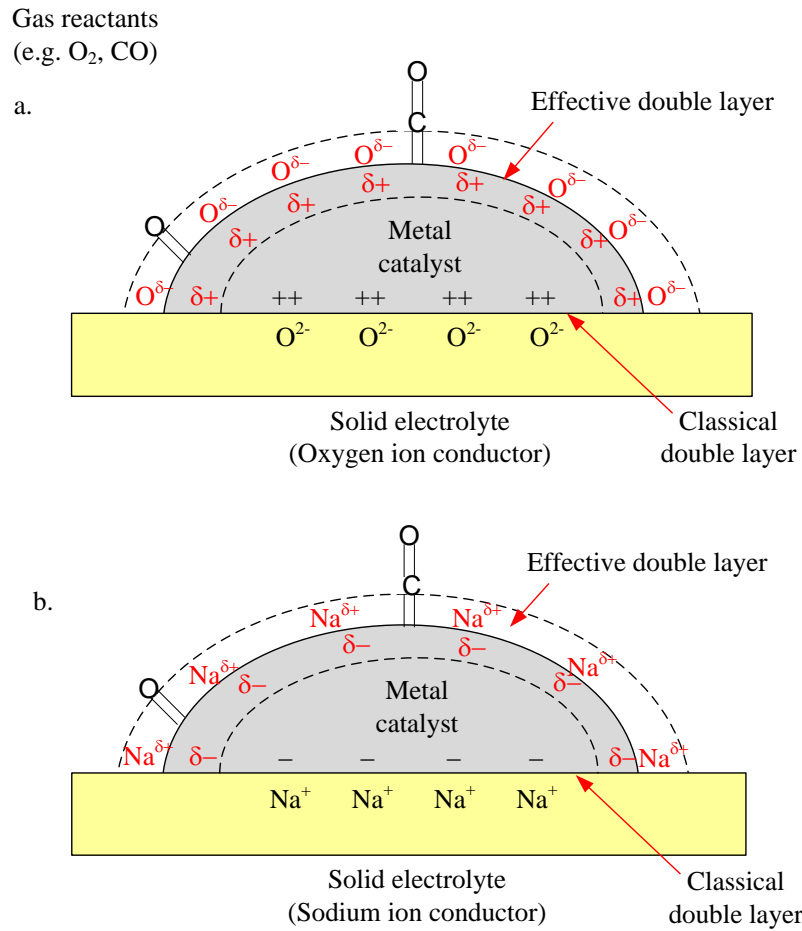
Figure 0.4. Schematic representation of a metal electrode deposited on an oxygen ion conducting membrane (a) and a sodium ion conducting membrane (b), showing the location of the effective double layer created at the metal-gas interface due to potential-controlled ion migration (backspillover). Adapted from [2].

1.7.4.2. Work function changes

The work function, Φ, of a solid surface (in eV) is the minimum energy required to extract an electron at the Fermi level, E_F of the solid to its ground state in vacuum at an infinite distance from the solid [2, 82]. The parameter Φ/e is termed as the extraction potential. According to Vayenas, a key role in understanding EPOC is the catalyst-electrode work function changes, $\Delta\Phi$, during electrical polarisation of the cell. The changes in the Ohmic-drop free catalyst potential with respect to a reference electrode, ΔV_{WR}, leads to the catalyst surface work function changes, $\Delta\Phi$, by:

$$\Delta\Phi = e\Delta V_{WR} \tag{2.58}$$

where e is the charge on the electron. The changes in V_{WR} can be induced by either using a potentiostat or galvanostat or by changing the gaseous composition [2, 83], while the work function changes can be measured at molecular level *in situ* by using a Kelvin Probe [84-85]. Equation 2.58 has been found to be valid up to at least 1 eV [75]. However, Metcalfe et al. found that the change in the electron extraction potential is linearly related to the change in the overpotential, but not on an equal basis [76, 86].

$$\Delta\Phi = \xi V_{WR} \tag{2.59}$$

where ξ depends on the catalyst morphology and operating conditions that kinetically determine the relative rates of spillover and removal of the spillover species via desorption or reaction [86-87]. Therefore, Equation 2.58 is expected to hold only in the case of low reactivity of the spillover species with fast surface diffusion [87].

As mentioned earlier, the change in the catalyst work function is caused by an electrochemically induced ionic spillover species that have lower reactivity than the chemisorbed gas phase reactant, resulting in a newly enhanced catalytic rate. The new catalytic rates can be related to the change in the work function and the applied overpotential by:

$$\ln(r/r_o) = \alpha(e\Phi - \Phi^*/k_b T) \tag{2.60}$$

$$\ln(r/r_o) = \alpha F (V_{WR} - V_{WR}^*)/RT \tag{2.61}$$

where r_o is the regular (open-circuit) catalytic rate, k_b is the Boltzmann constant, R is the universal gas constant and α is the catalyst- and reaction-specific constant (α normally between 1 and -1). The magnitude of electrochemical promotion is more commonly described by using the rate enhancement ratio, ρ, and the Faradaic efficiency, Λ:

$$\rho = r/r_o \tag{2.62}$$

$$\Lambda = \Delta r / (^I/_{nF}) \qquad (2.63)$$

where r is the electro-promoted rate, Δr is the difference in the electro-promoted and open-circuit rate, r_o, I is the applied current, F is the Faraday's constant. An electrochemical promotion is observed when $\rho \neq 1$ and $|\Lambda| > 1$.

1.7.5. *Promotional rules*

The promotional rules derived by Vayenas et al [88] allow the classification of catalytic reactions based on the catalytic rate dependence on the work function, Φ, or equivalently on the coverage of the electropositive (electron donor) or electronegative (electron acceptor) promoter species to four categories. A reactant, j is defined as electron donor (D) if it decreases the work function of a surface (e.g. hydrocarbon),

$$\partial \Phi / (\partial \theta_j)_{\theta i \neq j} < 0 \qquad (2.64)$$

and as an electron acceptor (A) when it increases in the work function of a surface (e.g. oxygen).

$$\partial \Phi / (\partial \theta_j)_{\theta i \neq j} > 0 \qquad (2.65)$$

where θi and θj correspond to the coverage of promoter i and reactant j on the surface.

The promotional rules classify reactions into four types: electrophobic, electrophilic, volcano and inverted volcano [2, 88]:

Electrophobic reactions: A reaction exhibits purely electrophobic behaviour when the kinetics are positive order in the electron donor (D) reactant and negative or zero order in the electron acceptor (A) reactant. Equivalently, the electron acceptor reactant (A) is strongly adsorbed and much more strongly adsorbed than the electron donor reactant (D).

$$\partial r / (\partial \Phi)_{p_A, p_D} > 0 \qquad (2.66)$$

Electrophilic reactions: A reaction exhibits purely electrophilic behaviour when the kinetics are positive order in the electron acceptor (A) reactant and negative or zero order in the electron donor (D) reactant. In this case, the electron donor reactant (D) is strongly adsorbed and much more strongly adsorbed than the electron acceptor reactant (A).

$$\partial r/(\partial \Phi)_{p_A,p_D} < 0 \tag{2.67}$$

Volcano-type reactions: A reaction exhibits volcano (maximum rate) type behaviour with respect to Φ when the kinetics also exhibited maximum with respect to A (at fixed p_D) and D (at fixed p_A) so that the rate is always positive order in A or D and at the same time negative (not zero) order in D or A, respectively. This means that both A and D are strongly adsorbed on the catalyst surface.

Inverted volcano-type reactions: A reaction exhibits inverted volcano (minimum-rate) type behaviour with respect to Φ when the kinetics are positive order in both A or D reactants. This means that both A and D are weakly adsorbed on the catalyst surface.

1.7.6.   *Pt/YSZ as model system*

The solid electrolyte system of Pt(O_2)/YSZ has been extensively studied in the past to enhance the understanding of many important fields such as fuel cells, electrochemical oxygen pumps and oxygen sensors [89-91]. The Pt(O_2)/YSZ system is also of great importance in the fundamental study of electrocatalysis and can be considered to be a model system that can be employed to understand the nature of oxygen pumping and spillover processes in electrochemical promotion of metal catalysts supported on oxygen-ion-conducting membrane solid electrolytes. The overall electrochemical reaction for the reduction of gaseous oxygen can be written in Kröger-Vink notation as:

$$O_{2(g)} + 4e^- + 2V_O^{\cdot\cdot} \leftrightharpoons 2O_O \tag{2.68}$$

where $V_O^{\cdot\cdot}$ is an oxygen vacancy in the lattice of zirconia, e^- is an electron and O_O is oxygen in the lattice [89]. The ionic oxygen species, O^{2-} from the zirconia lattice will be adsorbed at the tpb, and subsequently may desorb as O_2, or may react with a combustible molecule (e.g. CO or C_2H_4), or may migrate (backspillover) on the entire metal/gas interface acting as a strong electronegative promoter and causing electrochemical promotion [2].

One of the electrochemical techniques often used to investigate the $Pt(O_2)$/YSZ electrode system is cyclic voltammetry (CV). Vayenas et al showed that the CV technique can be used for estimation of the tpb length based on the amount of the electrocatalytically active oxygen reduced at the tpb [71]. In another study, the appearance of two cathodic peaks on the cyclic voltammograms has been ascribed to the presence of two oxygen species, the second being assigned to the backspillover oxygen ion species [73]. However, in more recent studies, it has also been reported that the appearance of the CV peaks under oxygen can be explained by the electrochemical formation of platinum oxide species (PtO_x) [89-90, 92]. The presence of more than two cathodic peaks has also been observed with prolonged anodic oxidation; this has been explained with the extension of the tpb from the Pt/YSZ binary interface towards the bulk of the metal controlled by solid diffusion [90]. In addition, the formation of PtO_x species during prolong anodic polarisation at 450^oC is associated with the accumulation of extra charge at the Pt-YSZ binary interface, the tpb and towards the bulk of the platinum electrode [93].

1.7.7. *EP of ethylene oxidation*

Ethylene oxidation is a well-studied reaction in EPOC [2]. It has been used as a probe reaction in many catalytic systems since it is a total oxidation leading to only one carbon species as the product. The kinetic studies of ethylene oxidation on platinum films deposited on YSZ at temperatures between 200 and 400^oC, together with solid electrolyte potentiometry (SEP) show that the activity of the atomic oxygen on the platinum surface is

proportional to the ratio of $p_{O_2}/p_{C_2H_4}$ [94]. The rate was found to be first order in ethylene and zero order in oxygen for low ethylene partial pressures. At higher ethylene partial pressure, the rate becomes first order in oxygen and almost zero order in ethylene. Using a Pt/YSZ system, the electrochemically induced rate increase up to a factor of 50 higher than the open-circuit rate and 74000 times higher than the rate of oxygen ion transport to the catalyst has been observed [26]. The rate enhancement was obtained under fuel-lean conditions, where the open-circuit catalytic rate is first order in ethylene and zeroth order in oxygen. This according to the rules of promotion refers to an electrophobic reaction. The application of positive overpotentials causes an increase to the work function of platinum that leads to the strengthening of the chemisorptive bond of platinum with an electron-donor adsorbate (ethylene) and consequently a weakening of the chemisorptive bond of with an electron-acceptor adsorbate (oxygen). This results in a decrease in the oxygen coverage on the platinum surface that was predominantly covered by oxygen and a decrease in the rate constants and activation energy, thus enhancing the rate of ethylene oxidation [2]. Vice-versa, an opposite effect to the rate of ethylene oxidation seen under positive polarisation is obtained with the application of negative overpotentials. However, in the case of ethylene oxidation, both positive and negative polarisation can cause a promotion depending on the gas-phase composition and on the ratio between the oxygen and ethylene partial pressures ($p_{O_2}/p_{C_2H_4}$) [27].

1.7.8.   *Practical applications of EPOC*

There are several industrial applications that are particularly relevant for EPOC commercialisation. One of those would be for activation of very slow processes that needed either extreme operating conditions or long retention times when using conventional technologies such as ammonia synthesis, total oxidations at reduced O_2 partial pressure or direct methane conversion to C_xH_y [95]. For example, it has been shown that the catalytic

activity of fully promoted industrial ammonia synthesis catalysts interfaced with a proton conductor ($CaIn_{0.1}Zr_{0.9}O_{3-\alpha}$) can be enhanced by up to 1300% with electrochemical promotion. The rate enhancement was 6 times larger than the electrochemically supplied protons [96]. This in principle could lead to a substantial decrease in the commercial operating temperature and pressure of ammonia synthesis reactors. Another possibility of application is in fuel cell technology. Both low (PEMFC) and high (SOFC) temperature fuel cells have been used as reactors (co-generators) for specific reactions under promoted conditions [6, 97-98]. For instance, Salazar and Smotkin showed that the isomerization of 2-3-dimethyl-1-butene to 2-3-dimethyl-2-butene can be enhanced over a thousand fold (ρ = 1230) by spillover of protons generated by the supply of low currents on carbon supported palladium catalyst in a polymer electrolyte fuel cell [97]. Recently, Vayenas proposed the idea of using a triode fuel cell where a third electrode together with an auxiliary circuit is introduced in addition to the anode and cathode. The enhancement of power output by the new device was found to be up to a factor of 8 [99]. Of recent interest, the electrochemical promotion has also been shown to enhance the rate of water gas shift reaction for production of high purity hydrogen which can be used by fuel cell application for power generation [5, 100].

From the environmental point of view, the use of EPOC in air pollution treatment either from stationary or mobile sources is also highly relevant. Air pollutants including volatile organic emissions, nitrogen oxides, hydrocarbons and carbon monoxide that pose several adverse effects to human health and to the environment can be converted into harmless emissions by using heterogeneous catalysis and suitable catalysts. Combining this conventional catalysis with EPOC could enhance the efficiency of using the high-cost metal catalysts, allow the tuning of the catalyst selectivity to desirable products and give the control of the reaction rate during a given electrocatalytic process. A reviews exists on the electrochemical promotion of reactions with environmental and industrial interest from 2002 to 2008 [6]. Studies dedicated on oxidation of hydrocarbons and CO has been conducted

since the early years of EPOC [26, 37, 42, 44, 101-103]. The rate of oxidation reactions can be easily enhanced by electrochemical promotion. Reduction of NO_x to N_2 on the other hand is harder to achieve and thus the study of the reaction is of major importance. In practice, the use of three-way catalysts (TWC) catalytic converter has also been successful to convert all three types of exhaust gases, i.e. hydrocarbons, CO and NO_x into CO_2, H_2O and N_2 provided the air to fuel ratio (AFR) is near stoichiometry. Under lean (high AFR) combustion, where significant fuel savings can be achieved, the classical TWC is not effective in reducing NO_x as the excess oxygen is competing for the reducing agents, particularly CO and the selectivity of the catalyst to N_2O is also increased. The more recent technologies of NO_x storage-reduction (NSR) where NO is stored under lean conditions and then released and reduced to N_2 by a reducing agent under rich conditions and selective catalytic reduction (SCR) by urea or hydrocarbons are able to operate under lean-burn conditions. The reaction of NO reduction in the presence of reducing gas such as ethylene, propene, CO and hydrogen has also been a subject of interest in the EPOC community [10, 104-107]. By far, the NO reduction by propene is the most studied systems in EPOC as it is the major constituent of the hydrocarbon component in automotive exhaust and is the industrial standard for catalyst testing [104].

1.7.9. *EP of NO reduction by propene*

In the presence of oxygen, electrochemical promotion studies were initially demonstrated on metal catalysts interfaced with YSZ solid electrolyte support, an oxygen ion conducting membrane. Foti et al [108] reported that a current (±5 μA) application to an Rh/YSZ system at 300°C enhanced the catalytic activity of NO reduction, but not the selectivity towards N_2. Nevertheless, the conversion of the reactants drops upon a simple heating from 300 to 400°C, due to oxidation of rhodium to rhodium oxide (Rh_2O_3). On the other hand, Williams et al [109] investigated the combination of Rh and silver (Ag) as a bimetallic catalyst deposited on YSZ for electrochemical promotion of NO reduction under lean-burn

conditions. Upon application of +100 mV, the bimetallic combination was found to improve the catalytic activity and selectivity at 386°C. Vernoux and his group [110] has also promoted the NO and C_3H_6 conversion in the presence of oxygen at stoichiometric AFR, over platinum deposited on YSZ by a negative current application (with the enhancement ratio of $\rho_{N_2} = \rho_{N_2O} = 1.9$ and $\rho_{CO_2} = 2$). The negative current application was suggested to increase the oxygen and NO coverage on platinum and decrease that of propene which was strongly adsorbed on the platinum surface. However, the selectivity to N_2 was not improved, and no electrochemical promotion was observed under lean burn conditions. This was explained to be due to the use of low operating temperature (280°C) which renders slow spillover-backspillover of oxygen between platinum and YSZ and insufficient ionic conductivity of YSZ. Nevertheless, their study using thin film iridium catalyst prepared using magnetron sputtering and interfaced with YSZ showed a high and durable NO conversion under lean burn conditions at 500°C [66]. High catalytic activity (more than 80% N_2 yield) was achieved between 350-500°C under stoichiometric conditions. The promotion efficiency was found to be structure sensitive; the most suitable catalyst film is one that contains large iridium particles (20 nm), and presents a high porosity and very low thickness (20–40 nm).

Using a different support, i.e. an alkali ion conducting solid electrolyte, e.g. NASICON, the catalytic activity and the selectivity of the platinum catalyst under lean burn conditions at 300°C were strongly enhanced by electrochemical promotion [111]. The strong increase in the selectivity to N_2 from 41 to 61% upon application of -100 mV shows that electrochemical promotion could be an effective solution for the selective catalytic reduction (SCR) of NO in lean-burn engine exhausts. NASICON was also demonstrated beforehand to have higher efficiency than β''-Al_2O_3 in electrochemical promotion of ethylene oxidation over platinum catalyst as it exhibited a better thermal stability and resistance to H_2O and a high ionic conductivity even at low temperatures [44]. Similarly the NO conversion and the N_2 selectivity were also found to be enhanced by sodium addition to Pt/γ-Al_2O_3 catalysts

[112]. The rate enhancement seen in the systems with sodium ion conductor can be rationalised by the sodium-induced NO dissociation which is the rate-limiting step for the production of N_2 [102, 104, 109, 113-115]. Sodium ions in sites adjacent to NO molecules has an electric field that can lower the energy of the NO antibonding orbital with respect to the Fermi level, thus increases charge transfer from the metal to the NO π* orbital. This increases the strength of NO-metal bond relative to propene-metal bond, accompanied by a decrease in the strength of the N-O bond, thus facilitating the NO dissociation. The subject of alkali modified metals and the fate of co-adsorbed molecules has also received detailed theoretical analysis from surface scientists [116].

Valverde and co-workers [64] showed that electrochemical promotion can markedly modify the catalytic activity and selectivity of a platinum catalyst film directly deposited on Na-β''-alumina support for SCR of NO by propene. The sample preparation technique, i.e. thermal decomposition of H_2PtCl_6 solution, produced a catalyst with high metallic dispersion which could be effective at very low temperature ($240^{\circ}C$). However, increasing gas phase oxygen concentration was observed to progressively reduce the overall catalytic activity of the system. Increasing reaction temperature was also found to further decrease the promotional effects, leading to a poisoning effect at $300^{\circ}C$ [24]. Valverde and his group also applied electrochemical promotion to the NO_x storage-reduction (NSR) catalyst technology with a Pt/K-β'-Al_2O_3 system [45]. Under negative polarization, NO was stored on the surface of platinum catalyst in the form of potassium nitrates, while under negative polarization, the catalyst was regenerated, and the stored nitrates were desorbed and reduced to N_2. The Pt/K-β'-Al_2O_3 system in a tubular reactor configuration was possible of working under fixed lean burn reaction conditions [117]. In addition, it was demonstrated that the system was also capable of storing CO_2 as potassium carbonates. Recently, a similar system was reported to be effective for removal of NO_x under wet reaction conditions [118].

1.8.   The influence of impurities

Impurities may be defined as any foreign species that is present in the bulk or on the catalyst surface possibly during the manufacturing of the precursor, via catalyst preparation or during the experimental duration. Impurities may have differing effects on the catalyst systems. They may act as poisons (blocking active sites and reducing catalytic activity) or they may in fact have a promoting role in the catalytic reaction. Although EPOC has been shown to be successful in numerous catalytic reactions over different catalytic systems, the role of impurities in the electrochemical and electrocatalytic behaviour of a catalyst system has not been studied in detail except the study on differently prepared platinum electrodes (with and without silicon containing additives) [11], and indeed the role of impurities is not fully understood. Mutoro et al showed that the segregation and/or migration of impurities such as silicon can also form oxides at the electrode-electrolyte interface or on the electrode surface and give rise to an additional peak in a platinum cyclic voltammogram under flow of oxygen [11]. They also indicated that most of the reported studies in EPOC contain only minor or no information of the content of impurity in the investigated materials. By using time-of-flight secondary ion mass spectrometry (tof-SIMS) the presence of impurities such as sodium, potassium, calcium, chromium, aluminium, carbon, silicon, magnesium and iron were detected on a YSZ (111) single crystal [11]. Using inductively-coupled plasma (ICP) analysis, Jalil et al from our group [119] also showed that fresh platinum paste/resin used in the present work may contain bulk impurities (after blank correction) such as bismuth, calcium, gold, zinc, iron, nickel, chromium and silicon, but the sintered platinum only appears to contain bismuth, silicon, calcium and lead. Other trace impurities such as sodium, potassium and magnesium were either below the detection limit or masked by the blank impurities from deionised water and aqua regia which were used for dilution. The presence of these impurities and the catalyst microstructure were also found to affect the shape of cyclic voltammogram under flow of 20 kPa oxygen.

In recent studies on the electrochemical oxygen exchange [15], Fleig and his group has also associated the rate limiting step of oxygen reduction over platinum thin-model electrode deposited on YSZ (100) single crystal with the presence of impurities at the three phase boundary. The presence of impurities may create new sites for oxygen chemisorption or storage in the form of interfacial oxide phase that act as finite oxygen reservoir between platinum and YSZ. It may also block the tpb and force the other mechanisms to be important. As EPOC generally involves backspillover processes via the tpb, we could only expect that similar effects may be incurred in the presence of an impurity. Therefore, in this research we investigate the role of impurities in EPOC by first looking at its consequence on oxygen charge transfer reaction in a Pt/YSZ system. The findings from such study will provide useful insights in understanding of the role of sodium on electrochemical promotion in the Pt/YSZ system.

Material and Methods

1.9.   Introduction

This chapter describes the material and methods that are used in all experiments. These include the preparation of solid electrolyte and catalyst-electrodes as well as the testing rig and reactor design. Also described is the procedure of sodium deposition on the catalyst film, the calculation of sodium coverage and the gases used in the experiments. The experimental procedures of the techniques used for surface characterisation, electrochemical measurements and kinetic study are also described in this chapter.

.

1.10.   Materials and preparation

1.10.1.   Solid electrolyte

The solid electrolyte is an oxygen-ion conducting membrane made of 8 mol% yttria-stabilised-zirconia (ZrO_2 Y_2O_3 or YSZ) powder provided by Praxair (Grade HSY8). It must be noted that some impurities may also be present in the YSZ powder (and pellet) that may influence the initial purity of the platinum catalyst film. According to the manufacturer the YSZ powder typically contains 100 ppm Na_2O, 100 ppm SiO_2 30 ppm Fe_2O_3 1000 ppm TiO_2, 2500 ppm Al_2O_3 and 100 ppm CaO. Approximately 2 g of YSZ powder were pressed under 3 kN uniaxially using Specac hydraulic press to form a dense pellet of approximately 20 mm diameter and 2 mm thickness. The pellet was sintered at 1500°C for 4 hours in air. The diameter and the thickness of the sintered pellet were approximately 15 mm and 1.5 mm.

1.10.2. Catalyst-Electrodes

The catalyst-electrodes were prepared by painting of metal resins/pastes on the YSZ solid electrolyte, i.e. platinum (Pt) to serve as both catalyst and working electrode (WE), and gold (Au) as the counter (CE) and reference electrodes (RE). To facilitate catalyst adhesion on the YSZ pellet, the surface was first ablated using an emery cloth. On one side of the pellet, a thin layer of platinum was deposited by painting a platinum resinate (Metalor M603B), followed by sintering at 850°C for two hours in air, while on the other side of the pellet, two gold films were deposited using gold resinate (Metalor A1118) and sintered at 800°C for two hours in air. For some experiments, a different platinum precursor was used (Heraeaus RP 10003-12 paste) and it was sintered at 850°C for 7 minutes. The electrodes were positioned as shown in Figure 0.1.
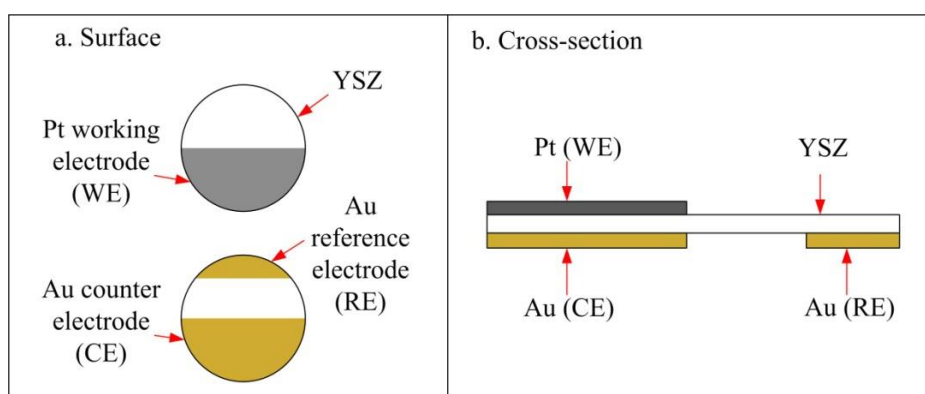
Figure 0.1. Schematic of a three electrode system in a single pellet configuration showing the position of the electrodes

The three electrode system as shown in Figure 0.1 is widely used because the electrical potential of the reference electrode does not change easily during the measurement. For an accurate measurement of the overpotentials of a working electrode against a reference electrode, the working and counter electrodes were attached symmetrically to the electrolyte, and the reference electrode positioned far from both working and counter electrodes [120]. From the literature, the reference electrode must be placed at least three electrolyte

thicknesses away from active electrodes to avoid potential gradients along the electrolyte [121]. The pellet was weighed before and after electrode deposition to determine the mass of the electrodes. Some of the samples used for work function measurements were prepared by electron beam deposition technique by an external collaborator. The working and counter electrodes were calculated to have a geometric projected surface area, A, of approximately 0.88 cm^2.

1.10.3.   *Sodium deposition*

As mentioned earlier sodium is the foreign species added on the catalyst/electrode as impurities. Sodium solutions of various concentrations were prepared by dilution of 1.0 N standard sodium hydroxide (NaOH) solution provided by Alfa Aesar. Sodium was then gradually deposited dropwise in increasing concentration onto the platinum catalyst surface using a micropipette. The volume of the NaOH solution droplets deposited on the catalyst is indicated in Table 0.1 (either 1 or 5 μL). The pellet was heated in the reactor in air for an hour at 400°C before starting the experiments. Table 0.1 summarises the estimated sodium loading (in terms of Na atoms cm^{-2} of platinum surface) and the percentage coverage of sodium on the platinum surface.

For the calculation of the platinum surface area we have assumed a platinum particle size of approximately 0.5 μm (based on SEM analysis of Sample A). For a film mass of around 10 mg and assuming spherical geometry of the platinum particles we can calculate an estimated platinum surface area of 56 cm^2 (this surface area is only used for the coverage calculation; for the current densities discussed later a geometric projected surface area is used instead). It has been found in the literature that full coverage corresponds to approximately 10^{15} Na atoms cm^{-2} [122-123]. Based on this value we can calculate the coverage of sodium from the different sodium loadings. Note that this calculation may overestimate the sodium coverage as it assumes that all of the NaOH solution has been

deposited on the platinum (without a presence on the YSZ support). This explains why a coverage above 100% is obtained for some samples. The platinum surface area of samples prepared by the electron beam method could not be determined by a similar approximation because the mass of platinum in the samples was not available. Samples A-W shown in Table 0.1 correspond to 21 different pellets, 18 of which were impregnated with various NaOH solutions. Samples A-C were used for SEM-EDX analysis, D for surface titration and electrochemical measurement, E-M for XPS analysis, N-T for work function measurements, U were also used for electrochemical measurements, while V and W were used for kinetic experiments. Samples E-M and W were prepared from Heraeus paste with a platinum mass of 5 mg, resulting in the calculated surface area of 28 cm^2.

Throughout the thesis, these samples are named as follows: Sample name *xyy*, where $x*10^{-yy}$ M corresponds to NaOH concentration of the most recent sodium deposition (e.g. A101 for sample A modified with 10^{-1}M NaOH). Unless otherwise stated the sodium loadings reported in Table 0.1 are cumulative values. Sodium loading with less than 1% Na coverage will be defined as low coverage, between 1 and 50% as medium coverage, while more than 50% will be referred to as high coverage. These will also be interchangeably referred to as low-, medium- or high-sodium modified samples respectively. It is important to note that the surface species of coverage higher than 10% must not be treated as impurities as such coverages would be expected to have very pronounced effects even on the nature of the catalyst. It is however, important for our work to study a wide range of sodium surface coverage in order to obtain a more complete picture of the role of sodium in the catalytic and electropromoted behaviour of the catalyst.

Table 0.1. Sodium loading and percentage of sodium coverage

Sample†	Volume NaOH mL	NaOH concentration M	Na atom	Na/Pt surface area atom cm^{-2}	% Na coverage
A000	\('clean' sample (painted, Metalor)				
B502	1.00 ± 0.25	5×10^{-02}	3.0×10^{16}‡	5.4×10^{14}	54
C101		1×10^{-01}	6.0×10^{16}‡	1.1×10^{15}	110
D000	'clean' sample (painted, Metalor)				
D112	5.00 ± 0.25	1×10^{-12}	3.0×10^{06}	5.4×10^{04}	5.4×10^{-09}
D108		1×10^{-08}	3.0×10^{10}	5.4×10^{08}	5.4×10^{-05}
D104		1×10^{-04}	3.0×10^{14}	5.4×10^{12}	0.54
D102		1×10^{-02}	3.0×10^{16}	5.4×10^{14}	54
D101		1×10^{-01}	3.3×10^{17}	5.9×10^{15}	590
E000	'clean' sample (painted, Heareus)				
F112	1.00 ± 0.25	1×10^{-12}	6.0×10^{05}‡	2.2×10^{04}	2.2×10^{-09}
G108		1×10^{-08}	6.0×10^{09}‡	2.2×10^{08}	2.2×10^{-05}
H104		1×10^{-04}	6.0×10^{13}‡	2.2×10^{12}	0.22
J103		1×10^{-03}	6.0×10^{14}‡	2.2×10^{13}	2.2
K102		1×10^{-02}	6.0×10^{15}‡	2.2×10^{14}	22
L502		5×10^{-02}	3.0×10^{16}‡	1.1×10^{15}	110
M101		1×10^{-01}	6.0×10^{16}‡	2.2×10^{15}	220
N000	'clean' sample (painted, Metalor)				
N104	5.00 ± 0.25	1×10^{-04}	3.0×10^{14}	5.4×10^{12}	0.54
N102		1×10^{-02}	3.0×10^{16}	5.4×10^{14}	54
P000	'clean' sample (painted, Metalor)				
Q104	5.00 ± 0.25	1×10^{-04}	3.0×10^{14}‡	5.4×10^{12}	0.54
R102		1×10^{-02}	3.0×10^{16}‡	5.4×10^{14}	54
S000	'clean' sample (ELD)				
S104	5.00 ± 0.25	1×10^{-04}	3.0×10^{14}	N/A	N/A
T000	'clean' sample (ELD)				
T102		1×10^{-02}	3.0×10^{16}	N/A	N/A
U000	'clean' sample (painted, Metalor)				
U504	1.00 ± 0.25	5×10^{-04}	3.0×10^{14}	5.4×10^{12}	0.54
U103		1×10^{-03}	9.0×10^{14}	1.6×10^{13}	1.6
U503		5×10^{-03}	3.0×10^{15}	6.5×10^{13}	6.5
U102		1×10^{-02}	9.0×10^{15}	1.6×10^{14}	16
U502		5×10^{-02}	3.6×10^{16}	6.5×10^{14}	65
U101		1×10^{-01}	9.0×10^{16}	1.6×10^{15}	160
V000	'clean' sample (painted, Metalor)				
V104	1.00 ± 0.25	1×10^{-04}	6.0×10^{13}	1.1×10^{12}	0.11
V102		1×10^{-02}	6.1×10^{15}	1.1×10^{14}	11
V502		5×10^{-02}	3.6×10^{16}	6.5×10^{14}	65
W000	'clean' sample (painted, Heareus)				
W502	1.00 ± 0.25	5×10^{-02}	3.0×10^{16}	1.1×10^{15}	110
W101		1×10^{-01}	9.0×10^{16}	3.2×10^{15}	320

†Sample xyy; NaOH concentration of recent deposition = $x*10^{-yy}$ M
‡Not cumulative

1.10.4. *Gases*

In this research the reaction gases used were either provided by BOC or Scientific and Technical Gases (ST Gas). Details of the gases used are shown in Table 0.2. The gases are diluted using helium to obtain desired concentrations.

Table 0.2. Gases used, the provider companies and the corresponding experiments

Reaction gases	Provider company	Experiments
20% O_2/He	BOC	Cyclic and linear sweep voltammetry, Surafce oxygen titration, All kinetic experiments
10% C_2H_4/He	BOC	Surafce oxygen titration, Kinetic experiements (C_2H_4 oxidation)
3000 ppm NO/He	ST Gas	Kinetic experiements (NO reduction by C_3H_6) Gas analyser calibration
3000 ppm C_3H_6/He	ST Gas	Kinetic experiements (NO reduction by C_3H_6)
1.5% C_3H_6/He	BOC	Kinetic experiements (NO reduction by C_3H_6)
CP Grade He (N5)	BOC	Gas dilution
1000 ppm N_2O/He	ST Gas	Gas analyser calibration
500 ppm NO_2/He	ST Gas	Gas analyser calibration
1% CO_2/He	ST Gas	Gas analyser calibration
2% O_2, 2% CO_2, 2% C_2H_4, balance in He	ST Gas	Mass spectrometer calibration
0.1% O_2, 0.1% C_3H_6, 0.1% CO_2, 0.1% N_2, 0.1% N_2O, balance in He	ST Gas	GC calibration

1.11. Experimental set-up

1.11.1. Electrochemical reactor

As mentioned in Chapter 2, two types of reactor are normally used for EPOC studies; one is the fuel cell type reactor where the catalyst-working electrode is exposed to the catalytic reactants and products but the counter and reference electrodes are in separate chamber and exposed to a reference gas such as air; while the other is the single chamber type reactor where all electrodes are exposed to the same reactant and product gases [2]. A single chamber reactor design was used in this research. The schematic and the actual picture of the single chamber electrochemical reactor are shown in Figure 0.2, while the cell configuration is as shown in Figure 0.3.
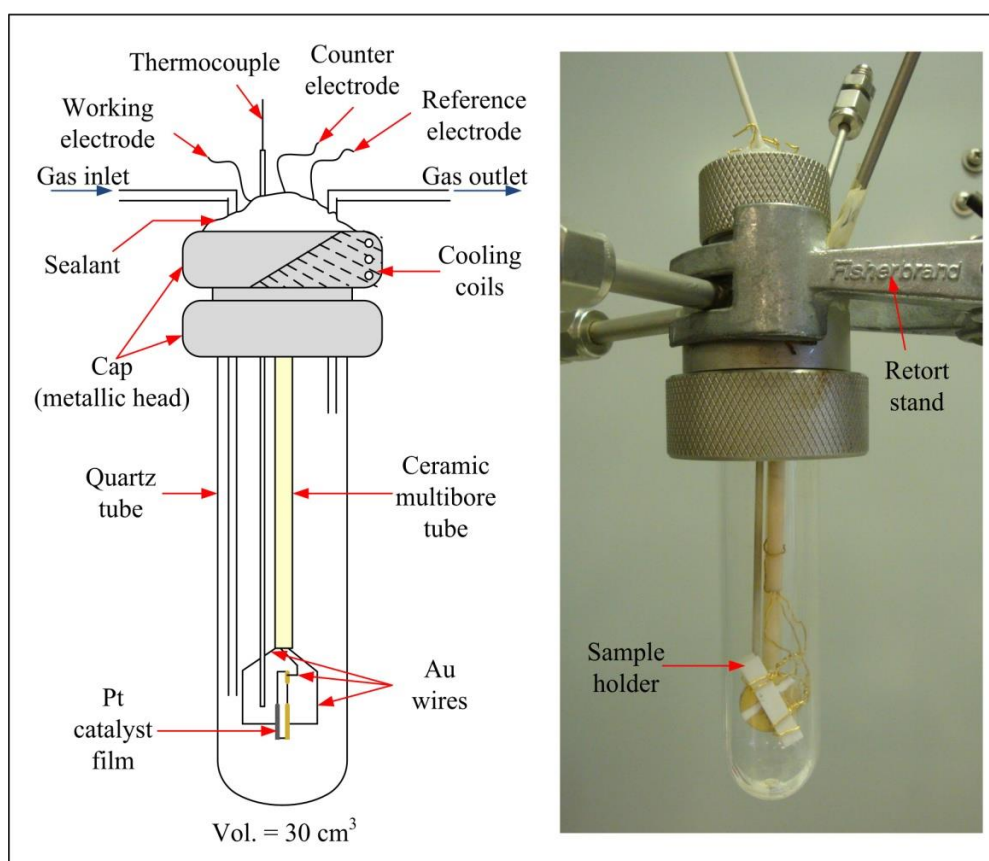
Figure 0.2. Schematic and actual picture of the single chamber electrochemical reactor
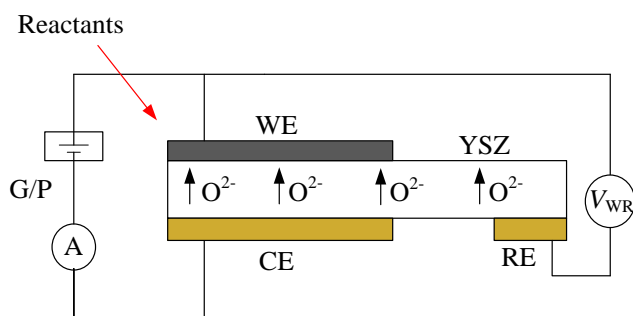
Figure 0.3. Cell configuration

The sample was mounted on a ceramic sample holder (Macor) and placed in an atmospheric pressure continuous flow quartz reactor of volume 30 cm^3. The reactor had a metallic cap on top and an O-ring was used in-between to secure from gas leak. This type of reactor has been shown to behave like a continuous-stirred tank reactor (CSTR) in the range of flow rate used, i.e. 100-200 ml (STP) min^{-1} [26]. The electrodes were connected to the Ivium potentiostat/galvanostat by gold wires (Alfa Aesar) that were kept separated using a ceramic multibore tube. Connection wires and thermocouple were inserted from the top, and sealed using a silicone sealant. The sealant at the top of the reactor was kept cooled by passing water through the cooling coils. The reactor was held in vertical position by a retort stand and placed into a Vecstar tube furnace. The operational temperature range was between 250-600°C. However, most electrochemical experiments were conducted at 350-400°C, because at this temperature, the activity of oxygen and platinum electrode deposited on YSZ is near maximum [2]. The actual temperature at the sample location was measured by SYSCAL KM330 hand held digital thermometer with a connecting K-type thermocouple. As shown in the cell configuration (Figure 0.3), the applied potential is measured against the RE, while the CE closes the electrical circuit for the current to flow. The experiments are performed by a potentiostat that effectively controls the voltage between the RE and WE, while measuring the current through the CE.

1.11.2. *Experimental rig*

A general schematic and the actual picture of the experimental rig are shown in Figure 0.4.
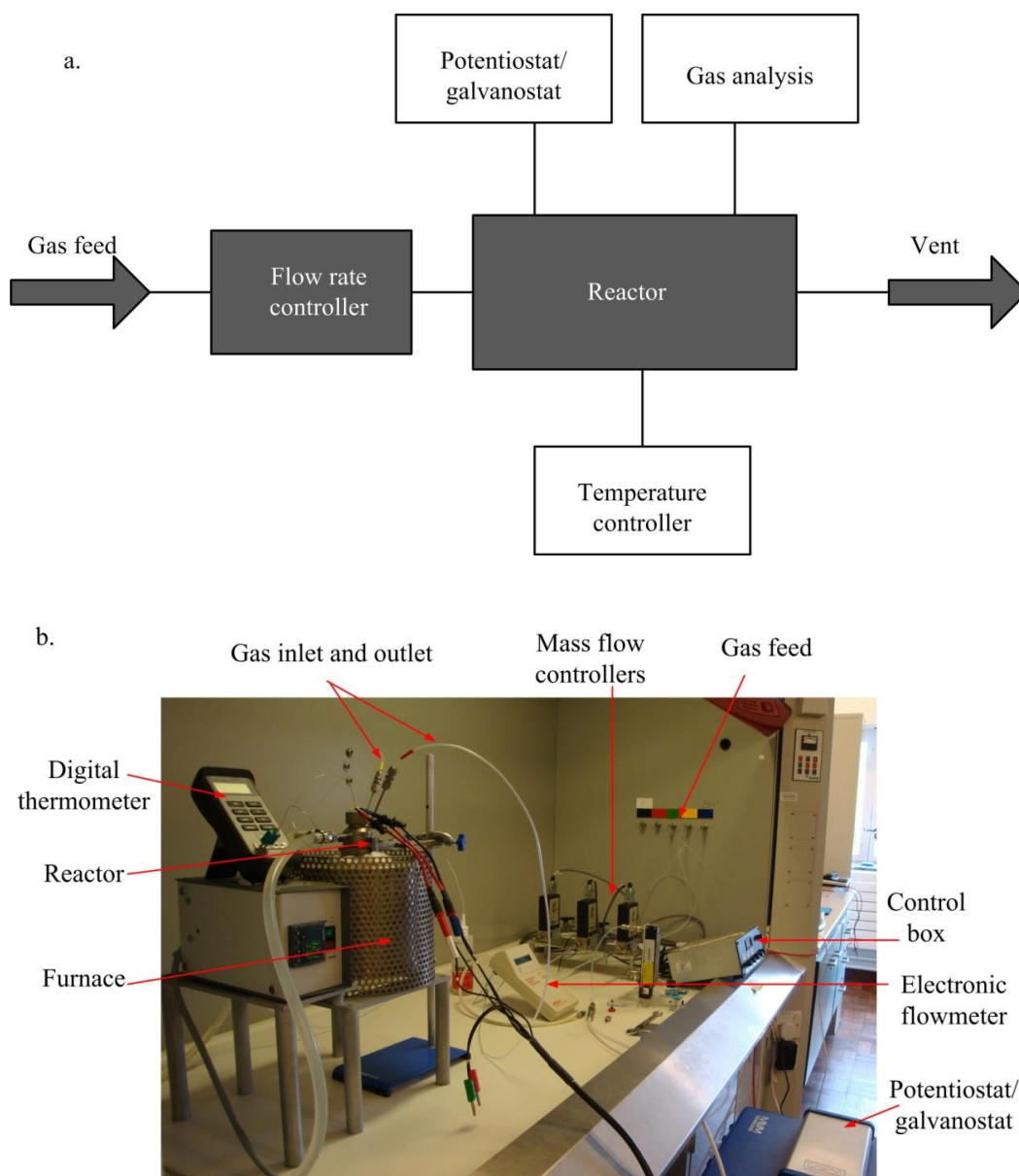
Figure 0.4. General experimental rig: (a) Schematic representation (b) Actual picture

The rig was constructed using stainless steel Swagelok compression fittings and Perfluoroalkoxy (PFA) tubing. The flow of gas to the electrochemical reactor was controlled by electronic mass flow controllers (MFCs) provided by Chell Hastings. Typical flowrate, f, was between 100-200 ml min^{-1} (at STP) and the flowrates were also measured at the outlet

using a Varian digital flow meter (1000 series). All experiments were conducted under atmospheric pressure. An Ivium Compactstat (potentiostat/galvanostat) was used for electrochemical measurement. The equipment for gas analysis is different for each experiment. This can be seen in Figure 0.5a-c that shows detailed experimental rigs for the study of oxygen charge transfer, ethylene oxidation and NO reduction by propene respectively. As can be seen in Figure 0.5a, the study of oxygen charge transfer involves mainly electrochemical experiments using a potentiostat, while ethylene oxidation and NO reduction by propene involves kinetic experiments as well. The gases were analysed using a BINOS 100 CO_2 analyser and an X-treme $NO-NO_2-N_2O$ analyser provided by Emerson (Figure 0.5b-c). The CO_2 analyser used a non-dispersive infra-red (IR) detector for CO_2 measurement, while the $NO-NO_2-N_2O$ analyser used both IR and ultraviolet (UV) detectors for measurements of NO (0 – 3000 ppm), N_2O (0 – 3000 ppm) and NO_2 (0 – 500 ppm). Pico dataloggers were used to record the analyser reading in voltage and report the data in percentage. As shown in Figure 0.5c, a CP3800 Varian gas chromatograph was used to intermittently monitor some of the reactant and product gases such as N_2O, N_2, O_2, C_3H_6 and CO_2.

a. Oxygen charge transfer experiments
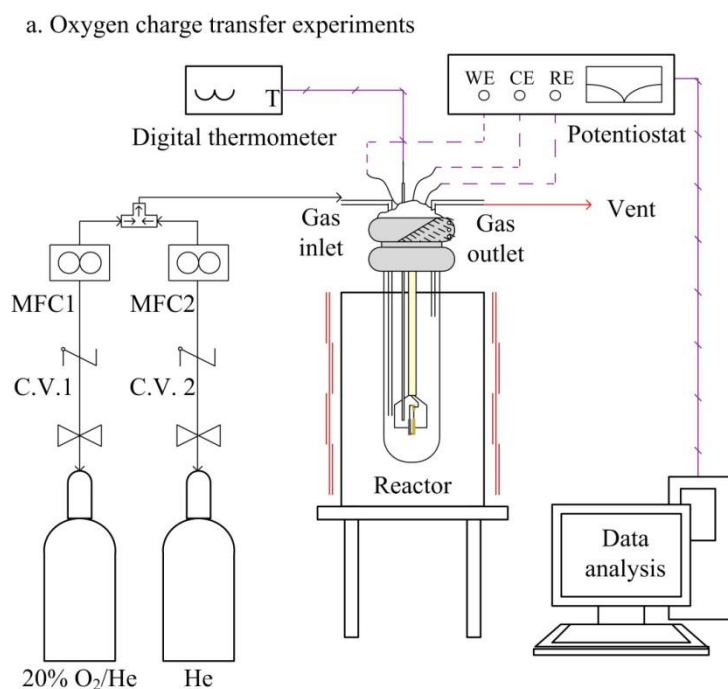
b. Ethylene oxidation experiments
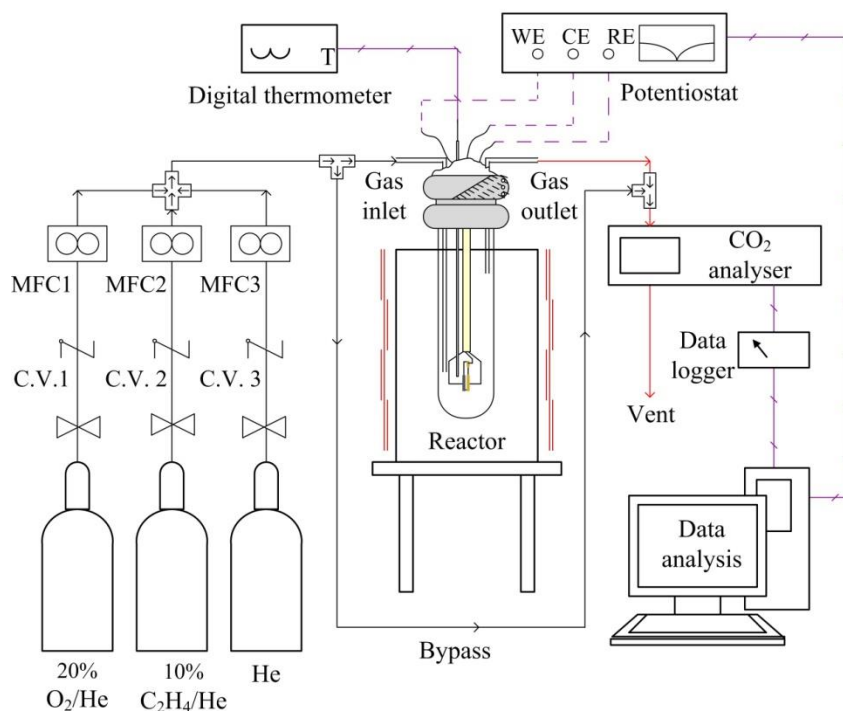
c. NO reduction by propene experiments
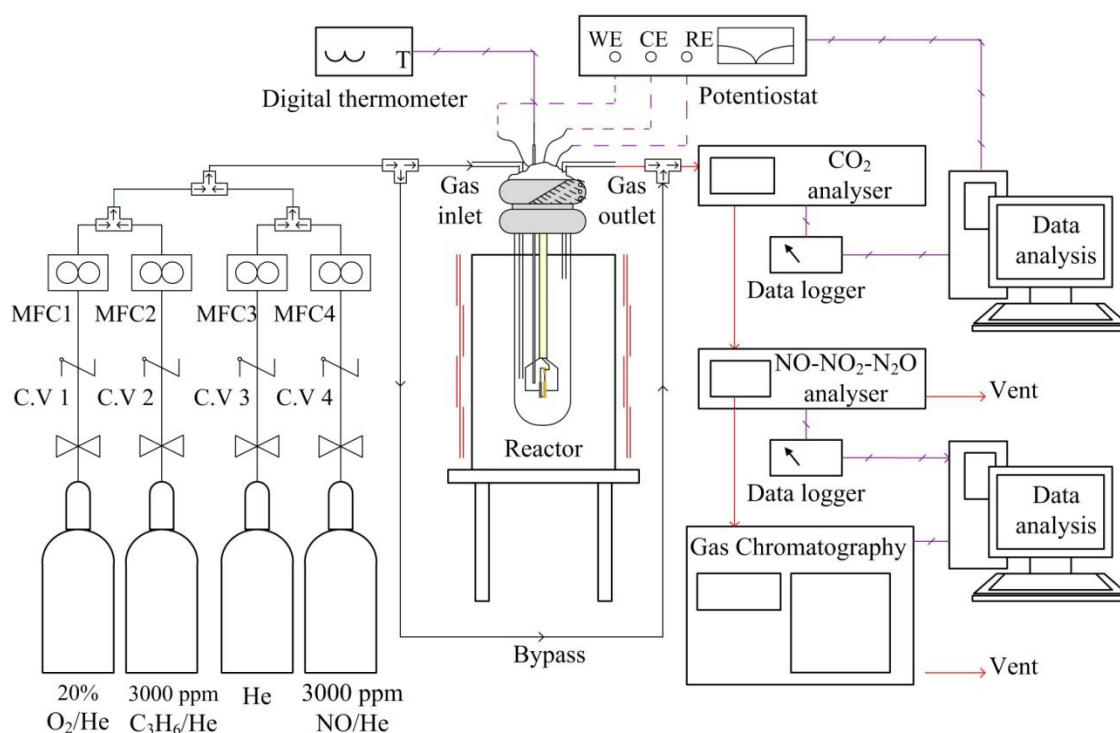
Figure 0.5. Detailed schematic of the experimental rig for (a) Oxygen charge transfer, (b) Ethylene oxidation and (c) NO reduction by propene experiments

1.12. Methodology

1.12.1. *Surface characterisation*

1.12.1.1. SEM-EDX

A scanning electron microscope consists essentially of a source of electrons, lenses for focusing them to a fine beam, facilities for sweeping the beam in a raster, arrangements for detecting electrons signals emitted by the specimen and an image-display system [124]. The SEM uses a focused beam of high-energy electrons to generate a variety of signals at the surface of solid specimens as shown in Figure 0.6. These signals include secondary electrons (that produce SEM images), backscattered electrons (BSE), diffracted backscattered electrons (EBSD that are used to determine crystal structures and orientations of minerals), photons (characteristic X-rays that are used for elemental analysis and continuum X-rays), visible light (cathodoluminescence - CL) and heat.

In this research, an environmental scanning electron microscope-field emission gun (FEI XL30 ESEM-FEG) was used. This instrument is different from conventional SEM as it allows specimens to be examined at conventional high vacuum mode or at relatively high chamber pressure environment. It offers high resolution secondary electron imaging at pressures as high as 10 Torr and sample temperatures as high as 1000°C. Using ESEM wet, oily, dirty, outgassing and non-conductive samples can be examined in their natural state without significant sample modification or preparation. The ESEM-FEG employed a stable, high brightness Schottky field emission source that allows high resolution/magnification and excellent signal to noise ratio in both regular high vacuum and environmental (wet) mode. This equipment is also fitted with EDX light element analysers to detect and quantify elements from beryllium upwards.
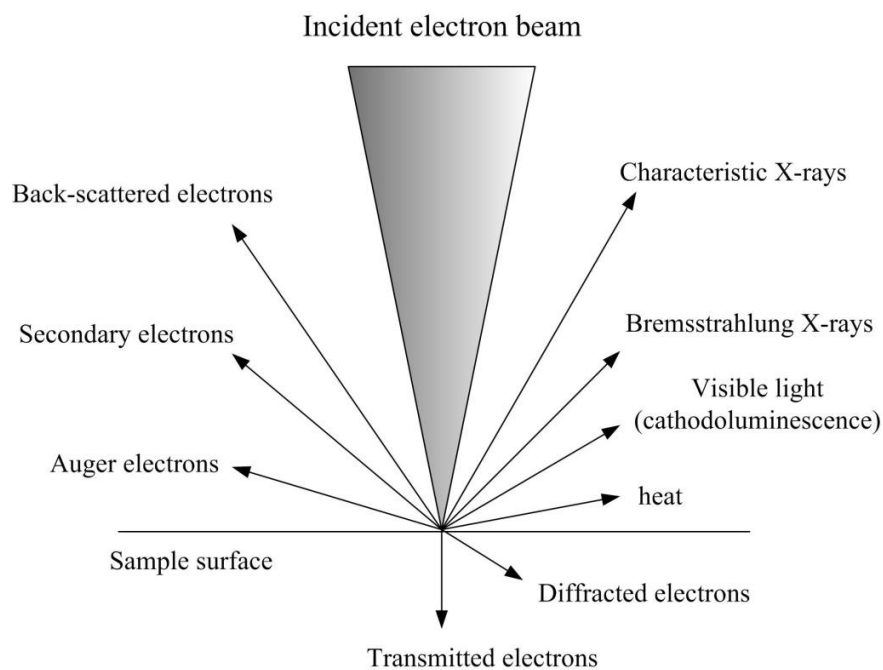
Figure 0.6. A variety of electrons (auger, secondary and back-scattered), X-rays (characteristic and Bremsstrahlung), light (cathodoluminescence) and heat (phonons) are emitted depending on the incident energy of the electron beam [125].

The measurement was conducted on both fresh and used platinum samples under high vacuum mode and at 20 kV without any pre-treatment. The fresh samples include one of the nominally 'clean' samples and one of the sodium-modified samples (with similar sodium coverage to the used sample). The elemental analysis was done using microanalysis (EDX) system by Rontec and Quantac software. It is important to note that the EDX measures elements present to a depth of several micrometers into the sample surface. Therefore, the results of EDX are not used to quantify the elemental constituents on the platinum surface, rather for simple identification and distribution mapping of significant elements such as platinum and sodium.

1.12.1.2. Surface titration

The active surface area of the catalyst film can be measured *in-situ* by means of isothermal surface titration method. The method has been used in many EPOC studies to determine the

active surface area of a catalyst [26, 37, 41]. The set-up of experiment is as shown in Figure 0.7. Throughout the entire procedure, the catalyst was maintained at a fixed temperature ($T = 400^{\circ}C$), so that the equilibrium oxygen coverage is near saturation and the reaction of chemisorbed O with ethylene is fast [2]. Prior to the surface titration, helium gas was flushed into the reactor for about 20 minutes. The platinum catalyst was then pre-saturated with oxygen at 20 kPa at a flow rate of 150 ml min^{-1} for a period of five minutes, assuming every active site of the platinum catalyst film was fully occupied on a one to one O:Pt ratio. An oxygen desorption step followed by exposing the catalyst to a helium stream at different desorption times (t_{He}) of at least eight times longer than the residence time of the reactor (V/f_v, where V is the volume of the reactor and f_v is the volumetric flow rate) [41]. The remaining adsorbed oxygen was then reacted with a reducing gas, e.g. ethylene, to produce CO_2. The product CO_2 area was recorded using a mass spectrometer. By integrating the CO_2 peak area, the amount N_O of O adsorbed on surface after desorption time t_{He} can be determined. One mole of carbon dioxide produced equals to three oxygen atoms consumed based on the reaction $C_2H_4 + 6O \rightarrow 2CO_2 + 2H_2O$. Assuming a first order process in oxygen for the ethylene oxidation, we can plot a natural logarithm of the calculated number of O moles consumed during the reduction step versus t_{He}. The exponential of the zero t_{He} intercept gives us the maximum number of oxygen adsorbed on the catalyst, N_O, which is equals to the active surface area of the platinum catalyst, N_G (mol Pt). The surface area in cm^2 can be calculated by

$$N_G = N_{Pt} * N_{AV} * A_{Pt\ atom} \tag{3.1}$$

where N_{AV} is the Avogadro number (6.023 x 10^{23} atoms mol^{-1}) and $A_{Pt\ atom}$ is the area (πr^2) occupied by one platinum atom with a radius, r, of 1.35 Å.
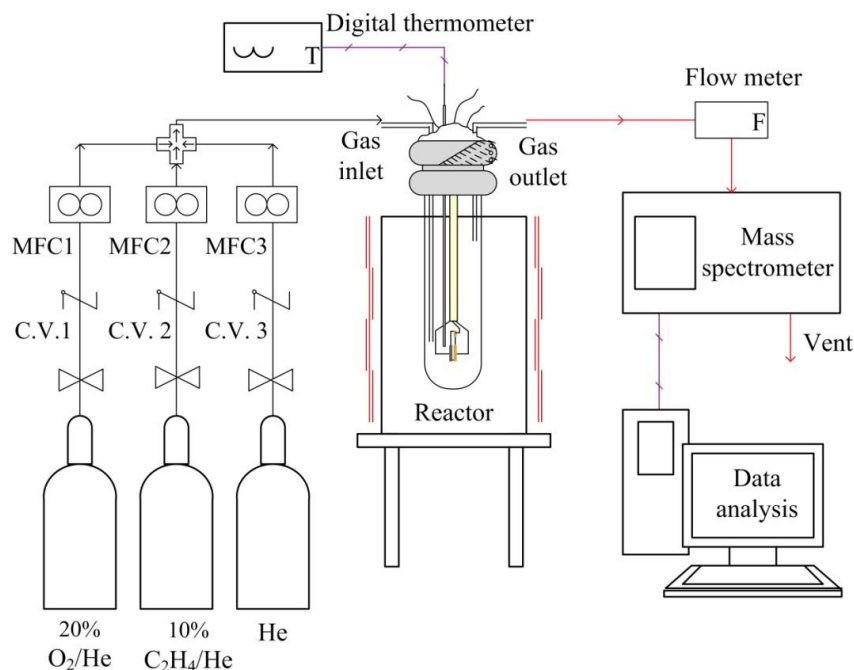
Figure 0.7. Experimental set-up for oxygen surface titration

1.12.1.3. XPS

An X-ray photoelectron spectroscopy consists of a source of primary radiation (soft X-rays, generally Al Kα or Mg Kα) and an electron energy analyser all contained within a vacuum chamber preferably operating in the ultra-high vacuum (UHV) regime [126]. The XPS concerns with the ejection of an electron from a core level by an X-ray photon of energy hv. The energy of the emitted photoelectrons is then analysed by the electron spectrometer and the data presented as a graph of intensity (usually expressed as counts or counts per second) versus electron energy - the X-ray induced photoelectron spectrum. The kinetic energy, KE, of the electron is measured by the spectrometer depending on the photon energy of the X-rays employed. The binding energy of the electron, BE, is the parameter which identifies the electron specifically, both in terms of its element and atomic energy level. The relationship between the parameters involved in the XPS experiment is:

$$BE = hv - KE - W \qquad (3.2)$$

where *hv* is the photon energy, KE is the kinetic energy of the electron, and W is the spectrometer work function. The process of photoemission is shown schematically in Figure 0.8, where an electron from the K shell is ejected from the atom (a 1s photoelectron). The photoelectron spectrum will reproduce the electronic structure of an element quite accurately since all electrons with a binding energy less than the photon energy will feature in the spectrum.
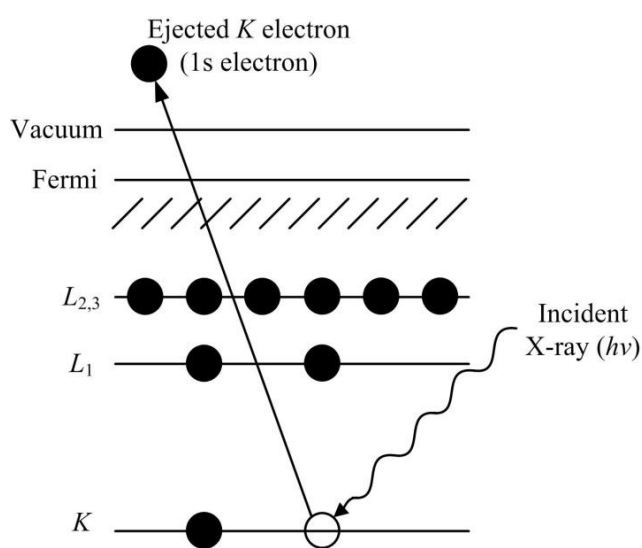
Figure 0.8. Schematic diagram of the XPS process showing the photionisation of an atom by the ejection of a 1s electron

The samples (E000-M101) used for the XPS measurements in this research were eight fresh platinum films made from Heraeus platinum paste and supported on YSZ solid electrolyte, seven of which were impregnated with variable concentration of NaOH solutions (ranging from 10^{-12} to 10^{-1} M). The calculated sodium coverages can be found in Table 0.1. After sodium impregnation the catalysts were dried in air for an hour at 400°C in similar manner to the samples used for kinetic studies. The XPS measurements were performed using a Thermo K-Alpha electron spectrometer with a monochromated Al Kα X-ray source (1486.6 eV, 1 eV = 1.6302×10^{-19} J) with a spot size of approximately 400 μm on the sample surface. The instrument has a hemi-spherical electron energy analyser; survey spectra were

taken at a pass energy of 200 eV and narrowscan spectra around the principal peaks of the elements present (e.g. C, O, Na and Pt) with a pass energy of 50 eV. The narrowscan spectra were taken from four points in a line for each of the 8 samples. These points on each line were about 2.5 mm apart as shown in Figure 0.9. For each line scan, the first three points were on the platinum film, and the last point was on the YSZ region. The base pressure in the analysis chamber was kept below 1×10^{-8} mbar during data acquisition. The pass energy of the analyser was set at 50 eV for the narrowscans, for which the resolution as measured by the full width at half maximum (FWHM) of the Ag $3d_{5/2}$ peak was 0.85 eV. The binding energies were referenced to Au using the manufacturer's automatic calibration software.
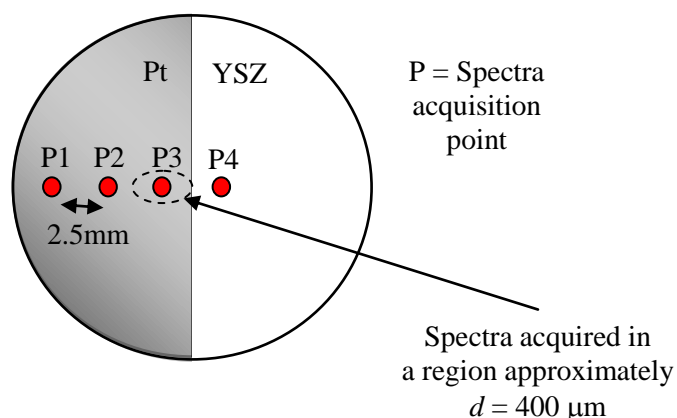
Figure 0.9. Schematic of the four acquisition points on each sample during XPS measurements.

1.12.1.4. Kelvin probe

Kelvin Probe is a non-contact and non-destructive vibrating capacitor device used to measure the work function of conducting materials or surface potential of semiconductor or insulating surfaces [127]. The technique measures the contact potential difference (CPD) between two surfaces brought in close proximity. Their Fermi levels align at the vacuum level at energies corresponding to the respective work functions. If the two metals are connected by a wire, electrons flow from the metal with the smaller work function to the

metal with the larger work function, causing the smaller work function metal to charge positively while the other charges negatively. The electron transfer process stops once the electric field between them compensates for the work function difference. In this equilibrated state, the potential associated with the electric field exactly equals the work function difference, i.e. the CPD, between the metals. Since this technique only measures the CPD, the work function measurement is only possible by calibration with a surface of known work function [128].

In this research, the work function measurements were conducted using a scanning Kelvin probe (SKP5050) located in a light-tight chamber (LE450) and illuminated by an automatic surface photovoltage light source (SPV020) provided by KP Technology Ltd. shown in Figure 0.10 and Figure 0.11a-b.
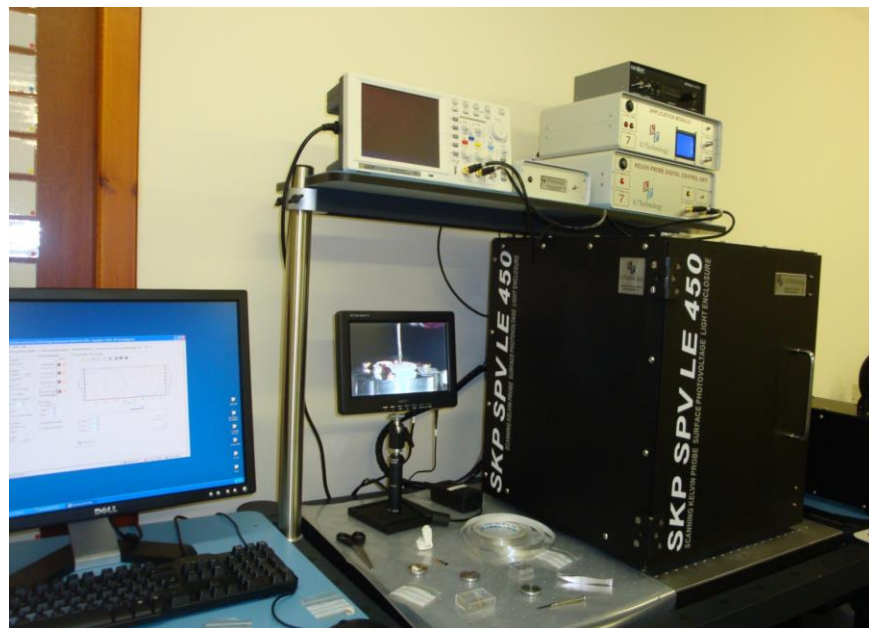
Figure 0.10. Work function measurement set-up. Kelvin probe is located in the black chamber.
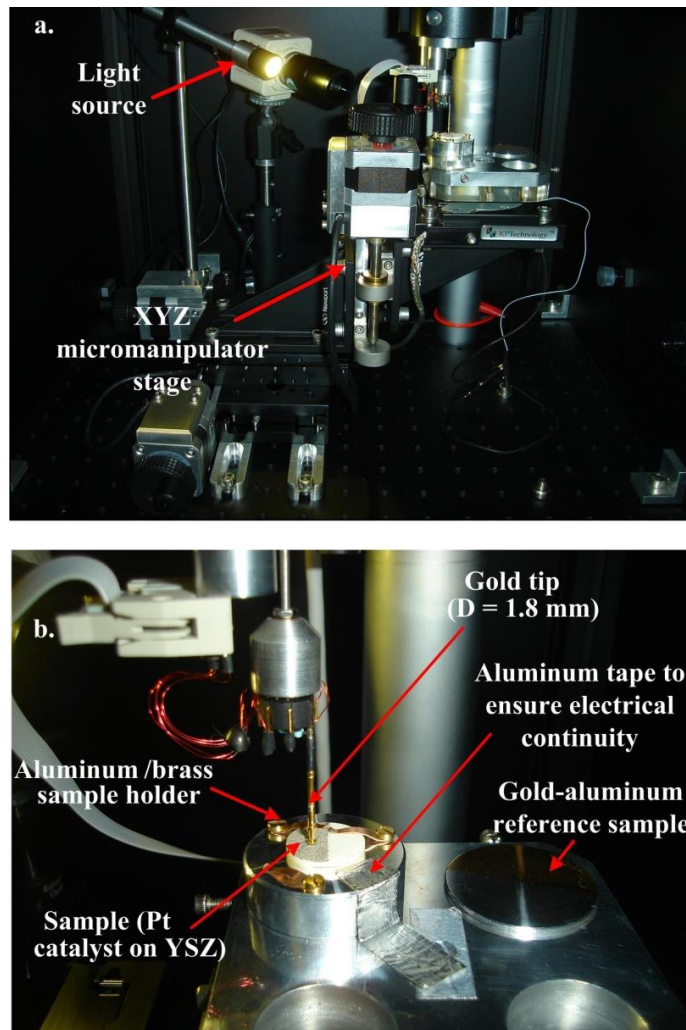
Figure 0.11. Kelvin Probe (SKP5050) in a light-tight chamber (LE450) (a); and a close-up of the sample and Au-Al reference on sample platform (b)

In the close-up of the Kelvin Probe in Figure 0.11b, we can see that the SKP has a 1.8 mm diameter gold-coated tip that vibrates just above the sample surface. The SKP works by producing the CPD between the vibrating tip and the sample surface. The mean spacing is computer-controlled and held constant during the measurement to avoid changes of parasitic capacity. The work function of the platinum catalyst is calibrated against a gold reference sample with known work function. The actual work function values are calculated with respect to the literature values of gold measured in vacuum using the photoelectric effect [129] as follows:

$$\Phi_{Au(lit.)} = 5.1 \text{ eV (PE)} \qquad\qquad (3.3)$$

$$5.1 - CPD_{tip\text{-}Au(ref.)} = \Phi_{tip} \qquad\qquad (3.4)$$

$$\Phi_{tip} + CPD_{tip\text{-}sample} = \Phi_{sample} \qquad\qquad (3.5)$$

It has been found, by the photoelectric effect, that metallic sodium has a work function of 2.1 eV while the work function of metallic platinum is 5.64 eV [129]. The work function of platinum interfaced with YSZ has been found to be around 5.14 eV [84]. It is anticipated that the addition of sodium on the platinum surface will lower the work function of the surface; the work function of a sodium-modified sample should lie between the values of 2.1 and 5.14 eV (possibly a lot closer to the value of the platinum surface). The actual work function change will depend upon the sodium coverage and the state of sodium species on the platinum surface (i.e. metallic, oxide, hydroxide or carbonate form) as well as the state of the platinum (metallic or oxide).

The work function measurements of the 'clean' platinum surface were conducted on four samples; two of the samples (N000, P000) were prepared by painting of a platinum resinate while the other two (S000 and T000) were prepared using electron beam deposition method. Three types of sodium-modified samples were tested. Sample N000 (platinum-painted) was impregnated with consecutive drops of NaOH solutions of 10^{-4} (N104, 0.54% Na coverage) and 10^{-2} M (N102, 54% coverage), and measurements were conducted after each impregnation. In addition, two independent platinum-painted samples, each modified with NaOH solutions of 10^{-4} (Q104, 0.54% coverage) and 10^{-2} M (R102, 54% coverage) were used for comparison. The two electron beam-prepared samples (S000 and T000) were also impregnated with NaOH solutions of 10^{-4} (S104) and 10^{-2} M (T102) and measurements were performed on each sample after each impregnation. The method of sodium deposition for all samples is as described in the catalyst preparation section (Section 3.2.3), except for

Samples N104, N102, S104 and T102 which were heated in air at a lower temperature of about 200°C for 20 minutes. For each sample, fifty data points were collected and averaged.

1.12.2. Cyclic and linear sweep voltammetry

Cyclic and linear sweep voltammetry techniques were mainly used to investigate the electrochemical behaviour of the Pt/YSZ system. These electrochemical techniques, especially cyclic voltammetry has high sensitivity towards (sub)monolayer(s) product formation and decomposition on an electrode/electrolyte interface. In a linear or cyclic voltammetry experiments, the working electrode (catalyst) potential is ramped linearly versus time and the current response at the working electrode is plotted against the potential applied to produce a voltammogram as shown in Figure 0.12a-d. As shown in the figure, the potential is first swept in a linear manner towards more reducing potential, and once it reaches the potential capable of inducing a reduction process of an electroactive species, current starts to flow and first peaks at E_{pc} (with i_{pc}) indicating a reduction is taking place. The current then drops due to depletion of the oxidising species on the electrode surface. In a cyclic voltammetry experiment, this is followed by a second peak at E_{pa} (with i_{pa}) when the process is reversed during a return scan (oxidation is occurring). The characteristics of the current depend on a number of factors including the rate of the electron transfer between metal and the electroactive species, the transport of material to and from the electrode surface, the chemical reactivity of the electroactive species as well as the voltage scan rate. The peak current or peak height, i_p, reflects the balance between an increase in the reduction or oxidation rate constant and a decrease in the surface concentration of an electroactive species [33]. The current-voltage curve preceding the i_p is determined by the electrode kinetics, while the part following the i_p reflects the rate at which the electroactive species diffuses to the electrode surface to replenish the decrease in the surface concentration.
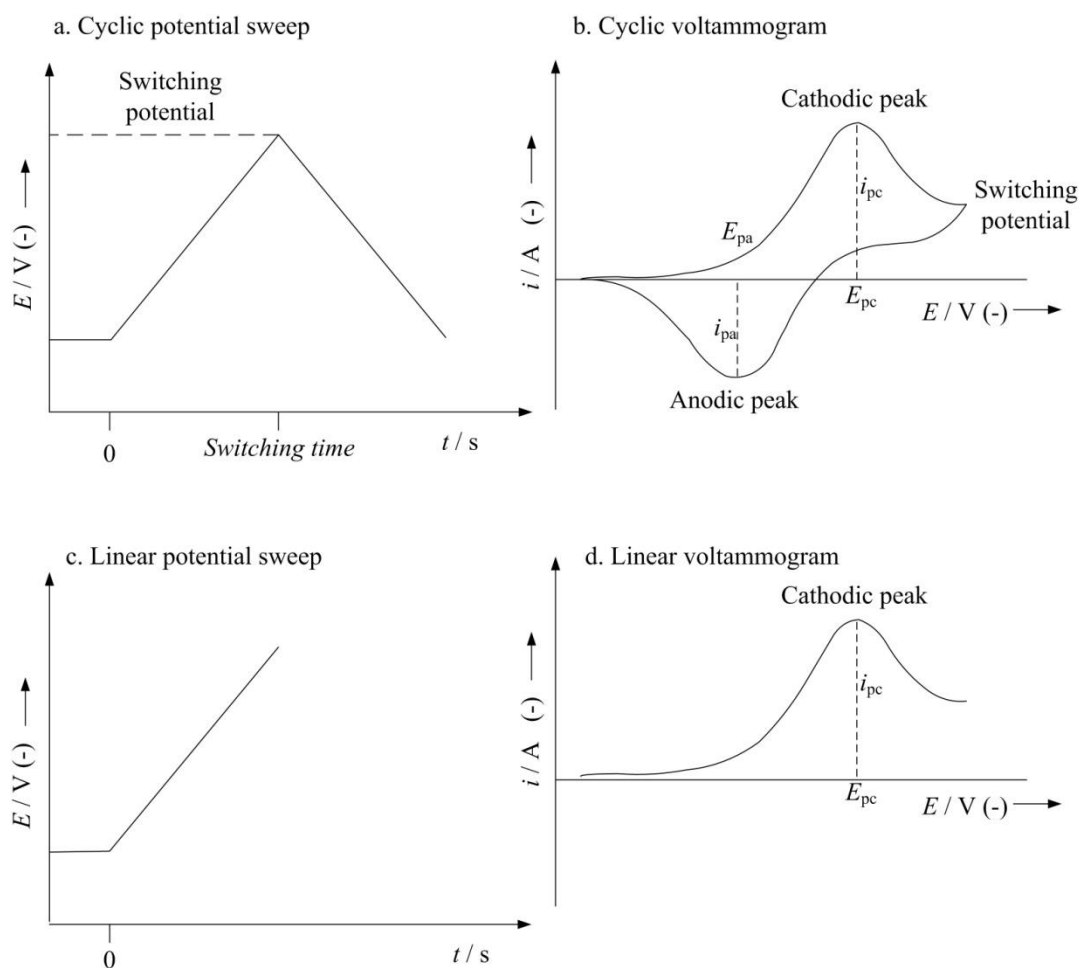
Figure 0.12. The potential sweep and the resulting voltammogram in the (a-b) cyclic voltammetry and (c-d) linear sweep voltammetry experiments.

In this research, the potential application and the current flowing between the catalyst (working electrode) and the counter electrode was respectively controlled and recorded using an Ivium Compactstat. The current density, i, (calculated based on the geometric projected surface area, $A = 0.88$ cm^2) was used to plot cyclic and linear sweep voltammograms against the potential between working and reference electrode, V_{WR}. All voltammograms shown in this chapter correspond to the third scan. The area under the cathodic peak, Q_{pc} (which corresponds to the charge transferred during this phase of oxygen reduction) was measured and integrated using graphing and data analysis software.

1.12.2.1. CV and LSV under non-reactive conditions

The experiments were conducted under 200 ml/min (STP) flow of 20 kPa O_2, at a temperature of 400°C. The scan rate was always fixed at 20 mV s^{-1} except when studying the effect of varying scan rates (where it was varied between 1 to 100 mV s^{-1}). For the purpose of studying the effect of reversal potential, E_r, on the system, the potential sweep was started from anodic potential ranged from 0.6-0.1 V to -0.8 V. In another study the anodic potential (+0.3 V) was held at different holding times, t_H, i.e. 5, 10, 20, 40, 100, 200, 300, 400, 600, 800 seconds before a linear sweep started. For the temperature study, CV experiments were conducted at different temperatures, i.e. 400, 450, 500, 550 and 600°C. In addition, steady state current-overpotential measurements were performed, where the system was polarised at different positive (+0.005 to +0.5 V) and negative potentials (-0.005 to -0.5 V) while the current was recorded at steady state conditions. This experiment was performed at 400, 500 and 600°C. All experiments were first conducted on a nominally 'clean' sample and subsequently on the sodium-modified samples after each sodium addition. As mentioned earlier (in Chapter 2), the uncompensated resistance between the working and reference electrodes results in a voltage (Ohmic) drop called the IR_u drop. The IR_u drop of approximately 0.9-2 mV was determined under 20 kPa oxygen at 350 and 400°C using a current-interrupt technique with an Ivium potentiostat/galvanostat. Since the IR_u value is small, it is not subtracted from the reported V_{WR}.

1.12.2.2. CV under reactive conditions

The NO reduction and ethylene oxidation experiments were performed on the same sample (Sample V). The NO reduction experiment was conducted after the latter took place following each sodium deposition. Under reactive conditions, the change in the reaction rates during CV experiments were also recorded using BINOS 100 CO_2 analyser and X-treme NO-NO_2-N_2O analyser. For ethylene oxidation, the CV experiment was conducted

under 200 ml/min (STP) flow of oxygen and ethylene mixture (oxygen partial pressure, p_{O_2} = 0.5 to 8 kPa and ethylene partial pressure, $p_{C_2H_4}$ = 0.5 kPa) at a temperature of 350°C. The scan rates, ν, were first set to be 5 mV s^{-1} for 'clean' (V000) and low-sodium modified samples (V104, 0.11% Na coverage). However, it appears that with increasing sodium coverage the reaction takes longer to respond to the change in the potential, so the scan rate was reduced to 2 mV s^{-1} for medium-sodium modified sample (V102, 11% Na coverage) and finally 1 mV s^{-1} for high-sodium modified sample (V502, 65% Na coverage).

For NO reduction by propene, the study was carried out under a flow of NO, oxygen and propene mixture (NO partial pressure, p_{NO} = 0.1 kPa, oxygen partial pressure, p_{O_2} = 0.5 to 5.0 kPa and propene partial pressure, $p_{C_3H_6}$ = 0.1 kPa) at a temperature of 350°C. The total gas flow rate in the experiments was set to be 100 ml min^{-1} (STP). The catalyst system was first subjected to different voltage scan rates, from ν = 5 to 100 mV s^{-1} under flow of 20 kPa oxygen to reproduce the result seen under non-reactive conditions. To obtain a reproducible CV, the catalyst was pre-treated under oxidising conditions with 30 ml min^{-1} flow of 20 kPa oxygen at 600°C for an hour. The experiments were also conducted separately under flow of single gas and reactive gas mixtures, where the scan rate was fixed at 20 mV s^{-1}. The feed composition of the gases consisted of either one of the following, and balanced with helium:

i. 0-5 kPa O_2

ii. 0.1 kPa NO

iii. 0.1 kPa C_3H_6

iv. 5 kPa O_2 and 0.1 kPa NO

v. 5 kPa O_2 and 0.1 kPa C_3H_6

vi. 0.1 kPa NO and 0.1 kPa C_3H_6

vii. 0.5 kPa O_2, 0.1 kPa NO and 0.1 kPa C_3H_6

viii. 1 kPa O_2, 0.1 kPa NO and 0.1 kPa C_3H_6

ix. 5 kPa O_2, 0.1 kPa NO and 0.1 kPa C_3H_6

To investigate the kinetics of NO reduction during the cyclic voltammetry experiments, lower scan rates were used; i.e. 5 mV s^{-1} for 'clean' sample (V000), 2 mV s^{-1} for low-sodium modified sample (V104, 0.11% Na coverage) and 1 mV s^{-1} for medium and high-sodium modified sample (V102, 11% and V502, 65% Na coverage respectively). The difference in the scan rates as mentioned earlier was due to the longer time needed for the sodium-modified system to achieve equilibrium on the surface. However, once the sodium coverage was increased, it was not possible to repeat any experiment for the 'clean' system or the system with lower sodium coverage.

1.12.3.   *Chronoamperometry*

The basis of chronoamperometry techniques is the measurement of the current response to an applied potential. In a potentiostatic transient EPOC experiment (chronoamperometric technique) as shown in Figure 0.13a-c, initially (at $t < 0$), current is zero, while the open circuit potential, E_o, and the unpromoted catalytic rate, r_o, can be recorded. At $t = 0$, the potentiostat is used to apply a controlled potential, E_1, between the catalyst-working electrode and the reference electrode. The potentiostat always fixes the current between the working and counter electrode so that the potential applied between the catalyst-working electrode and the reference electrode can be maintained at a desired value [2]. The current response and the change in the catalytic rate (to a promoted rate, r_1) can also be recorded. After a steady state is reached, the potential application is stopped, and the current is gradually discharged. The catalytic rate and electrode potential return to their initial unpromoted values.
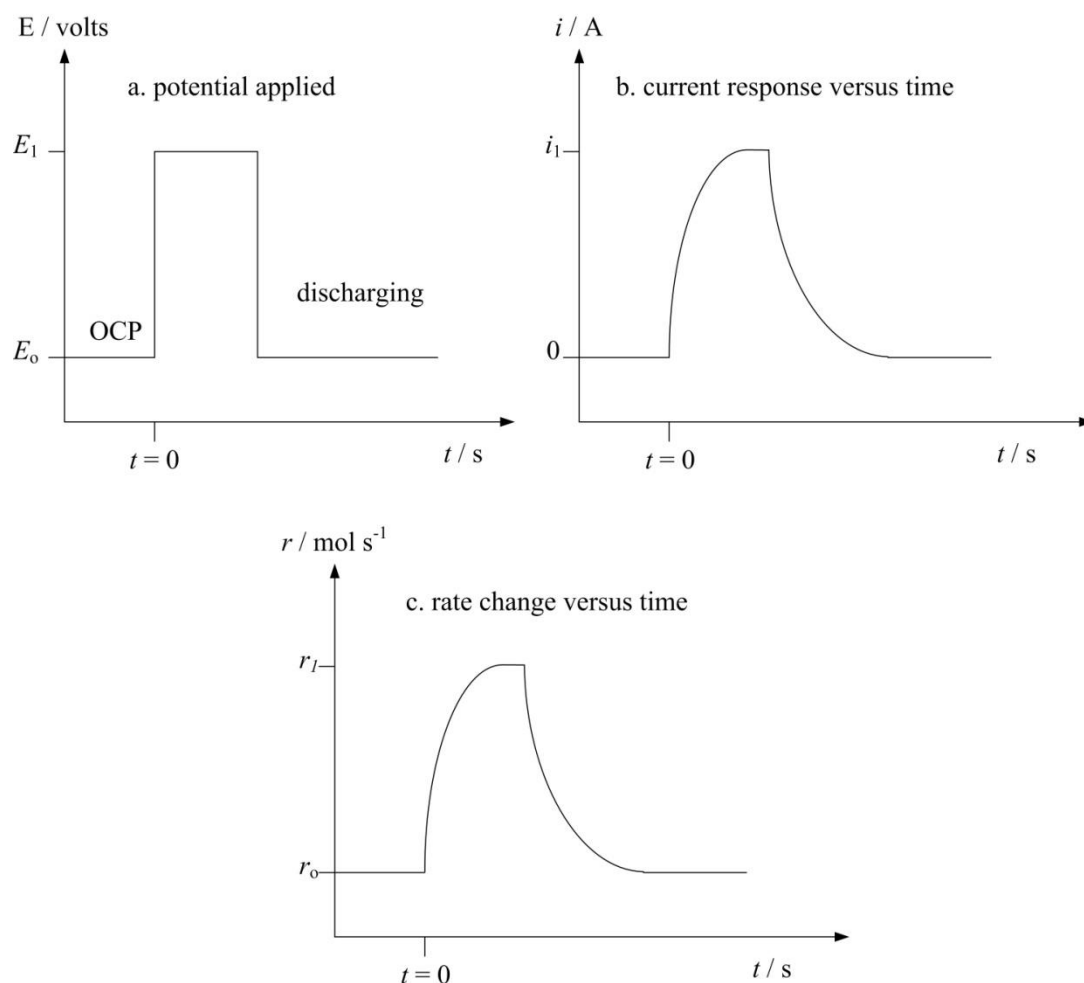
Figure 0.13. The chronoamperometric (potentiostatic transient) EPOC experiment: (a) Controlled-potential application, (b) current response and (c) change in the catalytic rate versus time in a potentiostatic transient EPOC experiment.

The transient experiments were conducted on the same sample (Sample V) used for cyclic voltammetry experiments under similar gas compositions and flow rates (for ethylene oxidation, $p_{O_2} = 0.5\text{-}8.0$ kPa, $p_{C_2H_4} = 0.5$ kPa and $f = 200$ ml min^{-1}, while for NO reduction, $p_{NO} = 0.1$ kPa, $p_{O_2} = 0.5\text{-}5.0$ kPa, $p_{C_3H_6} = 0.1$ kPa and $f = 200$ ml min^{-1}). During the transient experiments, once stable, the reaction rate was monitored for five minutes prior to polarisation (initial open-circuit rate), seven minutes during polarisation and approximately fifteen minutes after polarisation (in some cases the final open circuit step is longer as the return to the initial open circuit rate can be slower depending on the experimental conditions). For a temperature study, a different sample (Sample W) prepared from a

different platinum precursor (Heraeus) was used. This sample was first deposited with 1 μL of deionised water (which then appeared to show similar catalytic and electrocatalytic activity with the 'clean' sample), followed by 5×10^{-2} M NaOH and 0.1 M NaOH solutions (i.e. higher sodium concentration range) using the same sodium deposition method described in Chapter 3. The temperature was ramped from 250 to 525°C at 0.5°C min^{-1} while the NO, NO$_2$, N$_2$O and CO$_2$ concentrations (partial pressures) was recorded every minute. In the result section, the overpotential symbol, η, is used to indicate the constant potential applied during a potentiostatic transient experiment instead of V_{WR} (used for cyclic voltammetry) to differentiate the fact that the current is applied with respect to the open-circuit potential, OCP.

1.13. Reproducibility

This section concerns about the reproducibility of our main experiments, i.e. cyclic voltammetry and chronoamperometric (potentiostatic transient) EPOC experiments. In our initial studies, we have always used fresh samples to study the effect of variable coverage sodium on the Pt/YSZ system. We found from the cyclic voltammetry studies that sample preparation can significantly affect the voltammogram features under 20 kPa of oxygen flow. Therefore, we decided to use one sample for each set of experiments, and gradually add sodium in increasing concentration after each set of experiments was completed. For the cyclic voltammetry experiments under flow of 20 kPa oxygen we have studied four different samples. Although the coverage of sodium was not always the same for each sample (due to the difference in the amount of platinum or concentration of sodium hydroxide solution), it was found that the voltammogram features from the different samples show similar trends with respect to sodium coverage. For kinetic experiments of ethylene oxidation and NO reduction using chronoamperometric (transient) technique only one sample was studied with a complete set of experiments. On the same sample, the catalyst polarisations at V_{WR} = +1 and -1 V were repeated twice and similar behaviour were observed for the same potential

application. A second kinetic experiment of NO reduction was also carried out on a platinum sample prepared from a different platinum precursor (not shown in the thesis) at higher range of sodium concentrations, thus some differences in the magnitude of the catalytic activity and promotion were noted. The carbon balance for both ethylene oxidation and NO reduction experiments was found to be within 5%, while the nitrogen balance calculated using data from both NO-NO_2-N_2O analyser and GC (N_2) was within $2 - 20\%$ as the N_2 data is close to the GC detection limit. However, the N_2 production rates reported in Chapter 8 are calculated from N balance (NO_2, NO, N_2 and N_2O) instead of N_2 measured by the GC. An example for material balance calculation is shown in Appendix B.

Surface characterisation

1.14. Introduction

Surface characterisation of a catalyst and its support is very important for this is where a catalyzed reaction takes place. In this research several characterisation techniques were used. Scanning electron microscopy in combination with energy-dispersive X-ray microscopy (SEM-EDX) was used for high magnification imaging and elemental distribution mapping or area averaged/spot analysis. The use of EDX due to its low detection limit did not allow the quantification of the chemical constituents on the catalyst surface. This was done by using X-ray photoelectron spectroscopy (XPS). The XPS technique also allowed the determination of the chemical state of the elements that are present on the catalyst and solid electrolyte surface. The true surface area of the catalyst is too low to be accurately measured by using a BET technique, so an isothermal surface titration technique was used instead. In addition, a Kelvin probe was used for work function measurements. The Kelvin probe measures the change in the surface potential between a catalyst and a vibrating probe. This chapter discusses the results obtained from the surface characterisation experiments.

1.15. Results

1.15.1. SEM-EDX

The SEM images shown in Figure 0.1 are 1000x (left) and 10000x magnifications (right) of (a) fresh nominally 'clean' sample (A000), (b) fresh sodium-modified sample (B502, 54% Na coverage) and (c) used sodium-modified sample (V502, 65% Na coverage). Figure 0.1a shows that the platinum film consists of an irregular porous network. The platinum particle size is around 0.5 μm. Sodium deposition appears to have slightly blocked the pores in some part of the fresh platinum film as shown in Figure 0.1b. However, in some areas and in

different samples that are not shown, the structure of the platinum film does not appear to be significantly affected by sodium deposition. The used sample in Figure 0.1c shows a slight roughening on the film surface possibly due to a sintering effect. The used sample has been used in many experiments including cyclic voltammetry and kinetic experiments of ethylene oxidation and NO reduction by propene. The sample had also been exposed at temperatures up to 600°C. In the larger magnification picture of Figure 0.1c (right), we can observe that this has resulted in the segregation of the platinum particles, although the particle itself is still similar to the 'clean' sample.
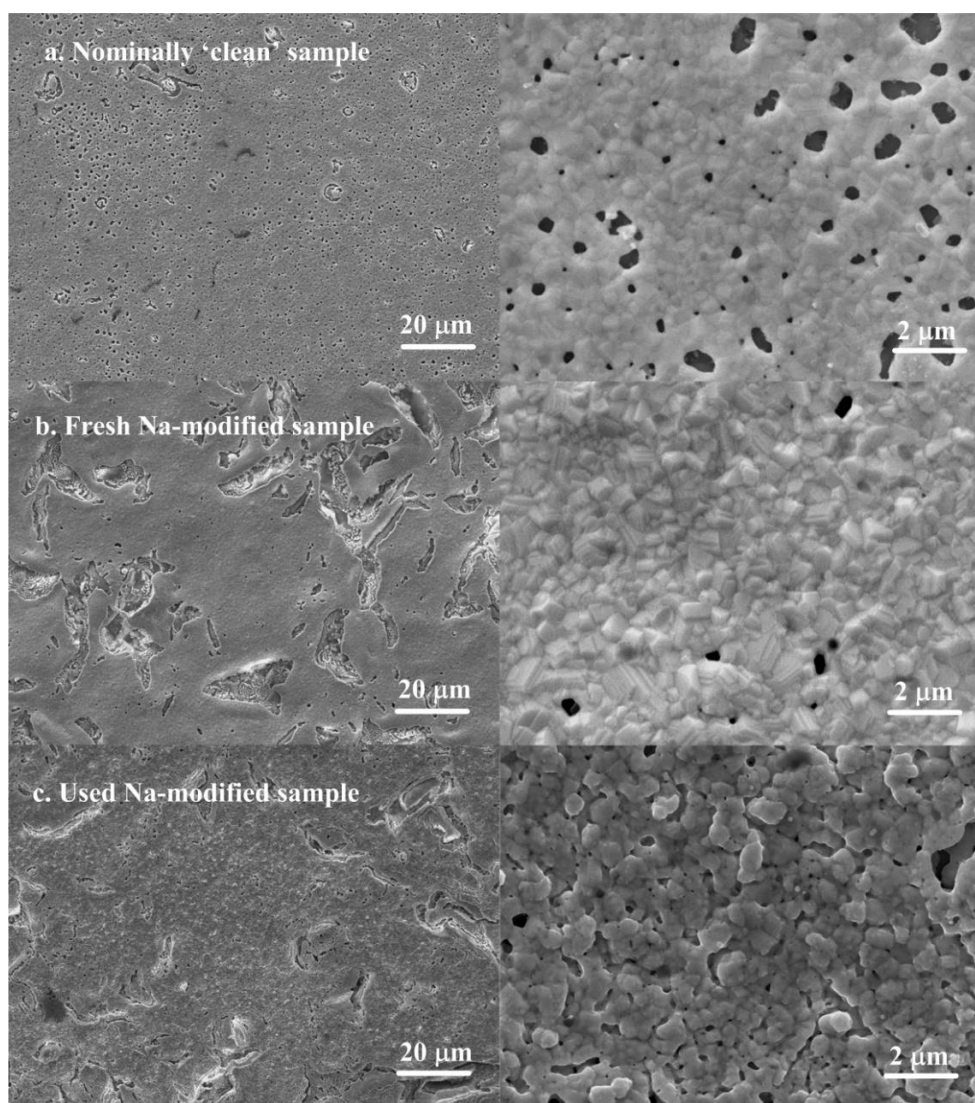
Figure 0.1. SEM images with magnification of 1000x (left) and 10000x (right): (a) Fresh 'clean' sample (A000); (b) Fresh Pt + 5x10^{-2}M NaOH (B502); (c) Used Pt + 5x10^{-2}M NaOH (V502).

The elemental distribution mapping of the fresh and used sodium-modified samples can be seen in Figure 0.2. The presence of sodium and platinum and also some additional impurities mainly potassium (K), calcium (Ca) and sulphur (S) was seen on the surface of the used sample. In Figure 0.2b, only potassium (apart from sodium and platinum) is shown on the map as it is the most significant one compared to calcium and sulphur. However, these additional impurities do not appear to be homogeneous on the sample surface, in fact they are only significant on the spot which is shown in Figure 0.2b. The accumulation of potassium and calcium could be originating from the de-ionised water used for dilution of NaOH solution and/or from the YSZ solid electrolyte, while sulphur could be associated with the hydrocarbon gases used in the reactions (the gas provider reported that sulphur is present in the gases used at ppb levels).
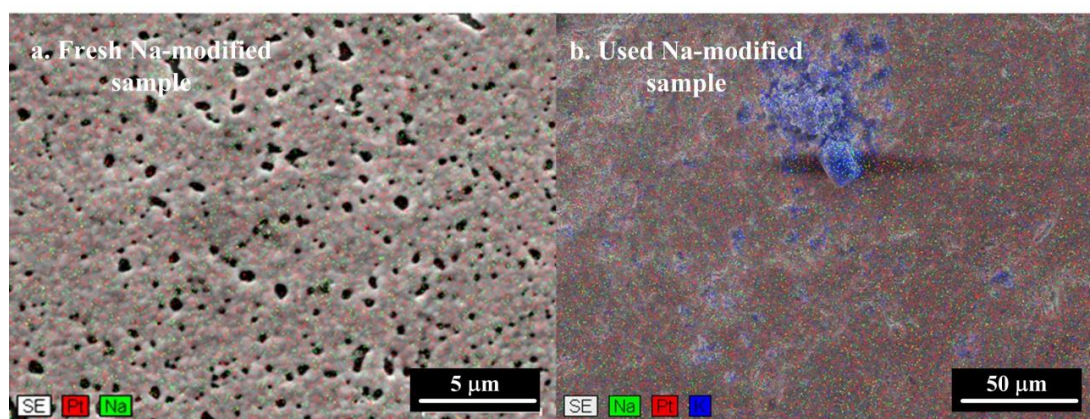
Figure 0.2. Elemental distribution mapping: (a) Fresh Pt + 10^{-1} M NaOH (110% Na coverage, C101); (b) Used Pt + 5×10^{-2} M NaOH (65% Na coverage, V502).

1.15.2. *Surface titration*

The plot of ln N_O versus t_{He} for the 'clean' and sodium-modified samples is shown in Figure 0.3 and the corresponding N_O values are listed in Table 0.1. It appears that within experimental error, low sodium coverage ($< 1\%$ Na coverage, D112 – D104) does not have a significant impact on the uptake of oxygen, N_O by the platinum catalyst. For higher sodium

coverage (10 – 100%, D102 – D101) there is at least four-fold increase of the apparent N_O, when compared to the 'clean' sample (D000). However, it should be noted that this method of catalyst active sites determination has significant uncertainties in term of data reproducibility when used for the sodium-modified samples. It was found that by consecutively repeating a titration experiment on the system with higher sodium coverage (D102 and D101), the amount of carbon dioxide produced and the associated N_O values in the subsequent experiments (not shown here) are lower than those obtained during the first run. The N_O values in Table 0.1 are estimated using the data from the first titration. Therefore, the N_O values of the different samples should only be used to show the relationship between the number of oxygen adsorbed and sodium coverage, not to accurately determine the platinum surface area corresponding to the different sodium coverages. As of the nominally 'clean' sample, the estimated active surface area is in the order of 4 x 10^{-6} mol Pt (~1000 cm^2). The surface area of the platinum film can also be estimated based on the mass of platinum film and the platinum particle size from SEM, assuming a spherical geometry, as discussed in Chapter 3.
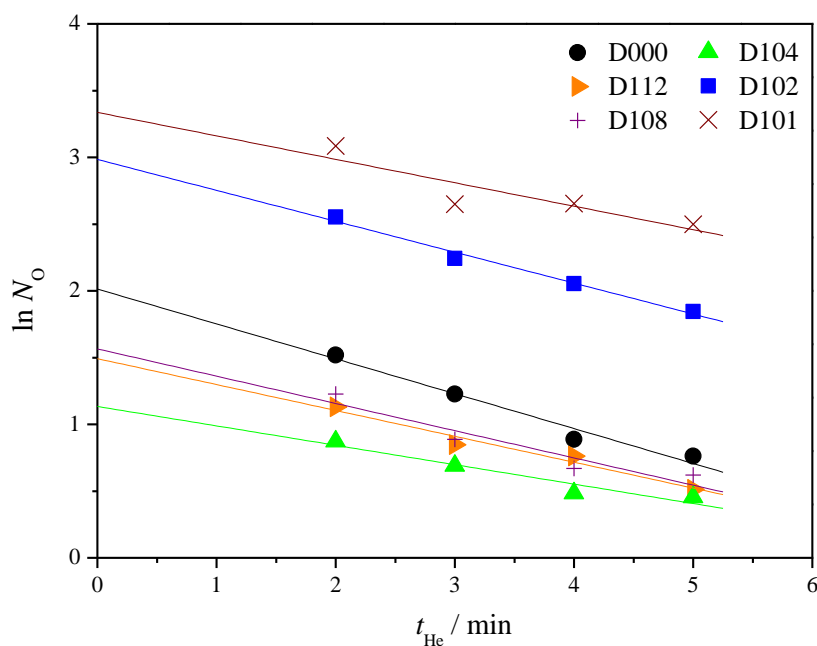
Figure 0.3. Plot of ln N_O versus the oxygen desorption time, t_{He}. Gas composition: 20 kPa O_2 and 10 kPa C_2H_4; Temperature: 400°C; Total flow rate: 150 ml min^{-1}.

Table 0.1. Maximum number of oxygen adsorbed by the platinum active sites over mass of platinum (10 mg). The standard error is calculated by the graphing software during linear fitting.

Sample	Oxygen adsorbed by Pt active sites, N_O
	μmol/mg
D000	0.55 ± 0.12
D112	0.45 ± 0.11
D108	0.48 ± 0.12
D104	0.31 ± 0.11
D102	1.98 ± 0.11
D101	2.81 ± 0.13

1.15.3.   XPS

Typical O 1s, Na1s, C 1s, and Pt 4f spectra of a nominally 'clean' Pt/YSZ catalyst system (E000) and the sodium-modified samples (F112-M101) are shown in Figure 0.4 (only those obtained from Point 3 are shown here). Similar spectra with respect to the peaks of O 1s, Na1s, C 1s, and Pt 4f were obtained for all other points in the platinum regions, except for some small shifts in the binding energies and slight changes in the peak intensities probably due to non-homogeneity in sodium distribution on the catalyst surface. Figure 0.5 shows an example of the acquired spectra (Sample L502 only) at different acquisition points.

The nominally 'clean' sample in Figure 0.4a exhibited two main O 1s components at binding energies of 530.2 and 532.2 eV. The former indicates the presence of lattice oxygen, this signal belongs to the oxidic contribution of the YSZ [130], and the latter indicates the existence of oxygen from other groups such as hydroxides, carbonates and/or oxides on the surface of the platinum films [131-133]. Increasing the sodium coverage on the catalyst surface appears to reduce the O 1s signal arising from the solid electrolyte (the first peak), while at the same time increases the second peak suggesting that this peak may be associated with sodium. From Figure 0.4b broad peak for Na 1s can be seen for the 'clean' sample, as well as for the samples of low sodium coverage (below 1%). This broad peak, which could

represent more than one chemical states of sodium on the catalyst platinum surface, such as sodium carbonates (binding energy 1071.50 eV), sodium oxide (binding energy 1072.50 eV) or hydroxides (binding energy 1072.59 eV), becomes sharper and larger at medium to high sodium coverage, while there appears to be a shift in the Na 1s binding energy from 1070.50 eV for Sample G102 (11% coverage) to 1071.5 eV for Samples H502 and J101. The presence of carbonate species can be further confirmed by the C 1s spectra (shown in Figure 0.4c) at a binding energy of 289.2 ± 0.2 eV for Samples H502 and J101. Note that under reaction conditions where carbon dioxide is present in the reactor as the product of ethylene oxidation, it is possible that the carbonate species may be formed on all samples regardless of the nominal sodium coverage. Harkness et al. also showed using XP and TPD spectra that sodium species deposited on platinum is in the form of sodium carbonate [134]. The C 1s peak around 284 eV is normally assigned to graphitic carbon that may originate from impurities on the catalyst surface due to sample preparation and handling.

The binding energy of Pt $4f_{7/2}$ at 70.8 ± 0.3 eV in Figure 0.4 (for Point 3) indicates that the platinum catalyst on all samples is in metallic form [131]. This suggests that sodium coverage does not have a significant effect on the chemical state of the platinum catalyst. However for L502 in Figure 0.5, sodium addition appears to shift the Pt $4f_{7/2}$ peak to a higher binding energy at 72.3 ± 0.3 eV at Point 1, which is indicative of platinum hydroxide species [131]. On the other hand, the Zr $3d_{5/2}$ binding energy of 182.5 ± 0.6 eV and Y $3d_{5/2}$ binding energy of 157.1 ± 0.5 eV from Point 4 spectra in Figure 0.5 correspond to the YSZ solid electrolyte. The Y $3d_{5/2}$ signal is only measurable on Point 4, probably because it is masked by the platinum film on the other three spectra acquisition points. In addition, we have also measured the Si $2p_{3/2}$ peak as it was reported before that the presence of silicon on a platinum catalyst can affect oxygen-reduction cathodic peak behaviour during a cyclic voltammetry [11]. The Si $2p_{3/2}$ binding energy of 102.4 ± 0.4 eV was detected only on the spectrum of Point 4 of all samples (spectra not shown here) probably because it is also masked by the platinum film on the other spectra acquisition points (P1-P3).
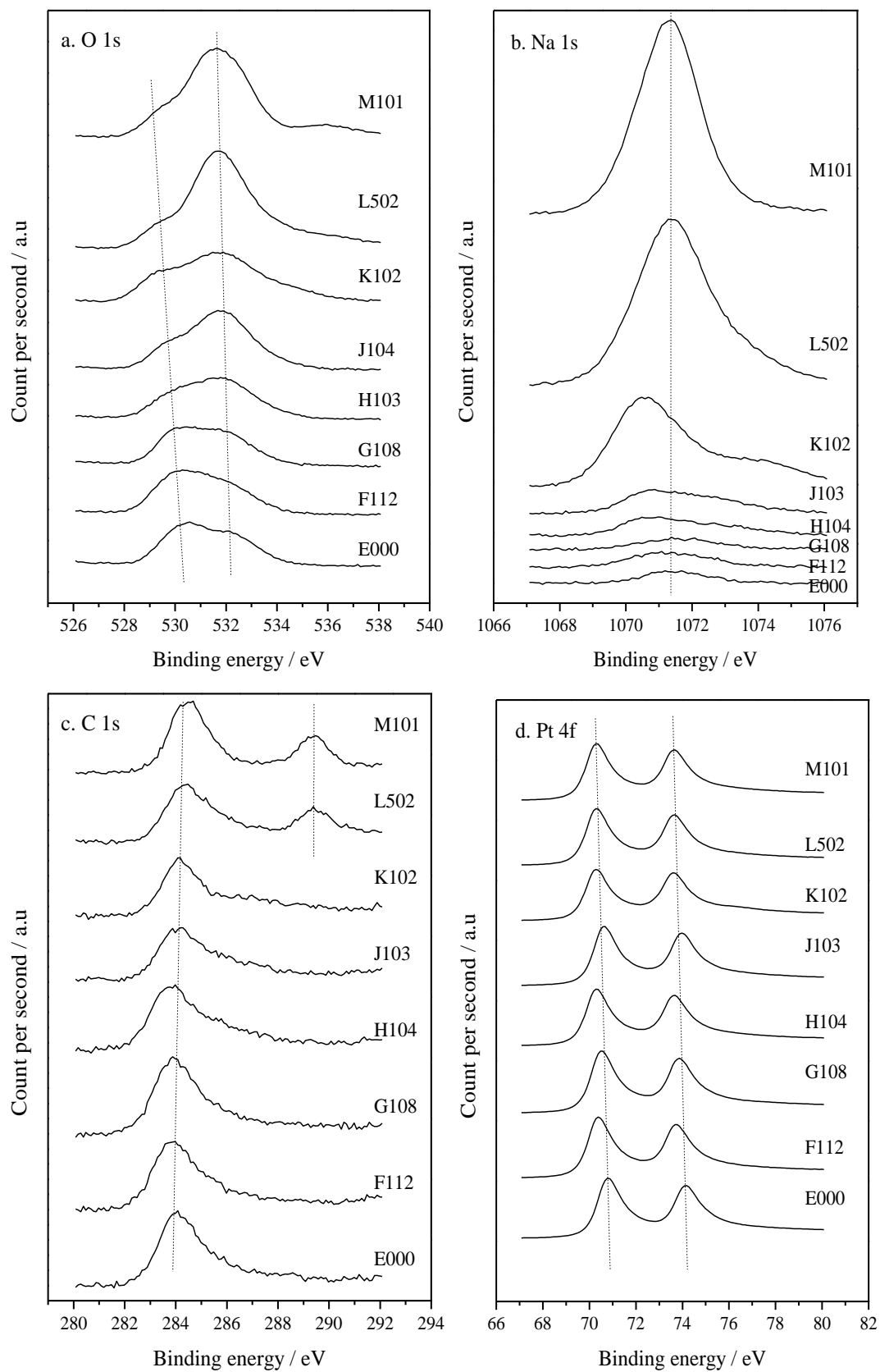
Figure 0.4. XP spectra of the nominally 'clean' and sodium-modified samples
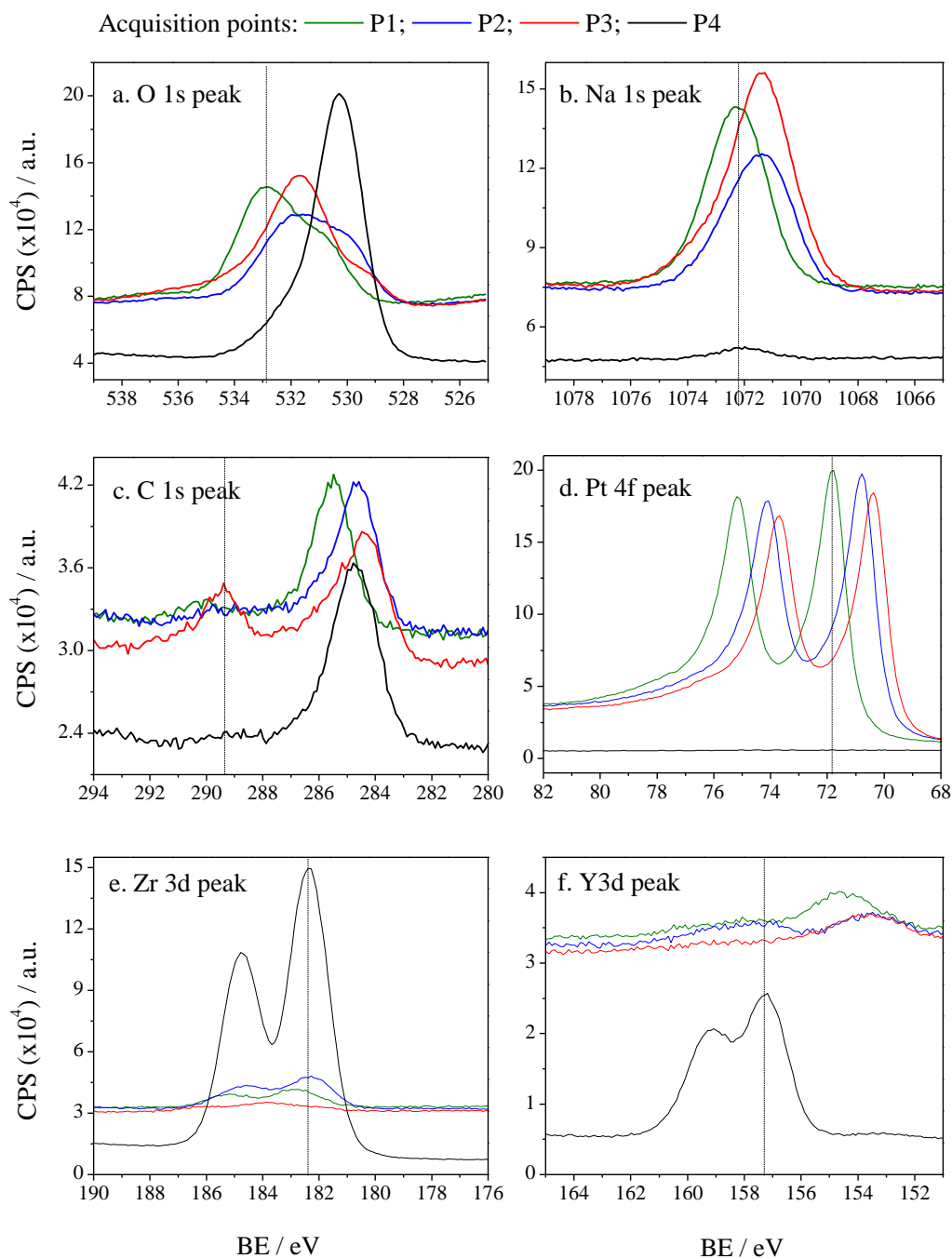
Figure 0.5. XP spectra of Sample L502 (110% Na coverage) as a function of the spectra acquisition points

The intensity of the Na 1s signals for all samples on the four different acquisition points are plotted against the nominal % sodium coverage in Figure 0.6. An increase in sodium coverage increases the Na 1s intensity. It appears that sodium is non-uniformly distributed on each acquisition point (the highest scatter is observed for the sample with the highest

sodium coverage). The Na 1s peak in Point 4 on the YSZ could be due to an overflow of sodium solution during preparation from the platinum region and also from sodium impurities pre-existing on the YSZ electrolyte (the manufacturer reports that the 8 mol% YSZ powder contains approximately 100 ppm Na_2O). As we can see from Figure 0.6 the nominally 'clean' sample (B000) appears to have similar Na 1s peak intensity to the samples of low sodium coverage (<1% sodium coverage, Samples F112 to H104). This could possibly be due to impurities pre-existing on the platinum surface and the de-ionised water used to prepare the NaOH solutions (pre-existing impurities will be more significant for solutions of low NaOH concentration and thus for samples of low coverage). In fact, ICP analysis showed that the de-ionised water contains 1.47 ppm sodium (1 μL of de-ionised water is equivalent to about 0.07% sodium coverage).
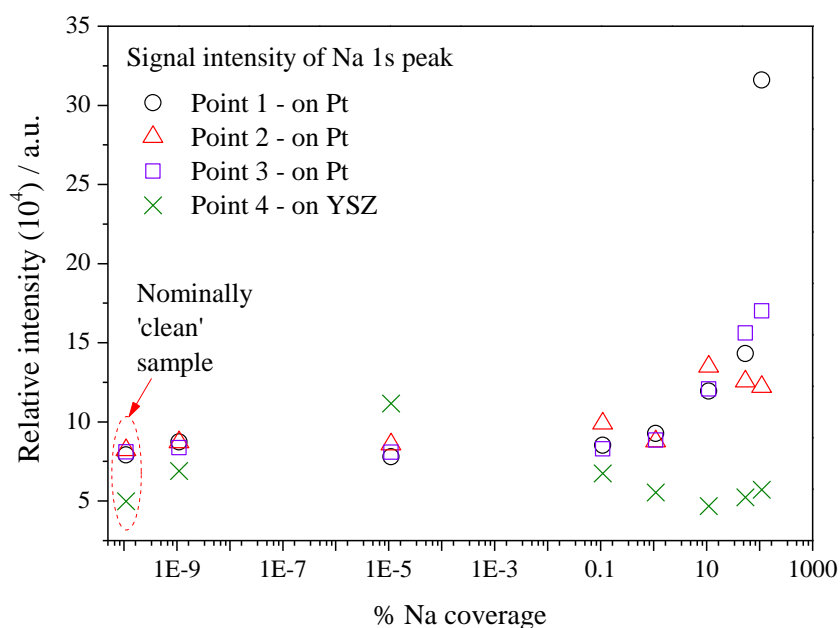
Figure 0.6. Relative signal intensity of sodium versus nominal % sodium coverage

We have also analysed a used sample (W101) using the XPS technique. The sample was previously used for NO reduction experiments in the temperature range between 250 to 525°C. The Na 1s spectra of the used sample is compared with the 'clean' ones (E000) and a fresh sodium-modified sample (M101) of nearest sodium coverage in Figure 0.7. Using the

CasaXPS software, the atomic ratio of platinum, sodium, silicon, calcium and potassium over zirconia for each acquisition points of the fresh and used samples shown in Figure 0.7 is calculated and listed in Table 0.2. The ratio of Na/Pt is also included.
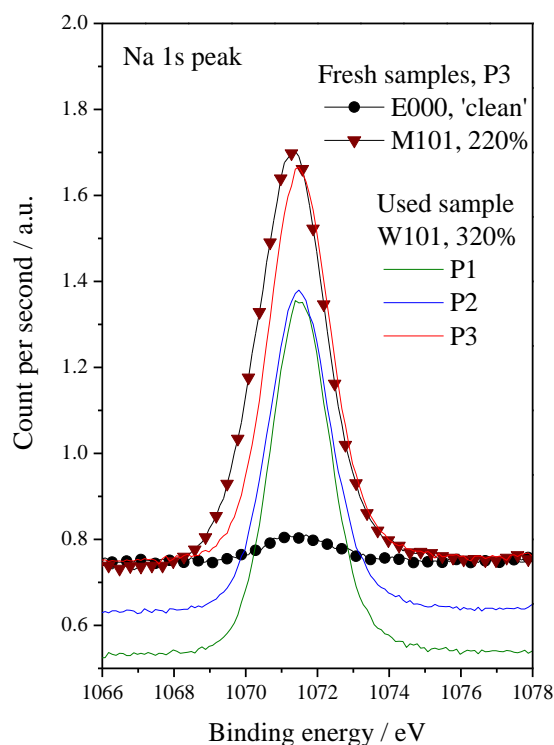
Figure 0.7. Comparison between XP spectra of fresh and used samples, P1-P3 are spectra acquisition points on the platinum surface, while P4 is on the YSZ

As we can see in Figure 0.7, the Na 1s peaks of the used sample (W101, 320% Na coverage) appear to be similar to the fresh sodium modified sample (M101, 220% Na coverage). In a previous study, the Na 1s peak was found to be reduced after being used due to the evaporation of sodium species [134]. The binding energies of the Na 1s peak shown in Figure 0.7 also do not appear to be significantly affected by the sample use, indicating that the sodium species before and after experiments are in similar chemical state. We can also see in Table 0.2, that the Na/Zr ratio on the YSZ (Point 4) has been increased to a higher value compared to the fresh sample, possibly because of the mobility of sodium species from the catalyst surface to the YSZ surface or the migration of sodium from the bulk to the surface of YSZ due to a sintering effect. Apart from that, silicon, calcium and potassium also

appear to populate the surface of the used sample. Table 0.2 shows an increase in the ratio of Si/Zr, Ca/Zr and K/Zr on the surface of the used sample compared to that observed on the fresh samples, possibly also due to the sintering effects. Calcium and potassium have both been observed using the EDX technique discussed earlier, but the quantification of the elements was not possible. In addition we did not observe any peak indicating the presence of sulphur components on the sample surface using XPS, although sulphur was previously detected using EDX.

Table 0.2. Atomic concentration ratio of Pt, Na, Si, Ca and K over Zr compared between fresh and used samples. Na/Pt ratio is lso included. E000 is 'clean' sample, M101 is fresh sample with nominal coverage of 220%, and W101 is aged sample with 320% nominal sodium coverage.

Atomic concentration	Acquisition point	Fresh samples		Used sample
		E000	*M101*	*W101*
Na/Pt	P1	0.03	0.81	0.65
	P2	0.03	0.51	0.49
	P3	0.03	0.35	0.47
	P4			
Pt/Zr	P1	0.92	0.98	0.46
	P2	0.92	0.81	0.62
	P3	0.92	0.98	0.70
	P4			
Na/Zr	P1	0.27	1.00	0.61
	P2	0.25	0.82	0.61
	P3	0.23	0.97	0.68
	P4	0.03	0.06	0.41
Si/Zr	P1			0.62
	P2			0.63
	P3			0.71
	P4	0.01	0.01	0.26
Ca/Zr	P1			0.31
	P2			0.33
	P3			0.32
	P4			0.31
K/Zr	P1			0.27
	P2			0.23
	P3			0.31
	P4			0.19

1.15.4. Kelvin Probe

The results of the Kelvin Probe work function measurement on 'clean' and sodium-modified polycrystalline platinum surface are shown in Figure 0.8. The work function values measured for S000 and T000 samples are quite close to the literature values [129], while the painted samples (N000 and P000) have lower values of about 5.2 eV. This shows that N000 and P000 samples have a higher initial surface contamination, oxide cover and/or higher porosity (for a porous platinum film the Kelvin probe will measure the average work function of platinum and YSZ rather than pure platinum, as would be the case for a fully dense sample) than S000 and T000, and provides the basis that this method can be used to measure the changes in platinum work function caused by sodium modification and subsequent oxide layer accumulation. The electron-beam prepared S000 and T000 samples show work function change of 200 and 250 meV when modified with 10^{-4} M (S104) and 10^{-2} M (T102) NaOH respectively. The change in the work function is most likely due to the NaOH dipole concentration on the platinum surface. Work function changes are not very clear in the painted samples probably because the platinum surface is less well defined and has more initial impurities compared to the electron-beam prepared samples. In any case in all samples, the 10^{-2} M solution of NaOH (54% Na coverage) causes a larger work function (dipole) change than those deposited with the 10^{-4} M solution of NaOH (0.54% Na coverage). Sodium species appear to form a dipole with a positive outer charge lowering the work function by around 200 meV. This is in agreement with the literature studies that showed a decrease in metal work function caused by adsorption of alkali such as sodium [122, 135].
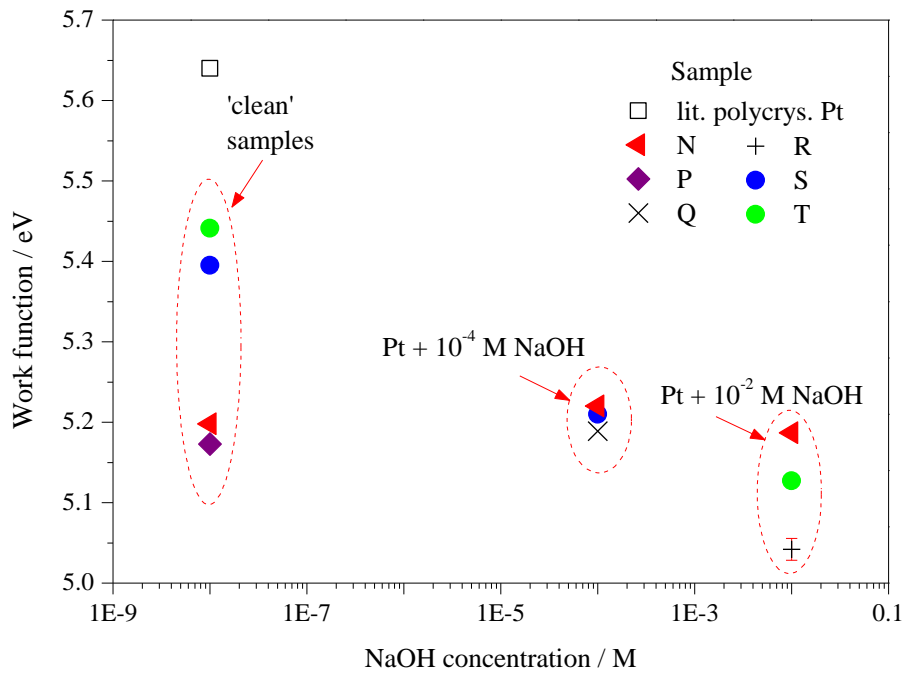
Figure 0.8. Work function measurements on polycrystalline platinum film prepared by painting of platinum resinate on YSZ (Samples N, P, Q and R) and using electron beam deposition technique (S and T). All measurements performed at ambient temperature and pressure. The literature work function of the polycrystalline platinum is 5.64 eV in vacuum (measured using the photoelectric effect).

1.16. Summary

The key findings from the surface characterisation experiments carried out on the Pt/YSZ system are as follows:

(i)   From the SEM analysis, we found that sodium may partially block the pores of the platinum film.

(ii)   From the surface oxygen titration, there is an indication that sodium addition could enhance the oxygen uptake by the catalyst.

(iii)   The XPS analysis shows that sodium may occupy the platinum surface in the form of sodium carbonate, hydroxide and/or oxide.

(iv)   The Kelvin probe measurement on the electron-beam prepared samples shows that sodium addition reduces the platinum work function however it is difficult to measure the work function changes on the painted samples under atmospheric conditions.

These findings could be a good basis to hypothesize the role of sodium in the Pt/YSZ system under dynamic or reaction conditions in the next chapter.

Experimental Hypothesis

1.17. Introduction

The role of sodium on the Pt/YSZ system under non-reactive and reactive conditions is predicted. Non-reactive condition refers to the condition when the system was under continuous flow of 20 kPa oxygen and at a temperature between 400-600°C. For reactive conditions, the system was under a flow of a mixture of 0.5 kPa ethylene and 0.5 kPa oxygen (variable to 1.5, 3 and 8 kPa) for ethylene oxidation study or under a flow of a mixture of 0.1 kPa nitric oxide, 0.1 kPa propene and 0.5 kPa oxygen (variable to 1 and 5 kPa) for NO reduction by propene experiments. Both reactions were conducted at 350°C. For NO reduction some kinetic experiments were also done within the temperature range of 250 – 525°C (for a temperature study).

1.18. Non-reactive conditions

In this section, the focus will be on the role of sodium on oxygen charge transfer in the Pt/YSZ system. The main techniques used to study the oxygen charge transfer were cyclic and linear sweep voltammetry. Based on our previous results from the characterisation techniques and the literature studies, we can expect the sodium deposition to affect the oxygen charge transfer in a number of ways.

(i) Sodium species could adopt a spectator role in the charge transfer reaction and simply occupy the platinum active sites.

(ii) Sodium may modify the charge transfer reaction by creating new sites for, or modifying the kinetics of, oxygen storage, adsorption and diffusion from the gas phase, possibly through modification of the binding strength of oxygen on the catalyst surface.

It is expected that these effects will be evidenced on the voltammogram features as schematically presented in Figure 0.1.
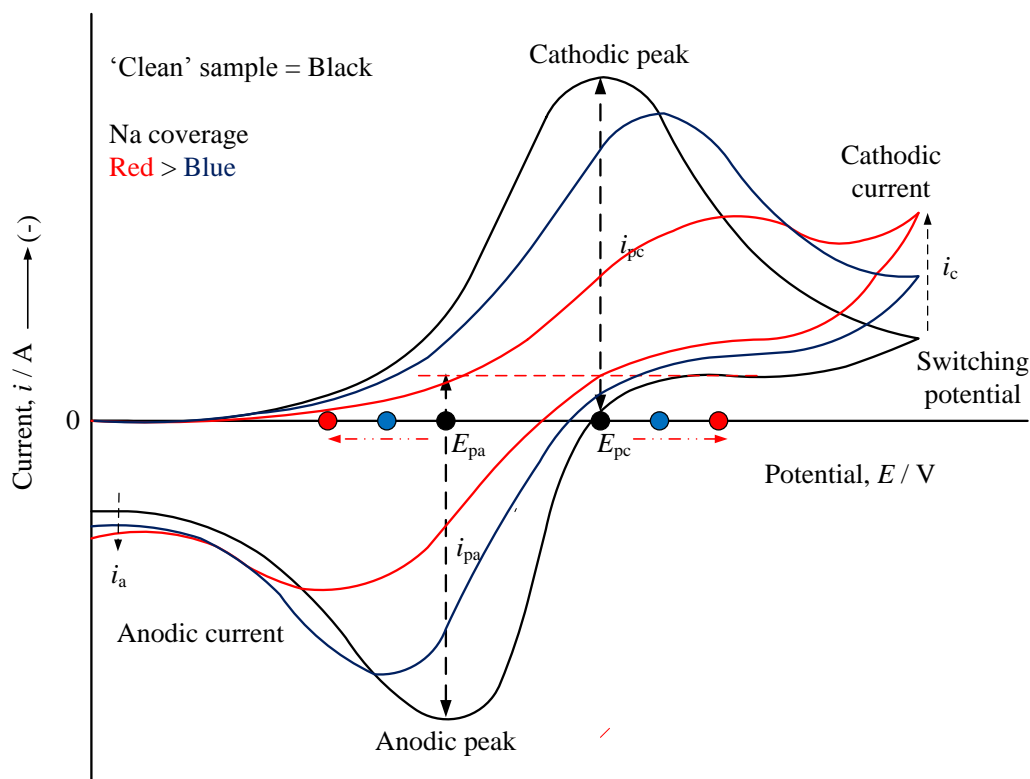
Figure 0.1. Schematic of a cyclic voltammogram showing the expected feature modification by sodium addition

The schematic is an example of a reversible system, but in our case the system could be irreversible. For a reversible charge transfer reaction [28], where there is no surface interaction between the electrode and the reactants, the electron transfer is fast and the ratio of the reverse and the forwards current equals to one. The position of the peak potentials, E_p, for a reversible system is independent of scan rate, while the peak current, i_p is proportional to the square root of the scan rate, $v^{1/2}$. For an irreversible charge transfer reaction [28], where the electron transfer is slow, the forward and the reverse current is not symmetrical, depending on the rate of the reduction or oxidation processes. The position of the peak potentials is dependent on the scan rate because the equilibrium at the surface is no longer establishing rapidly. In the case of oxygen reduction, the voltammogram features could also

be affected by oxygen adsorption on the electrode surface and oxygen diffusion that follows. The black line in Figure 0.1 represents a nominally 'clean' sample while the other two correspond to two sodium-modified samples with different coverage. The red line represents higher sodium coverage than the blue line.

Case (i) may be manifested as a lower rate of oxygen charge transfer in the cyclic voltammetry experiments through the tpb sites blocking. As a result we could expect to see a reduction in the anodic and cathodic peak height (maximum current densities), i_{pa} and i_{pc}, as well as the peak area, A_{pc}, of a voltammogram with increasing sodium coverage as shown in Figure 0.1. If sodium addition modifies the kinetics of oxygen storage, adsorption and diffusion from the gas phase (Case (ii)); on the one hand we could expect to see a shift in the peak positions, E_{pa} and E_{pc}, to more oxidizing or more reducing conditions respectively as indicated in Figure 0.1 by blue and red circle symbols on the x-axis. On the other hand, we could expect to see a change in the anodic and cathodic current densities (i_a and i_c) or total current densities perhaps due to an increase in the supply of oxygen from the adsorbed/stored oxygen species that in turn enhances the flux of oxygen towards the electrode surface. Case (ii) may also result in catalyst promotion if the system is exposed to reaction conditions. The catalyst promotion has been seen in the past in studies with e.g. sodium-conducting supports for electrocatalysis [21, 64, 112, 136]. However, under non-reactive conditions (as is the case studied here) we would not be able to observe such promotion.

1.19. Reactive conditions

Next we will put forward a conceptual model that will allow us to evaluate the role of sodium addition on the catalytic and electropromoted properties of the Pt/YSZ system. Based on the literature [36, 122] and our previous work in Chapter 4 we have seen that sodium addition lowers the work function of platinum. Sodium is known as an

electropositive promoter (electron donor) with low work function and ionisation potential. When such species is adsorbed on the platinum surface, some of the electronic charge will be transferred from the species to platinum, and the positive charge from the sodium species together with an induced negative charge in the metal will create dipoles at the surface resulting in a lower platinum work function. This implies that sodium will function as an electronic promoter in a way that is analogous to the role of the promoting species supplied to the catalyst during polarisation (EPOC experiments), i.e. by changing the work function of a catalyst, thus modifies the relative binding energy strength of chemisorbed reactant species on the catalyst and affects the catalytic properties. Sodium may also directly interact with the catalyst, thus modifying the activity of active sites in the vicinity of the sodium species (short range effect), such as increasing the oxygen adsorption. Moreover, sodium species may interact with the gas phase reactants by creating different reaction intermediates that can affect the catalytic reaction rate. When studying the electropromoted behaviour of a catalyst system, the addition of another type of promoter (oxygen ions in the case studied here) leads to a very complex systems where possible interaction not only between each promoting species and the reaction components (i.e. catalyst, reactants and intermediates) but also between the two types of promoters could influence the behaviour of the reaction. We can therefore anticipate that a very complex model would be required in order to fully predict and explain the behaviour of such system. In this work we will, in the first instance, test a very simple model by making certain assumptions about the interactions between all important species in the systems. To that effect we will initially disregard any short range effects caused by sodium addition and also any interaction between the sodium and oxygen promoting species. We would anticipate this assumption to be valid at low promoter coverage (both sodium and oxygen ions) where the promoting species may have enough distance between them on the catalyst surface so that no significant electrostatic interaction would be possible. Under these assumptions we would expect equal work function changes to cause equal rate modification regardless of the origin of the work function change (i.e. sodium addition ex situ or oxygen spillover in situ by electrical polarisation) and that the

total rate change observed as a result of the combined promotion by sodium and oxygen species could be predicted by the total catalyst work function change.

In this case (using an oxygen ion conducting support) polarisation will cause the supply (positive polarisation) or removal (negative polarisation) of oxygen promoting species to and from the catalyst surface. On a plot of the reaction rate versus the changes in the catalyst work function ($\Delta\Phi$) the y-axis intercept (for $\Delta\Phi = 0$) would correspond to the open circuit rate (no supply of oxygen ion promoter due to polarisation) of a nominally 'clean' pellet (no sodium promoter). All other points along the rate curve could be accessed either by imposing an electrical overpotential to cause a work function change equal to $\Delta\Phi_{el}$ or by fixing the sodium coverage (by external deposition) so that a work function change equal to $\Delta\Phi_{Na}$ is obtained[2]. We must note that as sodium addition causes the work function of platinum to decrease we would only be able to access positive work function changes by polarisation (i.e. by oxygen ion supply and not sodium promotion). Based on this simple model we would expect that a combination of electrical polarisation ($\Delta\Phi_{el}$) and sodium addition ($\Delta\Phi_{Na}$) would have an additive effect on the reaction rate (i.e. would cause a rate change corresponding to the total work function change $\Delta\Phi_{tot} = \Delta\Phi_{el} + \Delta\Phi_{Na}$).

Using our simple model, we expect that the sodium addition will affect the catalytic activity in a way that can be predicted from the nature of the reaction, i.e. electrophilic, electrophobic, volcano or inverted volcano. As mentioned earlier, according to Vayenas reaction classification [88] for purely electrophilic reaction the rate decreases as the work function of the catalyst increases, while for purely electrophobic reaction the rate increases for increasing work function. For volcano-type reaction, the rate shows minimum at $\Delta V_{WR} = 0$, and in contrast the rate shows maximum at $\Delta V_{WR} = 0$ for an inverted-volcano reaction. Electrophilic, electrophobic, volcano and inverted volcano behaviour are as described in

---

[2] In EPOC studies the change in the catalyst work function due to electrical polarisation ($\Delta\Phi_{el}$) is linked to the applied potential between the working and reference electrodes (V_{WR}) or overpotential via the relation: $\Delta\Phi_{el} = \xi e \Delta V_{WR}$, where ξ depends on operating conditions and electrode morphology [I.S. Metcalfe, Journal of Catalysis, 199 (2001) 247-258]. This has been discussed in Chapter 2.

Chapter 2; the first two are shown by Equations 2.66 and 2.67 respectively. Here, we will describe the case of an electrophilic reaction where the rate increases with negative work function changes. For such a reaction we expect that sodium addition and negative polarisation (i.e. removal of oxygen ions from the catalyst surface) would have a qualitatively similar effect, i.e. a rate increase when compared to the rate of a clean sample under open circuit conditions as shown in Figure 0.2.
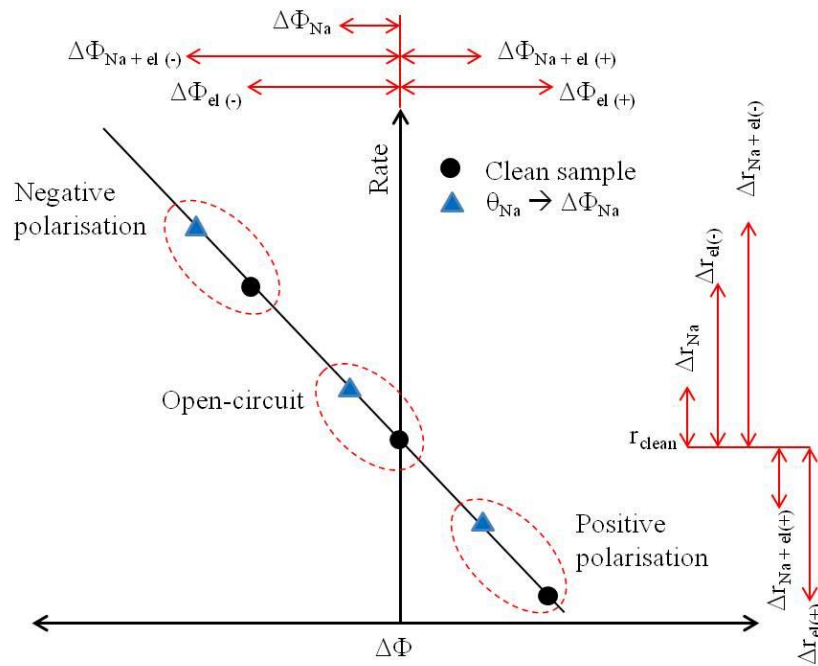
Figure 0.2. Schematic representation of promotional model for an electrophilic reaction. The model is based on work function changes caused by sodium addition and/or electrical polarisation. The shape of the rate curve is arbitrary and only used for illustration purposes.

The magnitude of the rate enhancement would depend upon the polarisation and the sodium coverage (in Figure 0.2 a case where the work function change as a result of sodium coverage is smaller than that caused by electrical polarisation is shown). The combined effect of sodium coverage and electrical polarisation (in the case of this simple model) can be predicted as the rate enhancement caused as a result of the total work function change imposed on the system (i.e. the addition of electrically- and sodium-coverage-induced work function changes, $\Delta\Phi_{Na+el(-)}$). In the case of positive polarisation, where polarisation is

expected to cause a rate decrease, we would expect the combined effect of sodium addition and polarisation to be less pronounced (rate decrease) than what is observed on a clean sample, as sodium addition effectively lowers the combined work function change (i.e. $\Delta\Phi_{Na+el(+)} < \Delta\Phi_{el(+)}$). In this case the promoting effect of sodium (electropositive promoter) and oxygen ions (electronegative promoter) would have an opposite effect on the induced rate modification. If the sodium coverage is sufficiently high we could even expect a rate increase at positive polarisation (compared to the rate of the clean pellet under open circuit) as the positive work function change caused by polarisation is negated by the negative work function changed caused by sodium addition.

Of course the change in the work function of the metal reflects not only the interaction between the adsorbed sodium and the metal but also the interaction of the sodium and the metal with the other adatoms within the adsorbate overlayer. As mentioned earlier, the presence of alkali species has been found to stabilise adsorbed oxygen atoms on the alkali modified sites due to direct interaction between sodium and oxygen, and stabilise the molecular oxygen (precursor) while decreasing the activation barrier for oxygen dissociation due to enhanced backdonation of electron density into the $1\pi*$ antibonding orbitals of oxygen molecules [2, 137]. Based on this, we can also expect that alongside the work function changes, varying sodium coverage will also affect the adsorption of oxygen on the platinum catalyst. At low coverage, sodium has been shown to exhibit a strong positive ionic character and may be uniformly distributed on the metal surface. The coverage of oxygen will be low possibly due to the electronic transfer of electrons towards platinum surface atoms or by electrostatic influence; under these conditions ethylene (electron donor) would be more strongly adsorbed. On the other hand, at higher sodium coverage, sodium may take a more pronounced metallic character, and enhance the adsorption of oxygen with regard to the increase in the oxygen sticking coefficient for dissociative oxygen adsorption on the platinum surface. In the presence of ethylene which is strongly adsorbed on a 'clean' platinum surface, we can expect that sodium addition will also modify the relative strength

of oxygen (electron acceptor) adsorption in comparison to the adsorption of an electron donor (i.e. ethylene). This possible change in the adsorption strength of the reactants could also change the promotional behaviour of the reaction and a shift between electrophilic and electrophobic behaviour could be observed.

Oxygen charge transfer

1.20. Introduction

In this chapter the role of sodium surface species in the modification of a Pt/YSZ catalyst system under non-reactive conditions is discussed. Cyclic and linear sweep voltammetry techniques were mainly used to investigate the kinetics of the charge transfer reaction. The overall electrochemical reaction for the reduction of gaseous oxygen in a Pt/YSZ system is shown in Kröger-Vink notation by Equation 2.68 in Chapter 2. Considering only the *tpb* process, the charge transfer reaction is shown in Equation 6.1:

$$O_{(tpb)} + 2e^- \leftrightarrow O^{2-} \tag{6.1}$$

where $O_{(tpb)}$ is the atomic oxygen adsorbed at the Pt-YSZ-gas interface (tpb). $O_{(tpb)}$ can be created either by adsorption of oxygen from the gas phase and diffusion to the tpb (Equation 6.2), or by the reverse of Equation 6.1 (oxidation of ionic oxygen species from the YSZ electrolyte).

$$\tfrac{1}{2}O_{2(g)} \rightarrow O_{(a)} \rightarrow O_{(tpb)} \tag{6.2}$$

1.21. Results and discussion

1.21.1. Current-overpotential measurement

The 'clean' and sodium-modified systems were first characterised using a steady state current-overpotential measurement. Figure 0.1 shows the log current density-overpotential plots for Sample D at different sodium coverage from 5 to 500 mV for both cathodic and anodic regions. As observed, the cathodic region is mass transfer limited at overpotentials higher than 0.3 V indicating that there is slow supply of oxygen species to the *tpb*. This is not the case for the overpotentials in the anodic region. Similar behaviour of the

current density is seen on all samples except for D108 which shows mass transfer limitation in the anodic region as well. Due to the asymmetric character of the current density-overpotential behaviour in the linear region (where $\eta < RT/F = 60$ mV) the exchange current densities of the different samples were not calculated. The cathodic limiting current densities of the different samples varied from 4-18 $\mu A \ cm^{-2}$. No clear trend can be observed in the cathodic limiting current densities as a result of the sodium addition on the sample. From the results shown in Figure 0.1 it appears that sodium addition does not significantly affect the current-overpotential behaviour of the Pt/YSZ catalyst electrode under non-reactive conditions. This is also possibly because the samples have mostly low sodium coverage (from 10^{-9} to 54%).
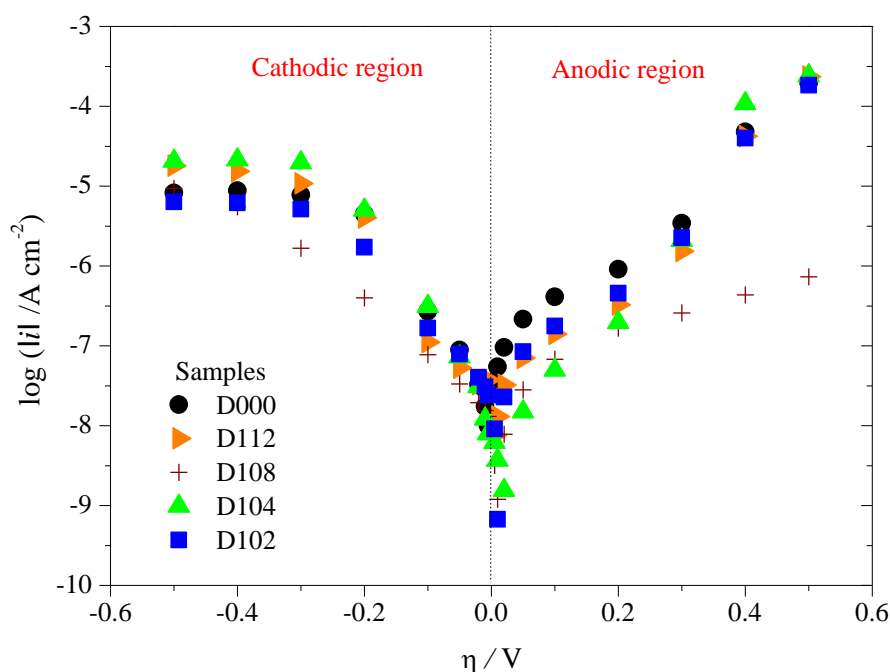
Figure 0.1. Steady state log current density-overpotential plots obtained at 20 kPa O_2 with 'clean' and sodium-modified platinum electrodes supported on YSZ. Gas composition: 20 kPa O_2; Temperature: 400°C; Total flow rate: 200 ml min^{-1}.

1.21.2.   Cyclic voltammetry

Figure 0.2 shows a typical voltammogram of a 'clean' platinum film (U000) exposed to a gas mixture of oxygen (p_{O_2} = 20 kPa) and helium. Figure 0.2a shows the cyclic voltammogram when a voltage is swept at ν = 20 mV s^{-1} from A to C and back to A (Figure 0.2b). The resulting current versus time is shown in Figure 0.2c while the voltammogram under flow of helium only (blank experiment) is shown in Figure 0.2d. The oxygen reduction and oxidation processes on the platinum electrode give rise to two peaks at V_{WR} = B and D respectively. The peak at V_{WR} = B (-0.12 V) is sharp and marked as Peak C for cathodic peak, while the small Peak A at V_{WR} = D (0.12 V) is the anodic peak. The cathodic peak involves the reduction of oxygen at the tpb (Equation 6.2), while the anodic peak corresponds to the oxidation of oxygen ions (from the bulk of the electrolyte) to oxygen at the tpb (the reverse of Equation 6.2)[3]. The sharp cathodic peak may indicate that oxygen adsorption and/or oxygen surface diffusion are slower than charge transfer. It should be noted that there is a number of studies disagreeing with the assignment of the cathodic peak (solely) to a tpb process. Kenjo et al. [92] assigned this peak to platinum oxide decomposition at the Pt/YSZ interface, while the group of Comninellis assigned the cathodic features in CV to both a tpb related process (spillover oxygen) and other interfacial processes (monolayer and bulk platinum oxide formation) [93]. Similarly, Bultel et al. [138] assigned the cathodic peak to the reduction of electrochemically produced oxygen species (either from the chemisorbed oxygen or a platinum oxide layer). Mutoro et al. suggested that this cathodic peak may not be caused only by spillover oxygen or platinum oxide but could also be influenced by the presence of impurities [11]. In a recent study, Pöpke et al. emphasized the role of platinum oxide in the electrode system Pt(O$_2$)/YSZ as its formation and decomposition is considered to affect the oxygen exchange rate [13]. In the work presented here, we are looking at the effect of sodium addition on the Pt/YSZ catalyst

---

[3] The peak height (at *i* maximum) of the anodic Peak A, i_{pa}, is not shown here as Peak A is broad and ill-defined for most samples. Peak A is smaller than Peak C indicating that the O(tpb) is primarily formed from the gas phase oxygen via Equation 6.2.

system and since the same pellet has been used both in the form of 'clean' and sodium-modified samples (for Sample U), the cause of the difference in the characteristics of the cathodic peak (area, height and position) is expected to be the different sodium coverage of the samples.
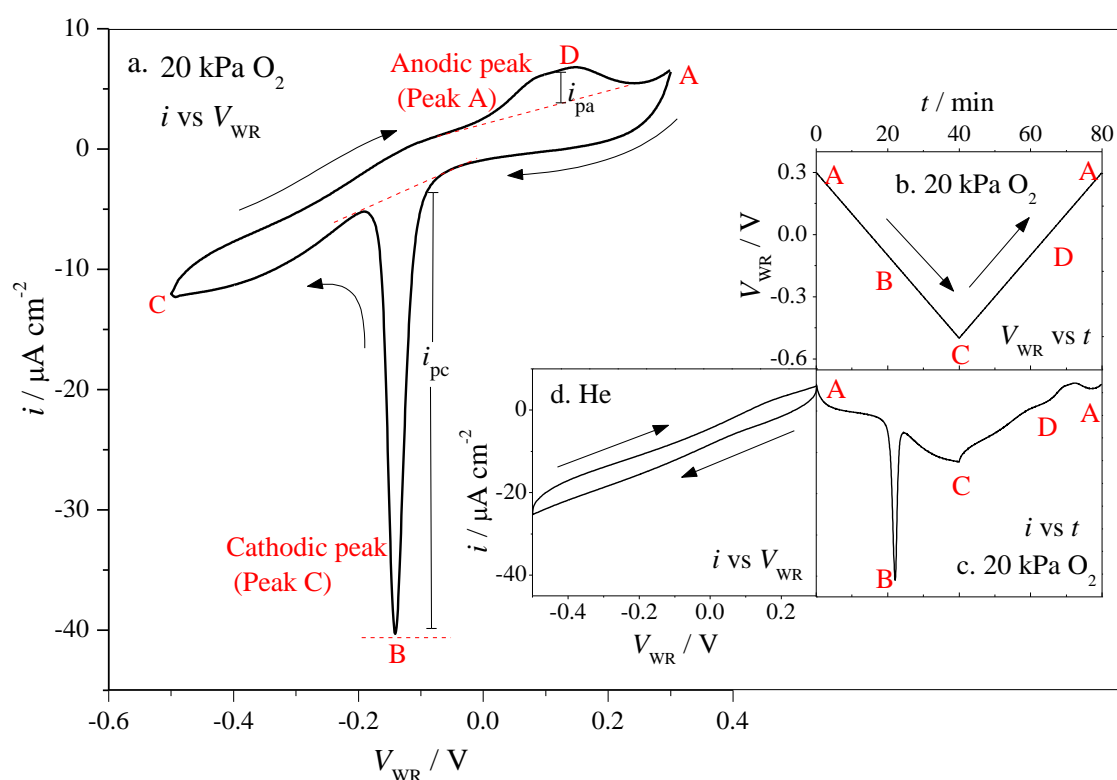
Figure 0.2. Typical platinum cyclic voltammogram under flow of oxygen: (a) Current density, i, versus potential between working and reference electrodes, V_{WR}, (b) V_{WR} versus time, t, (c) i versus t and (d) Blank experiment (He only), i versus V_{WR}. Gas composition: (a-c) 20 kPa O_2 (d) He; Scan rate, $\nu = 20$ mV s^{-1}; Temperature: 400°C; Total flow rate: 200 ml min^{-1}.

Figure 0.3a-g shows the voltammograms of Sample U at different sodium coverage and at varying scan rates from 1 to 100 mV s^{-1}, while Figure 0.4 shows the relationship between the cathodic peak height, $i_{pc,}$ and the square root of the scan rate, $\nu^{1/2}$. As shown in Figure 0.3a there is hysteresis in the voltammogram which indicates that the oxygen charge transfer reaction is an irreversible process [71, 139]. This is also true for the sodium-modified samples (Figure 0.3b-g). From Figure 0.4, the measured cathodic peak height (at

90

maximum current density), i_{pc}, is found to be proportional to the square root of the scan rate, $\nu^{1/2}$, indicating a diffusion-controlled process. This indicates that the oxygen charge transfer reaction taking place in the system studied here is not only a case of simple adsorption but is also controlled by the diffusion of oxygen to the tpb. Yi et al. [73] have also found a linear relationship between peak height and $\nu^{1/2}$ in their studies of the Pt/YSZ interface. However in the work conducted by Vayenas et al. on a different Pt/YSZ system [71] a linear dependence of peak height on ν was found. It is possible that the diffusion limited charge transfer process observed for the sample studied here is due to a combination of the thickness and porosity of the platinum film. We must note that preliminary experiments (not shown here) performed on 'clean' platinum films prepared by electron beam method did not show any peaks. These samples had a platinum film thickness of only 75 nm compared to approximately 10 μm of the painting platinum films.

From Figure 0.3, we can see that the cathodic peak potential, E_{pc}, always shifts towards more negative potential with increasing scan rate. This is a characteristic of electrode reactions with slow electron transfer kinetics which are often referred to as irreversible processes [28]. Under such conditions, the current needs more time to respond to the applied potential because the kinetics of the reaction are 'slow' and thus the equilibria are not established rapidly in comparison to the voltage scan rate [140]. Additionally, we also observe an increase in the total current with increasing scan rate. In liquid electrochemistry this can be explained by considering the thickness of the diffusion layer surrounding the electrode and the time taken to record the voltammogram [141]. The longer it takes to scan the voltammogram, the thicker the diffusion layer. Consequently the flux to the electrode surface is considerably smaller, and the magnitude of the current which is proportional to the flux towards electrode will be lower at slow scan rates and higher at high scan rates. This also explains the increase in the peak height, i_{pc} with scan rate, as i_{pc} according to Fick's law, indicates the concentration gradient of oxygen near the electrode, which is controlled by the diffusion layer thickness [33]. Perhaps in our case, the increase in the current densities is

related to the slow diffusion to the tpb and reflects the amount of oxygen available for the charge transfer process; for a faster scan rate, more oxygen is available to take part in the electrode reaction, while for a slower scan rate, some of the adsorbed oxygen may have diffused away from the electrode.
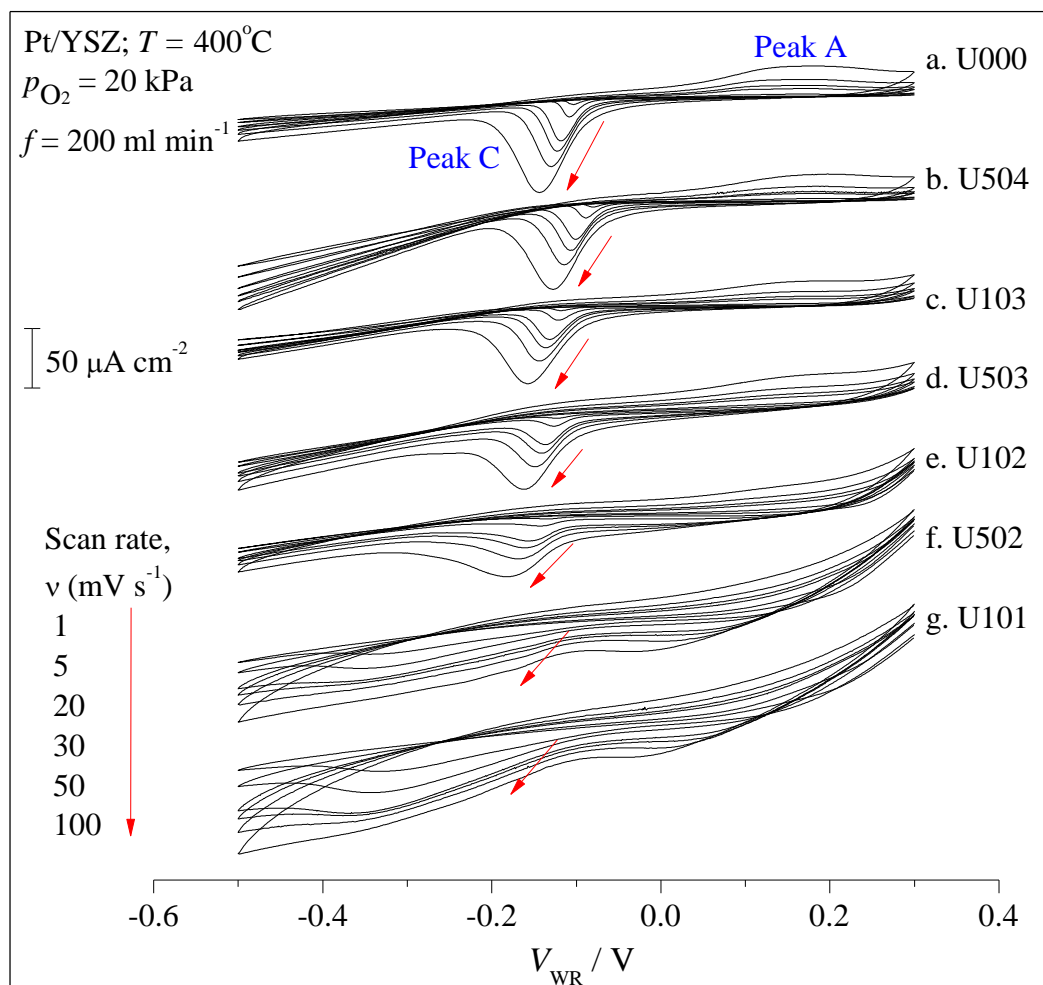
Figure 0.3. Cyclic voltammograms with varying scan rates and sodium loading (a-g). U000 is 'clean' sample, while the others refer to U000 that was modified with NaOH addition in increasing concentrations. Gas composition: 20 kPa O_2; Temperature: 400°C; Total flow rate: 200 ml min^{-1}.
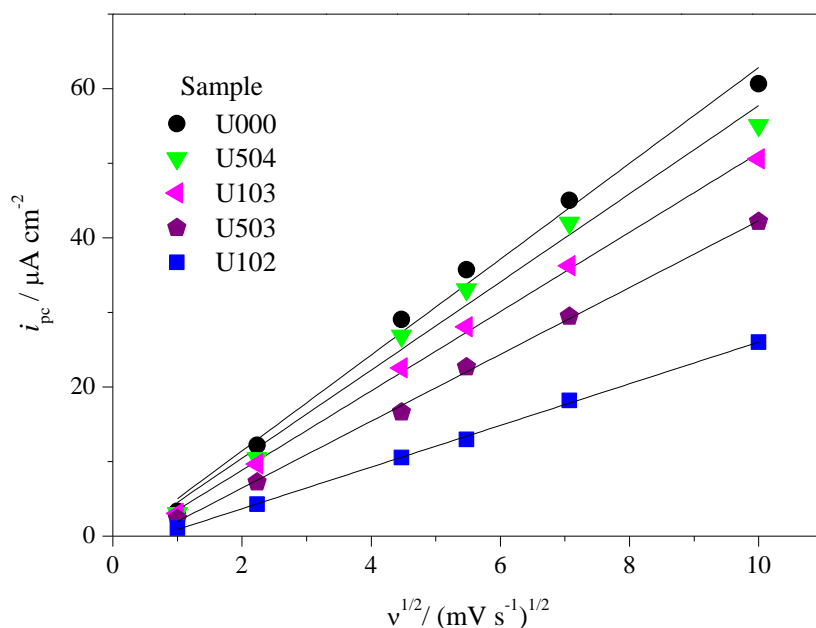
Figure 0.4. Relationship between cathodic peak height, i_{pc} and square root of the scan rate, $\nu^{1/2}$. Conditions as in Figure 6.3.

Table 0.1. Effect of sodium coverage on the cathodic peak potential, E_{pc}, cathodic peak height, i_{pc}, and the charge transferred during oxygen reduction, Q_{pc}. The values shown were calculated for a scan rate of 20 mV s^{-1}, other scan rates showed the same trends

Sample	% Na coverage	E_{pc} (mV)	i_{pc} (µA cm^{-2})	Q_{pc} (µC)
U000	N/A	-118	29	49
U504	0.54	-101	27	53
U103	1.6	-131	23	57
U503	6.5	-137	17	44
U102	16	-154	11	35
U502	65	N/A	N/A	N/A
U101	160	N/A	N/A	N/A

Similar i_{pc} versus ν behaviour as with the 'clean' sample is observed for the sodium-modified voltammograms of Samples U504 to U101 shown in Figure 0.3b-g. In addition, the cathodic peak height, i_{pc}, of Samples U504 – U101 decreases with increasing sodium loading as shown in Figure 0.4 and Table 0.1, indicating a decrease in the charge transfer rate as suggested in Case (i) in Chapter 5 possibly due to tpb sites blocking. However, the cathodic peak area or charge transferred during oxygen reduction, Q_{pc}, does not appear to be

significantly affected by sodium addition for sodium coverage up to approximately 16% as it only reduces by approximately 30% from Sample U000 to Sample U102 (as shown in Table 0.1) without following a discernible pattern. At high sodium coverage (> 50%), the cathodic peak of Samples U502 and U101 shown in Figure 0.3f-g disappears completely. It is possible that the cathodic peak for these samples has in fact simply shifted to lower overpotentials. A shift of the cathodic peak potential towards more negative values is also observed for the other sodium-modified samples (U504 – U102) as can be seen in Table 0.1. This suggests that, as a result of sodium addition, oxygen becomes more strongly bound to the catalyst thus requiring more reducing overpotentials to be removed (Case (ii)). Oxygen can be bound to sodium on the platinum surface in the form of oxides, hydroxides and carbonates [142], or even in the form of sodium-platinum-oxygen complexes [112]. This is also in agreement with the XPS findings that show the presence of these species on the surface of the catalyst.

Another parameter affected by the sodium addition is the observed current density at high overpotentials which increases significantly at sodium coverage above 50% as seen in Figure 0.3f-g. The increase in current density indicates that high sodium coverage could facilitate oxygen supply from the gas phase to the electrode surface through modification of the oxygen storage, oxygen surface diffusion or oxygen adsorption processes as discussed in Case (ii) of Section 5.2. As mentioned earlier, an increase in the oxygen supply to the electrode would cause an increase in the flux towards the electrode, and in turn enhance the current.

1.21.3.   Linear sweep voltammetry

Linear sweep voltammetry was performed at a scan rate of 20 mV s^{-1} for different holding times (t_H) at an anodic potential of $E_H = 0.3$ V. Figure 0.5 shows the obtained voltammograms.
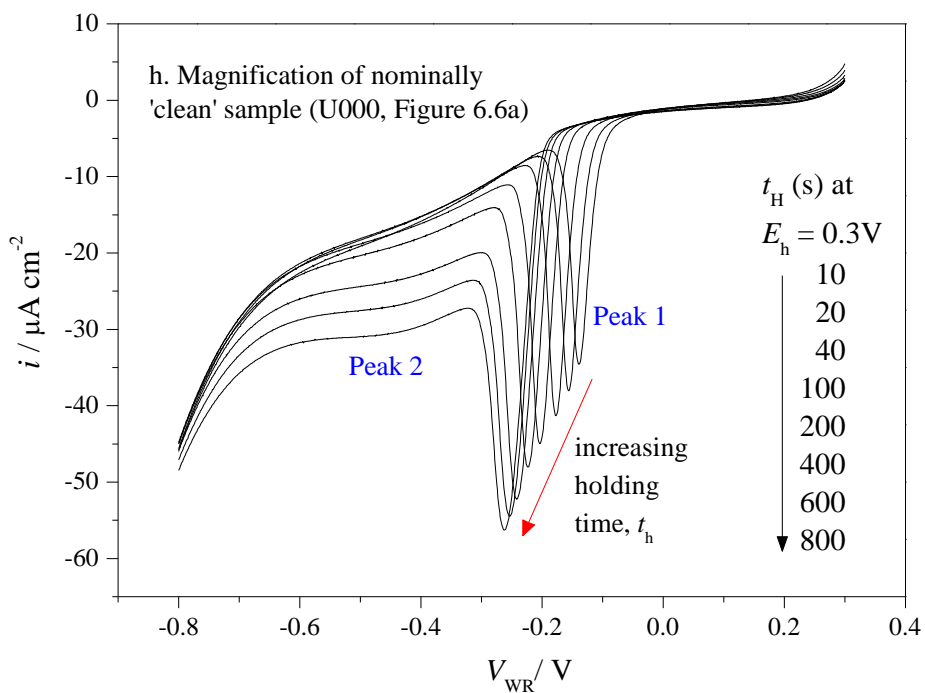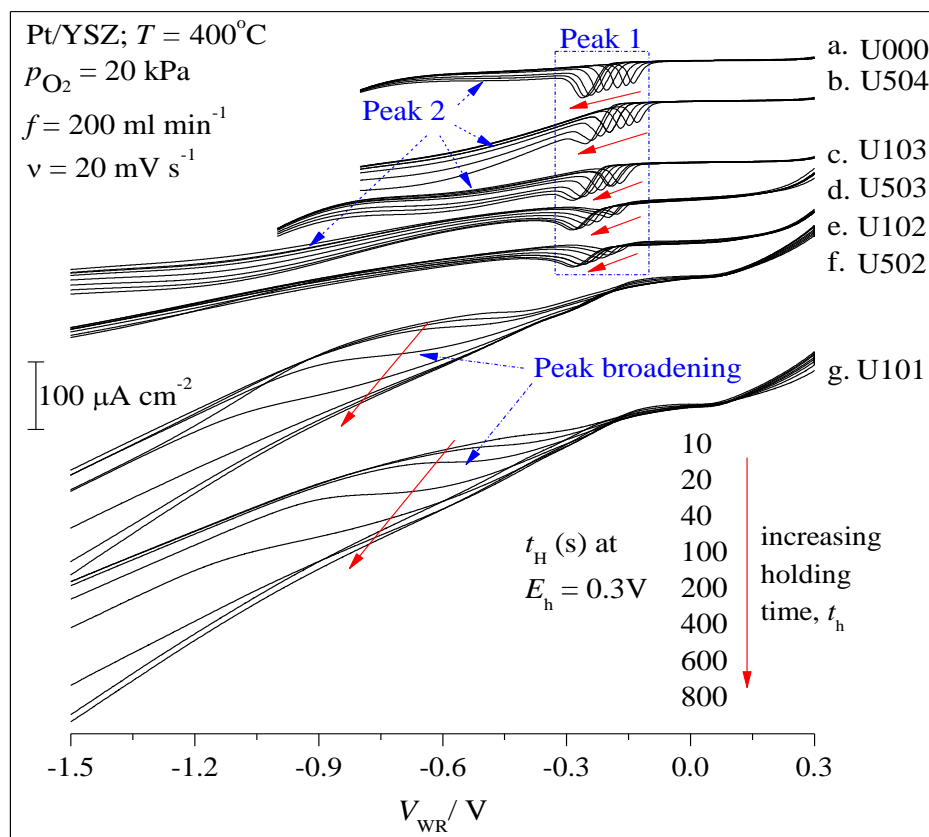
Figure 0.5. Linear sweep voltammograms with varying holding time, t_H at constant anodic potential ($E_H = 0.3$ V): (a – g) Sample with varying sodium loading. U000 is 'clean' sample, while the others refer to U000 that was modified with NaOH addition in increasing concentrations; (h) Magnification of Sample U000. Gas composition: 20 kPa O_2; Temperature: 400°C; Scan rate: 20 mV s^{-1}; Total flow rate: 200 ml min^{-1}.

We can see that as t_H progresses from 10 to 800 s the cathodic peak potential, E_{pc} becomes more negative suggesting that fixing the anodic potential for longer times not only increases the amount but also the binding strength of oxygen. There are actually two peaks on the 'clean' sample (U000) shown in Figure 0.5a (magnification shown in Figure 0.5h); the first one is very pronounced and the same as the cathodic peak discussed in Figure 0.2 and Figure 0.3, while the second peak is very broad and appears only when the potential is held for $t_H =$ 200 s or longer. These peaks were previously used to explain the origin of EPOC [2], by assigning the first one to a highly reactive oxygen species from the gas phase, and the second one to a strongly bonded, thus less reactive, oxygen (back) spillover species. Mutoro *et al*. [11] compared the CV features between two platinum electrodes from the same source, one with and one without intentionally deposited silicon from glass particles. It was observed that additional cathodic peaks were featured only by the sample contaminated with silicon. In the work presented here, we cannot disprove this theory as silicon is often added in platinum pastes as a sintering aid and was also present in the emery cloth used to polish the YSZ pellets. From the XPS result discussed in Chapter 4 we also found that silicon exist on the YSZ surface. However, as the focus of this work is to study the effect of the sodium loading on the charge transfer reaction, the origin of the second peak was not investigated further.

An increase in sodium coverage causes the cathodic peaks' heights to reduce and the peak potentials to become more negative. Sodium coverage up to 16% (U504-U102) does not appear to extensively affect the first peak, but the shift in the second peak towards more cathodic overpotentials is quite significant. At sodium coverage from 65-100% (Figure 0.5f-g, Samples U502 and U101), both peaks also appear to have shifted significantly. This cathodic peak shift was already observed for the cyclic voltammetry experiments as discussed earlier. In addition, and in accordance to previous findings for Samples U502 and U101, all the recorded peaks become broad and ill-defined, possibly masked by an increase in the current density as well. This corroborates our earlier findings about sodium addition

causing oxygen to be more strongly bound on the catalyst surface (case (ii)). These as discussed in Chapter 5 and in the previous cyclic voltammetry experiments would be due to sodium modifying the kinetics, or create new sites for oxygen adsorption, oxygen diffusion and/or oxygen storage. As mentioned in Chapter 5, under reaction conditions, such effects may result in the catalyst promotion. This will be investigated in Chapters 7 and 8.

1.21.4.   *Temperature study*

Figure 0.6 shows the effect of temperature on the cyclic voltammograms of 'clean' (D000) and sodium-modified samples between 5.4 x 10^{-9} and 54% Na coverage (D112, D104 and D102). The inset scatter plots in Figure 0.6 show the change in the cathodic peak position, $E_{pc,}$ (above) and cathodic peak height, $i_{p,}$ (bottom) as a function of the operating temperatures, T. In general, the total current density of all voltammograms is increased with increasing temperature from 400 to 600°C. The 'clean' sample (D000) in Figure 0.6a show that with an increase in the operating temperature, the E_{pc} increases and shifts towards more positive potential, while the i_{pc} increases gradually. The positive shift in the E_{pc} with temperature is similar to previous work [71, 73] and may be related to the increase in the exchange current density, i_{o}, which reflects the intrinsic rate of electron transfer. As shown in Figure 0.6, sodium addition also does not appear to change this behaviour. On the other hand, Vayenas and his group found that as a function of temperature, the i_{pc} of similar system first increases to a maximum near 500°C and then decreases sharply and vanishes near 600°C [71, 73]. The increase in the i_{pc} with T is attributed to kinetic reasons, generally because of the increase in the exchange current density, i_{o}, while the subsequent decrease is attributed to thermodynamic reasons, i.e. decrease in the adsorbed oxygen, and therefore the available oxygen at the tpb with increasing T. In our case, i_{pc} for the 'clean' sample does not appear to be decreased by the temperature at 600°C, possibly because of the difference in the morphology and thickness of the platinum film. Sodium addition appears to cause two general effects, one is to reduce the overall i_{pc} compared to the 'clean' sample and the other

is to reduce the i_{pc} towards zero from 550°C. The first one may be explained by sodium blocking the active sites, thus reducing the electrocatalytic activity of platinum catalyst. The second effect is similar to that observed in the previous EPOC studies and may indicate the presence of impurities in those cases. In addition, Figure 0.6d indicates that high sodium coverage may increase the total current density of the voltammogram, similar to that discussed in the previous sections.
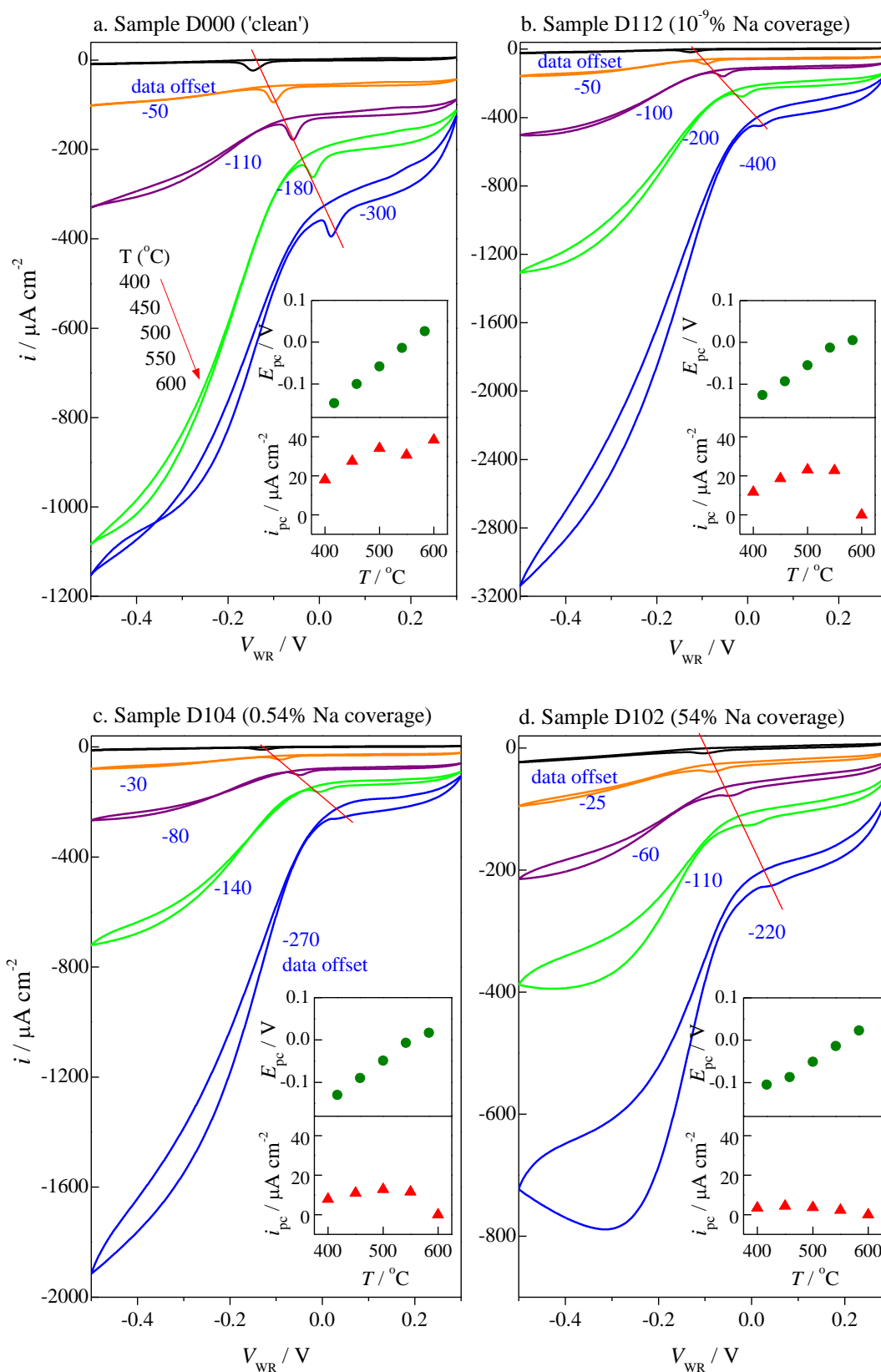
Figure 0.6. CV at different sodium coverage under varying temperature from 400 to 600°C. Inset graph: Cathodic peak position (top), peak height (bottom) versus temperature. Gas composition: 20 kPa oxygen; $f = 200$ ml min^{-1}; $v = 20$ mV s^{-1}. Sample D108 is not shown because peak is not clear. The CVs at the different temperatures are plotted with an offset (µA cm^{-2}) from the CV at 400°C.

1.22. Summary

To summarise the findings from the cyclic voltammetry experiments, we can see that:

(i)   Low sodium coverage reduces the cathodic peak height, indicating a decrease in the charge transfer possibly by sodium blocking of the tpb sites

(ii)   Sufficient sodium coverage (more than 1% Na coverage) causes the cathodic peak potential to shift towards more negative values indicating that oxygen is now more strongly bound on the catalyst surface

(iii)   High sodium coverage (more than 50% Na coverage) causes the current density at high overpotentials (and also the total current density) to increase, suggesting that sodium enhances oxygen storage, surface diffusion and/or adsorption.

Linear sweep voltammetry experiments also shows that oxygen becomes more strongly bound to the catalyst with increasing sodium coverage, requiring more reducing overpontentials to be removed.

Ethylene Oxidation

1.23. Introduction

The chapter discusses the role of sodium on the catalytic and electrocatalytic properties of the Pt/YSZ system. Cyclic voltammetry and chronoamperometry (potentiostatic transient experiments) were used as the means to investigate the effect of adding variable-coverage sodium to the catalyst system. Ethylene oxidation is the probe reaction in this study. The kinetics and mechanism of ethylene oxidation over platinum films interfaced with doped zirconia have been well-studied in the past [2, 26]. The ethylene oxidation reaction is written as follows:

$$C_2H_{4(g)} + 3O_{2(g)} \xrightarrow{\text{Pt}} 2CO_{2(g)} + 2H_2O_{(g)} \tag{7.1}$$
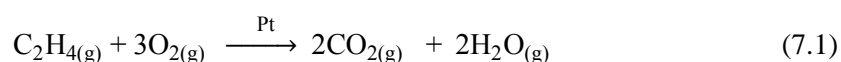
1.23.1. Reaction rate calculation

The parameter measured from the experiments discussed in Chapter 3 was p_{CO_2}. The reaction rates which are reported in the following sections were calculated as follows:

$$\text{Rate} = \frac{[CO_2]}{100} \times F_m \tag{7.2}$$

where $[CO_2]$ is the partial pressure of CO_2 (kPa), F_m is the total molar flow rate measured at STP from the outlet of the reactor. From the ideal gas equation at STP we have:

$$F_m = \frac{F_V}{60} \left(ml\ min^{-1} / s\ min^{-1} \right) \times \frac{1}{22400} (mol\ ml^{-1}) \Rightarrow$$

$$\Rightarrow F_m = 7.4 \times 10^{-7}\ F_V\ (mol\ s^{-1}) \tag{7.3}$$

where F_V is the measured volumetric flow rate in ml min^{-1} (STP). Combining Equations 7.2 and 7.3 produces the final expression for the reaction rate calculation, while dividing with the platinum electrode area, A gives the area specific rate:

$$\text{Rate CO}_2 \left(\text{nmol s}^{-1} \text{ cm}^{-2} \right) =$$

$$= 10^9 (\text{nmol/mol}) \times {[CO_2]}/{100} \times \left[7.4 \times 10^{-7} \times {F_V}/{A} \right] (\text{mol s}^{-1} \text{cm}^{-2}) \quad (7.4)$$

The reaction rates for ethylene oxidation are reported in nmol s^{-1} to standardise with the NO reduction study which has smaller reaction rates. A maximum of 5% error is expected to be associated with the rate measurements as per the accuracy of the analytical equipment used for the CO_2 detection. When reporting transient rate data no error bars are used in the figures as rate changes can be seen as function of time. An error bar corresponding to 5% error is used in the plots where discreet rate data are shown.

The activity of the catalyst under reaction conditions is reported in the thesis as reaction rate instead of conversion as the second parameter depends on the characteristic of the reactor, e.g. the amount of material effectively by-passed and the volume of the dead zone, whereas the reaction rate is an intrinsic property. Furthermore, the same reactor settings and total flowrate were always used for each set of experiments (under nonreactive and reactive conditions with either ethylene oxidation or NO reduction).

1.24. Results and discussion

1.24.1. Cyclic Voltammetry

First, cyclic voltammograms of the nominally 'clean' and sodium-modified samples (V000-V502) were recorded under flow of 3 kPa O_2 and 0.5 kPa C_2H_4 at 350°C. The current response (current density, i, versus the applied overpotential, V_{WR}) is shown in Figure 0.1a. The change in the area specific rate of CO_2 produced from ethylene oxidation during the

cyclic voltammetry experiment is depicted in Figure 0.1b and c as a function of the applied overpotential and the current density during polarisation respectively. As we can see in Figure 0.1a, the cyclic voltammograms do not show any significant cathodic peak while a sharp peak was observed for oxygen reduction under non-reactive conditions in Figures 6.3 and 6.4 in Chapter 6. This is possibly due to the fast oxygen consumption by ethylene. In Figure 0.1b we can observe that the rate change in the 'clean' and low sodium-modified systems follows a similar pattern, i.e. the CO_2 production rate is decreased by positive current densities and increased by negative values[4]. We can see that the reaction rate of the two systems reaches approximately the same minimum at current densities of the order of +20 μA cm^{-2} and the same maximum at current densities of about -15 μA cm^{-2}. The catalytic rate is clearly influenced by current densities in a similar way for the two samples. Our previous results in Chapters 4 and 6 also showed that at low sodium coverage (< 1%) sodium-containing species do not appear to have a significant role in the Pt/YSZ system, other than sodium poisoning the tpb.

Increasing sodium to medium and high coverages (V102-V502, 11-65%), on the other hand shows an increase in the reaction rates and the corresponding current densities. This indicates a possible positive effect of sodium on the catalytic activity of the Pt/YSZ system. At medium sodium coverage (V102, 11%) the reaction rates reaches minimum and maximum at more positive current densities than those seen with low sodium coverage; i.e. +40 and -10 μA cm^{-2} respectively. For the sample with high sodium coverage (V502, 65%), it appears that the rate shows minimum on both anodic and cathodic sides, around +110 and -15 μA cm^{-2}, and maximum at about +5 μA cm^{-2}. Next we investigate the rate changes

---

[4] In previous studies on the EPOC of ethylene oxidation over a platinum catalyst it has been found that positive polarisation generally enhances the rate of ethylene oxidation (i.e. the reaction shows electrophobic behaviour) [S. Bebelis, C.G. Vayenas, J. Catal., 118 (1989) 125, M. Stoukides, C.G. Vayenas, J. Catal., 70 (1981) 137]. However, it has also been found that at temperatures higher than 350°C (as in the case studied here) negative polarisation may also cause a small rate increase [C. Koutsodontis et al, Topics in Catalysis, 38 (2006) 157]. In addition, depending on the gas phase composition (i.e. the $p_{O_2}/p_{C_2H_4}$ ratio) it is possible to observe a rate enhancement under both positive and negative polarisation [S. Bebelis et al, Solid State Ionics, 129 (2000) 33].

observed for 'clean' and sodium-modified systems under a constant polarisation (at η = +1 V and -1 V).
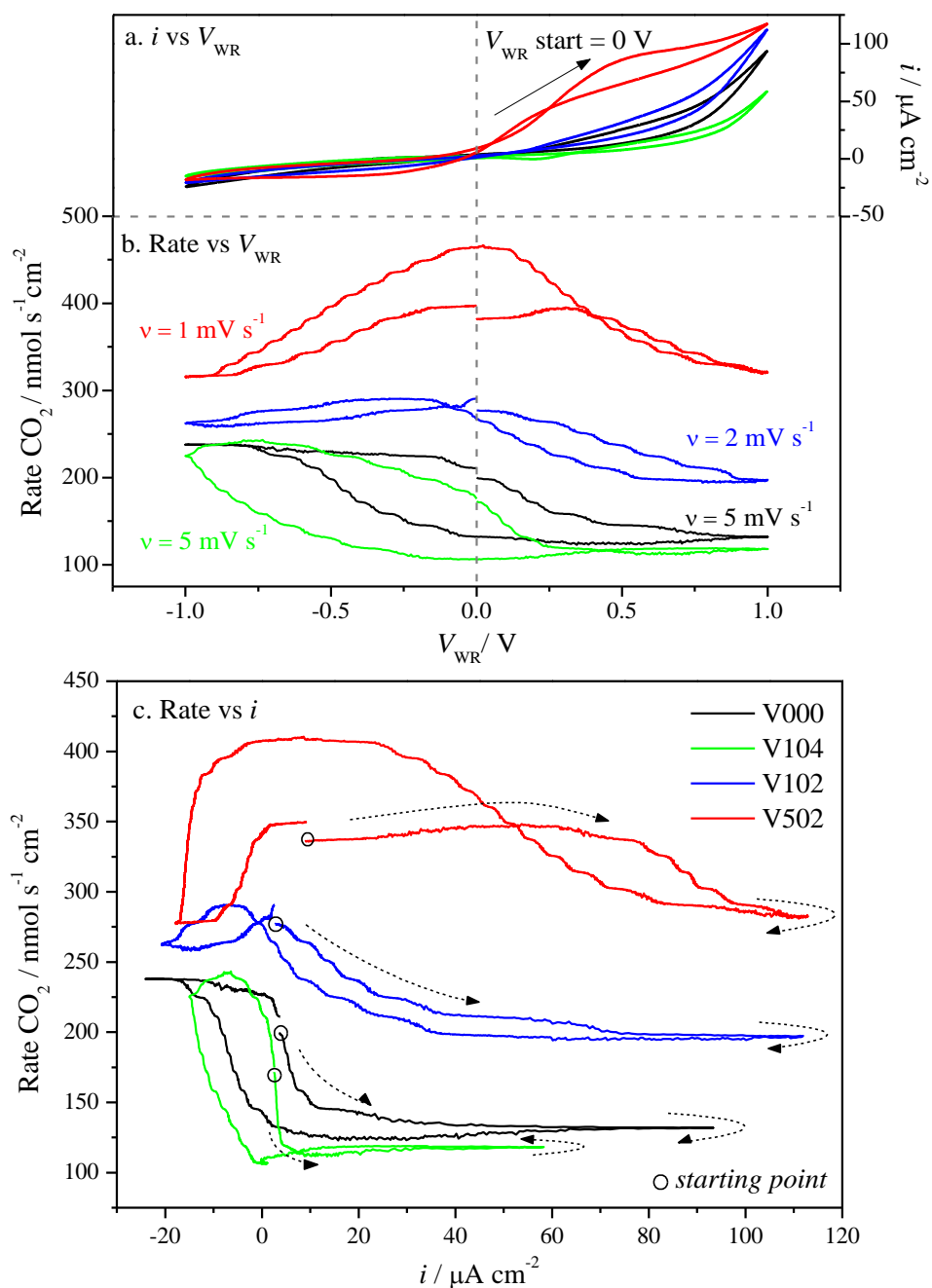
Figure 0.1. Cyclic voltammetry data: (a) i vs V_{WR}; (b) Rate vs V_{WR}; (c) Rate vs i. Reactant partial pressures: p_{O_2} = 3 kPa, $p_{C_2H_4}$ = 0.5 kPa; Temperature = 350°C; Total flow rate = 200 ml min⁻¹.

1.24.2. Kinetic studies

A series of potentiostatic transient (chronoamperometry) experiments were conducted on Sample V under various gas compositions; the oxygen partial pressure, p_{O_2}, was varied between 0.5 and 8 kPa, while ethylene partial pressure, $p_{C_2H_4}$, was kept constant at 0.5 kPa. Both open-circuit and polarisation experiments were conducted (as described previously in Chapter 3) on the 'clean' sample and also after each sodium addition (with 10^{-4}, 10^{-2} and 5×10^{-2} M NaOH). We will first discuss the open-circuit experiments.

1.24.2.1. Open-circuit conditions

Figure 0.2 shows the CO_2 production rate of all samples under open-circuit conditions; while Table 0.1 lists the rate enhancement ratio caused by sodium addition, ρ_{Na}. This enhancement ratio is defined as the open-circuit rate of the sodium-modified sample, $r_{o(Na\text{-modified})}$, over that of the 'clean' sample, r_o:

$$\rho_{Na} = r_{o(Na\text{-modified})}/r_o \qquad (7.5)$$

As we can see from Figure 0.2 the rate of CO_2 production is positive order with respect to oxygen partial pressure. This is true for all the samples (i.e. 'clean' and sodium-modified). This has also been consistently reported in the literature [26-27]. From Figure 0.2, we can see that sodium addition in general increases the open-circuit rate. This effect becomes more pronounced at high sodium coverage and for low oxygen partial pressure in the reaction mixture. Thus the highest enhancement ratios ($\rho \approx 4$) are observed in Table 0.1 for 65% sodium coverage and oxygen partial pressures up to 1.5 kPa (stoichiometric oxygen to ethylene ratio). The results obtained under open-circuit conditions are, in the first instance, in qualitative agreement with the proposed model (for an electrophilic reaction), in the sense that in general sodium addition resulted in an increase of the reaction rate as predicted by the model. Of course, whether this promotion is simply due to the work

function changes caused by sodium addition or also due to interactions between the surface species with the reactants and possibly the creation of extra sites for oxygen adsorption cannot be assessed at the moment and will be discussed in more detail next when the experiments under polarisation are discussed.
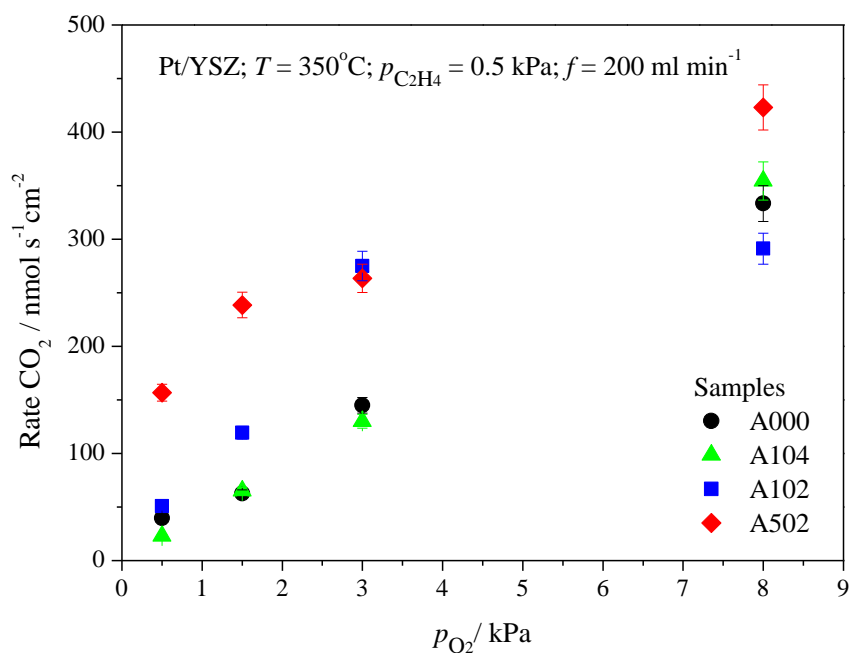
Figure 0.2. Open-circuit CO_2 production rate versus oxygen partial pressure. Reactant partial pressures, variable p_{O_2} = 0.5, 1.5, 3 or 8 kPa, $p_{C_2H_4}$ = 0.5 kPa; Temperature = 350^oC; Total flow rate = 200 ml min^{-1}.

Table 0.1. Rate enhancement ratio due to sodium addition, ρ_{Na}

p_{O_2} (kPa)	Rate enhancement ratio, ρ_{Na}		
	V104	V102	V502
0.5	0.58	1.29	3.96
1.5	1.04	1.90	3.81
3.0	0.90	1.90	1.82
8.0	1.06	0.87	1.27

1.24.2.2. Polarised conditions

Figure 0.3 and Figure 0.4 show the reaction rate transients during polarisation. As mentioned earlier, the reaction rate is monitored for five minutes prior to polarisation, 7 minutes (420 s) during polarisation and approximately 15 minutes after polarisation (in some cases the final open circuit step is longer as the return to the initial open circuit rate can be slower depending on the experimental conditions). In Figure 0.3a-b we can see the transients for an oxygen partial pressure of 3 kPa (results for lower partial pressures are shown in Appendix D with similar trends), while Figure 0.4a-b show the behaviour under an oxygen partial pressure of 8 kPa (high p_{O_2}). For both Figure 0.3 and Figure 0.4, figure a corresponds to negative polarisation with an overpotential of -1 V and figure b corresponds to positive polarisation with an overpotential of +1 V. In addition, Table 0.2 shows the rate enhancement ratios, ρ, and Faradaic efficiencies, Λ, observed under all experimental conditions studied here. The rate enhancement ratio and Faradaic efficiency as expressed in Equations 2.62 and 2.63 in Chapter 2 are re-written here:

$$\rho = r/r_o \tag{7.6}$$

$$\Lambda = \Delta r / \left({}^{I}\!/_{nF}\right) \tag{7.7}$$

where r_o is the open-circuit rate of the sample, r is the electro-promoted rate, Δr is the difference in the electro-promoted and open-circuit rate, I is the applied current and F is the Faraday's constant. The shaded areas in Table 0.2 are indicative of non-Faradaic enhancement of the reaction rates.
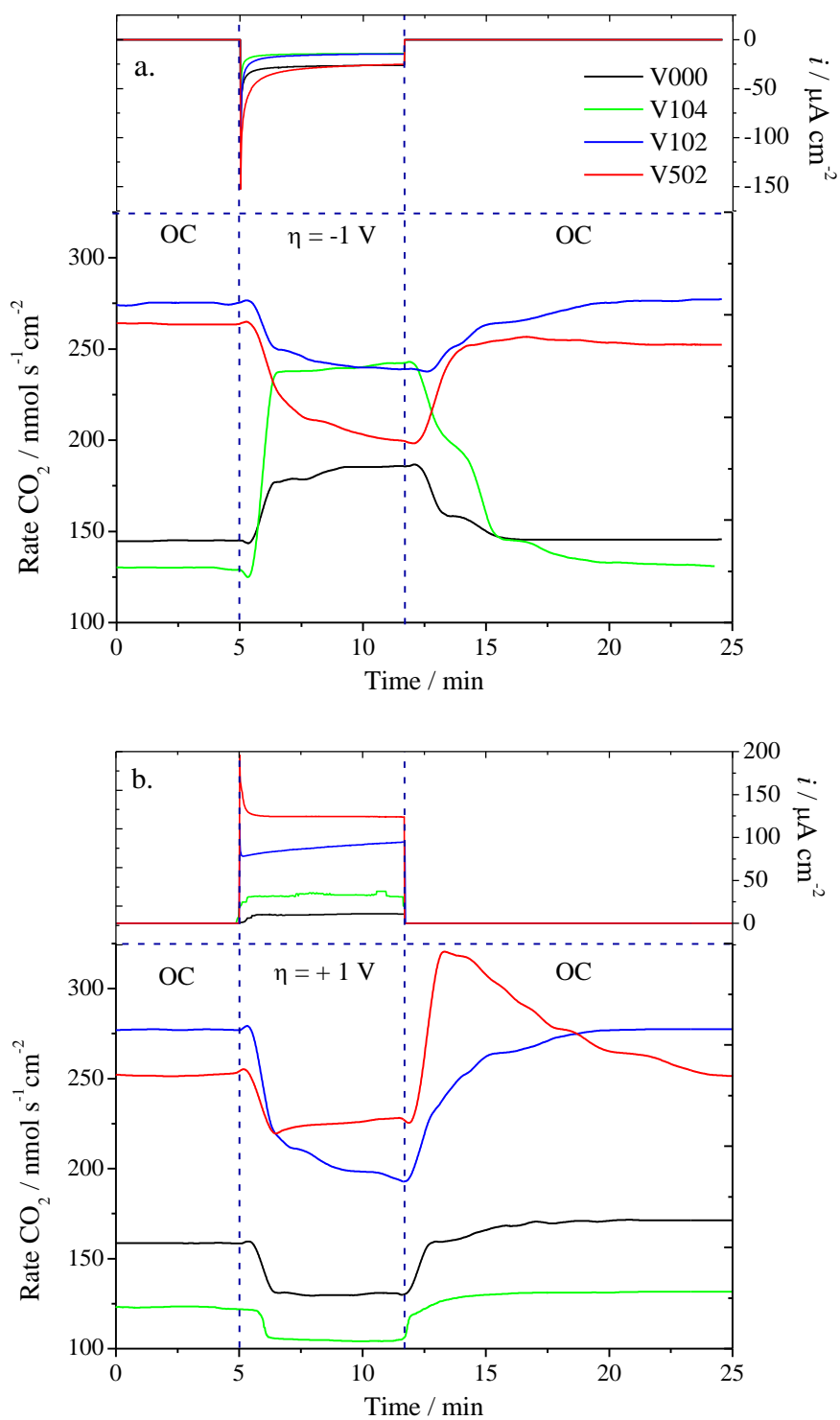
Figure 0.3. Transient plots under intermediate p_{O_2} and polarisations: (a) η = -1 V; (b) η = +1 V. Top: Current density, i versus time; Bottom: CO_2 versus time. Reactant partial pressures, p_{O_2} = 3 kPa, $p_{C_2H_4}$ = 0.5 kPa; Temperature = 350°C; Total flow rate = 200 ml min^{-1}.
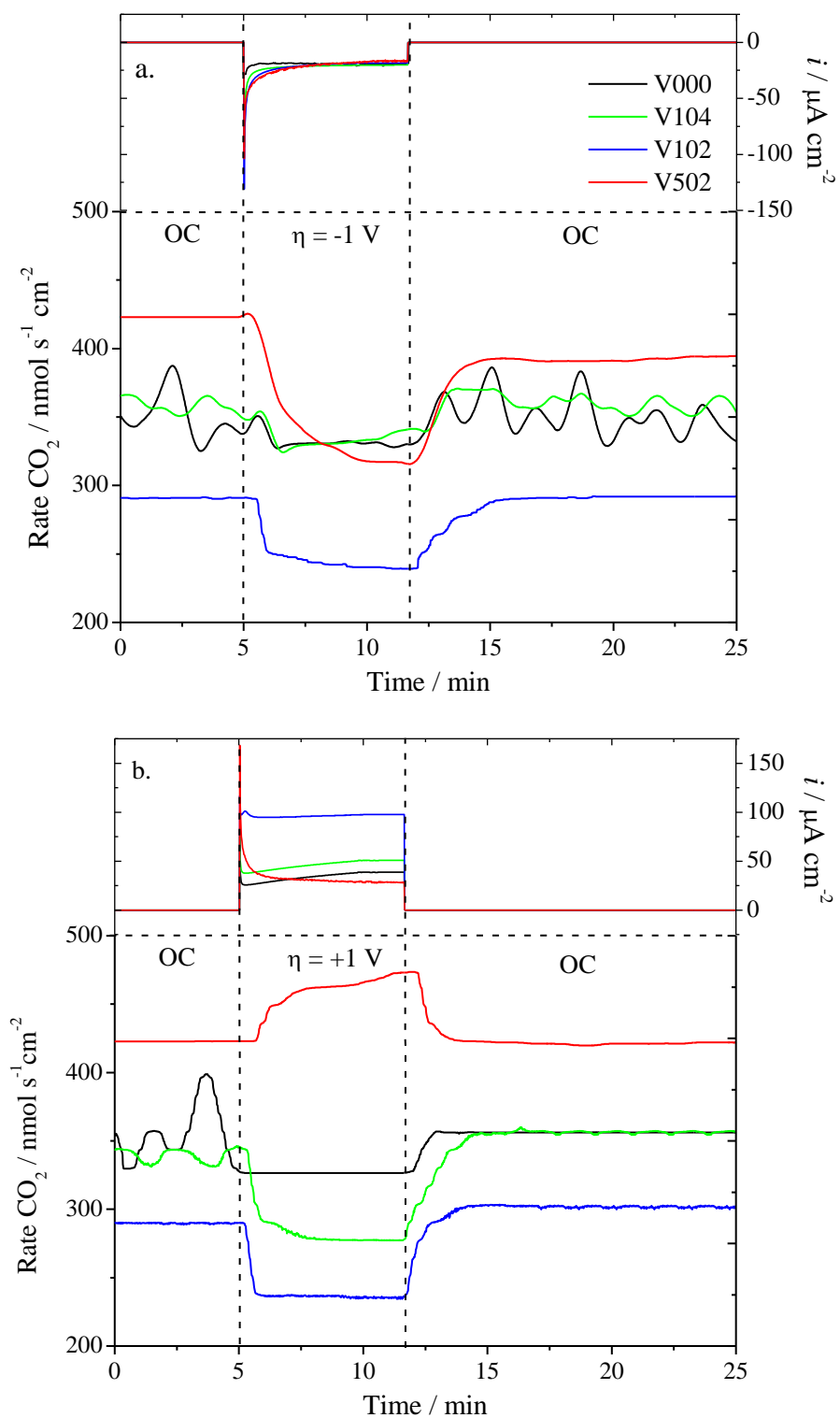
Figure 0.4. Transient plots under high p_{O_2} and polarisation: (a) $\eta = -1$ V; (b) $\eta = +1$ V. Top: Current density, i versus time; Bottom: CO_2 rate versus time. Reactant partial pressures, $p_{O_2} = 8$ kPa, $p_{C_2H_4} = 0.5$ kPa; Temperature = 350°C; Total flow rate = 200 ml min^{-1}.

Table 0.2. Rate enhancement ratios and Faradaic efficiencies of all samples

Negative polarisation

p_{O_2} (kPa)	$\rho_{(-1\,V)}$				$\Lambda_{(-1\,V)}$			
	V000	V104	V102	V502	V000	V104	V102	V502
0.5	1.35	2.23	1.30	1.01	-138	-505	-299	-55.2
1.5	1.27	2.03	1.32	0.83	-177	-871	-724	322
3	1.28	1.84	0.88	0.76	-330	-1323	336	473
8	1.00	0.94	0.83	0.75	-2.12	172	666	1170

Positive polarisation

p_{O_2} (kPa)	$\rho_{(+1\,V)}$				$\Lambda_{(+1\,V)}$			
	V000	V104	V102	V502	V000	V104	V102	V502
0.5	1.02	0.94	1.10	0.85	8.37	-65.7	29.5	-108
1.5	0.89	0.89	0.89	0.79	-148	-33.3	-84.9	-104
3	0.82	0.85	0.72	1.00	-1142	-157	-169	1.93
8	0.80	0.81	0.92	1.12	-1015	-283	-45.6	347

As can be seen here the reaction shows in general electrophilic behaviour for sodium coverage less than 1% (Sample V104) and oxygen partial pressure up to 3 kPa (i.e. fuel rich to mildly fuel lean conditions) since application of a negative potential (Figure 0.3a) leads to an increase of the reaction rate while positive potential causes a rate decrease (Figure 0.3b). This has also been observed in our previous work in the cyclic voltammetry section (Section7.2.1), where an increase in the rate of CO_2 production with negative polarisation (η = -1 V) and a decrease with positive polarisation (η = +1 V) was observed for the nominally 'clean' sample and the low-sodium modified sample (V104, 0.11% Na coverage). Under constant negative polarisation, the reaction rate increases non-Faradaically with a rate enhancement ratio maximum of 2.23 and a Faradaic efficiency up to -1300. As shown in Table 0.2, the reaction becomes volcano-type for oxygen partial pressures of 8 kPa (at all sodium coverages) while the oxygen partial pressure where volcano behaviour is first observed decreases with increasing sodium coverage (so for a sodium coverage of 65% the reaction exhibits volcano-type behaviour even at sub-stoichiometric oxygen to ethylene ratios, $p_{O_2}/p_{C_2H_4}$ = 1). In addition for a sodium coverage of 65% and an oxygen partial

pressure of 8 kPa the reaction becomes electrophobic as a rate enhancement (with $\rho = 1.1$ and $\Lambda = 272$) is only observed under positive polarisation (Figure 0.4b).

In addition, under high oxygen partial pressures (Figure 0.4a-b), we can observe that the clean sample and the one with low sodium coverage (0.11%, A104) behave in a similar way; i.e. both show an oscillation in the initial CO_2 production rate under open-circuit conditions. The rate is stabilised (to a slightly lower value) by means of polarisation, particularly when using positive overpotentials. We also note that for high sodium coverage (65%, A502) the rate takes a longer time to return to its initial value after depolarisation (full data not shown). This is an indication of a phenomenon known as permanent or 'persistent' EPOC that could be due to reasons such as stored promoting species (oxygen) on the catalyst surface (non-active sites) being released to the three-phase-boundaries (tpb) and its slow diffusion from the tpb towards the catalyst-gas interface [108, 143-144].

In terms of the current densities, it appears that the current density resulting from negative polarisation with -1 V does not vary significantly ($i = 16.9 \pm 2.7$ μA cm^{-2}) between the different sodium coverages as shown in the top of Figure 0.3a and Figure 0.4a and in Appendix D, suggesting that there may be a limiting current due to diffusion in the cathodic region. The presence of a limiting current in the cathodic region has also been shown previously in the steady state current versus overpotential measurement in Chapter 6. For positive polarisation, clearly the current densities of the high-sodium modified sample (V502, 65%) are always higher than the others except in the case under high p_{O_2} (8 kPa) as shown in Figure 0.4b when the reaction shows electrophobic behaviour. We have also seen previously under non-reactive conditions in Chapter 6 that high sodium coverage increases the anodic and cathodic current densities recorded during cyclic voltammetry experiments.

1.24.3. Discussion

The experimental data under varying sodium coverages and oxygen partial pressures exhibit the following key features:

- Increasing sodium coverage up to 65% appears to promote the open-circuit catalytic activity of the Pt/YSZ system for ethylene oxidation, but the sodium-induced rate enhancement is reduced by an increase in the oxygen partial pressure

- The system exhibits electrophilic behaviour at low sodium coverage and under rich fuel conditions to mild lean fuel conditions (p_{O_2} = 0.5-3 kPa), however this promotional behaviour appears to be changed to volcano and finally electrophobic by increasing oxygen partial pressure and sodium coverage

We will now test the work function dependence model proposed earlier on with the experimental data obtained in this work. We will initially consider the case of low oxygen partial pressures where the reaction showed electrophilic behaviour. Work function changes for samples of 0.11% and 11% coverage have been measured to be 0.2 and 0.25 eV respectively (as shown in Chapter 4). We must, however, note that these measurements were performed under ambient conditions and may as a result deviate from the work function changes caused by sodium addition under reaction conditions. The work function change (1.86 eV) caused by a sodium coverage of 65% was extrapolated assuming a linear dependence between work function and sodium coverage [2]. For the electrical polarisation we assume that $\Delta\Phi = e\Delta V_{WR}$. Figure 0.5 shows the rate dependence on work function change for an oxygen partial pressure of 1.5 kPa (data for other oxygen partial pressures are shown in Appendix D).
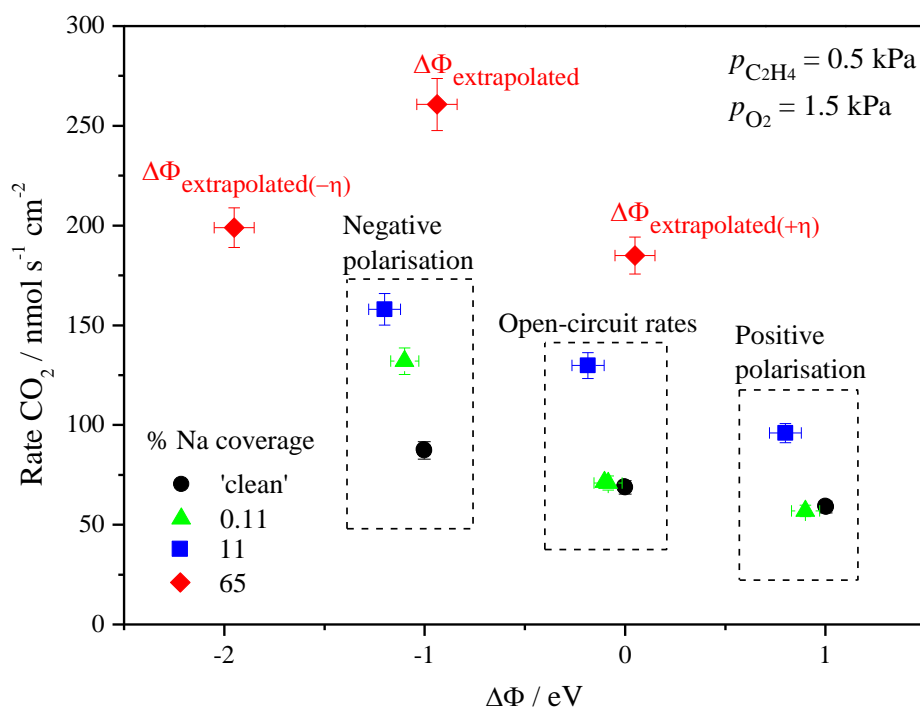
Figure 0.5. CO_2 production rate versus the change in the catalyst work function under stoichiometric fuel conditions. Reactant partial pressures, $p_{O_2} = 1.5$ kPa, $p_{C_2H_4} = 0.5$ kPa; Temperature = 350°C; Total flow rate = 200 ml min⁻¹.

The three sets of data in the dotted boxes correspond to the nominally 'clean' sample (circle) and those modified with 10^{-4} M (0.11% Na coverage, triangle) and 10^{-2} M (11% Na coverage, star) NaOH solutions. As we can observe in the figure in general the reaction rate changes at low sodium coverage (0.11%) follow the proposed work-function dependent behaviour for an electrophilic reaction, where negative polarisation generally enhances the reaction rate due to a decrease in the catalyst work function, while positive polarisation reduces the reaction rate as it increases the catalyst work function. While we can comment on a qualitative agreement between the proposed model and the experimental data, we can also notice some deviations from the model that suggest further interaction between either the two promoting species or between the promoters and the reactants or any reaction intermediates. In particular, we can observe that while a sodium coverage of 0.11% does not significantly change the reaction rate it induces a much higher electropromoted rate at negative polarisation than that of a clean pellet. This suggests that there is an interaction between the oxygen species leaving the catalyst surface and the sodium species existing on

113

the catalyst surface. The total rate increase for the sodium-modified electropromoted sample is not therefore equal to the addition of the rate changes from sodium addition and polarisation alone. This can be seen in Figure 0.3 and Figure 0.4. Moreover, as discussed earlier on and is also shown in Figure 0.3 at high sodium coverage the reaction changes behaviour to volcano-type. It has been postulated that at high sodium coverage we may expect to find a stronger interaction between the sodium and the oxygen from the gas phase due to the metallic character of sodium on the catalyst surface that enhances oxygen adsorption.

The decrease in the work function is known to enhance the heat of adsorption and thus the chemisorptive bond strength of electronegative (electron acceptor) adsorbates, and decrease the heat of adsorption and thus the chemisorptive bond strength of electropositive (electron donor) adsorbates [88]. Vayenas justified the promotion induced by electronic promoters in terms of this work function dependent adsorption model [2, 40-41, 134], whereby the sodium induced work function decrease results in increased oxygen (electron acceptor) surface coverage at the expense of ethylene (electron donor) due to the respective increase and decrease in the adsorption energy. The reaction rate is enhanced as the oxygen adsorption increases in the cases where the reaction rate is shown to be first-order in oxygen. The same analogy can be used here to explain the increase in the reaction rate with a decrease in the catalyst work function by sodium addition and negative polarisation. Note that under closed-circuit conditions, there are two promoter species in the system, i.e. the deposited sodium (electropositive promoter) and the electrochemically supplied oxygen (electronegative promoter) which have contradictory effect on the catalyst work function. The electronegative oxygen anion, as opposed to the electropositive sodium cations, is known to increase the metal work function, thus strengthening the chemisorptive bond of electropositive (electron donor) adsorbates, and weakening the chemisorptive bond of electronegative (electron acceptor) adsorbates [2]. For an electrophilic reaction, an increase in the electronegative promoter decreases the reaction rates as it increases the metal work

function, while for an electrophobic reaction the decrease in the work function by an increase in the electropositive promoter decreases the reaction rate. This explains why the magnitude of the reaction rate changes caused by sodium addition and positive polarisation (where oxygen promoter is supplied to the metal surface) is dependent on the contradictive effect exhibited by both types of promoters. On the contrary, sodium addition and negative polarisation (where oxygen promoter is removed from the metal surface) can thus decrease the metal work function and synergistically enhances the reaction rate.

Next we will further discuss the role of sodium on the changing behaviour of the reaction under EPOC conditions. As mentioned earlier the reaction behaviour changes with increasing oxygen partial pressure and sodium coverage from electrophilic, to volcano and finally to electrophobic. This is shown schematically in Figure 0.6a, while Figure 0.6b illustrates this shifting behaviour with experimental data. Under polarisation, the electrophilic behaviour observed at low sodium coverage and under low oxygen partial pressure can simply be explained by stronger ethylene (electron donor reactant) adsorption, in accordance to the more ionic character sodium exhibits at low coverage, in comparison to oxygen (electron acceptor reactant) adsorption. An increase in sodium coverage (and also gas phase oxygen) however may result in an increase in oxygen coverage, and possibly also modify the competitive adsorption between oxygen and ethylene, as sodium becomes more metallic. In the intermediate region of sodium coverage and oxygen partial pressure volcano behaviour should then be observed (where both reactants are strongly adsorbed), while at high sodium coverage, when eventually the oxygen becomes more strongly adsorbed than the ethylene, the electrophobic behaviour can occur. In the intermediate region of sodium coverage and oxygen partial pressure volcano behaviour was observed (where both reactants are strongly adsorbed), while at high sodium coverage, when eventually the oxygen gets more strongly adsorbed than the ethylene, the electrophobic behaviour can occur.

a. Schematic

i. Electrophilic   ii. Volcano   iii. Electrophobic

Sodium coverage and gas phase oxygen concentration (p_{O_2})
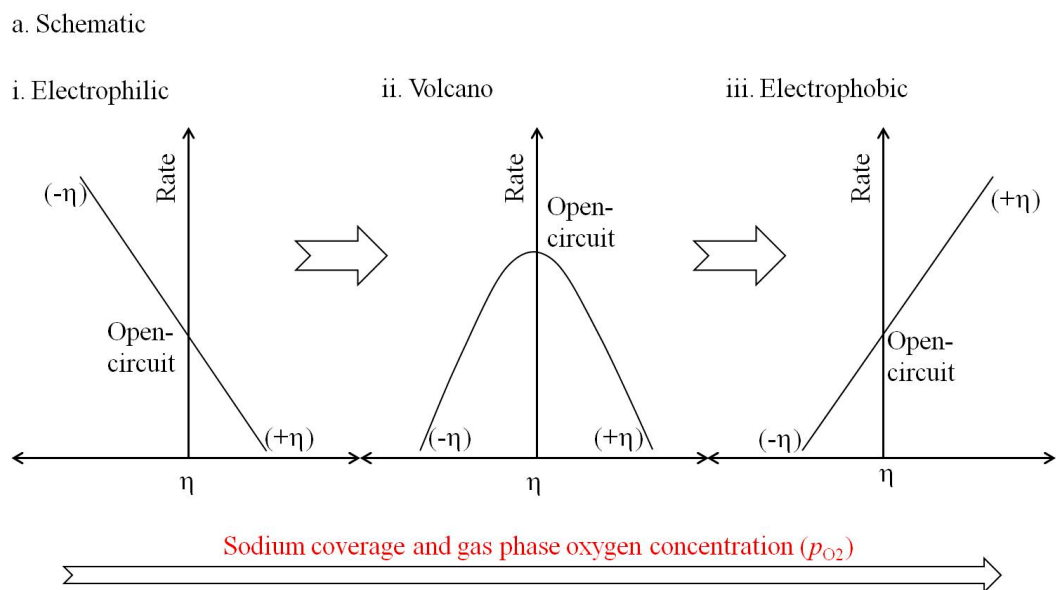
b. Experimental data
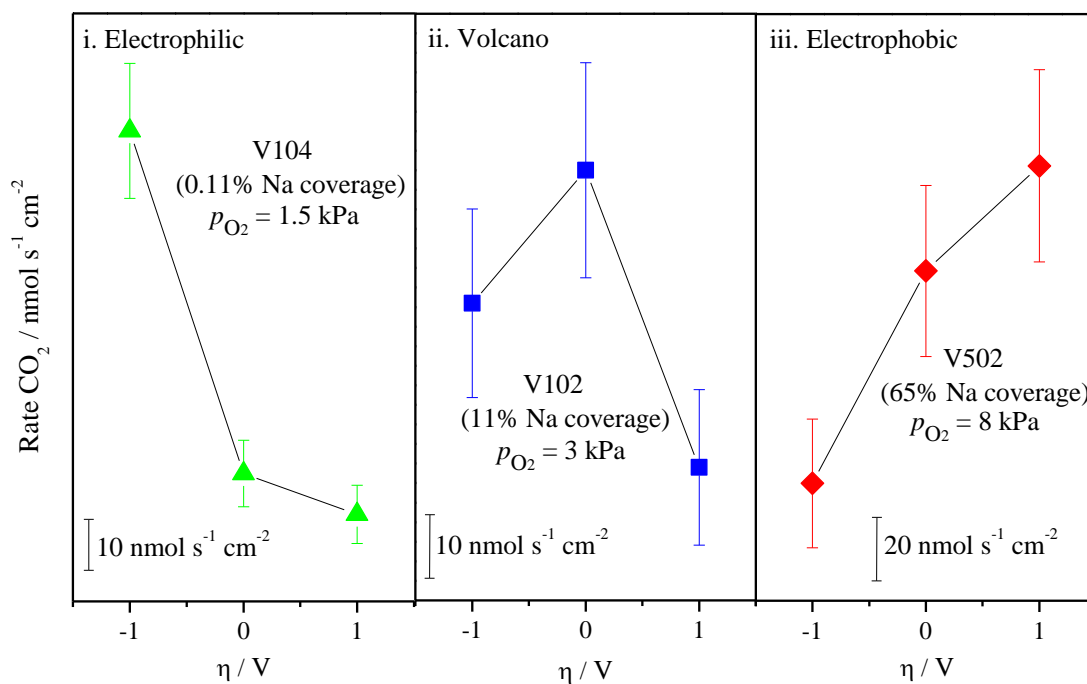
Figure 0.6. The behavioural changes as a function of sodium coverage and oxygen partial pressure: (a) Schematic representation and (b) Experimental data (example for each case)

The influence of oxygen partial pressure on the behaviour of the reaction may also be explained by the observed (in the literature [145]) change in the nature of the sodium

species on the catalyst surface. At low coverage sodium has a more ionic character while, as its coverage increases sodium become more metallic in nature and therefore interaction with an electron acceptor adsorbate (such as oxygen) may become more significant. This could strengthen the chemisorptive bond of oxygen thus lowering the necessary oxygen partial pressure to change the reaction to volcano-type (and eventually electrophobic). This refers to Table 0.2 where we can see that the oxygen partial pressure where volcano behaviour is first observed decreases with increasing sodium coverage.

This change in the apparent behaviour of the reaction, which is caused primarily by the sodium addition, is in fact a manifestation of the complexity of the interaction between all the species (reactive, promoting and catalyst) of this catalytic system. The fact that the presence of surface species has such an effect on the catalyst properties could be used to explain some of the differences in experimental results presented by different research groups on similar catalyst systems where the raw materials are often obtained from different sources. As an example, while most studies conducted on the electrochemical promotion of ethylene oxidation on Pt/YSZ show that the reaction exhibits electrophobic behaviour for a wide range of conditions [26, 55] in our work the reaction showed clear electrophilic behaviour for a nominally clean pellet; this may simply be due to the presence of different impurities on the raw materials used for the preparation of the different samples. This suggests that while surface species may not be necessary for the occurrence of EPOC they can significantly affect the behaviour of the system.

1.25. Summary

The study presented here showed that the presence of foreign surface species on a catalyst can significantly affect its catalytic and electrocatalytic properties. We cannot however, based on the evidence obtained from this work assess the necessity of such surface species for the occurrence of EPOC. In the case of sodium addition onto a platinum catalyst the

observed behavioural changes have been partially explained by a model that considers work function changes caused by each promoter species independently. The model can, for low sodium coverage predict an additive effect between sodium addition and polarisation. However, experimental results indicated that the two promoter species are not completely independent of each other especially at high sodium coverage. With increasing sodium coverage the reaction behaviour changes from electrophilic to volcano-type (possible to an increase in the chemisorptive bond strength of oxygen on the platinum catalyst), while for high sodium coverage, where the sodium is known to adopt a more metallic character, interaction with oxygen becomes more significant and the reaction shows electrophobic behaviour.

NO Reduction by Propene

1.26. Introduction

This chapter discusses the role of sodium surface species on the catalytic and electropromoted properties of the Pt/YSZ system for NO reduction by propene. In this case, the catalyst system is exposed to a feed composition of 0.1 kPa C_3H_6, 0.1 kPa NO and 0.5-5 kPa O_2, balanced in He. Under such conditions, the following reactions can take place in the Pt/YSZ system [110]:

$$C_3H_{6(g)} + \frac{9}{2}O_{2(g)} \rightleftharpoons 3CO_{2(g)} + 3H_2O_{(g)} \tag{8.1}$$

$$C_3H_{6(g)} + 9NO_{(g)} \rightleftharpoons 3CO_{2(g)} + \frac{9}{2}N_{2(g)} + 3H_2O_{(g)} \tag{8.2}$$

$$C_3H_{6(g)} + 18NO_{(g)} \rightleftharpoons 3CO_{2(g)} + 9N_2O_{(g)} + 3H_2O_{(g)} \tag{8.3}$$

$$NO_{(g)} + \frac{1}{2}O_{2(g)} \rightleftharpoons NO_{2(g)} \tag{8.4}$$
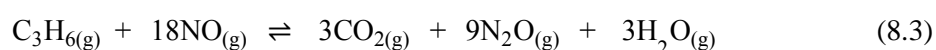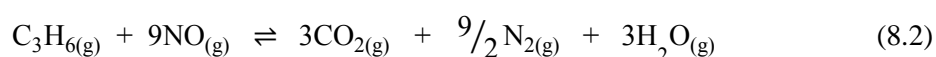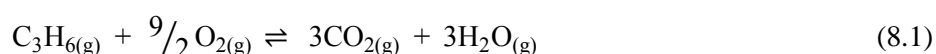
Cyclic voltammetry and chronoamperometry (potentiostatic transient) experiments were mainly used in this work. The results obtained from the experiments will be discussed based on the model proposed in Chapter 5 for reactive conditions and compared to the findings from the simpler probe reaction, i.e. ethylene oxidation study.

1.26.1. Reaction rates, catalytic activity and selectivity

The activity of the 'clean' catalyst and the sodium-modified ones was calculated from the measured concentrations (partial pressures) of CO_2, NO, NO_2 and N_2O (p_{CO_2}, p_{NO}, p_{NO_2} and p_{N_2O} respectively). The reaction rate calculations were as shown in Equations 7.2-7.4 of the previous chapter and re-written here:

$$\text{Rate } X \left(\text{nmol s}^{-1} \right) = [X]/100 \times F_m \tag{8.5}$$

where $[X]$ is the partial pressure of the gases (X could be any of CO_2, NO, NO_2 and N_2O) and F_m is the total molar flow rate measured at STP. From the ideal gas equation at STP we have:

$$F_m = F_V/60 \left(\text{ml min}^{-1}/\text{s min}^{-1} \right) \times 1/22400 \, (\text{mol ml}^{-1}) \Rightarrow$$

$$\Rightarrow F_m = 7.4 \times 10^{-7} \, F_V \, (\text{mol s}^{-1}) \tag{8.6}$$

where F_V is the measured volumetric flow rate in ml min^{-1} (STP). Combining Equations 8.5 and 8.6 produces the final expression for the reaction rate calculation, while dividing with the platinum electrode area, A gives the area specific rate:

$$\text{Rate } X \left(\text{nmol s}^{-1} \text{ cm}^{-2} \right) =$$

$$= 10^9 (\text{nmol/mol}) \times [CO_2]/100 \times \left[7.4 \times 10^{-7} \times F_V/A \right] (\text{mol s}^{-1} \text{cm}^{-2}) \tag{8.7}$$

The N_2 production rate was calculated based on the balance between the total nitrogen in the inlet (Total N_i) and the outlet (Total N_o) streams as shown in Equations 8.8- 8.9, followed by applying p_{N_2} in Equations 8.5-8.7. The inlet stream was passed through the bypass line as shown in the experimental rig (Figure 3.5) in Chapter 3 until stable Total N_i was achieved. The N_2 production was occasionally checked with GC to confirm validity of calculation.

$$\text{Total N} = p_{NO} + p_{NO_2} + 2(p_{N_2O}) \tag{8.8}$$

$$p_{N_2} = (\text{Total } N_i - \text{Total } N_o) / 2 \tag{8.9}$$

As showed in Equations 8.2, 8.3 and 8.4, NO reacts with C_3H_6 and/or O_2 to produce N_2, N_2O and also NO_2. The selectivity of NO to produce N_2 (Reaction 8.2) is desired. The catalyst selectivity to N_2, N_2O and NO_2 can be calculated as follows:

$$S_{N_2} = 100 * [p_{N_2} / (p_{N_2} + p_{N_2O} + 2p_{NO_2})]$$ (8.10)

$$S_{N_2O} = 100 * [p_{N_2O} / (p_{N_2} + p_{N_2O} + 2p_{NO_2})]$$ (8.11)

$$S_{NO_2} = 100 * [p_{NO_2} / (\frac{p_{N_2}}{2} + \frac{p_{N_2O}}{2} + p_{NO_2})]$$ (8.12)

where p_{N_2}, p_{N_2O} and p_{NO_2} are the partial pressure of N_2, NO_2 and N_2O in the outlet gas, respectively. Under the conditions studied, the C_3H_6 conversion is between 5 to 40% (depending on p_{O_2} and sodium coverage), whereas the NO conversion is below 5% (differential rate). As mentioned in Section 7.1.1, no error bars are used in the figures for transient data as rate changes can be seen as function of time. An error bar corresponding to 5% error is used in the plots where discreet rate data are shown based on the accuracy of $NO-NO_2-N_2O$ analyser for NO, N_2O and N_2O detection.

From the CO_2 production, we also calculate the percentage of CO_2 produced from direct propene oxidation and indirectly from NO reduction via reactions 8.2 and 8.3. From Equations 8.2 and 8.3 we can see that for every 3 moles of CO_2 produced, 4.5 moles of N_2 and 9 moles of N_2O are produced respectively. Therefore the CO_2 produced from NO reduction and oxidation can be calculated as follows:

$$S_{CO_2\text{-red}} = [(X_{CO_2\text{-}N_2} * p_{N_2}) + (X_{CO_2\text{-}N_2O} * p_{N_2O})] / \text{total } p_{CO_2}$$ (8.13)

$$S_{CO_2\text{-ox}} = 1 - S_{CO_2\text{-red}}$$ (8.14)

where $X_{CO_2\text{-}N_2}$ (0.67) and $X_{CO_2\text{-}N_2O}$ (0.33) are the mole fractions of CO_2 produced with every N_2 and N_2O produced, while p_{N_2}, p_{N_2O} and p_{CO_2} correspond to the partial pressure of N_2, N_2O and CO_2 in the outlet gas.

1.27. Results and discussion

1.27.1. Cyclic voltammetry

1.27.1.1. General features

This section discusses the cyclic voltammetry experiments conducted under various gas compositions and sodium coverages, with some data obtained under non-reactive conditions to check for reproducibility. In Chapter 6 the CV technique has also been utilised as a means to investigate the role of variable-coverage sodium on oxygen charge transfer. Similar CV with varying scan rates to that discussed in Chapter 6 are revisited in Figure 0.1a, except that the CVs here were obtained at $350^{o}C$ and from a different sample that was used for both NO reduction and C_2H_4 oxidation experiments (Sample V). Typical platinum CVs under oxygen flow can be seen with the 'clean' sample (V000) in Figure 0.1a; there are two peaks in the anodic and cathodic regions, i.e. the anodic and cathodic peaks respectively. The anodic and cathodic peak currents densities, i_{pa} and i_{pc}, are increased with increasing scan rates as observed previously at $400^{o}C$ in Chapter 6. Low and medium sodium coverages (0.11%, V104 and 11%, V102) do not appear to significantly affect the voltammogram features, but high sodium coverage (65%, V502) causes a decrease in the i_{pc} indicating a slower rate of charge transfer possibly because of active sites blocking by sodium surface species. The shrink in the i_{pc} at high sodium coverage however is not accompanied by an increase in the total current densities as seen in Chapter 6. This could be due to several reasons such as different operating temperature ($350^{o}C$ instead of $400^{o}C$), different thickness and porosity of sample and exposure to various reaction conditions (the sample has undergone a series of ethylene oxidation and NO reduction experiments under different gas compositions and sodium coverages).

The CVs in Figure 0.1b-d are produced under O_2, NO and C_3H_6 gas mixtures with varying p_{O_2} (0.5, 1 or 5 kPa), while p_{NO} and $p_{C_3H_6}$ are kept constant at 0.1 kPa. Here we can see that the exposure to the reaction mixture has removed the sharp cathodic peak (as well as

the barely detected anodic peak) seen under oxygen flow in Figure 0.1a, and sharply increased the current density at high overpotential, V_{WR} = -1 V. The current density at V_{WR} = -1 V is decreased by sodium addition, while increasing sodium coverage to 65% (V502) appears to increase the thickness (i.e. hysteresis at V_{WR} = 0) of the voltammogram, and consequently the total current densities. An increase in the total current densities has also been observed under non-reactive conditions in Chapter 6. This can be attributed to the enhancement of oxygen adsorption, oxygen diffusion and/or oxygen storage at high sodium coverage. This enhances the oxygen supply to the electrode, resulting in an increase in the flux towards the electrode as well as the current densities. As can be seen from Figure 0.1b-d, increasing the oxygen partial pressure in the reaction mixture also results in enhanced current densities, similar to the effect caused by increasing sodium coverage.
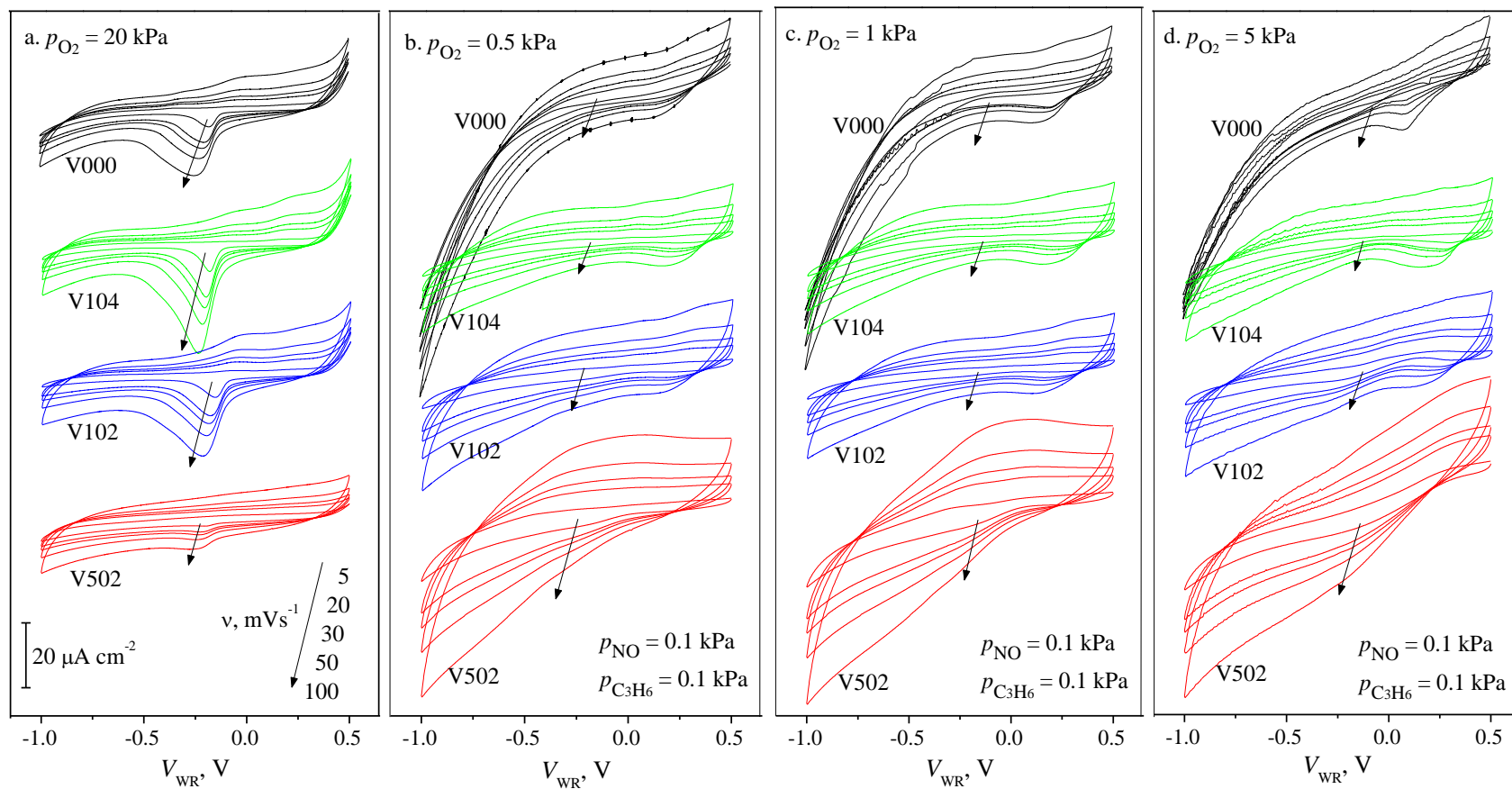
Figure 0.1. Platinum cyclic voltammograms of 'clean' and sodium-modified samples with varying scan rates: (a) Oxygen flow; p_{O_2} = 20 kPa; (b-d) Flow of O_2, NO and C_3H_6 gas mixture (p_{O_2} = 0.5, 1 or 5 kPa, p_{NO} = 0.1 kPa, $p_{C_3H_6}$ = 0.1 kPa). Temperature: 350°C; Total flow rate: 100 ml min^{-1}.

To further understand the CVs, similar experiment was also performed under single gas exposure and several gas mixtures i.e. (a) O_2, (b) NO, (c) C_3H_6, (d) O_2 and NO mixture, (e) O_2 and C_3H_6 mixture, (f) NO and C_3H_6 mixture and (g-i) a mixture of O_2, NO and C_3H_6 with varying p_{O_2} (0.5, 1 and 5 kPa) but constant p_{NO} and $p_{C_3H_6}$ at 0.1 kPa. Only the CVs of Sample V104 are shown in Figure 0.2 as the other samples show similar current versus potential behaviour.
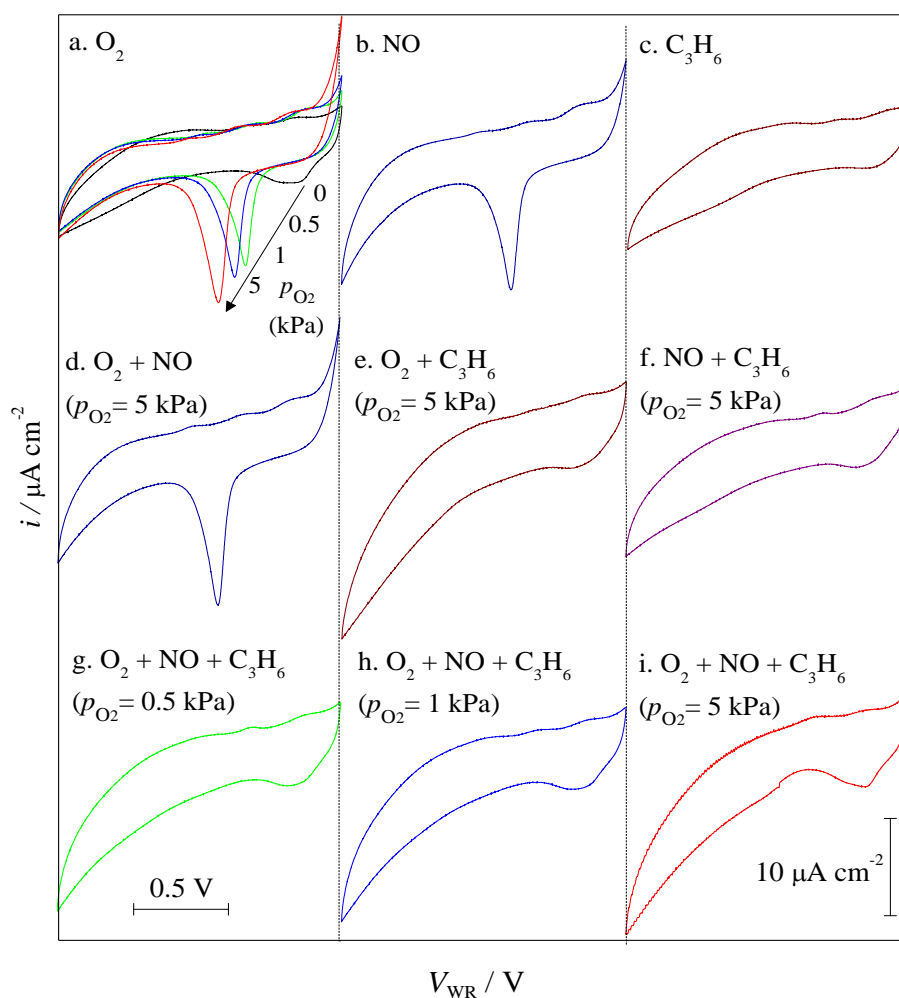
Figure 0.2. CV of Sample V104 (0.11% Na coverage) under various gas atmospheres: (a) 0-5 kPa O_2; (b) 0.1 kPa NO; (c) 0.1 kPa C_3H_6; (d) 5 kPa O_2 and 0.1 kPa NO; (e) 5 kPa O_2 and 0.1 kPa C_3H_6; (f) 0.1 kPa C_3H_6 and NO; (g) 0.5 kPa O_2, 0.1 kPa C_3H_6 and NO; (h) 1 kPa O_2, 0.1 kPa C_3H_6 and NO; (i) 5 kPa O_2, 0.1 kPa C_3H_6 and NO. Temperature: 350°C; Total flow rate: 100 ml min^{-1}; Voltage range: 0.5 to -1 V; V_{WR} start = 0.5 V; Scan rate, ν = 20 mV s^{-1}.

In Figure 0.2a, we can see again that increasing oxygen partial pressure increases the cathodic peak current density, i_{pc}, and shifts the cathodic peak position towards more negative potential. As discussed in Chapter 6 under non-reactive conditions, this could be due to oxygen being more strongly bround on the catalyst surface, thus more negative potential are required for the reduction process to take place. Figure 0.2b and d show that an exposure to NO does not affect the cathodic peak; the peak is in fact very similar to those produced under oxygen flow, whereas He and C_3H_6 (Figure 0.2a and c) eliminate the peak. This according to Dorado et al [146] whose work is on sodium ion conductor (Na-β''-Al_2O_3) suggests that the sodium promoter species does not form any surface compound with these species (i.e. He and C_3H_6). They also observed a cathodic and an anodic peak under gas mixture of 0-5% O_2, 0.2% NO and 0.2% C_3H_6 which are similar to that seen under oxygen flow, indicating the occurrence of an electrode reaction. The cathodic peak has been linked to the backspillover of sodium ions as detected by Makri et al. using scanning tunnelling microscopy [79, 146]. On the contrary, no significant peak can be observed in this study under gas mixture of 0.5-5% O_2, 0.1% NO and 0.1% C_3H_6 (Figure 0.2e-i). A small cathodic peak can be seen under positive potential in Figure 0.2e-i, but this peak also exists under flow of inert gas (helium) as shown in Figure 0.2a.

1.27.1.2. Reaction rates during CV

Sodium modification of the reaction rates during a cyclic voltammetry experiment was also investigated. Figure 0.3 and Figure 0.4 show the current response (reported as area specific current or current density, i) and the corresponding variation in the CO_2 production rate under low and high oxygen partial pressures; p_{O_2} = 0.5 kPa and 5 kPa respectively. The corresponding N_2 production rate is not shown because no significant rate changes versus the scanned potential were observed. The N_2 production will only be discussed under constant polarisation in the next section. From Figure 0.3a and Figure 0.4a, we can see that due to the use of higher scan rates, the current densities recorded for the 'clean' and low-sodium

modified samples (V000 and V104) are higher than those for medium and high-sodium modified samples (V102 and V502).
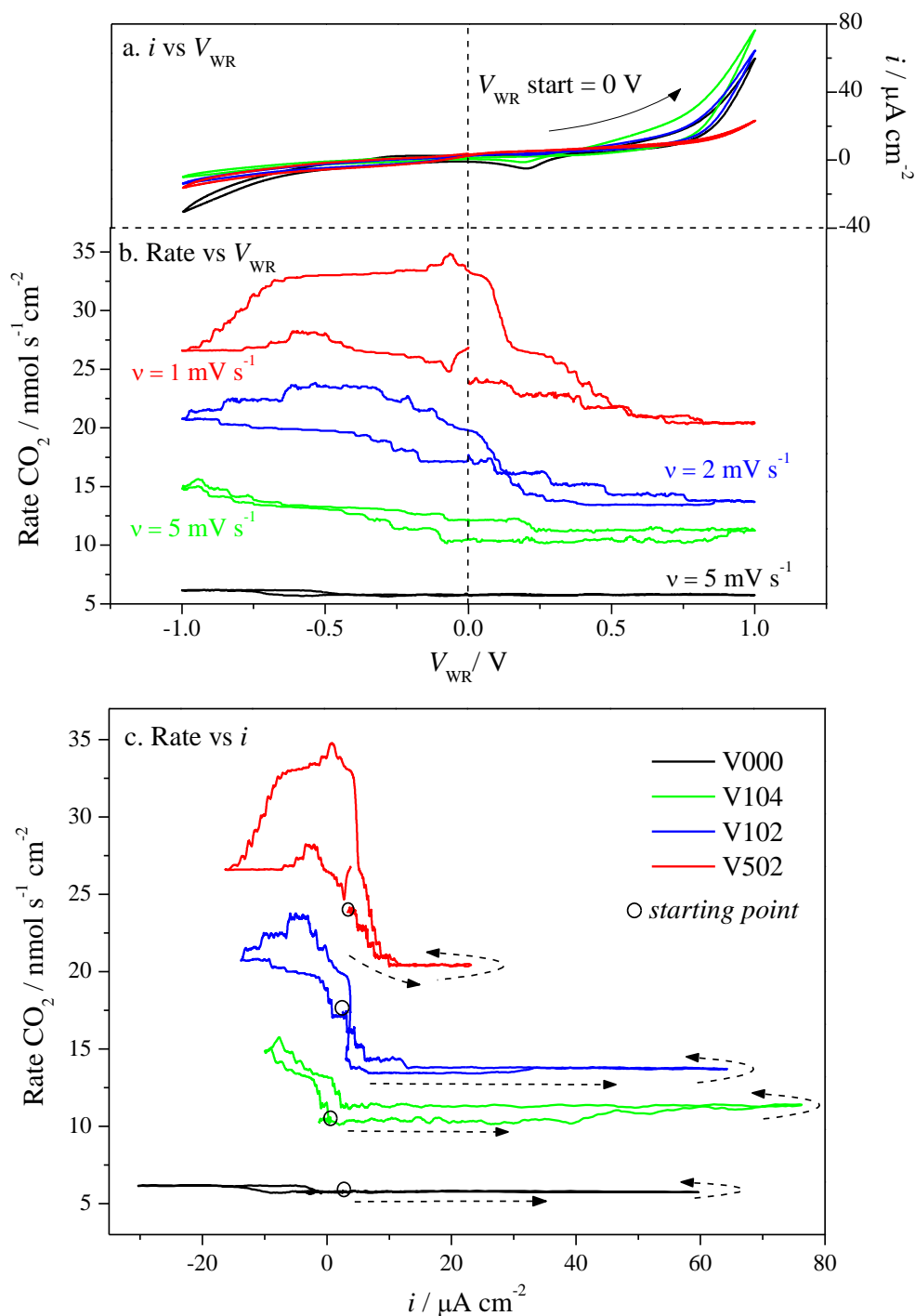
Figure 0.3. Cyclic voltammetry under low oxygen partial pressure: (a) i vs U_{WR}; (b) Rate vs U_{WR}; (c) Rate vs i. Reactant composition: $p_{O_2} = 0.5$ kPa, $p_{NO} = p_{C_3H_6} = 0.1$ kPa; Temperature = 350°C; Total flow rate = 100 ml min^{-1}.
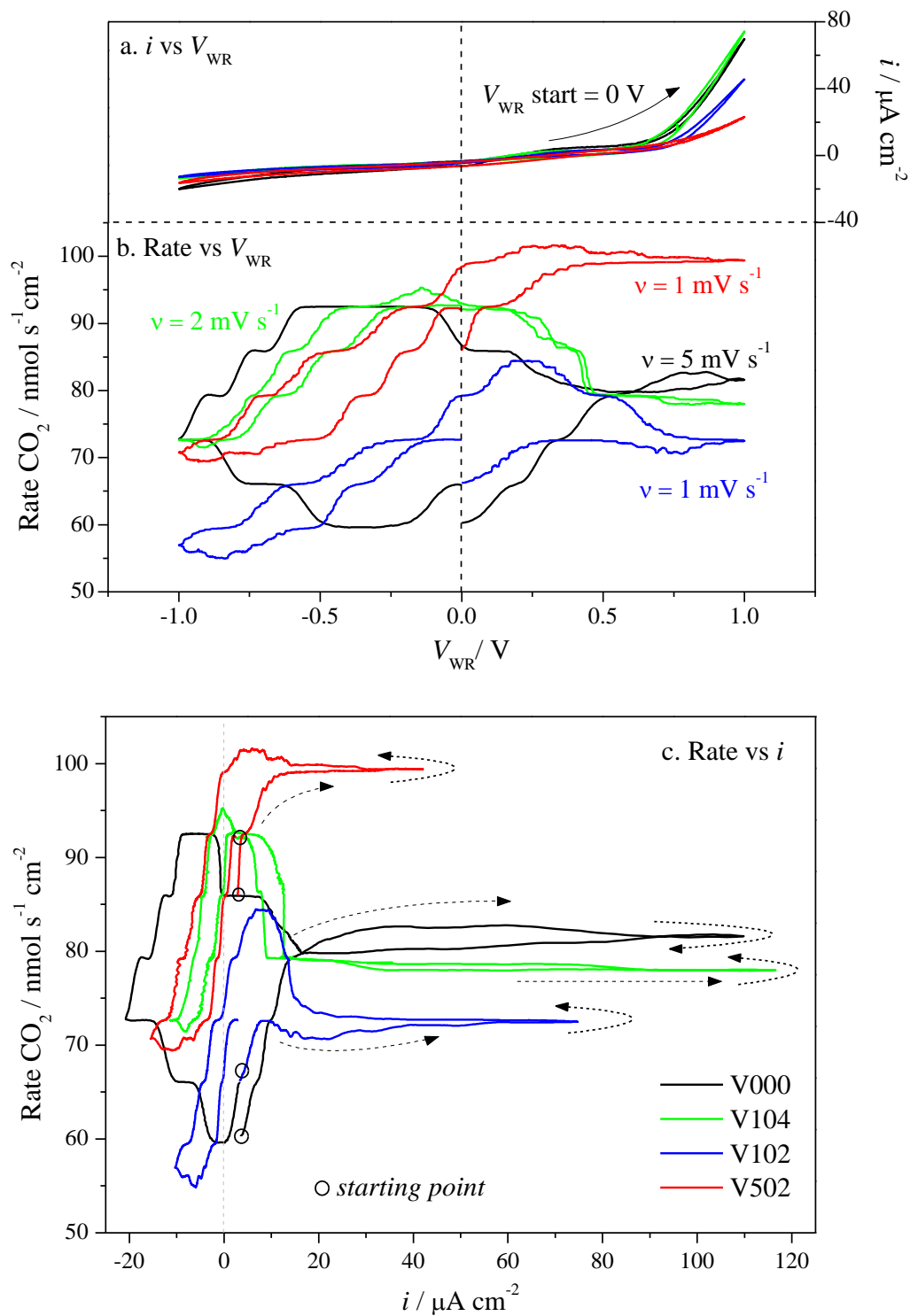
Figure 0.4. Cyclic voltammetry under high oxygen partial pressure: (a) i vs U_{WR}; (b) Rate vs U_{WR}; (c) Rate vs i. Reactant composition: $p_{O_2} = 5$ kPa, $p_{NO} = p_{C_3H_6} = 0.1$ kPa; Temperature = 350°C; Total flow rate = 100 ml min^{-1}.

As can be seen in Figure 0.3b-c under low p_{O_2} (0.5 kPa), the CO_2 production rates are generally higher in the cathodic region than in the anodic region, indicating that the system shows electrophilic behaviour. The 'clean' sample achieves rate maximum at i around -10 µA cm^{-2}. As we increase the sodium coverage from 0.11 to 65% (V104 < V102 < V502), it appears that the current density at which maximum rate is achieved also shifts towards more positive values (-8 < -5 < 1 µA cm^{-2}). This has also been seen under ethylene oxidation in Section 7.4.1. Under high p_{O_2} (5 kPa), we can see that the reaction rates in Figure 0.4b reach minimum in the cathodic region and maximum towards more anodic potentials. For instance, the reaction rates of the 'clean' (V000) and low-sodium modified samples (0.11%, V104) in Figure 0.4c find maximum at $i \approx$ -4 µA cm^{-2} and near zero-current respectively, while the medium (11%, V102) and high-sodium modified samples (65%, V502) reach maximum at $i \approx$ 5 µA cm^{-2}. At high sodium coverage (65%, V502), the reaction rate achieves maximum in the anodic region and minimum in the cathodic region; indeed an indication of electrophobic behaviour, in contrast to the electrophilic behaviour seen under low oxygen partial pressure in Figure 0.3. It becomes clear that as seen during the ethylene oxidation experiments discussed in Chapter 7, increasing sodium coverage and oxygen partial pressure also causes this reaction to become electrophobic. In between the coverages, volcano-type behaviour is also observed where the reaction rate is maximum at zero current density (V_{WR} = 0), and minimum under both positive and negative overpotentials e.g. as clearly shown by low sodium coverage (0.11%, V104) in Figure 0.4c. In addition, the low-sodium modified sample (0.11%, V104) in Figure 0.4 show similar initial rates to the 'clean' ones (V000); this has also been seen with ethylene oxidation under high p_{O_2} (8 kPa). The medium-sodium modified sample (11%, V102) has the lowest rates, while the high-sodium modified sample (65%, V502) has the highest rate. However, the reaction rates recorded during a CV experiment may also depend on the voltage scan rates whereby slower scan rates may be needed under certain reaction conditions to achieve surface equilibrium. For example the use of higher scan rate (5 mV s^{-1}) for the 'clean' sample (V000) under high p_{O_2}

produces a CV (in Figure 0.4) that is ill-defined and shows large variation in the reaction rates measured at the same potential (or current) on the reverse sweep.

1.27.2.   *Kinetic study*

1.27.2.1. Open-circuit conditions

First sodium modification of the reaction rates under open-circuit conditions (OC) will be discussed. Figure 0.5a and b show the open-circuit CO_2 and N_2 production rate as a function of oxygen partial pressure and sodium coverage. The corresponding sodium rate enahancement ratio, ρ_{Na} is shown in Table 0.1. As mentioned in Chapter 7, ρ_{Na} is defined as the open-circuit rate of the sodium-modified sample over the 'clean' sample's. The ratio, ρ_{Na} > 1, indicates that the reaction rate is promoted by sodium, while ρ_{Na} < 1 refers to rate inhibited by sodium. The magnitude of CO_2 (10^{-8} mol $s^{-1}cm^{-2}$) and N_2 (10^{-9} mol $s^{-1}cm^{-2}$) production rates observed in this study are comparable to the reaction rates reported in the study of NO reduction by C_3H_6 on Pt/Na-β''-Al_2O_3 system under slightly different feed composition of NO/C_3H_6/O_2 (0.2%/0.2%/0.5-5%), and at lower temperature (T = 240°C) [64]. Typical open-circuit voltages (OCV) of the system are between -100 to -300 mV.

As shown in Figure 0.5a, the CO_2 production rates of the 'clean' and sodium-modifed samples are generally increased by increasing oxygen partial pressures from p_{O_2} = 0.5 to 5 kPa. Sodium addition at low coverage (0.11%, V104) first appears to reduce the reaction rate, while further increase in sodium coverage up to 65% (V502) re-increases the reaction rate. For instance, the low-sodium modified sample (0.11%, V104) shows r_{CO_2} = 5, 10 and 59 nmol s^{-1} cm^{-2} under p_{O_2} = 0.5, 1 and 5 kPa respectively, which are lower than r_{CO_2} = 13, 33 and 77 nmol s^{-1} cm^{-2} exhibited by the nominally 'clean' sample (V000) under similar p_{O_2}. At high sodium coverage (65%, V502) the open-circuit rates are increased to 60, 67 and 100 nmol s^{-1} cm^{-2} under p_{O_2} = 0.5, 1 and 5 kPa respectively, with ρ_{Na} up to 4.62.
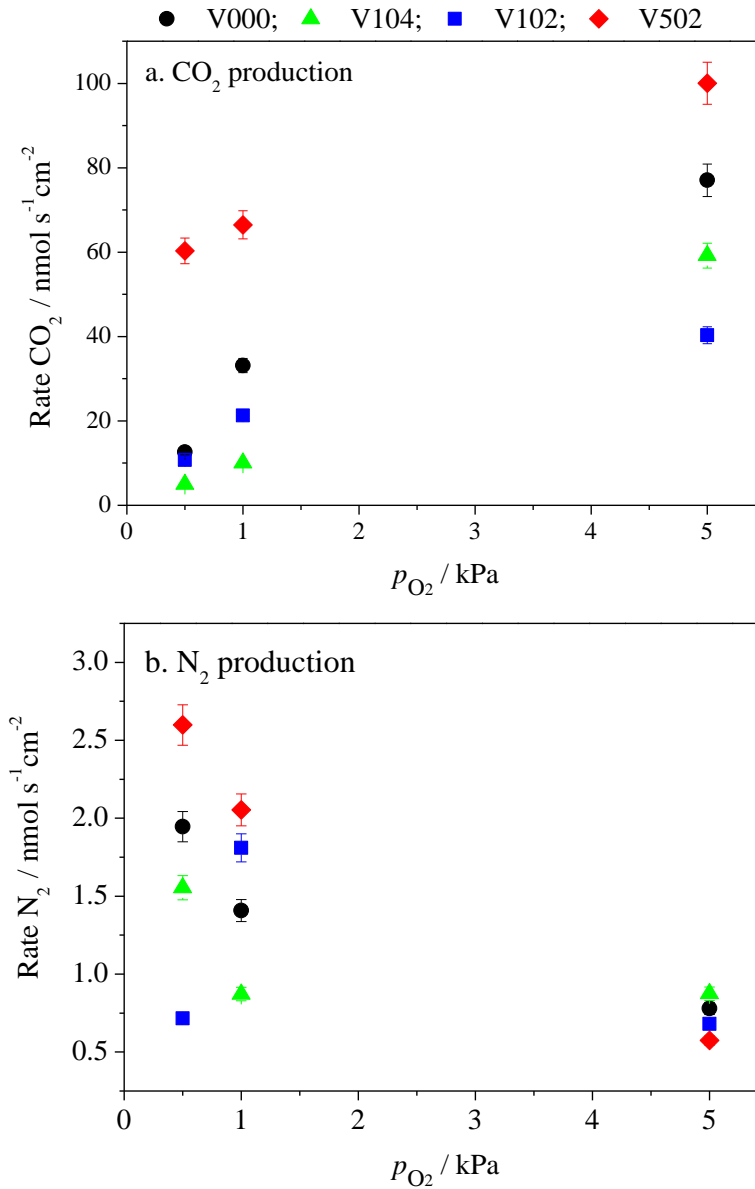
Figure 0.5. Open-circuit rates under varying oxygen partial pressures from $p_{O_2} = 0.5$-5 kPa: (a) CO_2 production and (b) N_2 production. Temperature: 350^oC; Total flow rate: 100 ml min^{-1}

Table 0.1. Rate enhancement ratio caused by sodium addition, ρ_{Na}

p_{O_2}	ρ_{Na} (CO_2 production)			ρ_{Na} (N_2 production)		
(kPa)	V104	V102	V502	V104	V102	V502
0.5	0.38	0.85	4.62	0.78	0.31	1.22
1	0.30	0.64	2.03	0.61	1.13	1.35
5	0.77	0.52	1.30	0.81	0.95	0.81

Similar to that seen for CO_2 production, the N_2 production rates in Figure 0.5b are generally decreased at low sodium coverage (0.11%, V104) and increased at high sodium coverage (65%, V502) with ρ_{Na} up to 1.35, which is not very significant. On the contrary, the N_2 production rates are reduced by increasing the oxygen partial pressure from $p_{O_2} = 0.5$ to 5 kPa. Under excess oxygen ($p_{O_2} = 5$ kPa) the N_2 production rates of all samples are low, possibly limited by the decrease in the N_2 selectivity which will be discussed later on. As can be seen from Table 0.1, the increase in the CO_2 and N_2 production appears to be more pronounced at high sodium coverage and under low oxygen partial pressures. This is similar to that seen under ethylene oxidation experiments in Chapter 7 where the reaction rate was also enhanced significantly at high sodium coverage and under low oxygen partial pressures.

1.27.2.2. Polarised conditions

Figure 0.6, Figure 0.7 and Figure 0.8 show the reaction rate transients under varying oxygen partial pressures; i.e. 0.5, 1 and 5 kPa respectively. Figures a and b correspond to negative polarisation ($\eta = -1$ V), while figures c and d refer to positive polarisation ($\eta = +1$ V). The CO_2 production rate is shown in figures a and c, while the N_2 production rate can be found in figures b and d. Table 0.2 and Table 0.3 list the rate enhancement ratio, ρ, and Faradaic efficiencies, Λ, corresponding to the polarisation with negative or positive overpotentials ($\eta = -1$ V or +1 V). From Figure 0.6 and Figure 0.7, we can see that under near-stoichiometric fuel conditions ($p_{O_2} = 0.5$ and 1 kPa) negative polarisation appears to promote the CO_2 and N_2 production of the low-sodium modified sample (0.11%, V104) with ρ_{CO_2} up to 2.26, $\Lambda_{CO_2} \approx -88$, and ρ_{N_2} up to 1.50, $\Lambda_{N_2} \approx -3$ respectively, while positive polarisation ($\eta = +1$ V) on the other hand, either inhibits or does not affect the CO_2 and N_2 production rates. Such behaviour indicates that the reaction is electrophilic. The reaction behaviour then becomes volcano-type with an increase in sodium coverage to 11 and 65% under the same fuel conditions (where both negative and positive polarisations decrease the reaction rate, and

rate maximum is at $\eta = 0$ V). In addition, an increase in the oxygen partial pressure to $p_{O_2} =$ 5 kPa (fuel lean conditions) changes the reaction behaviour at 11 and 65% sodium coverage to electrophobic, as the reaction rates are now increased by positive polarisation, and decreased by negative polarisation. This changing behaviour can be clearly seen from Table 0.2 for CO_2 production and is consistent with that seen during the cyclic voltammetry experiment discussed in Section 8.2.1.2 and in ethylene oxidation study in Chapter 7. However, we can see from Table 0.3 that the reaction behaviour for N_2 production is quite complicated possibly because the selectivity to N_2 may also be affected by oxygen concentration and/or sodium coverage. The increase in the N_2 production rate is also mostly Faradaic ($\Lambda \approx 1$).

In addition, we can see from Figure 0.6 and Figure 0.7 that at a coverage of 65% and under near-stoichiometric fuel conditions ($p_{O_2} = 0.5$-1 kPa), the reaction rates appear to be enhanced once the positive polarisation is stopped. This is followed by a gradual decrease in the reaction rate. Similar behaviour has also been observed in Figure 7.4b for ethylene oxidation and in the study of NO reduction over Ir/YSZ catalysts but under negative polarisation [66]. Such behaviour under negative polarisation was suggested to be due to induced modification of the physiochemical properties of the electrochemical catalyst. It is possible that in this case such activation in the catalytic activity is due to an increase in the oxygen adsorbed or stored in the form of sodium surface species (carbonates, hydroxides, oxides or even Pt-Na-O complexes) that releases oxygen promoter when the positive polarisation is stopped. Next we will investigate the effect of sodium addition to the selectivity of N_2 and other product gases, N_2O and NO_2.
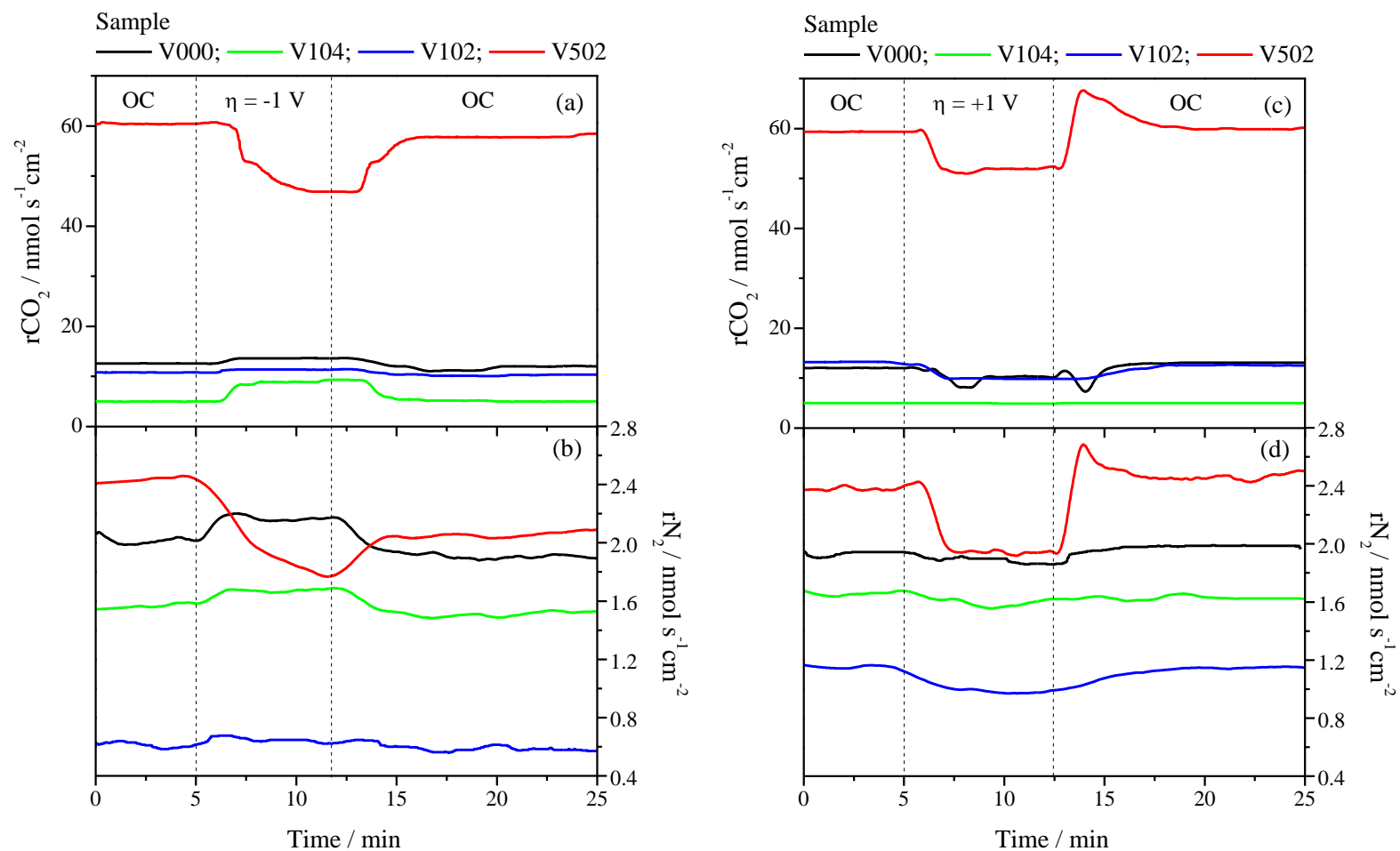
Figure 0.6. Transient plots under low oxygen partial pressure, p_{O_2} = 0.5 kPa. For η = -1 V (a) CO_2 production rate, (b) N_2 production rate and for η = +1 V (c) CO_2 production, (d) N_2 production rate. Other reactants: p_{NO} = 0.1 kPa, $p_{C_3H_6}$ = 0.1 kPa. Temperature: 350°C; Total flow rate: 100 ml min^{-1}.
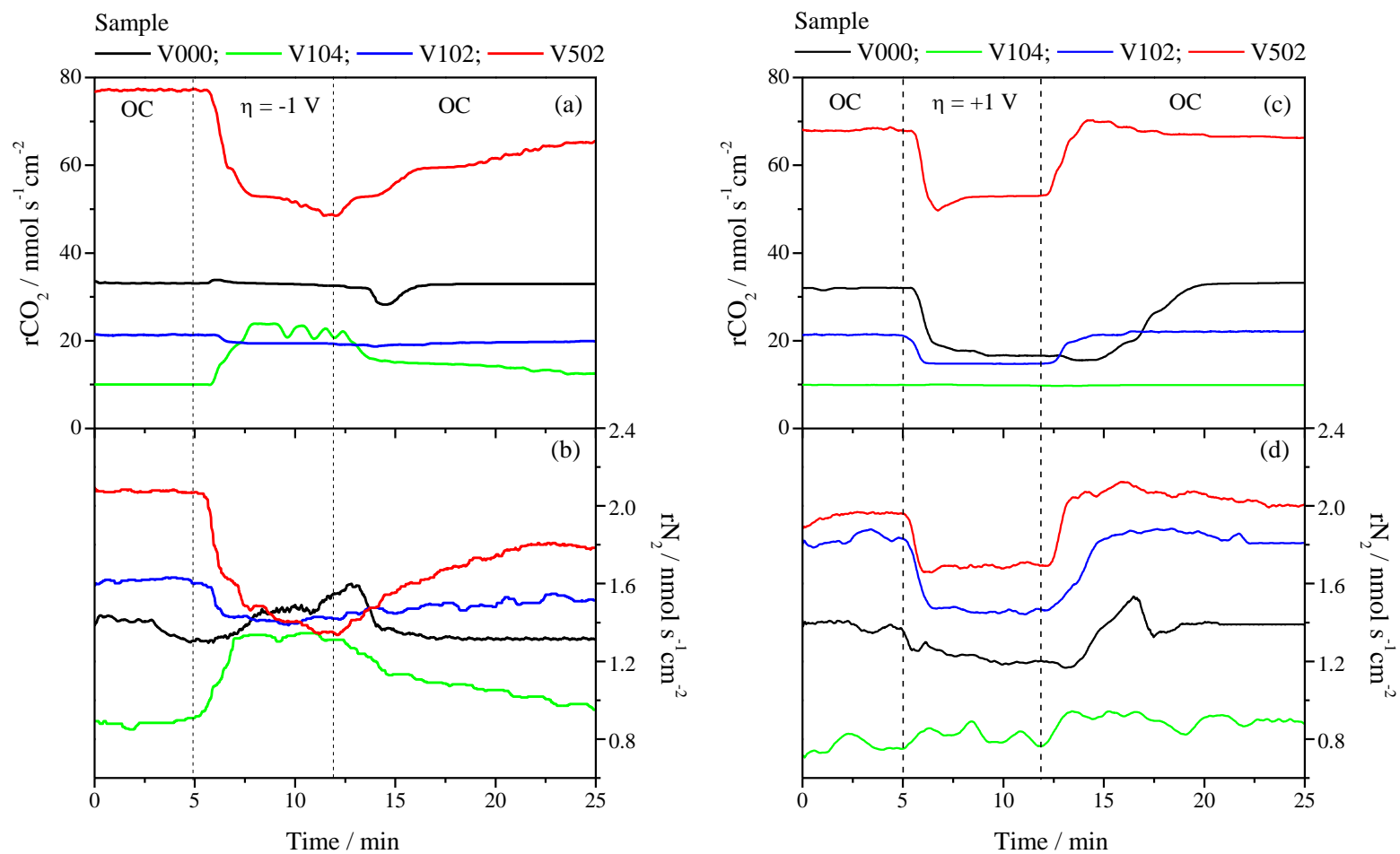
Figure 0.7. Transient plots under low oxygen partial pressure, $p_{O_2} = 1$ kPa. For $\eta = -1$ V (a) CO_2 production rate, (b) N_2 production rate and for $\eta = +1$ V (c) CO_2 production, (d) N_2 production rate. Other reactants: $p_{NO} = 0.1$ kPa, $p_{C_3H_6} = 0.1$ kPa. Temperature: 350°C; Total flow rate: 100 ml min^{-1}.
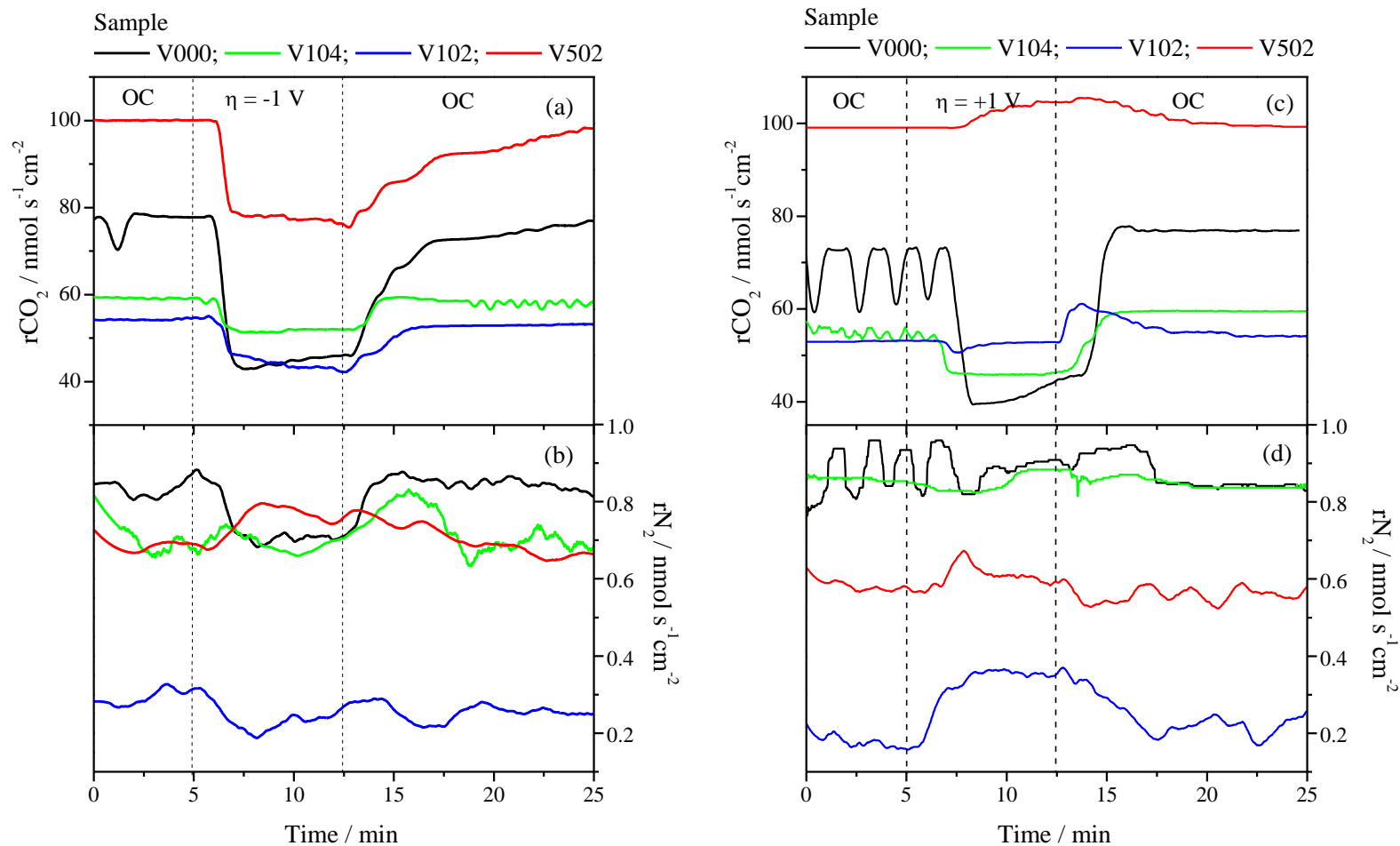
Figure 0.8. Transient plots under high oxygen partial pressure, $p_{O_2} = 5$ kPa. For $\eta = -1$ V (a) CO_2 production rate, (b) N_2 production rate and for $\eta = +1$ V (c) CO_2 production, (d) N_2 production rate. Other reactants: $p_{NO} = 0.1$ kPa, $p_{C_3H_6} = 0.1$ kPa. Temperature: 350°C; Total flow rate: 100 ml min^{-1}.

Table 0.2. Rate enhancement ratio and faradaic efficiency for CO_2 production. Shaded area show non-faradaic rate enhancement, while bold letters indicate faradaic rate increase.

Negative polarisation (η = -1 V)

p_{O_2}	ρ_{CO_2}				Λ_{CO_2}			
kPa	V000	V104	V102	V502	V000	V104	V102	V502
0.5	1.08	1.82	0.98	0.79	-6	-89	14	65
1	0.97	2.26	0.94	0.75	9	-88	11	243
5	0.59	0.88	0.80	0.78	199	91	11	255

Positive polarisation (η = +1 V)

p_{O_2}	ρ_{CO_2}				Λ_{CO_2}			
kPa	V000	V104	V102	V502	V000	V104	V102	V502
0.5	0.85	0.97	0.75	0.87	-14	-6	-7	-23
1	0.53	1.00	0.69	0.80	-43	0.3	-38	-119
5	0.68	0.84	1.01	1.05	-230	-140	6	31

Table 0.3. Rate enhancement ratio and Faradaic efficiency for N_2 production.

Negative polarisation (η = -1 V)

p_{O_2}	ρ_{N_2}				Λ_{N_2}			
kPa	V000	V104	V102	V502	V000	V104	V102	V502
0.5	**1.08**	1.08	0.87	0.78	**-1**	-3	1	3
1	**1.06**	1.50	0.89	0.68	**-1**	-3	1	7
5	0.85	0.88	0.92	**1.11**	1	1	1	**-1**

Positive polarisation (η = +1 V)

p_{O_2}	ρ_{N_2}				Λ_{N_2}			
kPa	V000	V104	V102	V502	V000	V104	V102	V502
0.5	0.99	0.96	0.78	0.82	-1	-3	-1	-1
1	0.86	**1.08**	0.80	0.84	-1	**1**	-2	-3
5	**1.10**	1.00	**1.26**	1.00	**1**	**1**	**1**	**1**

1.27.3. Selectivity

The selectivity of the system to nitrogen (S_{N_2}), nitrous oxide (S_{N_2O}) as well as nitrogen dioxide (S_{NO_2}) under open-circuit conditions is plotted against sodium coverage in Figure 0.9. Figure 0.9a shows that in general S_{N_2} is maximum (around 30%) under low p_{O_2} (0.5 kPa), which is near-stoichiometric fuel condition and decreases with increasing oxygen partial pressure. Under p_{O_2} = 0.5 kPa (red symbol), sodium addition up to 11% coverage (V102) appears to decrease the N_2 selectivity to around 10%, but further increase in sodium coverage to 65% (V502) restores the S_{N_2} to a value comparable to the 'clean' ones. Increasing p_{O_2} to 5 kPa (fuel lean conditions) drops the N_2 selectivity from around 30% to less than 10%. However, low selectivity to N_2 is not unexpected because the NO reduction over Pt/YSZ system is known to have narrow operating temperature window [147] and the selectivity to N_2O may be increased under excess oxygen. Under such condition (p_{O_2} = 5 kPa), the N_2 selectivity does not appear to be affected by sodium coverage.

As shown in Figure 0.9b the selectivity to N_2O at p_{O_2} = 0.5 kPa is increased by high sodium coverage (65%, V502) from around 5 to 20%, whereas increasing the oxygen partial pressure from p_{O_2} = 0.5 to 5 kPa does not appear to have an effect that is of any significance. Generally, the catalyst selectivity to N_2O (Reaction 8.3) is known to increase under excess oxygen [110, 147]. The catalyst selectivity to NO_2 (Reaction 8.4) is also shown in Figure 0.9c. High sodium coverage (65%, V502) appears to decrease the NO_2 selectivity under p_{O_2} = 0.5 kPa from around 60 to 40%, but an increase in the oxygen partial pressure to p_{O_2} = 5 kPa increases the catalyst selectivity to NO_2 to around 90%. This means that under this condition (fuel lean conditions) almost all of NO converted in the catalyst system is via oxidation of NO to NO_2, rather than the desirable NO reduction to N_2. A comparison was also made between the CO_2 produced by direct oxidation of C_3H_6 and indirectly from reduction of NO; it was found that almost 99% of the total CO_2 produced under high p_{O_2} is in fact from C_3H_6 oxidation, and only about 1% is from NO reduction by

C$_3$H$_6$. Apparently, under the studied conditions, this system is predominantly controlled by oxidative reactions rather than the reductive ones. This suggests that an investigation of the catalyst selectivity to NO reduction versus oxidation is of great relevance to this study.

Figure 0.10 compares the catalyst selectivity to either NO oxidation or reduction under varying oxygen partial pressure and applied overpotentials as a function of sodium coverage. We can see in Figure 0.10a that the selectivity of the 'clean' and low-sodium modified sample (V000 and V104) to oxidation and reduction of NO under near-stoichiometric condition (p_{O_2} = 0.5 kPa) is approximately 60:40. Increasing sodium coverage to 11% (V102) appears to increase the catalyst selectivity to NO oxidation, while reducing the selectivity to NO reduction with a 90:10 oxidation-reduction ratio. On the contrary, further increase in sodium coverage to 65% (V502) reduces the selectivity to NO oxidation, while enhancing the catalyst selectivity to NO reduction with approximately 50:50 oxidation-reduction ratio. However, this increase in NO reduction at high sodium coverage is also attributed to the increase in the N$_2$O production not only the desirable N$_2$. Increasing the oxygen partial pressure to p_{O_2} = 1 kPa (Figure 0.10b) does not appear to have significant effect on the oxidation-reduction selectivity ratio caused by the different sodium coverages, while further increase to p_{O_2} = 5 kPa (Figure 0.10c) enhances the catalyst selectivity at all sodium coverages to NO oxidation with an oxidation-reduction ratio of 80:20.
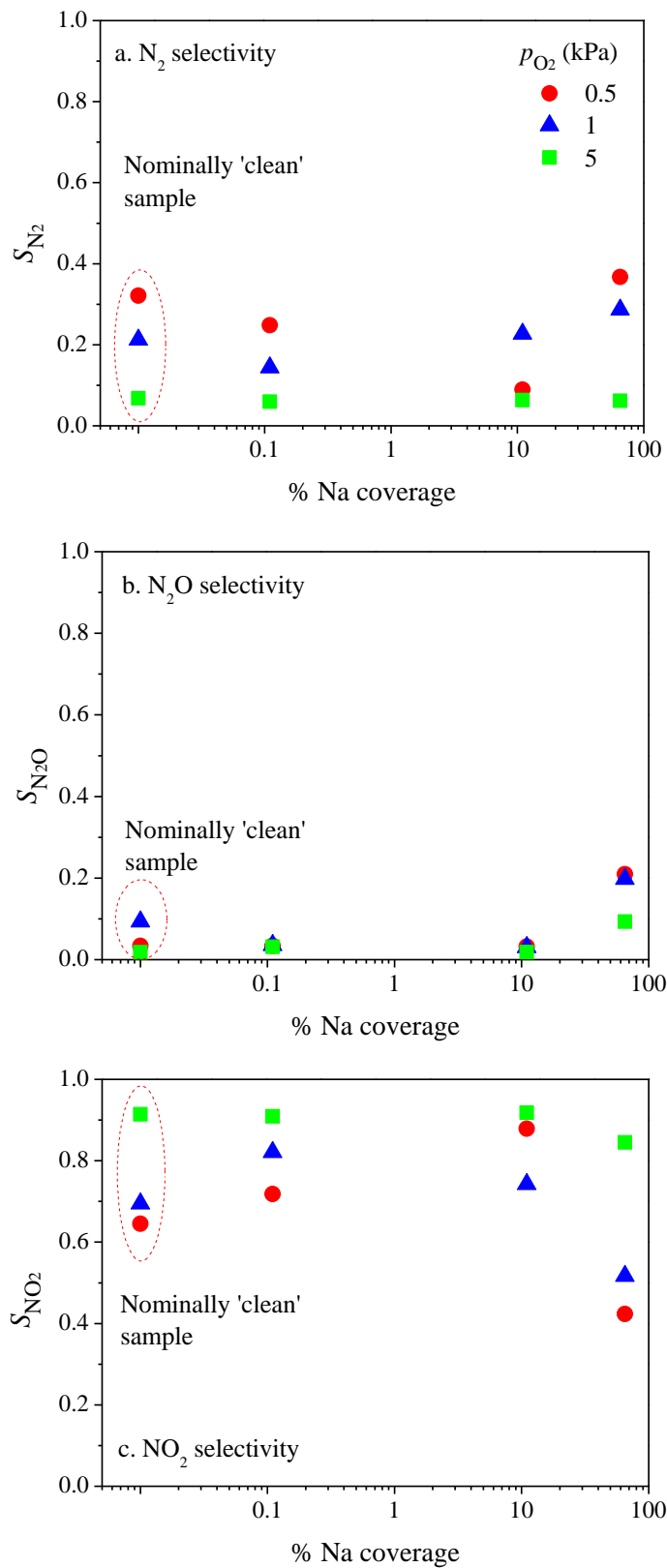
Figure 0.9. Catalyst selectivity under varying p_{O_2} and sodium coverage: Selectivity to (a) N_2, (b) N_2O and (c) NO_2 under open-circuit conditions. Gas composition: p_{O_2} = 0.5-5 kPa, $p_{NO} = p_{C_3H_6}$ = 0.1 kPa. Temperature: 350°C. Total flow rate: 100 ml min^{-1}
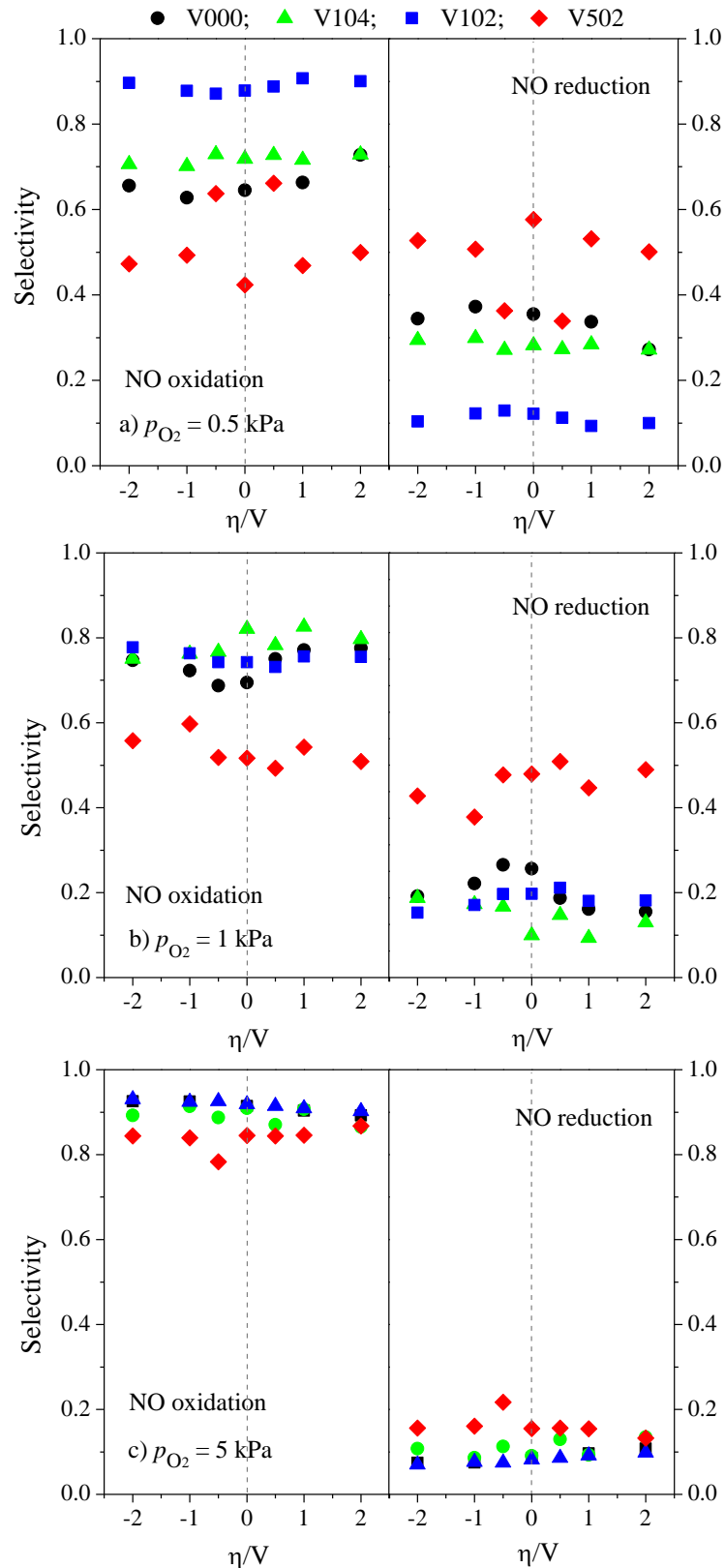
Figure 0.10. Selectivity to NO oxidation versus NO reduction under varying applied overpotentials and p_{O_2}; (a) 0.5 kPa; (b) 1 kPa and (c) 5 kPa. Other gas composition: p_{NC} = $p_{C_3H_6}$ = 0.1 kPa. Temperature: 350°C. Total flow rate: 100 ml min^{-1}.

1.27.4. *Temperature study*

The effect of temperature on the reaction rates was studied using a fresh sample prepared from Heraeus platinum paste. This sample has less platinum than Sample V (Metalor) used for previous experiments as mentioned in Chapter 3, thus sodium modification with 5×10^{-2} M and 10^{-1} M NaOH solutions resulted in higher sodium coverage range; i.e. 110 and 320% respectively (W502 and W101). Higher sodium coverage is used here as in the previous sections it was found to increase the catalytic activity and selectivity to NO reduction.

Figure 0.11a shows the CO_2 production rates, while Figure 0.11b exhibits the N_2 production rates under near-stoichiometric and fuel lean conditions (p_{O_2} = 0.5 and 5 kPa). The first and the second runs indicated in Figure 0.11a and b do not to equally match each other, especially for CO_2 production; their difference is the starting temperature (T_{start} = 250°C or 350°C respectively) and the second run was carried out on the next day. As we can see from Figure 0.11a, an increase in the temperature from 350 to 425°C under near-stoichiometric fuel conditions (p_{O_2} = 0.5 kPa) increases the CO_2 production rate of the 'clean' sample (2nd run) from around 25 to 135 nmol s^{-1} cm^{-2}. This is followed by a more gradual increase to 200 nmol s^{-1} cm^{-2} at 525°C possibly due to the reactor by-pass as mentioned in Section 7.1.1. Under the same condition, the nitrogen production rate (Figure 0.11b) peaks at a temperature around 425°C, but this is followed by a sharp decrease in the reaction rate. According to Burch and Millington [148], the onset of NO reduction and the maximum conversion of NO is always closely related to propene oxidation; the two reactions started at the same time and increased together until NO reduction reached maximum at a temperature close to complete oxidation of propene. A close example is an NO reduction study on a Pt/YSZ system under similar conditions (feed composition = 0.2% C_3H_6, 0.2% NO and 1% O_2, near-stoichiometric conditions) [110]. In that study it was found that maximum propene conversion to CO_2 can be achieved from a lower temperature, T = 295°C, while NO conversion goes through a maximum at a temperature when total hydrocarbon

conversion occurs. Above that temperature, the NO conversion into N_2 and N_2O decreases.
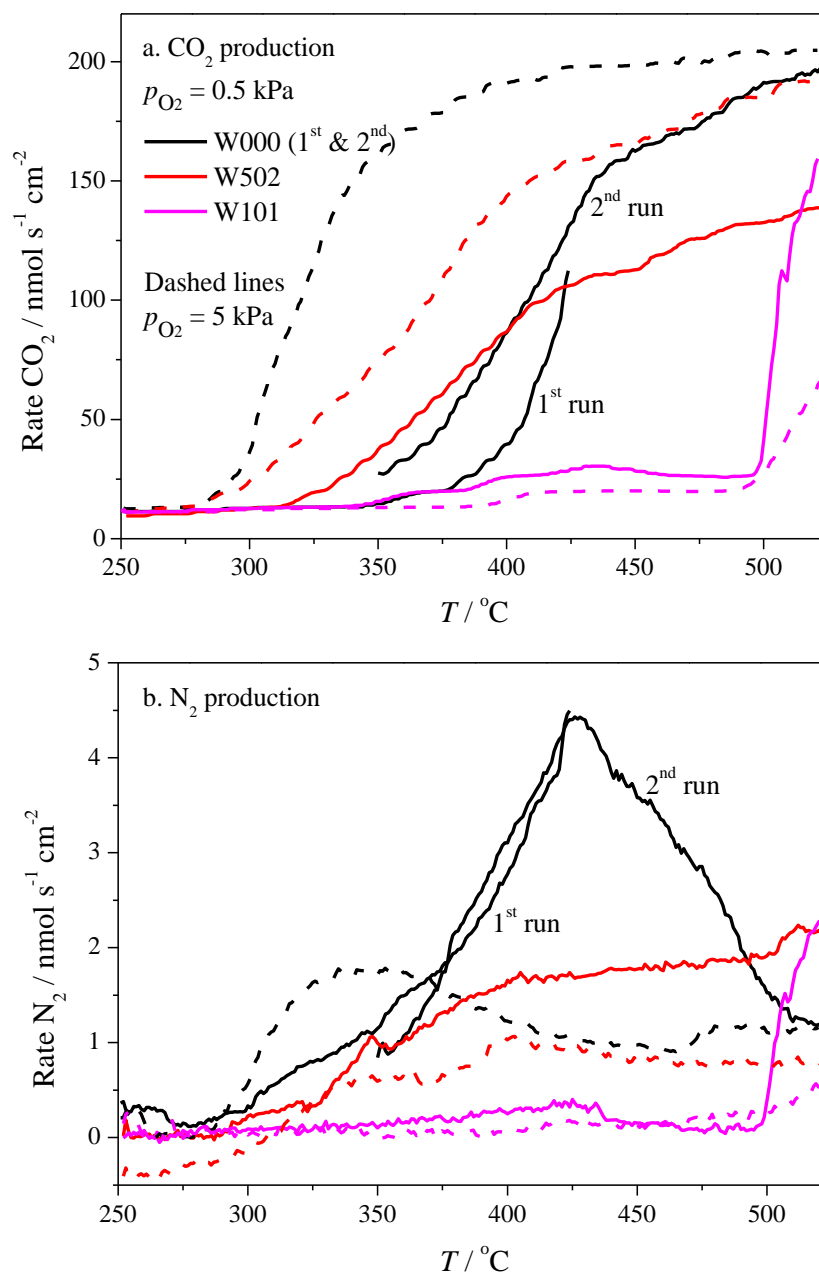
Figure 0.11. Reaction rates as a function of temperature under varying sodium coverage and oxygen partial pressure: (a) CO_2 production, (b) N_2 production. Gas composition: $p_{O_2} = 0.5$ and 5 kPa, p_{NO} and $p_{C_3H_6} = 0.1$ kPa. Temperature: 350°C. Total flow rate: 100 ml min^{-1}.

Unfortunately sodium addition at high coverages (110 and 320%) appears to slow down and inhibit both CO_2 and N_2 production within the studied temperature range, possibly

because the surface has been completely saturated by sodium. As we can see in Figure 0.11a, the CO_2 production of the sodium-modified sample (110% sodium coverage, W502) begins at a lower temperature (at approximately 315°C) than the 'clean' ones. However, it also reaches lower rates at temperatures around 425 and 550°C, compared to the 'clean' sample. At a very high sodium coverage (320%, W101) the CO_2 production takes place only after 500°C.

In addition, while the 'clean' sample in Figure 0.11b shows a decrease in the N_2 production rate after 425°C, the sample modified with 110% sodium coverage (W502) still shows a stable N_2 production rate up to the maximum temperature studied. This is consistent with the study of NO reduction over Pt/Na-doped γ-Al_2O_3 that also shows a wider operating temperature window with the promoted platinum catalyst compared to the unpromoted one [112]. Similar to CO_2 production, further increase in sodium coverage (230%, W101) also appears to suppress the N_2 production until the temperature reaches 500°C. We can also observe in Figure 0.11a that increasing the oxygen partial pressure to $p_{O_2} = 5$ kPa reduces the temperature at which both CO_2 and N_2 productions starts to occur to around $T = 300^o$C. Moreover, the temperature at which maximum N_2 production is achieved by the 'clean' sample is also reduced. Above 400°C, the reaction rates of the 'clean' sample and that modified with 110% Na coverage (W502) become comparable.

From Figure 0.12, we can see the proportion of the different nitrogen species produced as a function of temperature and oxygen partial pressure. In comparison to the near-stoichiometric fuel condition shown in Figure 0.12a, it is clear that the increase in the gas phase oxygen concentration enhances the production of NO_2 and N_2O, while at the same time inhibiting the production of N_2 (Figure 0.12b). From the literature [112], the production of NO_2 was found to take place after the propene conversion is complete, whereas the N_2O production is maximum after the temperature corresponding to 50% propene conversion is exceeded. Similar behaviour is seen in Figure 0.12b, where NO_2 production appear to increase after CO_2 production stops increasing, while N_2O production

reaches a maximum at the same temperature corresponding to half of the increase in CO_2 production, around $T = 325^{\circ}C$. Sodium addition at high coverage (110 and 320% Na coverage, W502 and W101) causes an even higher increase in the production of NO_2, while decreasing the N_2 and N_2O production rates (or the selectivity to NO reduction).
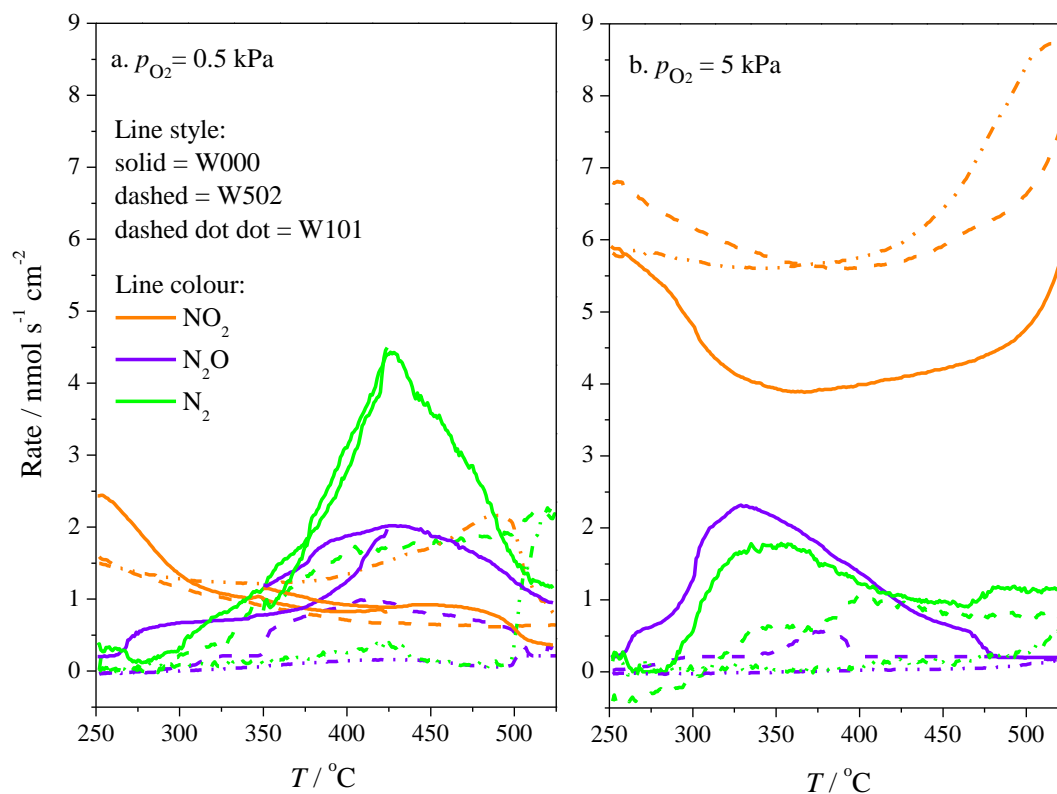
Figure 0.12. Production rate of N product gases as a function of temperature under varying sodium coverage and oxygen partial pressure, p_{O_2}: (a) 0.5 kPa (b) 5 kPa. Other gas composition: $p_{NO} = p_{C_3H_6} = 0.1$ kPa. Temperature: $350^{\circ}C$. Total flow rate: 100 ml min^{-1}.

1.27.5. Discussion

From the experimental data presented under varying sodium coverages and oxygen partial pressures, the following key features can be identified:

- An increase in sodium coverage up to 65% appears to enhance the open-circuit catalytic activity of the Pt/YSZ system for CO_2 and N_2 productions, but the sodium-

induced rate enhancement is decreased by an increase in the oxygen partial pressure

- The CO_2 production exhibits electrophilic behaviour at low sodium coverage (0.11%) and under near-stoichimetric fuel conditions (p_{O_2} = 0.5-1 kPa), however this reaction behaviour appears to be changed to volcano and finally electrophobic by increasing oxygen partial pressure from p_{O_2} = 0.5 to 5 kPa and sodium coverage from 0.11% to 65%.

- The N_2 production also generally exhibits electrophilic behaviour at low sodium coverage (0.11%) and near-stoichimetric fuel conditions (p_{O_2} = 0.5-1 kPa), but the reaction behaviour is more complicated (especially under fuel lean conditions) and only faradaic rate enhancement is observed.

- The catalyst selectivity to NO reduction is slightly enhanced by high sodium coverage, but largely decreased by an increase in oxygen concentration.

- High sodium coverage (110% and 320%) appears to slow down and/or inhibit the production of CO_2 and N_2 while NO_2 production is increased.

The result indicates that the open-circuit behaviour with respect to the variation in sodium coverage is similar to that observed for ethylene oxidation in Chapter 7 for CO_2 production. This behaviour may be partially explained by both work function dependent model and also the increase in oxygen adsorption depending on the coverage of sodium species on the platinum surface. We can anticipate that the electropromoted rate behaviour under this reaction system to be more complicated than that seen for ethylene oxidation as more reactants (and reaction intermediates) are involved. Here the reaction rate data under low oxygen partial pressure (p_{O_2} = 0.5 kPa) are also plotted versus the work function changes in Figure 0.13a-b, according to the work function dependent model proposed earlier (in Chapter 5). The model assumes that the reaction rate is influenced by the change in the

work function of the catalyst, which could either be caused by sodium addition or electrochemical polarisation. Based on our previous discussion, the model could be valid under low sodium coverage where sodium may primarily be in the ionic form rather than metallic and there is low lateral interaction between the surface ions. This may be consistent with the region where sodium addition only causes a shift in the cathodic peak potential of oxygen reduction as seen in Chapter 6. Based on Figure 0.13a-b, we can see that in general the CO_2 and N_2 production rates from this system follow the proposed work-function dependent behaviour for an electrophilic reaction, while at high sodium coverage (65%) the reaction shows volcano-type behaviour. The presence of sodium promoter species appears to complicate the reaction rate dependence on $\Delta\Phi$. We can see that at sodium coverages of 0.11 and 11%, the reaction rates are lower than the 'clean' ones. Data for higher oxygen partial pressures (p_{O_2} = 1 and 5 kPa) are shown in Appendix D. Similar behaviour observed under p_{O_2} = 0.5 kPa can be seen for CO_2 production under higher oxygen partial pressures, but the N_2 production data are not very significant. In general the N_2 production under p_{O_2} = 5 kPa follows a reaction rate dependence on $\Delta\Phi$ for an electrophobic reaction, where a negative polarisation decreases the reaction rate, and positive polarisation increases the reaction rate. Moreover rate enhancement for N_2 is mostly Faradaic.
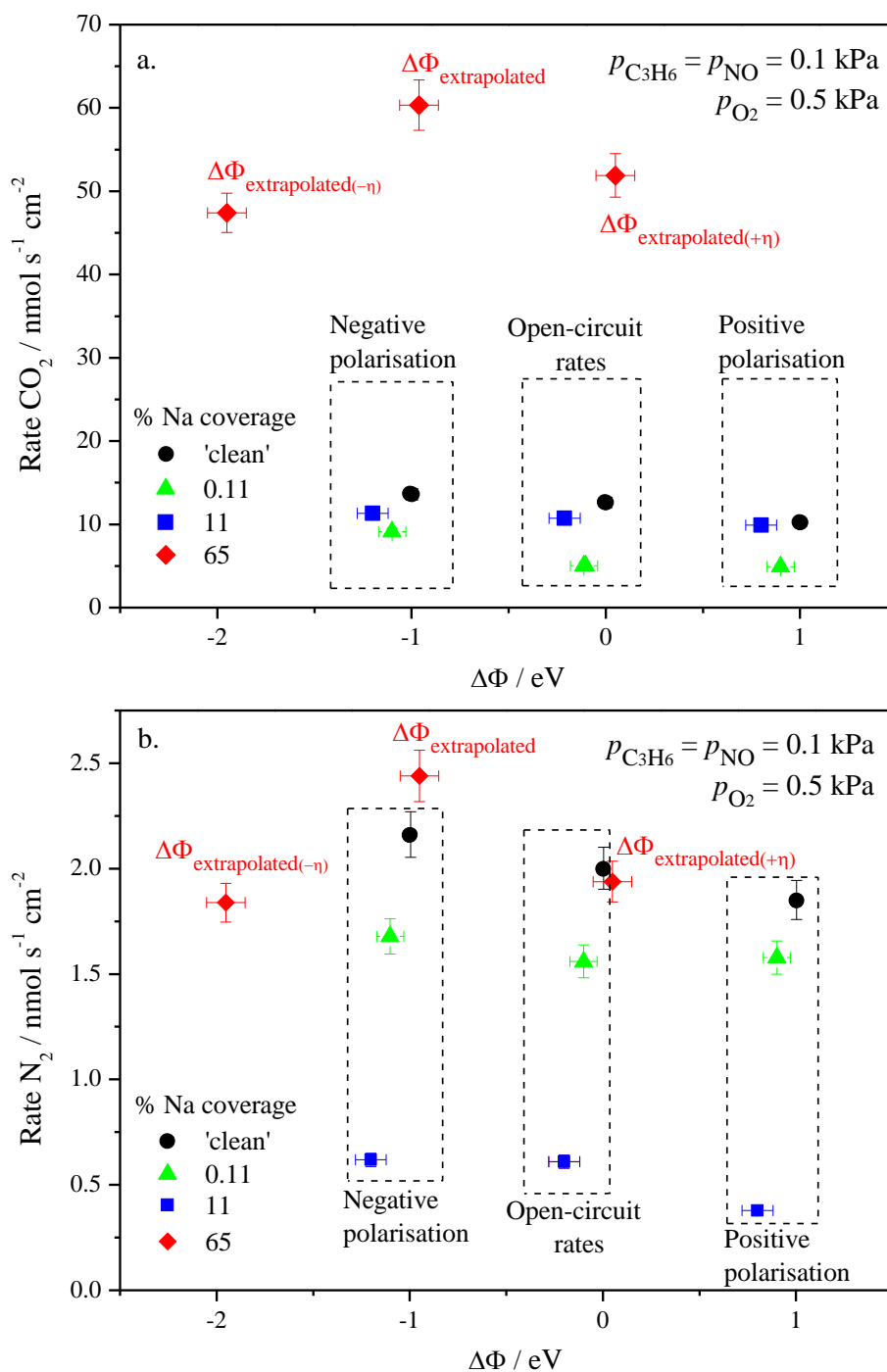
Figure 0.13. Reaction rate versus work function changes under near-stoichiometric fuel conditions. (a) CO_2 production (b) N_2 production. Gas composition: p_{O_2} = 0.5 kPa, p_{NO} = 0.1 kPa, $p_{C_3H_6}$ = 0.1 kPa. Temperature: 350°C. Total flow rate: 100 ml min^{-1}

Next we will see whether an increase in the coverage of sodium and gas phase oxygen also modifies this reaction behaviour from electrophilic to volcano and finally

electrophobic, as seen under ethylene oxidation in Chapter 7. This shifting behaviour is shown in the top (CO_2 production) and the bottom (N_2 production) of Figure 0.14. Note that for N_2 production this trend applies only up to a medium coverage of sodium (11%). At high sodium coverage a rather complex behaviour can be observed under fuel lean conditions with the reaction behaviour changes from electrophobic to electrophilic with increasing sodium coverage. This possibly accounts for the decrease in the selectivity to N_2 and the increase in the selectivity to NO_2 under fuel lean conditions as discussed in Section 8.2.3. In one case at low sodium coverage (0.11%, V104) and under low p_{O_2} (0.5 kPa) which is not shown here, the reaction even shows inverted volcano behaviour. Lintanf et al. [65] has also observed an slight increase in the NO conversion over Pt/YSZ system by applying positive overpotentials (+2 V) while a more drastic enhancement was seen under negative polarisation (-2 V).
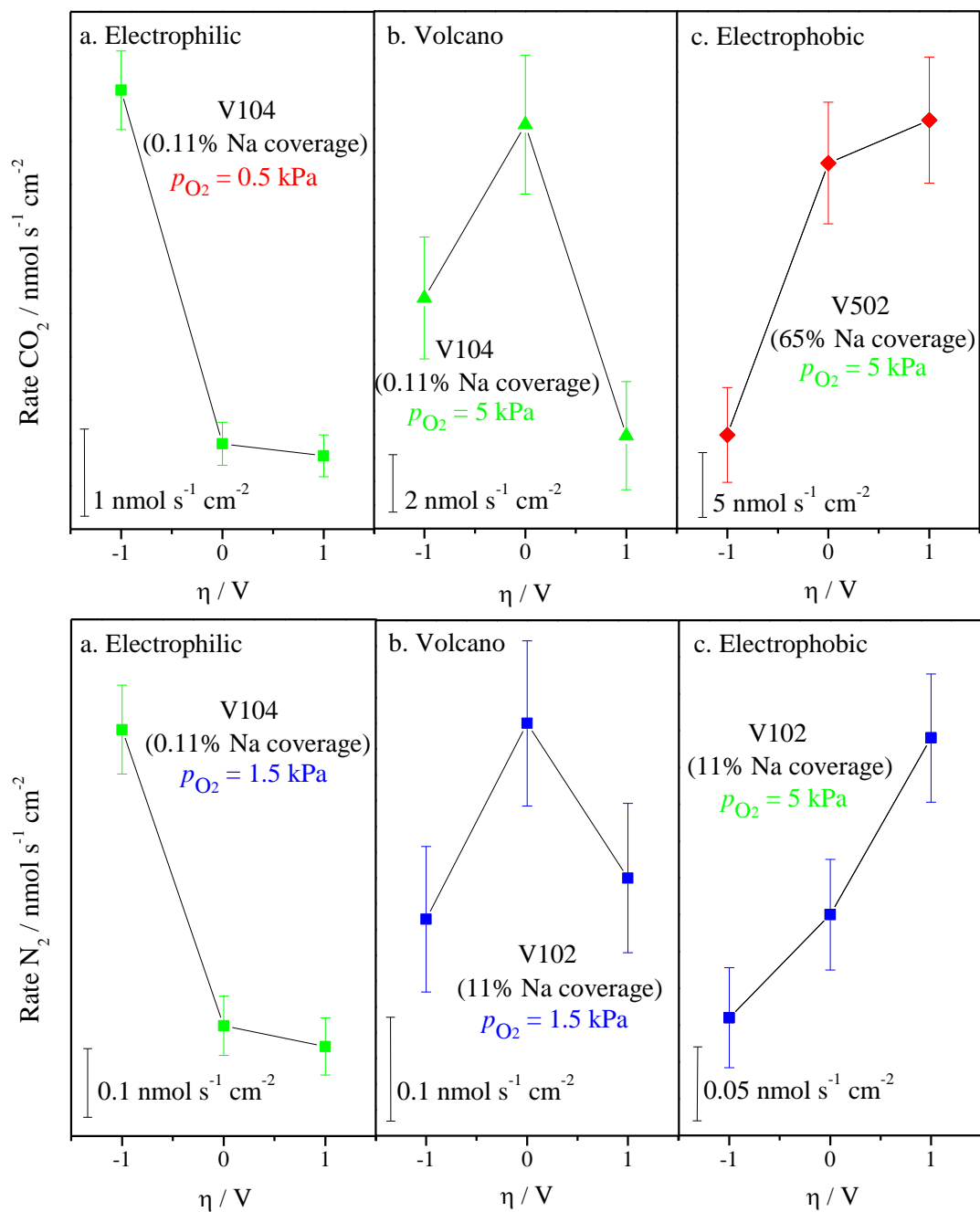
Figure 0.14. An example for each case of the changing behaviour from (a) electrophilic to (b) volcano and (c) electrophobic with increasing sodium coverage and oxygen partial pressure: CO_2 production (top) and N_2 production (bottom). Other gas composition: p_{NO} and $p_{C_3H_6} = 0.1$ kPa. Temperature: 350^oC. Total flow rate: 100 ml min^{-1}.

The effect of sodium as an electropositive promoter on the adsorption strength of oxygen (an electron acceptor adsorbate) has been described in Chapter 7. Based on the discussion, the rate increase at high sodium coverage may also be due to the sodium species

being more metallic rather than ionic. This enhances the coverage of oxygen on the platinum active sites, and if a reaction is initiated by an increase in oxygen adsorption (as shown in the case of ethylene oxidation), the reaction rate will be increased. Similarly, the CO_2 production from propene oxidation in this study is also shown to have a positive order relation with oxygen. Therefore the reaction rate is increased by an increase in oxygen coverage at high sodium coverage. On the other hand the NO reduction may be enhanced by sodium addition by the influence from the electrostatic field of the alkali cation on adjacent co-adsorbed molecules. Alkali acts to lower the NO $2\pi^*$ antibonding orbital energy below the Fermi energy and increase backdonation of electron density from the metal surface to the NO $2\pi^*$ antibonding molecular orbitals, resulting in enhanced molecular NO-metal bond strength and promotion of the NO dissociation [2, 149]. Therefore, it was proposed that in the presence of propene (an electropositive adsorbate) which is strongly adsorbed on the catalyst as long as it is not completely oxidised, sodium addition acts to (i) increase the adsorption strength of electronegative adsorbates such as NO and oxygen at the expense of propene and (ii) weaken the N-O bond in the adsorbed molecule which facilitates the NO dissociation [113, 149-151]. NO dissociation was suggested in the previous studies as the key initiating step to the formation of N_2 and N_2O, followed by the combination of adsorbed N or NO to form either N_2 or N_2O [104, 147, 149]:

$$NO_{(a)} \rightarrow N_{(a)} + O_{(a)} \tag{8.13}$$

$$N_{(a)} + N_{(a)} \rightarrow N_2 \tag{8.14}$$

$$N_{(a)} + NO_{(a)} \rightarrow N_2O_{(a)} \tag{8.15}$$

An increase in the reaction rate by applying negative polarisation and vice-versa, a decrease in the reaction rate with positive polarisation (i.e electrophilic behaviour) at low sodium coverage and under low oxygen partial pressure can be rationalised as follows

[112]. An application of negative overpotentials decreases the work function of platinum, thereby weakens the platinum chemical bond with electron donor adsorbates such as propene and strengthens the bond with electron acceptor adsorbates such as NO and oxygen. Consequently, an increase in the coverage of NO and oxygen on the platinum surface which is predominantly populated by propene can be expected. This leads to the promotion of propene oxidation and NO reduction. An application of positive overpotentials on the other hand increases the work function of platinum. This weakens the platinum bonds with electron acceptor adsorbates (NO and oxygen) and strengthens the electron donor ones (C_3H_6), leading to a further decrease in oxygen coverage which is already low compared to propene coverage. As a result we can see the decrease in the production of CO_2 and N_2.

In addition, the presence of reducing gas such as propene in the NO reduction system has been shown to be important to create a reduced platinum site for NO adsorption [147-148]. The platinum sites will be re-oxidised after NO dissociation, but the presence of propene allows removal of $O_{(a)}$ and thus re-reduce the platinum sites for a start of a new cycle. An adequate presence of oxygen in the reaction mixture was also found to help in the creation of hydrocarbon-free sites on the platinum catalyst for NO adsorption, the sites otherwise predominantly occupied by propene or propene-derived carbonaceous species if the propene was not completely oxidised [64, 152]. Under excess oxygen, because of the large and fast supply of $O_{(a)}$ from gas phase oxygen the platinum sites may become inactive for NO adsorption as they remain in an oxidised state, and instead the NO_2 production increases [147]. This could explain the reduction in the N_2 production and N_2 selectivity, while the NO_2 production increases under fuel lean conditions as shown in Figure 0.12b.

As discussed previously under ethylene oxidation, at high sodium coverage, sodium could also impose an additional effect on the catalyst system, and not only act as electronic promoter (that causes work function change and modify the chemisorptive bond energy between metal catalyst and adsorbates, and thus the competitive adsorption between

reactants and enhances/inhibits the reaction rate). Among the possibilities mentioned is the creation of extra sites for oxygen adsorption and/or storage in the form of oxides, hydroxides, carbonates and/or Pt-Na-O complexes. This is consistent with the region (sodium coverage) where an increase in the total current density of cyclic voltammograms was recorded under non-reactive and reactive conditions, and where an increase in the open-circuit catalytic rates was observed. Additionally we have also mentioned the possibility of sodium poisoning the platinum active sites. This is evidenced in under the temperature study in Section 8.2.4 where the CO_2 and N_2 production are severely reduced or slowed down by sodium addition at high coverage (110 and 320%, W502 and W101). In the previous work on sodium promoter, the catalyst poisoning by sodium compounds at high sodium coverage has also been shown during high negative polarisations [104, 115].

1.28. Summary

From the results under NO reduction system, especially based on the CO_2 production we have been able to verify the findings observed in Chapter 7 under ethylene oxidation experiments. It was found that at low coverage sodium is more ionic and plays electronic promoter role by causing changes in the catalyst work function, thus affecting the catalyst adsorption bond strength with the reactants. At high sodium coverage, sodium acts to enhance the adsorption of oxygen and NO as it becomes more metallic, and this affect the competitive adsorption between oxygen and NO (electron acceptors, together with the NO dissociation) and C_3H_6 (and electron donor). These affect the reaction rates and the promotional behaviour, suggesting that the presence of an impurity at various coverages in a catalyst system may cause the variations seen in the electrochemical promotion studies by the different groups. However, based on the results here we have no clear evidence as to whether an impurity such as sodium is needed for the occurrence of EPOC.

Summary and Future Work

1.29. Summary

In this chapter we will summarise the conclusions drawn from the experiments conducted for this project. As mentioned earlier the aim of this project is to investigate the role of impurities in electrochemical promotion of catalysis. One of the questions is to know whether impurities are required for an electrochemical promotion to occur. In order to do this we have systematically deposited sodium in increasing concentration on a platinum catalyst interfaced on YSZ solid electrolyte and studied the change in the physical, electrochemical, catalytic and electrocatalytic properties of the catalyst due to sodium modification.

From the SEM analysis, we found that sodium may partially block the pores of the platinum film, whereas the Kelvin probe measurement under atmospheric condition shows that sodium addition decreases the work function of the catalyst. In addition, the surface oxygen titration at constant temperature indicates that increasing sodium coverage could enhance the oxygen uptake by the catalyst. These oxygen species may accumulate on the platinum surface in the form of sodium carbonate, hydroxide and/or oxide compounds as showed by the XPS analysis. Based on this we have come to the assumptions that sodium may act as spectator species that can cause active sites blocking or can in fact modify the kinetics, or create new sites for, oxygen adsorption, oxygen diffusion and/or oxygen storage depending on the coverage. The simplest way to investigate this is first by probing the change in the oxygen charge transfer in the Pt/YSZ system.

The study of sodium role on oxygen charge transfer reaction made use of the cyclic and linear sweep voltammetry techniques, which are very useful for *in situ* investigation of the changes in the activity of electroactive species at the surface of an electrode. From the cyclic voltammetry experiments we found that low sodium coverage does not affect

significantly the oxygen charge transfer reaction, except possibly by blocking some of the tpb sites and slowing down the rate of charge transfer. This accounts for about 30% changes in the charge transferred during a reduction process caused by sodium addition from about 1 to 16% sodium coverage. Within this range it was found that the reduction peak potential shifts towards more negative values indicating that oxygen has been more strongly bound on the catalyst surface. This CV finding was confirmed by the linear sweep voltammetry experiment which also shows that oxygen becomes more strongly bound to the catalyst with increasing sodium coverage, requiring more reducing overpontentials to be removed. At high coverage (more than 50%), sodium causes the current density at high overpotentials (and consequently the total current density) to increase. This is evidence that sodium could enhance, or create new sites for, oxygen adsorption, diffusion and/or oxygen storage on the platinum catalyst. To investigate whether this effect can result in the promotion of catalyst activity, the Pt/YSZ system was then subjected to studies under reactive conditions using a model reaction, i.e. ethylene oxidation and a case study on NO reduction by propene.

Under reactive conditions, cyclic voltammetry and potentiostatic transient experiments were used to investigate the kinetics of ethylene oxidation and NO reduction by propene. We proposed that sodium may act as an electronic promoter in a similar way it works in electrochemical promotion by altering the work function of the platinum catalyst [2], thus changing the relative strength of oxygen and ethylene adsorption or in the case of NO reduction by propene, the relative strength of NO, oxygen and propene adsorption. A decrease in the work function by sodium addition enhances the adsorption of electron acceptor adsorbates (e.g. O and NO). This promotes the rate of ethylene and propene oxidation which are shown to be positive order in oxygen under the studied conditions, while the adsorption of NO adsorption is accompanied by NO dissociation which was proposed to be key initiating steps for the formation of N_2 and N_2O [147, 149]. The catalytic effect is more pronounced at high sodium coverage and under near-stoichiometric

conditions. Under polarised conditions, both reactions in general show electrophilic behaviour except for NO reduction to N_2 under fuel lean conditions (p_{O_2} = 5 kPa) which shows more complex behaviour. For an electrophilic reaction, both negative polarisation and sodium addition may additively contribute to a decrease in the catalyst work function, and increase the reaction rates, while positive polarisation and sodium addition may decrease the reaction rate resulting from the total increase in the work function which is less pronounced than that cause by the positive polarisation alone.

It can be clearly seen from the model system that increasing sodium coverage and gas phase oxygen concentrations (partial pressures) results in behavioural changes from electrophilic to volcano-type and finally to electrophobic at high sodium coverage and under fuel lean conditions. The change in the reaction behaviour is due to the difference in the nature of sodium surface species at the different sodium coverages under varying oxygen concentrations. Sodium is present in the form of ionic species at low coverage, in the region where sodium causes the work function change, whereas at high coverage, sodium may become more metallic and have higher propensity to react with the co-adsorbed species such as oxygen or NO. As anticipated, the proposed work function dependent model appears to be valid only at low sodium coverage where the interactions between the surface species and with the reaction components are insignificant. This would be in the region where only the overpotential shift towards more negative overpotentials was observed during the cyclic voltammetry experiments. At high sodium coverage (> 50%), sodium interactions with other surface species (e.g. oxygen promoting species) and reaction components or intermediates becomes stronger, resulting in enhanced oxygen adsorption (and NO in the case of NO reduction). This is consistent with the high total current density observed during cyclic voltammetry experiments and high open-circuit catalytic rates observed on samples modified with high sodium coverage (65%).

The promotional effect is more complicated under NO reduction system where more reaction components and intermediates are involved. There are parallel oxidation and

reduction reactions taking place i.e. oxidations of C_3H_6 to CO_2 and NO to NO_2 and reductions of NO to N_2 and N_2O, which result in a complex reaction behaviour especially under fuel lean conditions. The slight increase in the selectivity to NO reduction at high sodium coverage and under near-stoichiometric conditions can be explained by sodium enhancing NO molecular adsorption which is accompanied by NO intra-molecular dissociation. Increasing oxygen concentration in the gas phase to $p_{O_2} = 5$ kPa (fuel-lean conditions) reduces the reaction rate and the selectivity to N_2 and N_2O and instead enhances the NO oxidation into NO_2. At very high sodium coverage (> 100%), sodium also appears to cause catalyst poisoning. The CO_2 and N_2 production rate becomes slower and decreased. Although the actual N_2 production rate is reduced by addition of sodium at a coverage of 110%, the sodium-modified catalyst appears to have bigger operating temperature window.

From the findings, we can conclude that sodium can have an additive role (as electronic promoter) in electrochemical promotion of catalysis depending on its coverage. The presence of sodium at different coverages can result in behavioural changes and affect the magnitude of promotion. There is however no clear evidence that impurities such as sodium are required for the occurrence of EPOC.

1.30.   Future work

Based on the study, we found that there are several issues that can be further investigated. For instance, our XPS analysis showed that sodium forms carbonate, hydroxide and/or oxides compounds under ambient conditions. To understand the nature of the sodium-containing species under operating conditions, an in-situ XPS investigation of the sodium-modified samples under high temperature and reactive conditions can be preformed. In addition, an *in situ* XPS investigation of the sodium-modified samples under polarised condition may be conducted to investigate whether electrical polarisation can in

fact generate oxygen promoter species from the sodium-containing species and affect the electrocatalytic properties of the catalyst.

In addition, we realised that in order to fit in our reaction data with more representative work function changes according to the proposed work function dependent model, it is important to carry out *in situ* work function measurement of the different sodium coverages under reaction conditions, high temperature and polarisation conditions. This can be done by using a Kelvin probe but the electrochemical reactor must be customised to fit in the probe in micrometer distance above the catalyst surface.

In this research, the role of sodium in modification of the catalytic and electrocatalytic properties of the platinum catalyst has been investigated using ethylene oxidation and NO reduction by propene. In both cases the oxygen partial pressures are varied, but ethylene, propene and NO partial pressures were kept constant to simplify the study. An investigation of kinetic reactions should also include the effect of the other reactants in the catalyst system. Perhaps to understand more of the role of sodium in the system, we can also carry out the kinetic experiments under varying ethylene, propene and NO partial pressures. In addition, studies with different catalyst systems such as palladium or rhodium based catalysts may also be conducted in the future as these two may have better performance for NO reduction by propene. If our proposed model on the sodium modification of platinum catalytic and electrocatalytic activities is reproducible, then we may be able to predict the role of sodium in the different systems. Other than that, we can extend the studies on different impurity species such as potassium, silicon or sulphur.

References

[1] M. Stoukides, C.G. Vayenas, Journal of Catalysis, 70 (1981) 137-146.

[2] C.G. Vayenas, Bebelis, S., Pliangos, C., Brosda, S. and Tsiplakides, D., Electrochemical Activation of Catalysis: Promotion, Electrochemical Promotion, and Metal-Support Interactions, Kluwer Academic/Plenum Publishers, New York, 2001.

[3] C.G. Vayenas, S. Bebelis, S. Neophytides, The Journal of Physical Chemistry, 92 (1988) 5083-5085.

[4] C.G. Vayenas, S. Bebelis, S. Ladas, Nature, 343 (1990) 625-627.

[5] S. Souentie, L. Lizarraga, A. Kambolis, M. Alves-Fortunato, J.L. Valverde, P. Vernoux, Journal of Catalysis, 283 (2011) 124-132.

[6] A. Katsaounis, Journal of Applied Electrochemistry, 40 (2010) 885-902.

[7] F. Matei, D. Ciuparu, C. Jiménez-Borja, F. Dorado, J.L. Valverde, S. Brosda, Applied Catalysis B: Environmental, 127 (2012) 18-27.

[8] A. Hammad, S. Souentie, E.I. Papaioannou, S. Balomenou, D. Tsiplakides, J.C. Figueroa, C. Cavalca, C.J. Pereira, Applied Catalysis B: Environmental, 103 (2011) 336-342.

[9] G. Rothernberg, Catalysis: Concepts and Green Applications, Wiley-VCH, Weinheim, 2008.

[10] I.R. Harkness, R.M. Lambert, Journal of Catalysis, 152 (1995) 211-214.

[11] E. Mutoro, B. Luerßen, S. Günther and J. Janek, Solid State Ionics, 180 (2009) 1019-1033.

[12] G. Fóti, A. Jaccoud, C. Falgairette, C. Comninellis, Journal of Electroceramics, 23 (2009) 175-179.

[13] H. Pöpke, E. Mutoro, C. Raiß, B. Luerßen, M. Amati, M.K. Abyaneh, L. Gregoratti, J. Janek, Electrochimica Acta.

[14] S.P. Yoon, S.W. Nam, S.-G. Kim, S.-A. Hong, S.-H. Hyun, Journal of Power Sources, 115 (2003) 27-34.

[15] A.K. Opitz, M.P. Hörlein, T. Huber, J. Fleig, Journal of The Electrochemical Society, 159 (2012) B502-B513.

[16] J. Gaube, H.F. Klein, Applied Catalysis A: General, 350 (2008) 126-132.

[17] A.R. de la Osa, A. De Lucas, J.L. Valverde, A. Romero, I. Monteagudo, P. Coca, P. Sánchez, Catalysis Today, 167 (2011) 96-106.

[18] J. Haber, M. Nattich, T. Machej, Applied Catalysis B: Environmental, 77 (2008) 278-283.

[19] Y. Wu, M. Liu, Z. Ma, S.t. Xing, Catalysis Today, 175 (2011) 196-201.

[20] Y. Zhai, D. Pierre, R. Si, W. Deng, P. Ferrin, A.U. Nilekar, G. Peng, J.A. Herron, D.C. Bell, H. Saltsburg, M. Mavrikakis, M. Flytzani-Stephanopoulos, Science, 329 (2010) 1633-1636.

[21] P. Vernoux, F. Gaillard, C. Lopez, E. Siebert, Solid State Ionics, 175 (2004) 609-613.

[22] A. Billard, P. Vernoux, Topics in Catalysis, 44 (2007) 369-377.

[23] S. Bebelis, H. Karasali, C.G. Vayenas, Solid State Ionics, 179 (2008) 1391-1395.

[24] F. Dorado, A. de Lucas-Consuegra, C. Jiménez, J.L. Valverde, Applied Catalysis A: General, 321 (2007) 86-92.

[25] C. Pliangos, I.V. Yentekakis, S. Ladas, C.G. Vayenas, Journal of Catalysis, 159 (1996) 189-203.

[26] S. Bebelis, C.G. Vayenas, Journal of Catalysis, 118 (1989) 125-146.

[27] S. Bebelis, M. Makri, A. Buekenhoudt, J. Luyten, S. Brosda, P. Petrolekas, C. Pliangos, C.G. Vayenas, Solid State Ionics, 129 (2000) 33-46.

[28] A.J. Bard, L.R. Faulkner, Electrochemical Methods: Fundamentals and Applications, 2 ed., John Wiley & Sons, 2001.

[29] F.C. Walsh, A First Course in Electrochemical Engineering, The Electrochemical Consultancy, Hants, England, 1993.

[30] A.C. Fisher, Eectrode Dynamics, Oxford University Press, Oxford, 1996.

[31] C.G. Zoski, Handbook of Electrochemistry, in, Elsevier, Amsterdam, The Netherlands, 2007.

[32] G. Prentice, Electrochemical Engineering Principles, Prentice Hall, Upper Saddle River, New Jersey, 1991.

[33] A.C. Fisher, Electrode Dynamics, Oxford University Press, 1996.

[34] D. Pletcher, A First Course in Electrode Process, The Electrochemical Consultancy, Hants, England, 1991.

[35] M. Bowker, The Basis Applications of Heterogeneous Catalysis, Oxford University Press, Oxford 1998.

[36] T. Aruga, Y. Murata, Progress in Surface Science, 31 (1989) 61-130.

[37] I.V. Yentekakis, C.G. Vayenas, Journal of Catalysis, 111 (1988) 170-188.

[38] S. Bebelis, N. Kotsionopoulos, Solid State Ionics, 177 (2006) 2205-2209.

[39] S. Neophytides, C.G. Vayenas, Journal of Catalysis, 118 (1989) 147-163.

[40] C.G. Vayenas, S. Bebelis, I.V. Yentekakis and H.G. Lintz, Catalysis Today, 11 (1992) 303-438.

[41] C.G. Vayenas, S. Bebelis, M. Despotopoulou, Journal of Catalysis, 128 (1991) 415-435.

[42] A. Kaloyannis, C.G. Vayenas, Journal of Catalysis, 182 (1999) 37-47.

[43] P. Vernoux, F. Gaillard, L. Bultel, E. Siebert, M. Primet, Journal of Catalysis, 208 (2002) 412-421.

[44] P.D. Petrolekas, S. Brosda, C.G. Vayenas, Journal of The Electrochemical Society, 145 (1998) 1469-1477.

[45] A. de Lucas-Consuegra, Á. Caravaca, P. Sánchez, F. Dorado, J.L. Valverde, Journal of Catalysis, 259 (2008) 54-65.

[46] A. de Lucas-Consuegra, F. Dorado, C. Jiménez-Borja, A. Caravaca, P. Vernoux, J.L. Valverde, Catalysis Today, 146 (2009) 293-298.

[47] A. de Lucas-Consuegra, F. Dorado, C. Jiménez-Borja, J.L. Valverde, Applied Catalysis B: Environmental, 78 (2008) 222-231.

[48] I.V. Yentekakis, C.G. Vayenas, Journal of Catalysis, 149 (1994) 238-242.

[49] D. Tsiplakides, S.G. Neophytides, O. Enea, M. Jaksic, C.G. Vayenas, Journal of The Electrochemical Society, 144 (1997) 2072-2078.

[50] A. Thursfield, S. Brosda, C. Pliangos, T. Schober, C.G. Vayenas, Electrochimica Acta, 48 (2003) 3779-3788.

[51] I.M. Petrushina, V.A. Bandur, F. Cappeln, N.J. Bjerrum, Journal of The Electrochemical Society, 147 (2000) 3010-3013.

[52] S.G. Neophytides, D. Tsiplakides, P. Stonehart, M.M. Jaksic, C.G. Vayenas, Nature, 370 (1994) 45-47.

[53] I. Garagounis, V. Kyriakou, C. Anagnostou, V. Bourganis, I. Papachristou, M. Stoukides, ChemInform, 42 (2011) no-no.

[54] A.D. Frantzis, S. Bebelis, C.G. Vayenas, Solid State Ionics, 136–137 (2000) 863-872.

[55] S. Bebelis, C.G. Vayenas, Journal of Catalysis, 138 (1992) 588-610.

[56] M. Marwood, C.G. Vayenas, Journal of Catalysis, 170 (1997) 275-285.

[57] C. Pliangos, C. Raptis, T. Badas, C.G. Vayenas, Solid State Ionics, 136–137 (2000) 767-773.

[58] C. Pliangos, I.V. Yentekakis, X.E. Verykios, C.G. Vayenas, Journal of Catalysis, 154 (1995) 124-136.

[59] O.A. Mar'ina, V.A. Sobyanin, V.D. Belyaev, Materials Science and Engineering: B, 13 (1992) 153-155.

[60] I.V. Yentekakis, Y. Jiang, S. Neophytides, S. Bebelis, C.G. Vayenas, Ionics, 1 (1995) 491-498.

[61] S. Wodiunig, V. Patsis, C. Comninellis, Solid State Ionics, 136–137 (2000) 813-817.

[62] D. Tsiplakides, J. Nicole, C.G. Vayenas, C. Comninellis, Journal of The Electrochemical Society, 145 (1998) 905-908.

[63] M. Marwood, C.G. Vayenas, Journal of Catalysis, 178 (1998) 429-440.

[64] F. Dorado, A. de Lucas-Consuegra, P. Vernoux and J.L. Valverde, Applied Catalysis B: Environmental, 73 (2007) 42-50.

[65] A. Lintanf, E. Djurado, P. Vernoux, Solid State Ionics, 178 (2008) 1998-2008.

[66] P. Vernoux, F. Gaillard, R. Karoum, A. Billard, Applied Catalysis B: Environmental, 73 (2007) 73-83.

[67] G. Beck, H. Fischer, E. Mutoro, V. Srot, K. Petrikowski, E. Tchernychova, M. Wuttig, M. Rühle, B. Luerßen, J. Janek, Solid State Ionics, 178 (2007) 327-337.

[68] E. Mutoro, C. Koutsodontis, B. Luerssen, S. Brosda, C.G. Vayenas, J. Janek, Applied Catalysis B: Environmental, 100 (2010) 328-337.

[69] E. Mutoro, B. Luerssen, S. Günther, J. Janek, Solid State Ionics, 179 (2008) 1214-1218.

[70] C.G. Vayenas, S. Bebelis, Catalysis Today, 51 (1999) 581-594.

[71] C.G. Vayenas, A. Ioannides, S. Bebelis, Journal of Catalysis, 129 (1991) 67-87.

[72] G. Fóti, V. Stanković, I. Bolzonella, C. Comninellis, Journal of Electroanalytical Chemistry, 532 (2002) 191-199.

[73] J. Yi, A. Kaloyannis, C.G. Vayenas, Electrochimica Acta, 38 (1993) 2533-2539.

[74] D. Tsiplakides, S. Neophytides, C.G. Vayenas, Solid State Ionics, 136–137 (2000) 839-847.

[75] S. Ladas, S. Bebelis, C.G. Vayenas, Surface Science, 251-252 (1991) 1062-1068.

[76] D.A. Emery, P.H. Middleton, I.S. Metcalfe, Surface Science, 405 (1998) 308-315.

[77] S. Ladas, S. Kennou, S. Bebelis, C.G. Vayenas, The Journal of Physical Chemistry, 97 (1993) 8845-8848.

[78] S.G. Neophytides, D. Tsiplakides, C.G. Vayenas, Journal of Catalysis, 178 (1998) 414-428.

[79] M. Makri, C.G. Vayenas, S. Bebelis, K.H. Besocke, C. Cavalca, Surface Science, 369 (1996) 351-359.

[80] R. Imbihl, J. Janek, Solid State Ionics, 136–137 (2000) 699-705.

[81] C.G. Vayenas, D. Tsiplakides, Surface Science, 467 (2000) 23-34.

[82] H. Reiss, The Journal of Physical Chemistry, 89 (1985) 3783-3791.

[83] D. Poulidi, I. Metcalfe, Journal of Applied Electrochemistry, 38 (2008) 1121-1126.

[84] D. Tsiplakides, C.G. Vayenas, Journal of The Electrochemical Society, 148 (2001) E189-E202.

[85] D. Tsiplakides, C.G. Vayenas, Solid State Ionics, 152–153 (2002) 625-639.

[86] D.A. Emery, P.H. Middleton, I.S. Metcalfe, Journal of The Electrochemical Society, 146 (1999) 2194-2198.

[87] I.S. Metcalfe, Journal of Catalysis, 199 (2001) 247-258.

[88] C.G. Vayenas, S. Brosda, C. Pliangos, Journal of Catalysis, 203 (2001) 329-350.

[89] C. Tsaofang, K.J. Walsh, P.S. Fedkiw, Solid State Ionics, 47 (1991) 277-285.

[90] A. Jaccoud, G. Fóti, C. Comninellis, Electrochimica Acta, 51 (2006) 1264-1273.

[91] E.L. Shoemaker, M.C. Vogt, F.J. Dudek, Solid State Ionics, 92 (1996) 285-292.

[92] T. Kenjo, Y. Yamakoshi, K. Wada, Journal of The Electrochemical Society, 140 (1993) 2151-2157.

[93] A. Jaccoud, C. Falgairette, G. Fóti, C. Comninellis, Electrochimica Acta, 52 (2007) 7927-7935.

[94] C.G. Vayenas, B. Lee, J. Michaels, Journal of Catalysis, 66 (1980) 36-48.

[95] N.A. Anastasijevic, Catalysis Today, 146 (2009) 308-311.

[96] C.G. Yiokari, G.E. Pitselis, D.G. Polydoros, A.D. Katsaounis, C.G. Vayenas, The Journal of Physical Chemistry A, 104 (2000) 10600-10602.

[97] M. Salazar, E.S. Smotkin, Journal of Applied Electrochemistry, 36 (2006) 1237-1240.

[98] F.M. Sapountzi, M.N. Tsampas, C.G. Vayenas, Catalysis Today, 127 (2007) 295-303.

[99] S.P. Balomenou, F. Sapountzi, D. Presvytes, M. Tsampas, C.G. Vayenas, Solid State Ionics, 177 (2006) 2023-2027.

[100] C. Kokkofitis, M. Ouzounidou, A. Skodra, M. Stoukides, Solid State Ionics, 178 (2007) 475-480.

[101] A. Kaloyannis, C.G. Vayenas, Journal of Catalysis, 171 (1997) 148-159.

[102] I.V. Yentekakis, G. Moggridge, C.G. Vayenas, R.M. Lambert, Journal of Catalysis, 146 (1994) 292-305.
[103] C. Pliangos, I.V. Yentekakis, V.G. Papadakis, C.G. Vayenas, X.E. Verykios, Applied Catalysis B: Environmental, 14 (1997) 161-173.
[104] I.V. Yentekakis, A. Palermo, N.C. Filkin, M.S. Tikhov, R.M. Lambert, The Journal of Physical Chemistry B, 101 (1997) 3759-3768.
[105] R. Lambert, I. Harkness, I. Yentekakis, C. Vayenas, Ionics, 1 (1995) 29-31.
[106] O.A. Marina, I.V. Yentekakis, C.G. Vayenas, A. Palermo, R.M. Lambert, Journal of Catalysis, 166 (1997) 218-228.
[107] A. Palermo, R.M. Lambert, I.R. Harkness, I.V. Yentekakis, O. Mar'ina, C.G. Vayenas, Journal of Catalysis, 161 (1996) 471-479.
[108] G. Fóti, O. Lavanchy, C. Comninellis, Journal of Applied Electrochemistry, 30 (2000) 1223-1228.
[109] F.J. Williams, M.S. Tikhov, A. Palermo, N. Macleod, R.M. Lambert, The Journal of Physical Chemistry B, 105 (2001) 2800-2808.
[110] B. Béguin, F. Gaillard, M. Primet, P. Vernoux, L. Bultel, M. Hénault, C. Roux, E. Siebert, Ionics, 8 (2002) 128-135.
[111] P. Vernoux, F. Gaillard, C. Lopez, E. Siebert, Journal of Catalysis, 217 (2003) 203-208.
[112] P. Vernoux, A.Y. Leinekugel-Le-Cocq, F. Gaillard, Journal of Catalysis, 219 (2003) 247-257.
[113] I.V. Yentekakis, M. Konsolakis, R.M. Lambert, N. Macleod, L. Nalbantian, Applied Catalysis B: Environmental, 22 (1999) 123-133.
[114] I.V. Yentekakis, A. Palermo, M.S. Tikhov, N.C. Filkin, R.M. Lambert, Electrochemical promotion in emission control catalysis: The role of Na for the Pt-catalysed reduction of NO by propene, in: A.F. N. Kruse, J.M. Bastin (Eds.) Studies in Surface Science and Catalysis, vol. Volume 116, Elsevier, 1998, pp. 255-264.
[115] F.J. Williams, A. Palermo, M.S. Tikhov, R.M. Lambert, Surface Science, 482–485, Part 1 (2001) 177-182.
[116] N.D. Lang, S. Holloway, J.K. Nørskov, Surface Science, 150 (1985) 24-38.
[117] A. de Lucas-Consuegra, A. Caravaca, M.J. Martín de Vidales, F. Dorado, S. Balomenou, D. Tsiplakides, P. Vernoux, J.L. Valverde, Catalysis Communications, 11 (2009) 247-251.
[118] A. de Lucas-Consuegra, Á. Caravaca, F. Dorado, J.L. Valverde, Catalysis Today, 146 (2009) 330-335.
[119] M.R. Jalil, N. Ibrahim, D. Poulidi, I.S. Metcalfe, Solid State Ionics.
[120] M. Nagata, Y. Itoh, H. Iwahara, Solid State Ionics, 67 (1994) 215-224.
[121] S.B. Adler, B.T. Henderson, M.A. Wilson, D.M. Taylor and R.E. Richards, Solid State Ionics, 134 (2000) 35-42.
[122] W. Schröder, J. Hölzl, Solid State Communications, 24 (1977) 777-780.
[123] J. Cousty, R. Riwan, Surface Science, 204 (1988) 45-56.
[124] S.J.B. Reed, Electron Microprobe Analysis and Scanning Electron Microscopy in Geology, in, Cambridge University Press, Cambridge, 2005.
[125] Geochemical Instrumentation and Analysis, by Darrel Henry, Louisiana State University, http://serc.carleton.edu/research_education/geochemsheets/electroninteractions.html, 25 November 2012.
[126] J.F. Watts, J. Wolstenholme, An Introduction to Surface Analysis by XPS and AES, John Wiley & Sons, West Sussex, 2003.
[127] The Kelvin Probe, 2012, http://www.kelvinprobe.com/whatis-kelvinprobe.html, 26 November 2012.
[128] Kelvin Probe Measurements, 2012, http://rsl.eng.usf.edu/Pages/Tutorials.htm, 26 November 2012.
[129] D.R. Lide, CRC Handbook of Chemistry and Physics, in, CRC Press/Taylor and Francis, Boca Raton, Florida, 2009.

[130] S.G. Neophytides, S. Zafeiratos, S. Kennou, Solid State Ionics, 136–137 (2000) 801-806.

[131] T. Grzybek, G.C. Maiti, D. Scholz, M. Baerns, Applied Catalysis A: General, 107 (1993) 115-124.

[132] S. Dahle, F. Voigts, W. Maus-Friedrichs, Thin Solid Films, 520 (2012) 1842-1846.

[133] NIST X-ray Photoelectron Spectroscopy Database 2000, National Institute of Standards and Technology (NIST), http://srdata.nist.gov/xps/, 12 November 2012.

[134] I.R. Harkness, C. Hardacre, R.M. Lambert, I.V. Yentekakis, C.G. Vayenas, Journal of Catalysis, 160 (1996) 19-26.

[135] J. Hölzl, F.K. Schulte, Work function of metals in Solid surface physics / contributions by J. Hölzl, F.K. Schulte, H. Wagner, Springer-Verlag, Berlin 1979.

[136] M. Konsolakis, N. Macleod, J. Isaac, I.V. Yentekakis, R.M. Lambert, Journal of Catalysis, 193 (2000) 330-337.

[137] M. Kiskinova, G. Rangelov, L. Surnev, Surface Science, 150 (1985) 339-350.

[138] L. Bultel, C. Roux, E. Siebert, P. Vernoux, F. Gaillard, Solid State Ionics, 166 (2004) 183-189.

[139] A.J. Bard, L.R. Faulkner, Electrochemical Methods : Fundamentals and Applications, 2 ed., John Wiley & Sons, 2001.

[140] Linear Sweep and Cyclic Voltametry: The Principles, 2012, Department of Chemical Engineering and Biotechnology, University of Cambridge, http://www.ceb.cam.ac.uk/pages/linear-sweep-and-cyclic-voltametry-the-principles.html, 24 September 2012.

[141] R.G. Compton, C.E. Banks, Understanding voltammetry, 2nd Edition ed., Imperial College Press, London, 2011.

[142] A. de Lucas-Consuegra, F. Dorado, J.L. Valverde, R. Karoum, P. Vernoux, Journal of Catalysis, 251 (2007) 474-484.

[143] S. Souentie, C. Xia, C. Falgairette, Y.D. Li, C. Comninellis, Electrochemistry Communications, 12 (2010) 323-326.

[144] J. Nicole, D. Tsiplakides, S. Wodiunig, C. Comninellis, Journal of The Electrochemical Society, 144 (1997) L312-L314.

[145] J.C. Bertolini, P. Delichère, J. Massardier, Surface Science, 160 (1985) 531-541.

[146] F. Dorado, A. de Lucas-Consuegra, P. Vernoux, J.L. Valverde, Applied Catalysis B: Environmental, 73 (2007) 42-50.

[147] R. Burch, P.J. Millington, Catalysis Today, 26 (1995) 185-206.

[148] R. Burch, P.J. Millington, Catalysis Today, 29 (1996) 37-42.

[149] N. Macleod, J. Isaac, R.M. Lambert, Journal of Catalysis, 198 (2001) 128-135.

[150] M. Konsolakis, N. Macleod, J. Isaac, I.V. Yentekakis, R.M. Lambert, Journal of Catalysis, 193 (2000) 330-337.

[151] M. Konsolakis, I.V. Yentekakis, Journal of Hazardous Materials, 149 (2007) 619-624.

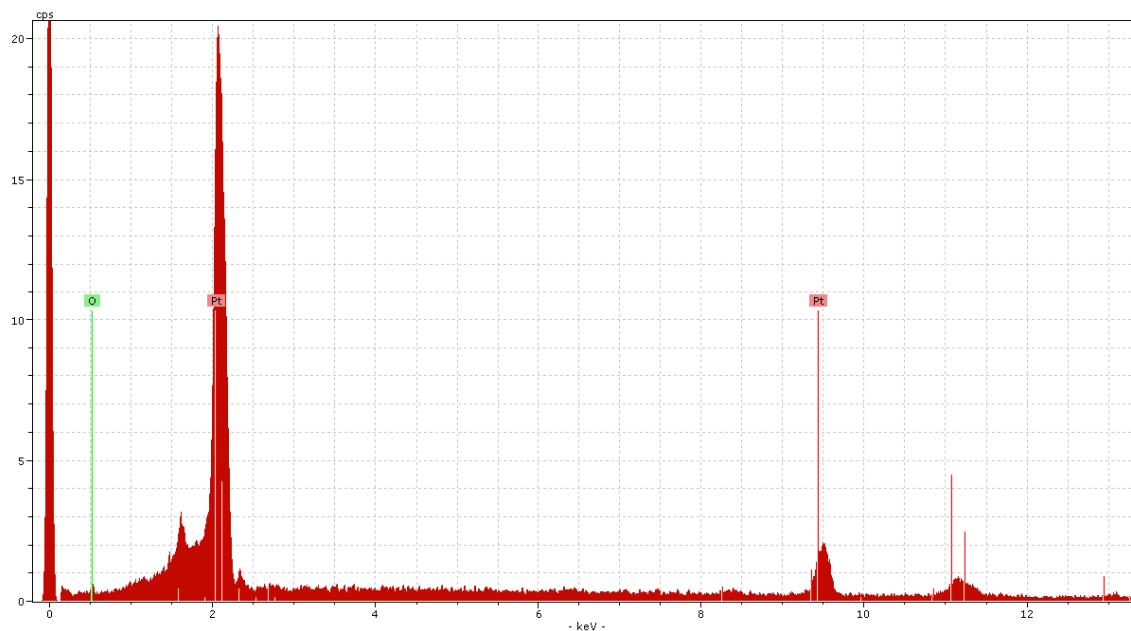[152] R. Burch, T.C. Watling, Catalysis Letters, 43 (1997) 19-23.

Appendices
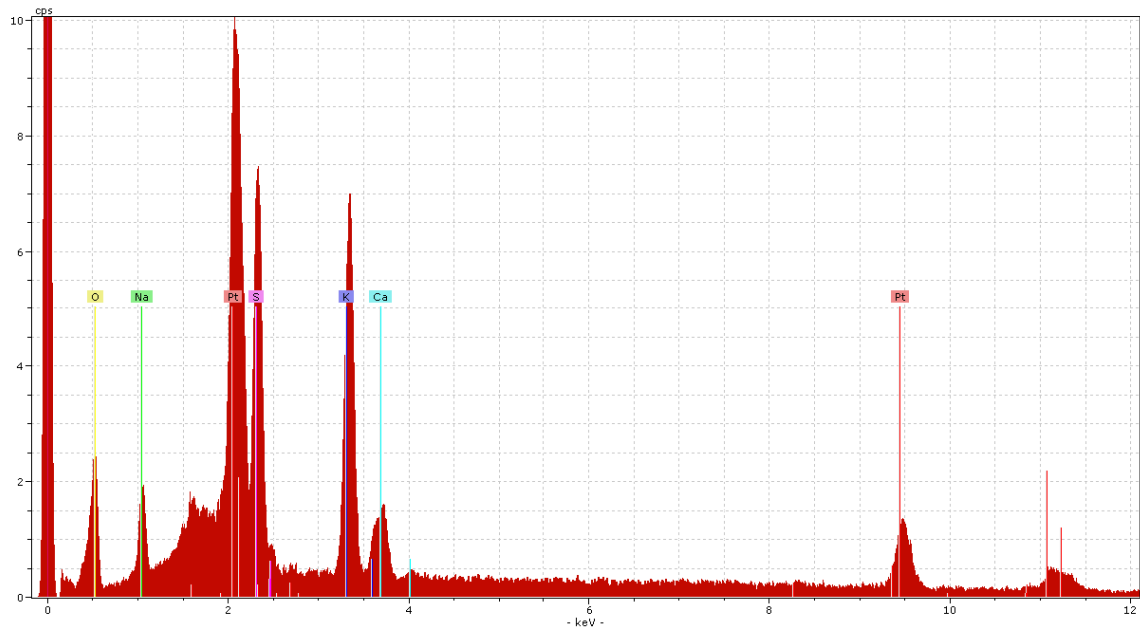
A. EDX spectra
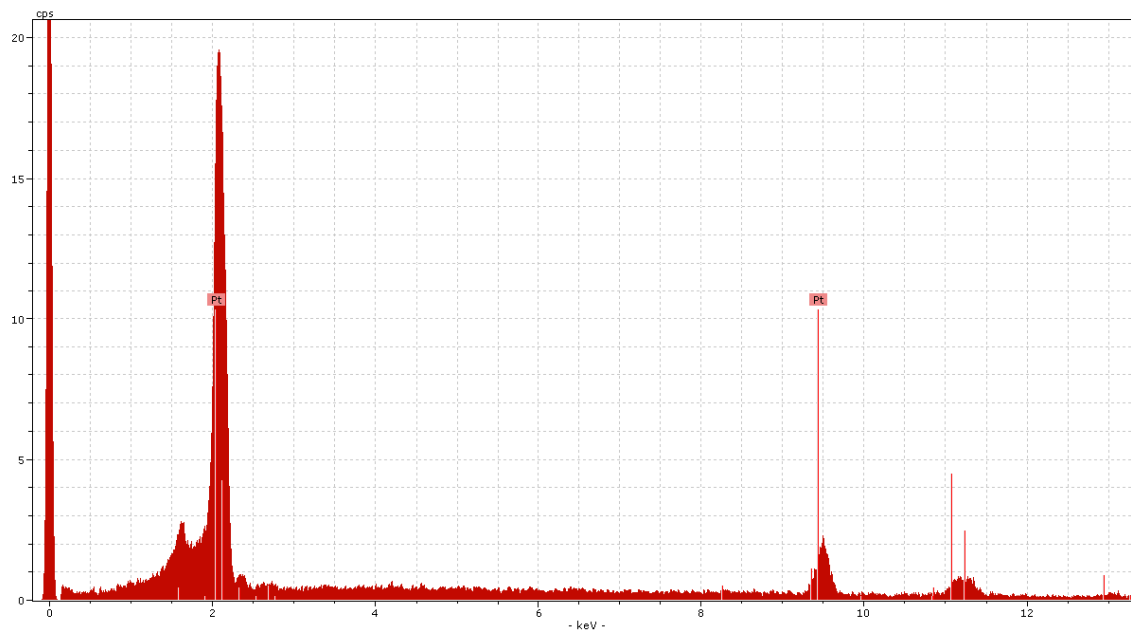
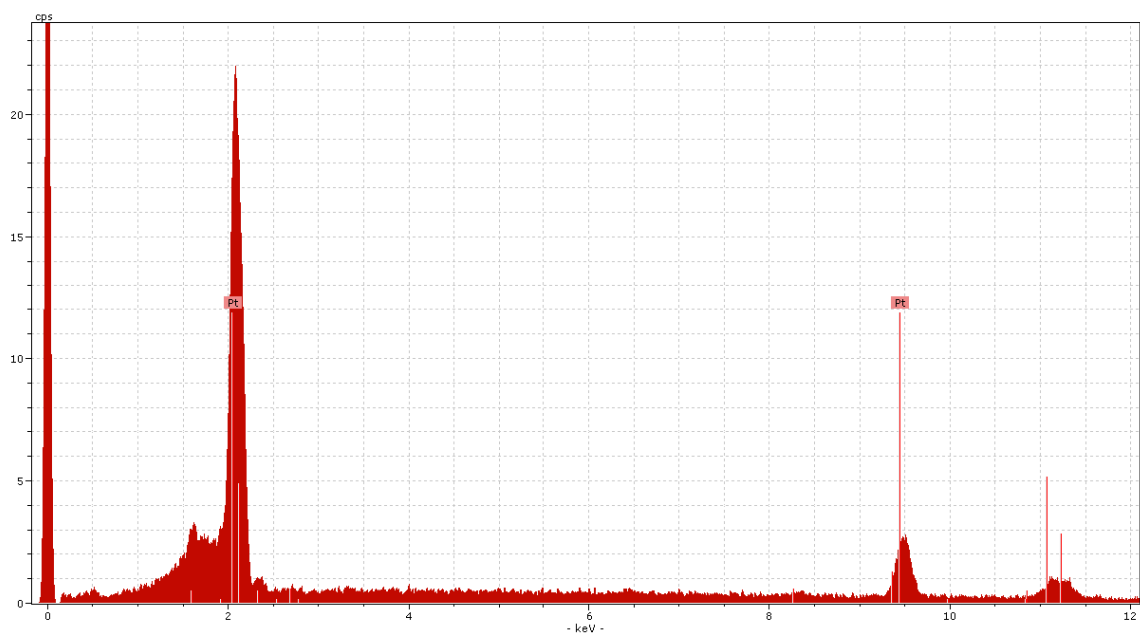a. Fresh 'clean' platinum sample
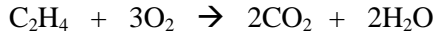

b. Fresh platinum sample modified with $5x10^{-2}$M NaOH

c. Used platinum sample (modified with $5x10^{-2}$ M NaOH) – Spot A

d. Used platinum sample (modified with $5x10^{-2}$ M NaOH) – Spot B

B. Material balance calculation

❖ C_2H_4 oxidation in Pt/YSZ system at 350^oC

$$C_2H_4 \; + \; 3O_2 \; \rightarrow \; 2CO_2 \; + \; 2H_2O$$

• An example for carbon balance calculation

$2*(C_2H_4)_{in} + (CO_2)_{in} = 2*(C_2H_4)_{out} + (CO_2)_{out}$

Using data from GC, for 8 kPa O_2 and 0.5 kPa C_2H_4 for a sodium modified sample (V502)
$(C_2H_4)_{in} = 0.58$ kPa, $(C_2H_4)_{out} = 0.46$ kPa, $(CO_2)_{out} = 0.18$ kPa, $(CO_2)_{in} \approx 0$
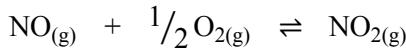
$(2*0.58) = (2*0.46) + 0.18$
$1.16 \approx 1.10 \rightarrow (1.16\text{-}1.10)/1.16*100 = 5.2\%$
For other conditions, carbon balance is closed within 1-5%.

❖ NO reduction by propene in Pt/YSZ system at 350^oC

Main reactions taking place
$$C_3H_{6(g)} \; + \; ^9\!/_2\, O_{2(g)} \; \rightleftharpoons \; 3CO_{2(g)} \; + \; 3H_2O_{(g)}$$
$$C_3H_{6(g)} \; + \; 9NO_{(g)} \; \rightleftharpoons \; 3CO_{2(g)} \; + \; ^9\!/_2\, N_{2(g)} \; + \; 3H_2O_{(g)}$$
$$C_3H_{6(g)} \; + \; 18NO_{(g)} \; \rightleftharpoons \; 3CO_{2(g)} \; + \; 9N_2O_{(g)} \; + \; 3H_2O_{(g)}$$
$$NO_{(g)} \; + \; ^1\!/_2\, O_{2(g)} \; \rightleftharpoons \; NO_{2(g)}$$
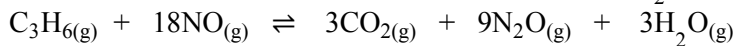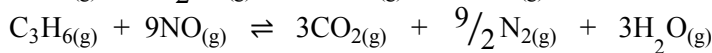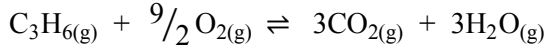
• An example for carbon balance calculation

$3*(C_3H_6)_{in} + (CO_2)_{in} = 3*(C_3H_6)_{out} + (CO_2)_{out}$

Using data from GC, for 5 kPa O_2, 0.1 kPa C_3H_6 and 0.1 kPa NO for a sodium modified sample (V502),

$(C_3H_6)_{in} = 0.10$ kPa, $(C_3H_6)_{out} = 0.08$ kPa, $(CO_2)_{out} = 0.05$ kPa, $(CO_2)_{in} \approx 0$
$(3*0.1) = (3*0.08) + 0.05$
$0.3 \approx 0.29 \rightarrow (0.3\text{-}0.29)/0.30*100 = 3.3\%$
For other conditions, carbon balance is closed within 2-5%.

• An example for nitrogen balance calculation

$(NO)_{in} + 2*(N_2)_{in} \; + \; 2*(N_2O)_{in} + (NO_2)_{in} \; = (NO)_{out} + 2*(N_2)_{out} \; + \; 2*(N_2O)_{out} + (NO_2)_{out}$

Using data from NO-NO_2-N_2O analyser and from GC (N_2 only), at 0.5 kPa O_2, 0.1 kPa C_3H_6 and 0.1 kPa NO for a 'clean' sample,

$(NO)_{in} = 0.9778$ kPa, $(N_2)_{out} = 0.016$ kPa, $(N_2O)_{out} = 0.0016$ kPa, $(NO_2)_{out} = 0.0524$
$(NO)_{out} = 0.9774$ kPa, $(N_2)_{out} = 0.019$ kPa, $(N_2O)_{out} = 0.0025$ kPa, $(NO_2)_{out} = 0.0237$

$0.9778 + (2*0.016) + (2*0.0016) + 0.0524 = 0.9774 + (2*0.019) + (2*0.0025) + 0.0237$
$1.0654 \approx 1.0445 \rightarrow (1.0654\text{-}1.0445)/1.0654*100 = 2\%$

For other conditions, carbon balance is closed within 8-20% because N_2 data from GC is close to the detection limit, however the reported N_2 production rates are calculated from N balance (NO_2, NO, N_2 and N_2O), instead of N_2 given by GC.

Some kinetic data from occasional checks on N_2 production under open-circuit conditions using GC to compare with N_2 calculated from nitrogen balance from NO, NO_2 and N_2O data from analyser. Total flow rate = 100 ml min^{-1}. $p_{NO} = p_{C_3H_6} = 0.1$ kPa

Sample	p_{O_2} (kPa)	N_2 concentration	
		GC reading (%)	Calculated from N balance (%)
V000	0.5	0.0028 ± 0.0004	0.0021
	1	0.0084 ± 0.0011	0.0016
	5	ND	0.0010
V104	0.5	0.0080 ± 0.0007	0.0018
	1	0.0036 ± 0.0005	0.0011
	5	ND	0.0009
V102	0.5	ND	0.0009
	1	0.0083 ± 0.0012	0.0022
	5	ND	0.0009
V502	0.5	0.010 ± 0.0006	0.0029
	1	0.0087 ± 0.0015	0.0024
	5	ND	0.0008

C. Data for non-reactive study

Cyclic voltammogram of reverse anodic potential under 20 kPa oxygen showing peak broadening and total current increase at high sodium coverage
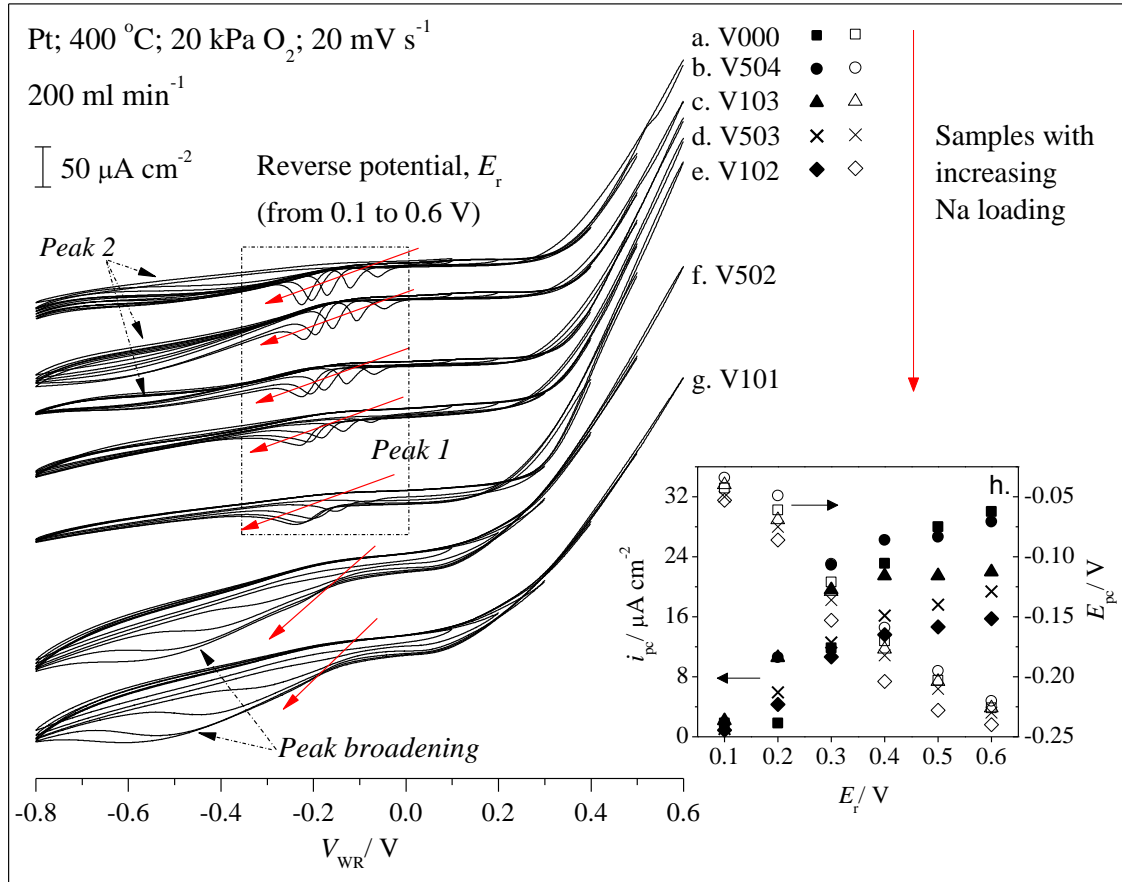
D. Data for reactive study

Potentiostatic transient data for low oxygen partial pressures, p_{O_2} = 0.5 and 1.5 kPa (near-stoichiometric conditions). Figure a shows negative polarisation, while figure b shows positive polarisation.

- p_{O_2} = 0.5 kPa

Pt/YSZ; p_{O_2}= 0.5 kPa; $p_{C_2H_4}$= 0.5 kPa; T = 350°C; f = 200ml min^{-1}

Pt/YSZ; p_{O_2}= 1.5 kPa; $p_{C_2H_4}$= 0.5 kPa; T = 350°C; f = 200ml min^{-1}
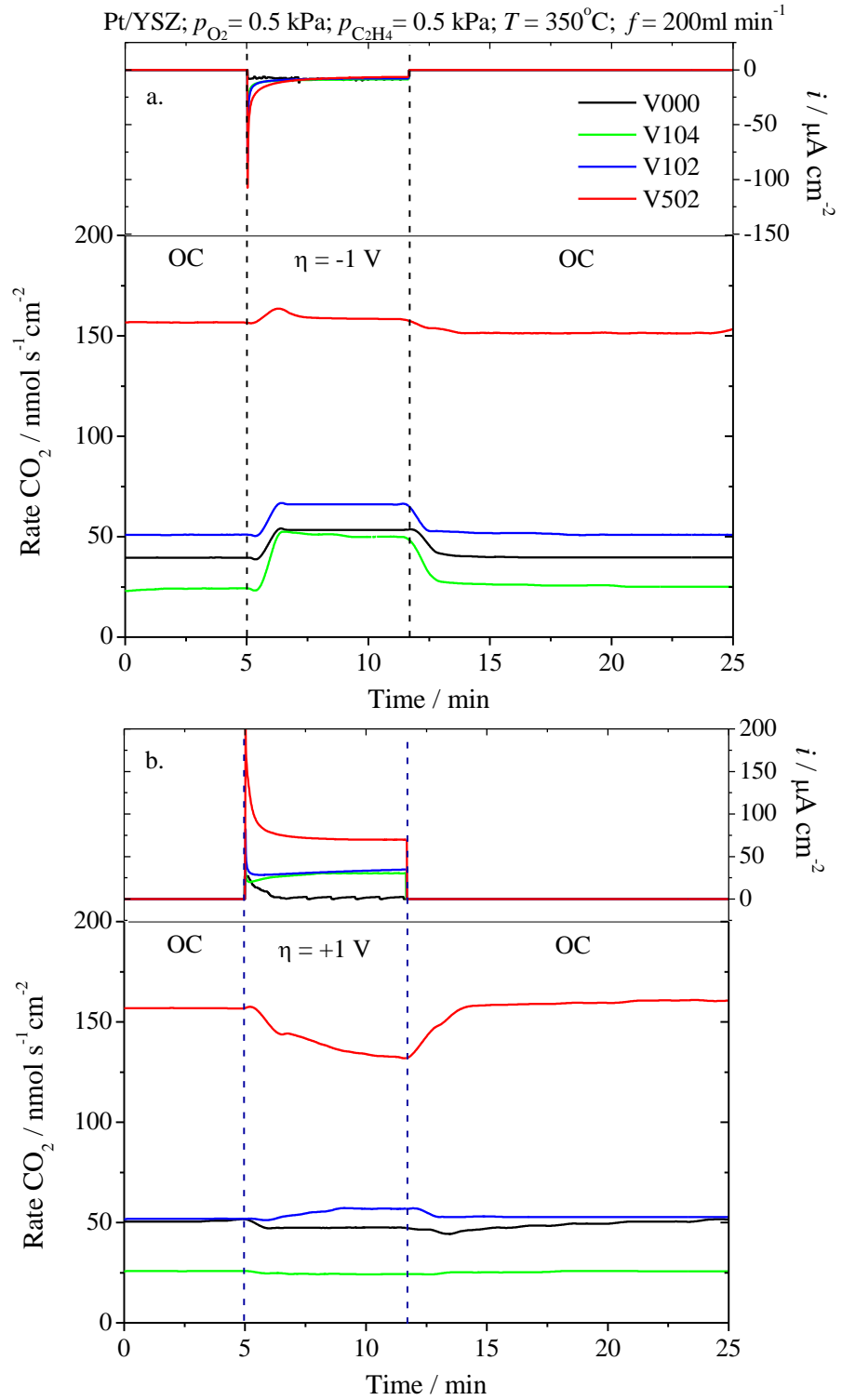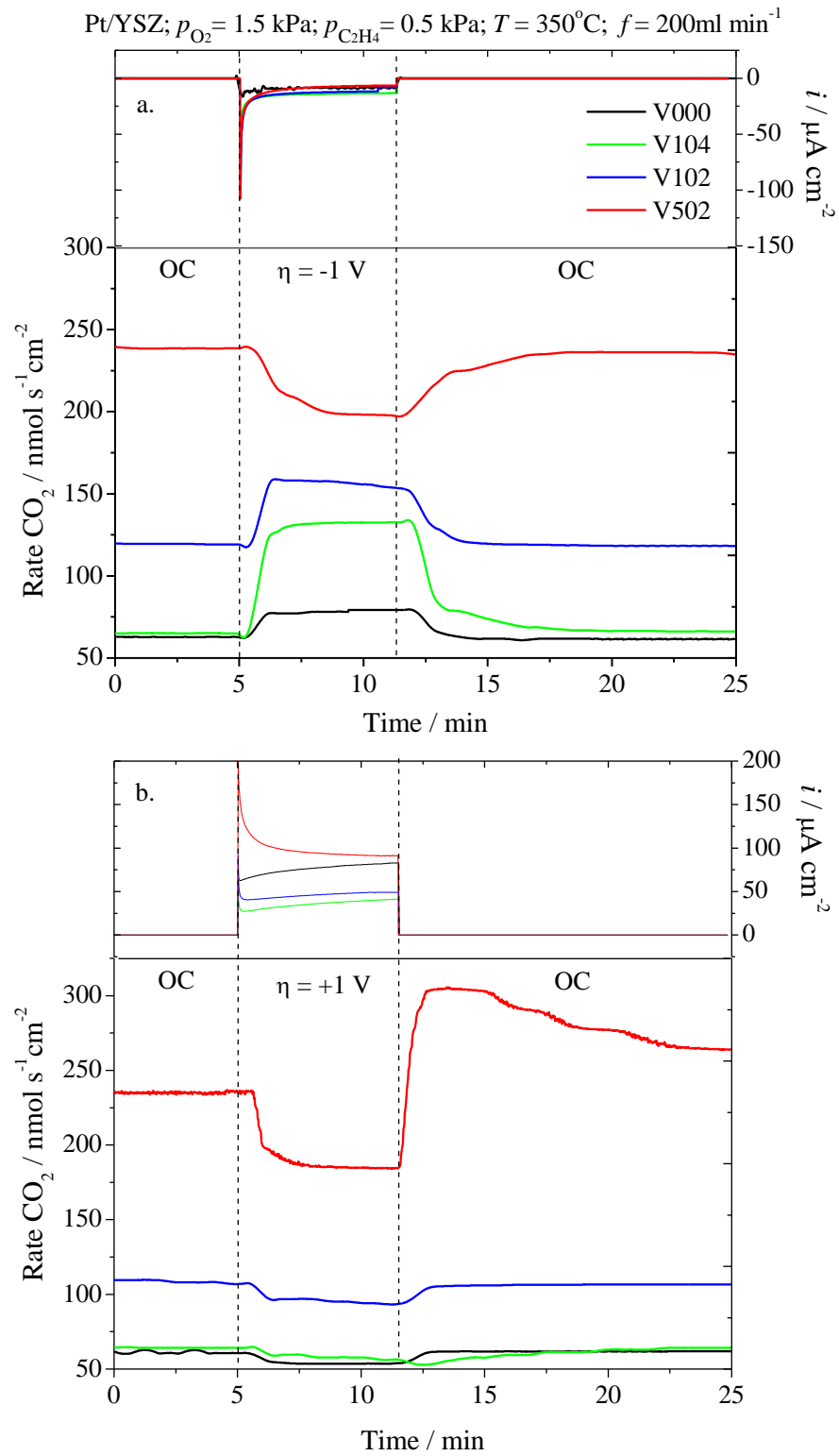
- **Rate dependence on work function change for oxygen partial pressures varying from 0.5 to 8 kPa**

Figure a only shows the CO_2 production rate under open-circuit conditions, where Δr is assumed to be caused only by $\Delta\Phi_{Na}$. Figure b includes the effect of applying electrical polarisation to the system, so the rate change, Δr, is caused by the total work function change, $\Delta\Phi_{tot} = \Delta\Phi_{Na} + \Delta\Phi_{el}$. We can see that in general increasing the oxygen partial pressure causes the reaction rate dependence on changes in the work function to become more random.

1. **Ethylene oxidation**

Pt/YSZ; $T = 350^{\circ}C$; $p_{C2H4} = 0.5$ kPa; $f = 200$ ml min^{-1}

2. **NO reduction**

Pt/YSZ; $T = 350^{\circ}C$; $p_{NO} = p_{C3H6} = 0.1$ kPa

p_{O2} (kPa): ○ 0.5; △ 1; ◇ 5

a. CO_2 production

b. N_2 production

electrophobic under high p_{O2}

Rate / nmol s^{-1} cm^{-2}

$\Delta\Phi$ / eV
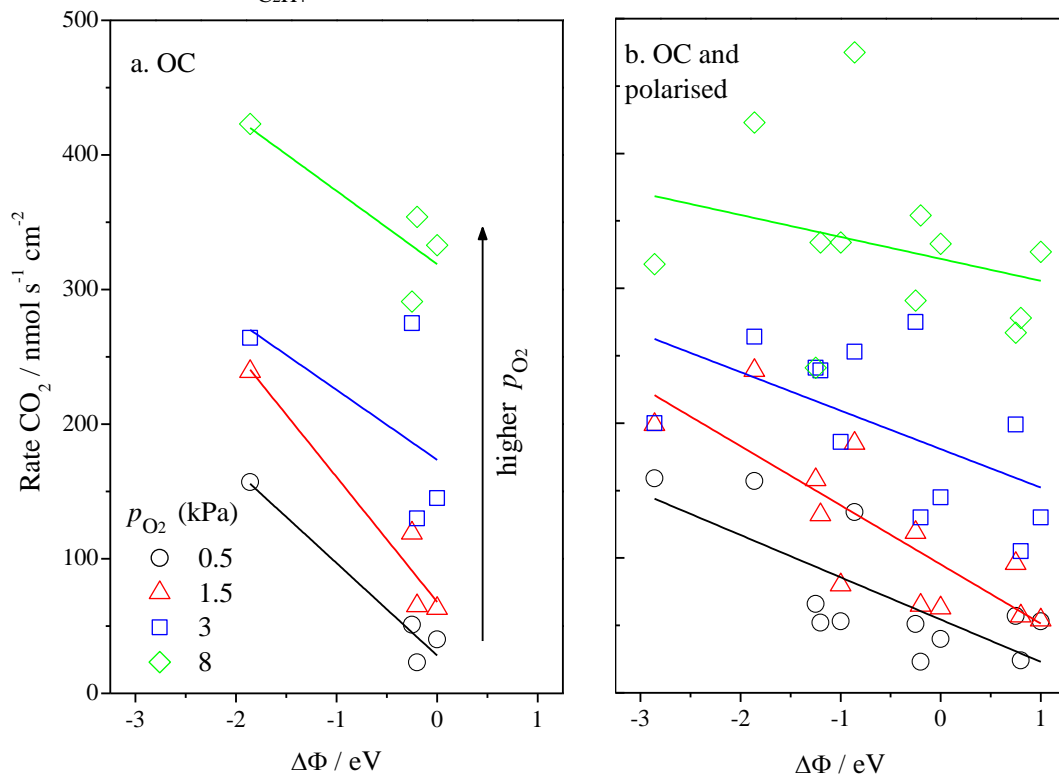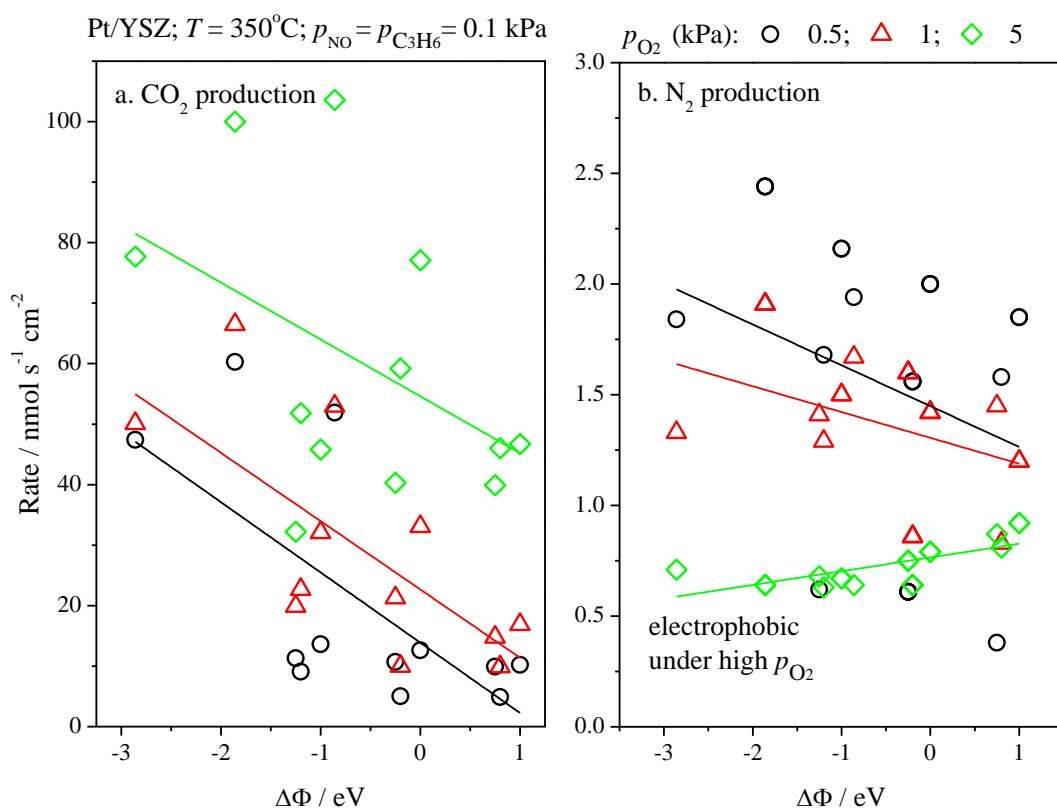
- **Reaction rate data under open-circuit and polarised conditions:**

Ethylene oxidation on Metalor platinum catalyst

$p_{C_2H_4}$ (kPa)	p_{O_2} (kPa)	rOC				r(-1V)			
		V000	V104	V102	V502	V000	V104	V102	V502
0.5	0.5	40	23	51	157	**53**	**52**	**66**	**159**
	1.5	63	65	119	239	**80**	**132**	**158**	199
	3	145	130	275	264	**186**	**239**	241	200
	8	333	354	291	423	**334**	334	241	318

$p_{C_2H_4}$ (kPa)	p_{O_2} (kPa)	rOC				r(+1V)			
		V000	V104	V102	V502	V000	V104	V102	V502
0.5	0.5	58	26	52	157	53	24	57	134
	1.5	61	64	109	235	54	57	96	185
	3	159	123	277	252	130	105	199	253
	8	342	343	290	426	276	278	267	**475**

NO reduction by propene on Metalor platinum catalyst:

i) CO_2 transients with Metalor sample, $T = 350^{o}C$ – CO_2 production rate. Shaded box is an increase more than 2 nmol s^{-1} cm^{-2}.

p_{O2} (kPa)	V000	V104	V102	V502	V000	V104	V102	V502
	rOC				r(-1V)			
0.5	13	5	11	60	**14**	**9**	11	47
1.0	33	10	21	67	32	**23**	20	50
5.0	77	59	40	100	46	52	32	78
	rOC				r(+1V)			
0.5	12	5	13	59	10	5	10	52
1.0	32	10	21	67	17	10	15	53
5.0	69	55	40	99	47	46	40	**104**

ii) N_2 transients with Metalor sample, $T = 350^{o}C$ – N_2 production rate. Shaded box is an increase more than 0.2 nmol s^{-1} cm^{-2}. nmol s^{-1} cm^{-2}.

p_{O2} (kPa)	V000	V104	V102	V502	V000	V104	V102	V502
	rOC				r(-1V)			
0.5	2.0	1.6	0.6	2.4	**2.2**	**1.7**	0.6	1.8
1.0	1.4	0.9	1.6	1.9	**1.5**	**1.3**	1.4	1.3
5.0	0.8	0.6	0.8	0.6	0.8	0.6	0.7	**0.7**
	rOC				r(+1V)			
0.5	1.9	1.7	0.5	2.4	1.9	1.6	0.4	1.9
1.0	1.4	0.8	1.8	2.0	1.2	0.8	1.5	1.7
5.0	0.8	0.8	0.7	0.6	**0.9**	0.8	**0.9**	0.6

- **Selectivity to N₂ versus nominal sodium coverage**

Pt/YSZ; $p_{NO} = p_{C_3H_6} = 0.1$ kPa; $T = 350^{\circ}$C; $f = 100$ ml min^{-1}
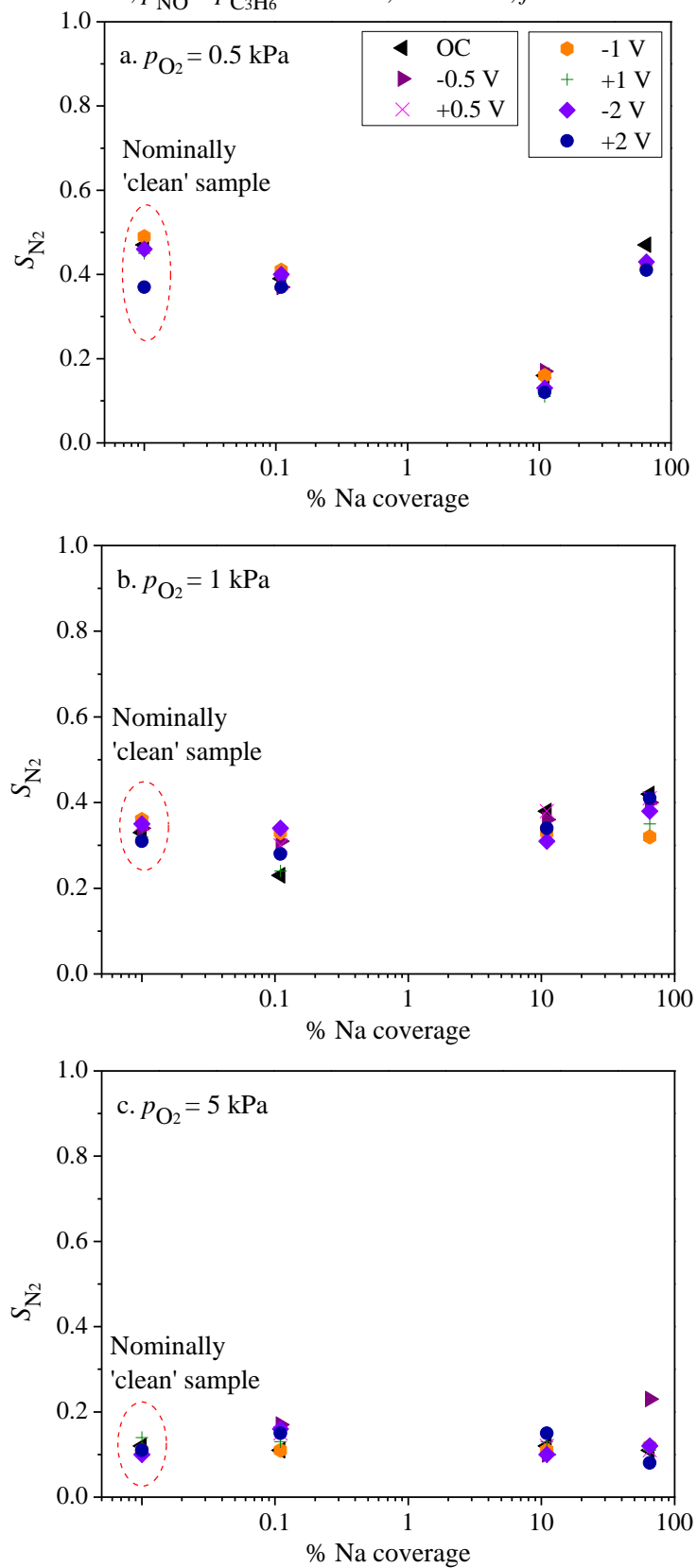
- **The effect of varying the applied overpotentials on sodium modification**

The example shown below is for Sample V502 (65% Na coverage) under fuel lean condition. No significant effect on the promotional behaviour is observed.

Pt/YSZ; p_{O_2}= 5 kPa; p_{NO}= $p_{C_3H_6}$= 0.1 kPa; T = 350°C

a. Negative polarisation,
V502 sample (65% Na coverage)

b. Positive polarisation,
V502 sample (65% Na coverage)

$\rho_{(+0.5\ V)}$= 1.0
$\Lambda_{(+0.5\ V)}$= -89
$\rho_{(+1.0\ V)}$= 1.0
$\Lambda_{(+1.0\ V)}$= -31
$\rho_{(+2.0\ V)}$= 1.1
$\Lambda_{(+2.0\ V)}$= -8
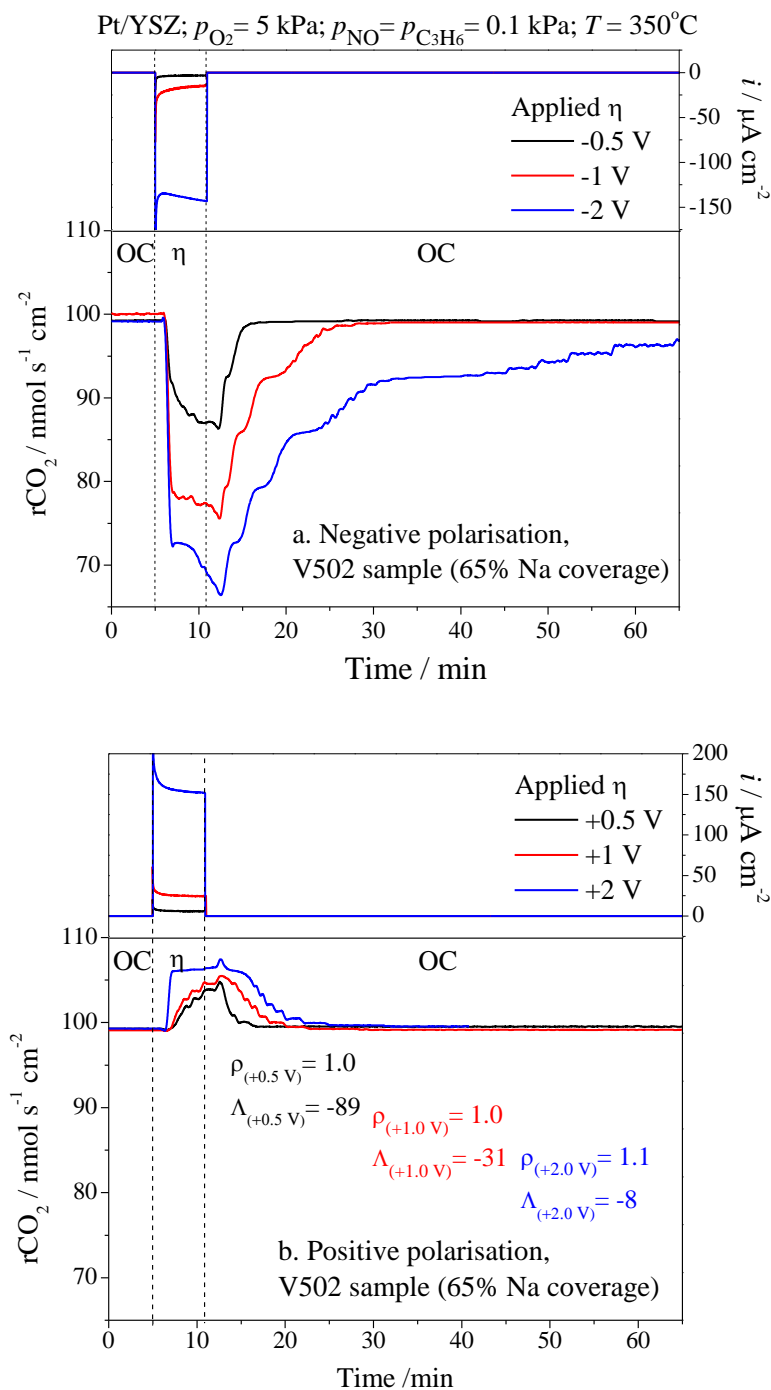
E. Publications

- Publication 1

The role of sodium surface species on oxygen charge transfer in the Pt/YSZ system

Naimah Ibrahim [a,b], Danai Poulidi [a], Maria Elena Rivas [a], Iain D. Baikie [c], Ian S. Metcalfe [a,*]

[a] School of Chemical Engineering and Advanced Materials, Newcastle University, Merz Court, Newcastle upon Tyne, NE1 7RU, UK
[b] School of Environmental Engineering, Universiti Malaysia Perlis, 02600 Arau, Perlis, Malaysia
[c] KP Technology Ltd., Burn Street, Wick, Caithness, KW1 5EH, Scotland, UK

ARTICLE INFO

ABSTRACT

The role of sodium surface species in the modification of a platinum (Pt) catalyst film supported on 8 mol% yttria-stabilised-zirconia (YSZ) was investigated under a flow of 20 kPa oxygen at 400 °C. Cyclic and linear sweep voltammetry were used to investigate the kinetics of the oxygen charge transfer reaction. The Pt/YSZ systems of both 'clean' and variable-coverage sodium-modified catalyst surfaces were also characterised using SEM, XPS and work function measurements using the Kelvin probe technique.

Samples with sodium coverage from 0.5 to 100% were used. It was found that sodium addition modifies the binding energy of oxygen onto the catalyst surface. Cyclic voltammetry experiments showed that higher overpotentials were required for oxygen reduction with increasing sodium coverage. In addition, sodium was found to modify oxygen storage and/or adsorption and diffusion increasing current densities at higher cathodic overpotential. Ex situ XPS measurements showed the presence of sodium hydroxide, carbonate and/or oxide species on the catalyst surface, while the Kelvin probe technique showed a decrease of approximately 250 meV in the work function of samples with more than 50% sodium coverage (compared to a nominally 'clean' sample).

1. Introduction

The solid electrolyte system of $Pt(O_2)/YSZ$ has been extensively studied in the past to enhance the understanding of many important fields such as fuel cells, electrochemical oxygen pumps and oxygen sensors [1,2]. The overall electrochemical reaction for the reduction of gaseous oxygen can be written as:

$$O_2(g) + 4e^- + 2V_O^{\bullet\bullet} \leftrightarrow 2O_O \quad (1)$$

where $V_O^{\bullet\bullet}$ is an oxygen vacancy in the lattice of zirconia, e^- is an electron and O_O is oxygen in the lattice [1]. The $Pt(O_2)/YSZ$ system is also of great importance in the fundamental study of electrocatalysis and can be considered to be a model system that can be employed to understand the nature of oxygen pumping and spillover processes in electrochemical promotion of metal catalysts supported on oxygen-ion-conducting membrane solid electrolytes. In electrochemical promotion of catalysis (EPOC), the supply of a small electrical current through an external circuit results in promoter species, such as oxygen ions being pumped towards the catalyst surface, and modifies the catalytic activity and selectivity of a reaction in a reversible and pronounced manner [3–5]. One of the electrochemical techniques often used to investigate

the $Pt(O_2)/YSZ$ electrode system is cyclic voltammetry (CV). The appearance of multiple cathodic peaks on the cyclic voltammograms has been used to identify the spillover oxygen anion species and to quantify the three-phase-boundary length [6]. However, it has also been reported that the appearance of the CV peaks under oxygen can be explained by the electrochemical formation of platinum oxide species (PtO_x) [1,2,7]. Recently, the presence of impurities (e.g. silicon) in the $Pt(O_2)/YSZ$ system has also been shown to influence the CV features [8]. However, the role of impurities in the electrochemical and electrocatalytic behaviour of a catalyst system has not been studied in detail and indeed the role of impurities is not fully understood. Impurities may have differing effects on catalyst systems. They may act as poisons (blocking active sites and reducing catalytic activity) or they may in fact have a promoting role in the catalytic reaction. (The term impurity is used here only to indicate an unknown type and amount of a foreign surface species on the catalyst.) Therefore, a systematic study is necessary to fully assess the effect of impurities on a catalyst system (in this case Pt/YSZ). In order to study the role of impurities, a known type and amount of a foreign species can be deposited on a nominally 'clean' catalyst surface. The term nominally 'clean' is used here as it is possible that a certain level of unknown and uncharacterised impurities may exist on any catalyst surface (due to the method of preparation, the purity of raw materials etc.). By gradually increasing a species concentration on the catalyst, we can systematically investigate the difference between the 'clean' and

* Corresponding author.
E-mail address: i.metcalfe@ncl.ac.uk (I.S. Metcalfe).

the contaminated systems while eliminating the effects of variation in electrode characteristics due to inconsistencies in the electrode preparation.

In this paper we investigate the effect of the presence of sodium species on oxygen charge transfer in a Pt/YSZ system using different characterisation techniques. Considering only the tpb process, the charge transfer reaction is shown in Eq. (2):

$$O(tpb) + 2e^- \leftrightarrow O^{2-} \tag{2}$$

where O(tpb) is the atomic oxygen adsorbed at the Pt-YSZ-gas interface (tpb). O(tpb) can be created either by adsorption of oxygen from the gas phase and diffusion to the tpb (Eq. (3)), or by the reverse of Eq. (2) (oxidation of ionic oxygen species from the YSZ electrolyte).

$$\frac{1}{2}O_2(g) \rightarrow O(a) \rightarrow O(tpb) \tag{3}$$

Sodium was chosen in this work as it is known to affect the activity of metal catalysts [9–12] by acting as a catalyst promoter. Additionally, it has been used as promoter in many EPOC catalytic reactions using sodium-ion conducting supports [13–15], particularly to enhance the rate of NO_x conversion [16,17]. Sodium deposition on the platinum surface could affect the catalyst system in a number of ways.

(i) Sodium species could adopt a spectator role in the charge transfer reaction and simply occupy the platinum active sites. This may be manifested as a lower rate of the charge transfer in the cyclic voltammetry experiments.

(ii) Sodium may modify the charge transfer reaction by creating new sites for, or modifying the kinetics of, oxygen storage, adsorption and diffusion from the gas phase, possibly through modification of the binding strength of oxygen on the catalyst surface.

We can see that in Case (ii) the sodium species have an effect on the platinum catalyst that may result in catalyst promotion if exposed to reaction conditions. This has been seen in the past in studies with, *e.g.* sodium-conducting supports for electrocatalysis [18]. However, under non-reactive conditions (as is the case studied here) we would not be able to observe such promotion.

In addition to the CV used in this work we also studied the effect of the sodium species on the work function of the catalyst/electrode. It has been found, by the photoelectric effect, that metallic sodium has a work function of 2.1 eV while the work function of metallic platinum is 5.65 eV [19]. The work function of platinum interfaced with YSZ has been found to be around 5.14 eV (this value can be used to establish an absolute electrode potential scale that would not depend upon the metal interfaced with the YSZ electrolyte) [20]. It is anticipated that the addition of sodium on the platinum surface will lower the work function of the surface; the work function of a sodium-modified sample should lie between the values of 2.1 and 5.14 eV (possibly a lot closer to the value of the platinum surface). The actual work function change will depend upon the sodium coverage and the state of sodium species on the platinum surface (*i.e.* metallic, oxide, hydroxide or carbonate form) as well as the state of the platinum (metallic or oxide). In order to determine the chemical state of species on the catalyst surface *ex situ* X-ray photoelectron spectroscopy (XPS) measurements were also performed.

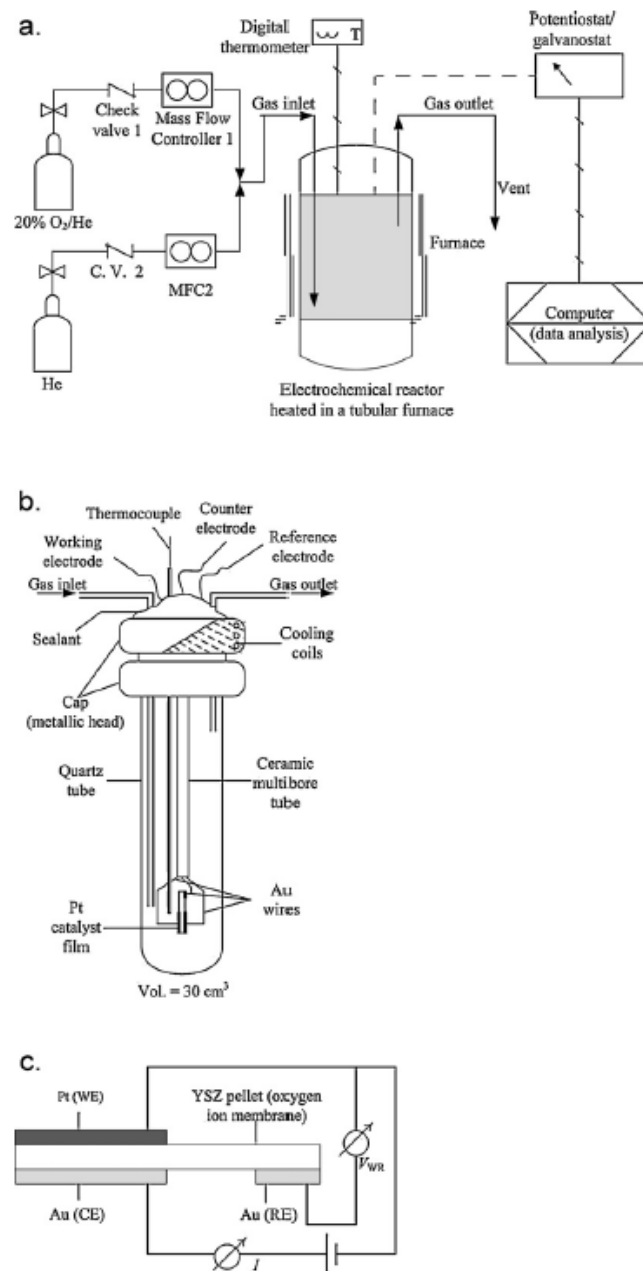## 2. Experimental

2.1. Experimental setup

The testing rig was constructed using stainless steel Swagelok compression fittings and Perfluoroalkoxy (PFA) tubing. The flow of gas to the electrochemical reactor was controlled by electronic mass flow controllers (MFCs) provided by Chell Hastings. The gases used were 20% O_2/He and CP grade He (N5) provided by BOC with typical flowrates around 200 ml min^{-1}. The flowrates were also measured at the outlet using a Varian® digital flow meter (1000 series). All experiments were conducted under atmospheric pressure and flow rates are given at STP. A single chamber type electrochemical reactor was used. An Ivium Compactstat was used for the electrochemical measurements. A schematic of the testing rig and electrochemical reactor can be seen in Fig. 1a and b, respectively.

2.2. Catalyst preparation

The solid electrolyte is an oxygen-ion conducting membrane made of 8 mol% yttria-stabilised-zirconia (YSZ) powder provided by Praxair. It must be noted that some impurities may also be present in the YSZ powder (and pellet) that may influence the initial purity of the platinum catalyst film. According to the manufacturer the YSZ powder typically contains 100 ppm Na_2O. Other impurities found in the powder are SiO_2 (100 ppm), Fe_2O_3 (30 ppm), TiO_2 (1000 ppm), Al_2O_3 (2500 ppm) and CaO (100 ppm). Approximately 2 g of YSZ powder were pressed uniaxially to form a pellet of approximately 20 mm diameter and 2 mm thickness. The pellet was sintered at 1500 °C for 4 h in air. The diameter of the sintered pellet was approximately 15 mm. To facilitate catalyst adhesion on the pellet, the surface was first scraped using an emery cloth. A thin layer of platinum was deposited on half of one side of the YSZ pellet by painting a platinum resinate (Metalor M603B), followed by sintering at 850 °C for 2 h in air. On the other side of the pellet, two gold films were deposited using gold resinate (Metalor A1118) and sintered at 800 °C for 2 h in air to serve as the counter and reference electrodes. For XPS analysis a different platinum paste was used (Heraeus) and it was sintered at 850 °C for 7 min. Some of the samples used in the work function measurement were prepared by electron laser deposition (ELD) by an external collaborator. A schematic of the three electrode system is shown in Fig. 1c. The working and counter electrodes were calculated to have a geometric projected surface area, A, of approximately 0.88 cm^2.

Sodium solutions of various concentrations were prepared by dilution of 1.0 N standard sodium hydroxide (NaOH) solution provided by Alfa Aesar. Sodium was then gradually deposited dropwise in increasing concentration onto the platinum catalyst surface using a micropipette. The volume of the NaOH solution droplets deposited on the catalyst is indicated in Table 1 (either 1 or 5 μl). The pellet was heated in the reactor in air for 1 h at 400 °C before starting the experiments. Table 1 summarises the estimated sodium loading (in terms of Na atoms cm^{-2} of platinum surface) and the percentage coverage of sodium on the platinum surface. For the calculation of the platinum surface area we have assumed a platinum particle size of approximately 0.5 μm (based on SEM analysis of Sample B). For a film mass of around 10 mg and assuming spherical geometry of the platinum particles we can calculate an estimated platinum surface area of 56 cm^2 (this surface area is only used for the coverage calculation; for the current densities discussed later a geometric projected surface area is used instead). It has been found in the literature that full coverage corresponds to approximately 10^{15} Na atoms cm^{-2} [21,22]. Based on this value we can calculate the coverage of sodium from the different sodium loadings. Note that this calculation may overestimate the sodium coverage as it assumes that all of the NaOH solution has been deposited on the platinum (without a presence on the YSZ support). This explains why a coverage above 100% is obtained for some samples. The platinum surface area of samples prepared by the ELD method could not be determined by a similar approximation because the mass of platinum in the

Fig. 1. Schematic representation of the experimental setup, (a) testing rig; (b) single chamber type electrochemical reactor; and (c) three electrode system.

samples was not available. Samples A–P shown in Table 1 correspond to fourteen different pellets, each impregnated with various NaOH solutions. Sample A was used for electrochemical measurements, B for SEM-EDX analysis, C–H for XPS analysis while J–P were used for work function measurements. Throughout the paper, these samples are named as follows: Pellet xyy, where $x \times 10^{-yy}$ M

corresponds to NaOH concentration of the most recent sodium deposition. Unless otherwise stated the sodium loadings reported in Table 1 are cumulative values, but the last deposition dominates. Table 2 lists all experiments conducted on the samples and the corresponding figures/tables in which the experimental results are shown.

Table 1

Estimation of sodium loading on platinum catalyst and percentage of sodium coverage. A000, B000, C000, J000, K000, N000 and P000 samples are 'clean' platinum catalysts, while the others are sodium-modified. Sample A was used for electrochemical experiments, Sample B for SEM study, Samples C, D, E, F, G and H for XPS analysis, while Samples J, K, L, M, N and P for work function measurements.

Sample[†]	Volume NaOH (μl)	NaOH concentration (M)	Na (atom)	Na/Pt surface area (atom cm^{-2})	% Na coverage
A000	'Clean' sample (painted)				
A504	1.00 ± 0.25	5×10^{-04}	3.0×10^{14}[‡]	5.4×10^{12}	0.54
A103		1×10^{-03}	9.0×10^{14}	1.6×10^{13}	1.6
A503		5×10^{-03}	3.9×10^{15}	7.0×10^{13}	7.0
A102		1×10^{-02}	9.9×10^{15}	1.8×10^{14}	18
A502		5×10^{-02}	4.0×10^{16}	7.2×10^{14}	72
A101		1×10^{-01}	1.0×10^{17}	1.8×10^{15}	180
B000	'Clean' sample (painted)				
B101	1.00 ± 0.25	1×10^{-01}	6.0×10^{16}[‡]	1.1×10^{15}	110
C000	'Clean' sample (painted)				
D104	1.00 ± 0.25	1×10^{-04}	6.0×10^{13}[‡]	2.2×10^{12}	0.22
E103		1×10^{-03}	6.0×10^{14}[‡]	2.2×10^{13}	2.2
F102		1×10^{-02}	6.0×10^{15}[‡]	2.2×10^{14}	22
G502		5×10^{-02}	3.0×10^{16}[‡]	1.1×10^{15}	110
H101		1×10^{-01}	6.0×10^{16}[‡]	2.2×10^{15}	220
J000	'Clean' sample (painted)				
K000					
J104	5.00 ± 0.25	1×10^{-04}	3.0×10^{14}[‡]	5.4×10^{12}	0.54
J102		1×10^{-02}	3.0×10^{16}	5.4×10^{14}	54
L104		1×10^{-04}	3.0×10^{14}[‡]	5.4×10^{12}	0.54
M102		1×10^{-02}	3.0×10^{16}[‡]	5.4×10^{14}	54
N000	'Clean' sample (ELD)				
P000					
N104	5.00 ± 0.25	1×10^{-04}	3.0×10^{14}[‡]	N/A	N/A
P102		1×10^{-02}	3.0×10^{16}[‡]	N/A	N/A

[†] Pellet xyy: Na concentration of recent deposition $= x \times 10^{-yy}$.

[‡] Not cumulative.

Table 2

List of the experiments conducted on each sample and the corresponding figures/tables in which the results are presented.

Experiments	Sample	Figure/table
SEM	B000–B101	Fig. 2
XPS	C000–H101	Fig. 3 (only C000 and F102 shown)
Cyclic voltammetry (including E_{pc}, t_{pc}, Q_{pc})	A000–A101	Table 3; Figs. 4 and 5
Linear sweep voltammetry	A000–A101	Fig. 6
Work function	J000–J102	Fig. 7
measurement	K000	
	L104	
	M102	
	N000–N104	
	P000–P102	

2.3. Sample characterisation

2.3.1. SEM-EDX analysis

A fresh pellet was used for SEM-EDX analysis. The SEM image of the 'clean' sample (B000) is shown in Fig. 2a, while Fig. 2b shows an SEM picture of Sample B000 after impregnation with a 0.1 M NaOH solution (Sample B101). The platinum film consists of an irregular porous network of approximately 10 μm thickness. As can be seen from the SEMs presented here, sodium deposition appears to have a small effect on the structure of the platinum film indicated by the induced surface roughness on the platinum particles. However, it needs to be noted that while the SEMs shown in Fig. 2 are of the same platinum film (before and after the sodium deposition) the areas of the film shown on the SEM are not the same. It was not possible to quantitatively analyse sodium by using SEM-EDX.

2.3.2. XPS analysis

XPS was performed on six fresh samples (C000–H101) using a VG Escalab 200R electron spectrometer provided with Al Kα X-ray source ($hv = 1486.6$ eV, 1 eV $= 1.6302 \times 10^{-19}$ J) and a hemispherical electron analyser. The base pressure in the analysis chamber was kept below 4×10^{-9} mbar during data acquisition. The pass energy of the analyser was set at 50 eV, for which the resolution as measured by the full width at half maximum (FWHM) of the Au $4f_{7/2}$ core level was 1.7 eV. The binding energies were referenced to C 1s peak at 284.6 eV due to adventitious carbon. Data processing was performed with an XPS peak programme; spectra were decomposed with a least squares fitting routine provided with the software with Gaussian/Lorentzian (90/10) product function and after subtracting a Shirley background.

2.3.3. Electrochemical measurements

Cyclic, (CV) and linear sweep voltammetry (LSV) are used in this study to characterise the changes in the electrochemical behaviour of the platinum catalyst modified by sodium deposition. With both techniques, a cyclic or linear voltage sweep was applied at a fixed scan rate, υ, while the current flowing between the catalyst (working electrode) and the counter electrode was recorded using an Ivium Compactstat. The current density, t, (calculated based on the geometric projected surface area, $A = 0.88$ cm^2) was plotted against the overpotential, V_{WR}, to produce cyclic and linear sweep voltammograms. All voltammograms shown in the figures in Section 3 correspond to the third scan. The area under the cathodic peak, Q_{pc} (which corresponds to the charge transferred during this phase of oxygen reduction) was measured and integrated using graphing and data analysis software.
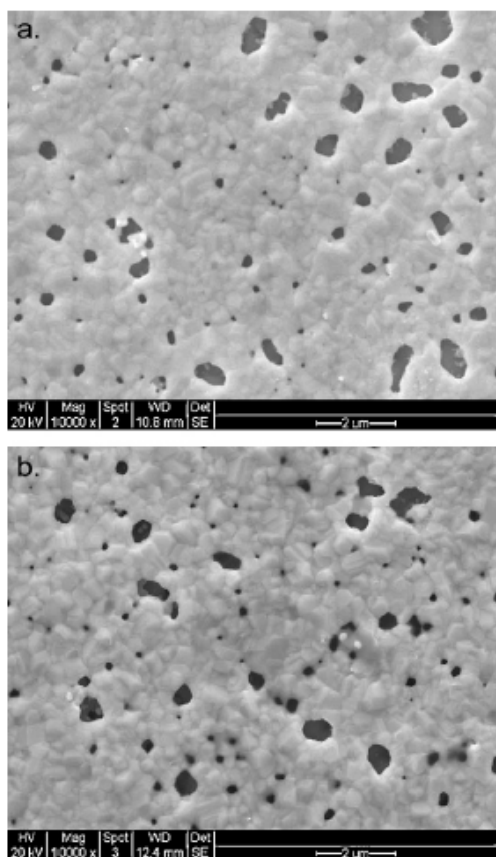
Fig. 2. SEM images: (a) B000 – 'clean' platinum sample; (b) B101 – platinum impregnated with 1×10^{-1} M NaOH.

2.3.4. Work function measurements

Work function measurements were conducted using a scanning Kelvin probe (SKP5050) located in a light-tight chamber (LE450) and illuminated by an automatic surface photovoltage light source (SPV020) provided by KP Technology Ltd. The SKP has a 1.8 mm diameter gold-coated tip that vibrates just above the sample surface. The SKP works in an off-null fashion and produces the contact potential difference between the vibrating tip and the sample surface. The mean spacing is computer-controlled and held constant during the measurement to avoid changes of parasitic capacity. The work function of the platinum catalyst is calibrated against a gold reference sample with known work function. The actual work function values are calculated with respect to the literature values of gold and platinum measured in vacuum using the photoelectric effect [19]. It should be noted that work function measurements on a sample surface using a vibrating non-contact Kelvin probe under ambient conditions are strongly influenced by the surface conditions and easily modified by adsorbed layers.

The work function measurement of the 'clean' platinum surface was conducted on four samples; two of the samples (J000, K000) were prepared by painting of a platinum resinate while the other two (N000 and P000) were prepared using ELD. Three types of sodium-modified samples were tested. Sample J000 (Pt-painted) was impregnated with consecutive drops of NaOH solutions of 10^{-4}

(J104) and 10^{-2} M (J102), and measurements were conducted after each impregnation. In addition, two independent Pt-painted samples, each modified with NaOH solutions of 10^{-4} (L104) and 10^{-2} M (M102) were used for comparison. The two ELD-prepared samples (N000 and P000) were also impregnated with NaOH solutions of 10^{-4} (N104) and 10^{-2} M (P102) and measurements were performed on each sample after each impregnation. The method of sodium deposition for all samples is as described in the catalyst preparation section (Section 2.2), except for Samples J104, J102, N104 and P102 which were heated in air at a lower temperature of about 200 °C for 20 min.

3. Results and discussion

3.1. XPS analysis

In order to analyse the chemical state of the elements and surface composition of the sintered Pt/YSZ, XPS measurements were performed on a nominally 'clean' (C000) and five sodium-modified samples (D104–H101 with 10^{-4} to 10^{-1} M NaOH). All samples tested showed Pt $4f_{7/2}$ binding energies around 72.0 eV that point to the presence of metallic platinum species (data not shown here). Fig. 3 shows the Na 1s component spectra for the 'clean' sample (Fig. 3a) and one of the sodium-modified samples, F102 (Fig. 3b). There is no Na 1s peak associated with the 'clean' sample (C000), while the sodium-modified sample shows an Na 1s peak at binding energies of 1071.4–1072.1 eV. This indicates the presence of hydroxide, carbonate and/or oxide species [23] on the Pt film probably due to sodium hydroxide addition and exposure to carbon dioxide in air.

3.2. Cyclic voltammetry

Fig. 4a shows a typical voltammogram of a 'clean' platinum film (A000) exposed to a gas mixture of oxygen (20 kPa) and helium scanned at varying scan rates from 1 to 100 mV s^{-1}. The cathodic peak (Peak C) involves the reduction of oxygen at the tpb (Eq. (2)), while the anodic peak, (Peak A), corresponds to the oxidation of oxygen ions (from the bulk of the electrolyte) to oxygen at the tpb (the reverse of Eq. (2)).[1] It should be noted that there is a number of studies disagreeing with the assignment of the cathodic peak (solely) to a tpb process. Kenjo et al. [7] assigned this peak to platinum oxide decomposition at the Pt/YSZ interface, while the group of Comninellis assigned the cathodic features in CV to both a tpb related process (spillover oxygen) and other interfacial processes (monolayer and bulk platinum oxide formation) [24]. Similarly, Bultel et al. [25] assigned the cathodic peak to the reduction of electrochemically produced oxygen species (either from the chemisorbed oxygen or a platinum oxide layer). Mutoro et al. [8] suggested that this cathodic peak may not be caused only by spillover oxygen or platinum oxide but could also be influenced by the presence of impurities. In a recent study, Pöpke et al. [26] emphasised the role of platinum oxide in the electrode system Pt(O₂)/YSZ as its formation and decomposition is considered to affect the oxygen exchange rate. In the work presented here, we are looking at the effect of sodium addition on the Pt/YSZ catalyst system and since the same pellet has been used both in the form of 'clean' and sodium-modified samples (for Sample A), the cause of the difference in the characteristics of the cathodic peak (area, height and position) is expected to be the different sodium coverage of the samples.

---

[1] The peak height (at t maximum) of the anodic Peak A, t_{pa}, is not shown here as Peak A is broad and ill-defined for most samples.
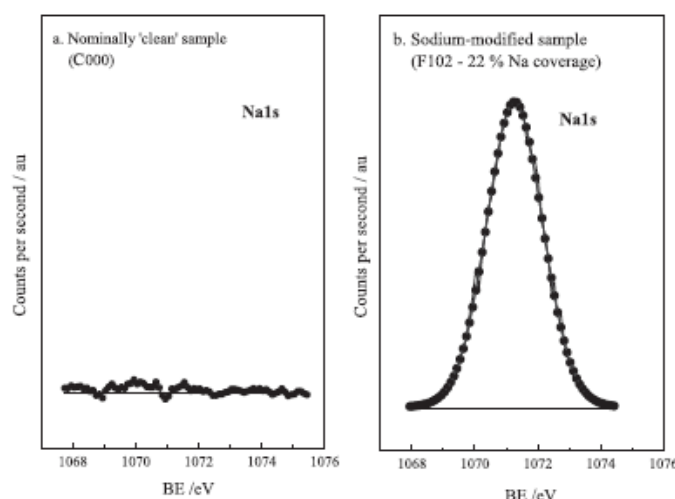
Fig. 3. XPS spectra of 'clean' and sodium-modified sample (with 10^{-2}M NaOH): (a) Na 1s C000 and (b) Na 1s F102.

As shown in Fig. 4a there is hysteresis in the voltammogram which indicates that the oxygen charge transfer reaction is an irreversible process [6,27]. This is also true for the sodium-modified samples (Fig. 4b–g). From Fig. 5, the measured cathodic peak height (at maximum current density), i_{pc}, is found to be proportional to the square root of the scan rate, $\upsilon^{1/2}$, indicating a diffusion-controlled process. This indicates that the oxygen charge transfer reaction taking place in the system studied here is not only a case of simple adsorption but is also controlled by the diffusion of oxygen to the tpb. Yi et al. [28] have also found a linear relationship between peak height and $\upsilon^{1/2}$ in their studies of the Pt/YSZ interface. However in work conducted by Vayenas et al. [6] on a different Pt/YSZ system

a linear dependence of peak height on υ was found. It is possible that the diffusion limited charge transfer process observed for the sample studied here is due to a combination of the thickness and porosity of the platinum film. We must note that preliminary experiments (not shown here) performed on 'clean' platinum films prepared by ELD did not show any peaks. These samples had a platinum film thickness of only 75 nm compared to approximately 10 μm of the painting platinum films.

Similar i_{pc} *versus* υ behaviour as with the 'clean' sample is observed for the sodium-modified voltammograms of Samples A504–A101 shown in Fig. 4b–g. In addition, the cathodic peak height, i_{pc}, of Samples A504–A101 decreases with increasing sodium loading as shown in Fig. 5 and Table 3. However, the cathodic peak area (Q_{pc}) does not appear to be significantly affected by sodium addition for sodium coverage up to approximately 72% as it only reduces by approximately 30% from Sample A000 to Sample A102 (as shown in Table 3). The cathodic peak of Samples A502 and A101 (shown in Fig. 4f and g) disappears completely. It is possible that the cathodic peak for these samples has in fact simply shifted to lower overpotentials. A shift of the cathodic peak
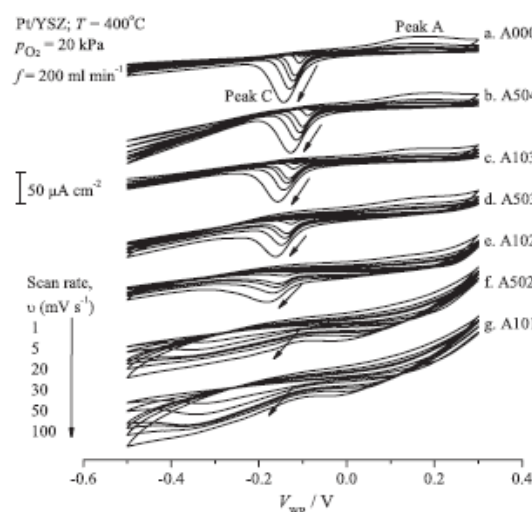

Fig. 4. Cyclic voltammograms with varying scan rates, υ and sodium loading: (a–g) Sample with varying sodium loading. A000 is 'clean' sample, while the others refer to A000 that was modified with NaOH addition in increasing concentrations. Gas composition: 20 kPa O_2; temperature: 400 °C; total flow rate: 200 ml min⁻¹.
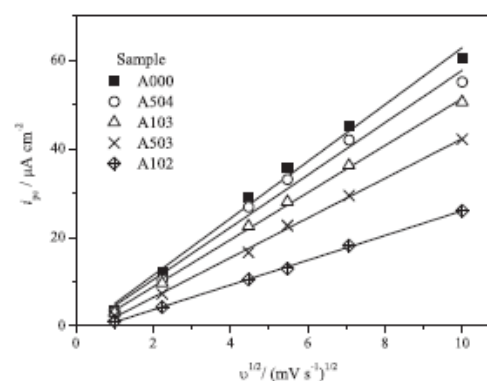

Fig. 5. Relationship between cathodic peak height, i_{pc} and square root of the scan rate, $\upsilon^{1/2}$ (conditions as in Fig. 4).

Table 3
Effect of sodium loading on the cathodic peak position, E_{pc}, cathodic peak height, I_{pc}, and charge transferred during oxygen reduction, Q_{pc}. The values shown were calculated for a scan rate of 20 mV s^{-1}, other scan rates showed the same trends.

| Sample	Cathodic peak position, E_{pc} (mV)	Cathodic peak height, I_{pc} (µA cm^{-2})	Charge transferred during oxygen reduction, Q_{pc} (µC)
A000	−118	29	49
A504	−101	27	53
A103	−131	23	57
A503	−137	17	44
A102	−154	11	35
A502	N/A	N/A	N/A
A101	N/A	N/A	N/A

potential towards more negative values is also observed for the other sodium-modified samples (A504–A102) as can be seen in Table 3. This suggests that, as a result of sodium addition, oxygen becomes more strongly bound to the catalyst thus requiring more reducing overpotentials to be removed (Case (ii)). Oxygen can be bound to sodium on the platinum surface in the form of oxides, hydroxides and carbonates [29], or even in the form of sodium-platinum-oxygen complexes [18]. This is also in agreement with the XPS findings that show the presence of these species on the surface of the catalyst. Another parameter affected by the sodium addition is the observed current density at high overpotentials which increases significantly at sodium coverage above 70% as seen in Fig. 4f and g. This indicates that sodium addition may facilitate oxygen supply to the three phase interface through modification of the oxygen storage, oxygen surface diffusion or oxygen adsorption processes (Case (ii)). To summarise the findings from the cyclic voltammetry experiments, we can see that the addition of sodium causes:

(i) the cathodic peak potential to shift towards more negative values indicating that oxygen is now more strongly bound on the catalyst surface,
(ii) the current density at high overpotentials to increase, suggesting that sodium enhances oxygen storage, surface diffusion and/or adsorption.

3.3. Linear sweep voltammetry

Linear sweep voltammetry was performed at a scan rate of 20 mV s^{-1} for different holding times (t_H) at an anodic potential of $E_H = 0.3$ V. Fig. 6 shows the obtained voltammograms. We can see that as t_H progresses from 10 to 800 s the cathodic peak potential, E_{pc} becomes more negative suggesting that fixing the anodic potential for longer times not only increases the amount but also the binding strength of oxygen. There are actually two peaks on the 'clean' sample (A000) shown in Fig. 6a (magnification shown in Fig. 6h); the first one is very pronounced and the same as the cathodic peak discussed in Fig. 4, while the second peak is very broad and appears only when the potential is held for $t_H = 200$ s or longer. These peaks were previously used to explain the origin of EPOC [30], by assigning the first one to a highly reactive oxygen species from the gas phase, and the second one to a strongly bonded, thus less reactive, oxygen (back) spillover species. Mutoro et al. [8] compared the CV features between two platinum electrodes from the same source, one with and one without intentionally deposited silicon from glass particles. It was observed that additional cathodic peaks were featured only by the sample contaminated with silicon. In the work presented here, we cannot disprove this theory as silicon is often added in platinum pastes as a sintering aid and was also present in the emery cloth used to polish the YSZ pellets. However, as the focus of this work is to study the effect of the sodium loading on the charge transfer reaction, the origin of the second peak was not investigated further.

An increase in sodium coverage causes the cathodic peaks' heights to reduce and the peak potentials to become more negative. At sodium coverage from 72 to 100% (Fig. 6f and g, Samples A502 and A101), both peaks appear to have shifted significantly. This cathodic peak shift was also observed for the cyclic voltammetry experiments as discussed earlier. In addition, and in accordance to previous findings for Samples A502 and A101, all the recorded peaks become broad and ill-defined. This corroborates our earlier
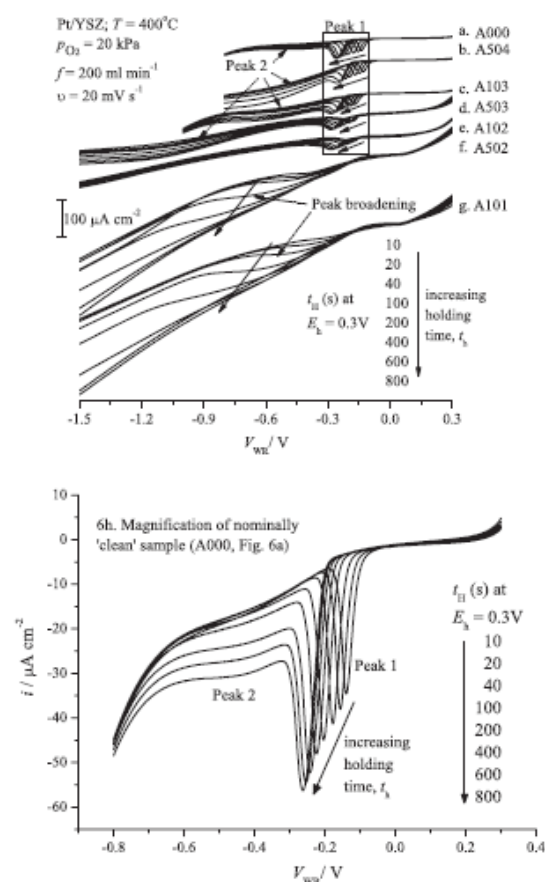
Fig. 6. Linear sweep voltammograms with varying holding time, t_H at constant anodic potential ($E_H = 0.3$ V): (a–g) sample with varying sodium loading. A000 is 'clean' sample, while the others refer to A000 that was modified with NaOH addition in increasing concentrations; (h) magnification of Sample A000. Gas composition: 20 kPa O$_2$; temperature: 400 °C; scan rate: 20 mV s^{-1}; total flow rate: 200 ml min^{-1}.
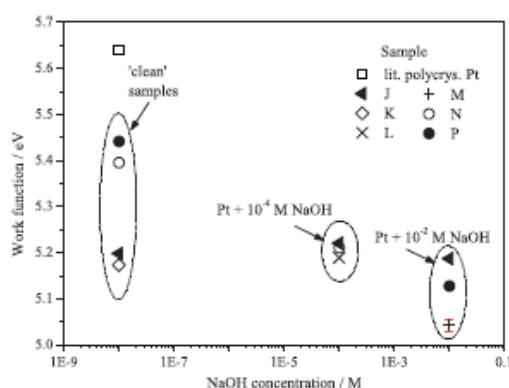
Fig. 7. Work function measurements on polycrystalline platinum film prepared by painting of platinum resinate on YSZ (Samples J, K, L and M) and using electron laser deposition (ELD) technique (Samples N and P). All measurements performed at ambient temperature and pressure. The literature work function of the polycrystalline platinum is 5.64 eV in vacuum (measured using the photoelectric effect).

findings about sodium addition causing oxygen to be more strongly bound on the catalyst surface.

3.4. Ex situ work function measurements

The results of the Kelvin Probe work function measurement on 'clean' and sodium-modified platinum films are shown in Fig. 7. The average work function of 'clean' platinum samples prepared by painting platinum resinate (J000 and K000) and 'clean' platinum samples prepared by ELD (N000 and P000) are compared to the literature-predicted work function of clean polycrystalline platinum. As mentioned earlier, it has been found [20] that the work function of porous platinum on YSZ differs by $\sim{-}500$ meV from the work function of pure platinum and has a value of 5.14 eV. The work function values measured for Samples N000 and P000 are quite close to the literature values for pure platinum [19], while the painted samples (J000 and K000) have lower values of about 5.2 eV that are closer to the value of 5.14 eV reported for porous platinum films on YSZ [20].

The ELD-prepared Samples N000 and P000 show a work function change of 200 and 250 meV when modified with 10^{-4} M (N104) and 10^{-2} M (P102) NaOH, respectively. The change in work function may be due to the NaOH dipole concentration on the platinum surface. It is also possible that the observed work function change could be due to the formation of carbonate and/or oxide species as well as platinum–sodium–oxygen complexes on the catalyst surface or even formation of platinum oxides due to the strengthening of the Pt—O bond as a result of the sodium addition [18]. Work function changes are not very clear in the painted samples probably because the platinum surface has more initial impurities compared to the ELD samples. In any case, in all samples a higher sodium coverage causes a larger work function change.

4. Conclusions

The catalyst system of a platinum film supported on a YSZ solid electrolyte was intentionally contaminated by depositing small amounts of NaOH solutions of varying concentrations (up to a 0.1 M solution). XPS analysis identified the presence of different sodium species (such as hydroxides, carbonates and/or oxides) on the platinum surface that may affect the behaviour of the catalyst. An electrochemical investigation of the effect of sodium on oxygen charge transfer was conducted under a flow of 20 kPa oxygen at 400 °C. Cyclic and linear sweep voltammetry experiments showed that sodium addition modifies oxygen storage, adsorption and/or diffusion on the catalyst surface. Oxygen becomes more strongly bound to the catalyst requiring more reducing overpentials to be removed. Work function measurements under atmospheric conditions showed a decrease of about 250 meV for higher than 50% sodium coverage compared to a 'clean' sample indicating that there is a difference in the chemical identity of the platinum surface as a result of sodium addition.

References

[1] C. Tsaofang, K.J. Walsh, P.S. Fedkiw, Solid State Ionics 47 (1991) 277.
[2] A. Jaccoud, G. Fóti, C. Comninellis, Electrochimica Acta 51 (2006) 1264.
[3] M. Stoukides, C.G. Vayenas, Journal of Catalysis 70 (1981) 137.
[4] C.G. Vayenas, S. Bebelis, S. Neophytides, The Journal of Physical Chemistry 92 (1988) 5083.
[5] S. Bebelis, C.G. Vayenas, Journal of Catalysis 118 (1989) 125.
[6] C.G. Vayenas, A. Ioannides, S. Bebelis, Journal of Catalysis 129 (1991) 67.
[7] T. Kenjo, Y. Yamakoshi, K. Wada, Journal of The Electrochemical Society 140 (1993) 2151.
[8] E. Mutoro, B. Luerßen, S. Günther, J. Janek, Solid State Ionics 180 (2009) 1019.
[9] I.V. Yentekakis, M. Konsolakis, R.M. Lambert, N. Macleod, L. Nalbantian, Applied Catalysis B: Environmental 22 (1999) 123.
[10] M. Konsolakis, I.V. Yentekakis, Journal of Hazardous Materials 149 (2007) 619.
[11] I.V. Yentekakis, R.M. Lambert, M.S. Tikhov, M. Konsolakis, V. Kiousis, Journal of Catalysis 176 (1998) 82.
[12] I.V. Yentekakis, R.M. Lambert, M. Konsolakis, V. Kiousis, Applied Catalysis B: Environmental 18 (1998) 293.
[13] P. Vernoux, F. Gaillard, C. Lopez, E. Siebert, Solid State Ionics 175 (2004) 609.
[14] A. Billard, P. Vernoux, Topics in Catalysis 44 (2007) 369.
[15] S. Bebelis, H. Karasali, C.G. Vayenas, Solid State Ionics 179 (2008) 1391.
[16] A. Katsaounis, Journal of Applied Electrochemistry 40 (2010) 885.
[17] F. Dorado, A. de Lucas-Consuegra, C. Jiménez, J.L. Valverde, Applied Catalysis A: General 321 (2007) 86.
[18] P. Vernoux, A.Y. Leinekugel-Le-Cocq, F. Gaillard, Journal of Catalysis 219 (2003) 247.
[19] D.R. Lide, CRC Handbook of Chemistry and Physics, CRC Press/Taylor and Francis, Boca Raton, Florida, 2009.
[20] D. Tsiplakides, C.G. Vayenas, Journal of The Electrochemical Society 148 (2001) E189.
[21] W. Schröder, J. Hölzl, Solid State Communications 24 (1977) 777.
[22] J. Cousty, R. Riwan, Surface Science 204 (1988) 45.
[23] T. Grzybek, G.C. Maiti, D. Scholz, M. Baerns, Applied Catalysis A: General 107 (1993) 115.
[24] A. Jaccoud, C. Falgairette, G. Fóti, C. Comninellis, Electrochimica Acta 52 (2007) 7927.
[25] L. Bultel, C. Roux, E. Siebert, P. Vernoux, F. Gaillard, Solid State Ionics 166 (2004) 183.
[26] H. Pöpke, E. Mutoro, C. Raiß, B. Luerßen, M. Amati, M.K. Abyaneh, L. Gregoratti, J. Janek, Electrochimica Acta 56 (2011) 10668.
[27] A.J. Bard, L.R. Faulkner, Electrochemical Methods: Fundamentals and Applications, 2 ed., John Wiley & Sons, 2001.
[28] J. Yi, A. Kaloyannis, C.G. Vayenas, Electrochimica Acta 38 (1993) 2533.
[29] A. de Lucas-Consuegra, F. Dorado, J.L. Valverde, R. Karoum, P. Vernoux, Journal of Catalysis 251 (2007) 474.
[30] C.G. Vayenas, S. Bebelis, C. Pliangos, S. Brosda, D. Tsiplakides, Electrochemical Activation of Catalysis: Promotion, Electrochemical Promotion, and Metal-Support Interactions, Kluwer Academic/Plenum Publishers, New York, 2001.

- Publication 2

SOLID STATE IONICS

The role of low coverage sodium surface species on electrochemical promotion in a Pt/YSZ system

Naimah Ibrahim [a,b], Mas Rahayu Jalil [a,c], Danai Poulidi [a], Ian S. Metcalfe [a,*]

[a] School of Chemical Engineering and Advanced Materials, Newcastle University, Merz Court, Newcastle upon Tyne, NE1 7RU, UK
[b] School of Environmental Engineering, Universiti Malaysia Perlis, 02600 Arau, Perlis, Malaysia
[c] Faculty of Civil and Environmental Engineering, Universiti Tun Hussein Onn Malaysia, 86400 Parit Raja, Batu Pahat, Johor, Malaysia

ABSTRACT

The effect of sodium-modification on the catalyst and electrocatalytic properties of a platinum catalyst supported on a YSZ solid electrolyte was studied. Increasing the sodium coverage on the catalyst surface appears to block some of the three-phase boundary (tpb) sites and reduces the rate of the charge transfer reaction. The promotion of the platinum surface reaction (ethylene oxidation) seems to a first approximation to be a function of the rate of oxygen supply or removal to or from the surface irrespective of whether this is contaminated by sodium or not (samples with sodium contamination require a higher overpotential to achieve the same current density as a clean sample because of poisoning in the tpb). At high negative polarisations (oxygen removed from the surface) the sodium contaminated samples show a significant increase in rate, possibly due to the decomposition of e.g. sodium hydroxides and carbonates.

© 2012 Elsevier B.V. All rights reserved.

1. Introduction

Electrochemical Promotion of Catalysis (EPOC) has been observed in a wide range of reactions performed on various metal catalysts supported on a number of different solid electrolytes [1–4]. In EPOC, or NEMCA (non-faradaic electrochemical promotion of catalysis), a small current supplied through an external circuit results in promoting species being pumped towards the catalyst surface, thus modifying the catalytic activity and selectivity of a reaction [5,6]. A recent study found that variations in the catalyst surface morphology and the presence of impurities on the catalysts may have a significant impact on the catalyst behaviour [7] and could play an important role in electrochemical promotion. Nevertheless, the role of impurities in EPOC has not been studied in detail except perhaps the influence of Si impurities and electrode morphology on the Pt(O₂)/YSZ system using cyclic voltammetry [7]. In this work, in order to systematically study the role of impurities in EPOC, a known type and amount of impurity (in this case sodium, Na) is gradually deposited in increasing amounts onto a nominally 'clean' catalyst surface (in this case platinum, deposited on yttria stabilised zirconia, YSZ) and the catalyst used for EPOC studies of ethylene oxidation.

2. Experimental

The catalyst/electrode and electrolyte materials used in the study were metal resinates provided by Metalor, UK and 8 mol% YSZ provided by Pi-Kem Ltd., UK. The platinum resinate was painted on two YSZ dense pellets of 15 mm diameter and 2 mm thickness and sintered at 850 °C for 2 h. The resulting samples have a platinum film of geometric projected surface area, $A = 0.88$ cm². One sample was used for the non-reactive study and the other was used under reactive conditions. A three electrode pellet system, with platinum as a working electrode/catalyst and gold as the counter and reference electrodes supported on a YSZ pellet, was mounted in a single chamber type electrochemical reactor (i.e. all electrodes were exposed to the same gas atmosphere) already described elsewhere [8]. The pellet system was either exposed to 20 kPa of oxygen at 400 °C (for non-reactive conditions) or a mixture of oxygen and ethylene at 350 °C (for reactive conditions). All experiments were conducted at atmospheric pressure. In the latter, the oxygen partial pressure was varied between $p_{O2} = 0.5$, 1.5, 3 and 8 kPa, while the ethylene partial pressure was kept constant at $p_{C2H4} = 0.5$ kPa. The gases used were 20% O₂/He and 10% C₂H₄/He provided by BOC, UK. The total gas flow in all experiments was 200 ml min⁻¹ (STP). Gas analysis was carried out by a BINOS 100 CO₂ analyser. Sodium was gradually deposited on the surface of the platinum catalyst dropwise using solutions of increasing concentrations prepared by dilution of 1 M NaOH, and dried in air at 400 °C in the same reactor. In the rest of the manuscript

the sodium-modified samples are referred to in terms of the sodium coverage. Table 1 shows the sodium loading of each sample used in this work. We must note that for the samples prepared using solutions of molarity less than 10^{-4} M it is possible that other impurities present in the de-ionised water used for dilution may affect the behaviour of the system as the sodium concentration of the solution will not be significantly higher that the concentration of those impurities. The sodium loading (atoms of sodium) per platinum surface area and the percentage of sodium coverage are also shown. For an estimation of the platinum surface area, a mean platinum particle size of 0.5 μm determined from SEM analysis (not shown here) was used; a spherical geometry was assumed. The 10 mg masses of the platinum films thus correspond to about 56 cm^2 of platinum surface area (note that because of the uncertainty in the platinum surface area specific rates and current densities reported later use the platinum projected area). The percentage of sodium coverage on the platinum surface is calculated assuming that full coverage (i.e. one monolayer of sodium) is achieved at sodium loading of approximately 10^{15} Na atoms cm^{-2} based on experimental values from the literature [9,10]. Sodium modification of the kinetics of the oxygen charge transfer reaction and ethylene oxidation on the Pt/YSZ system was investigated using cyclic voltammetry following on from an early study by Vayenas [11,12], and using EPOC-type electrocatalytic experiments [1,2]. The potential range used in the cyclic voltammetry experiments was from 0.3 to -0.5 V at a scan rate, $v = 30$ mV s^{-1} for the non-reactive study, and 1.0 to -1.0 V at $v = 5$ mV s^{-1} for reactive conditions.

3. Results

3.1. Non-reactive conditions (oxygen charge transfer reaction)

Fig. 1a shows cyclic voltammograms of the platinum catalyst exposed to an oxygen flow of 20 kPa at 400 °C, at a scan rate, $v = 20$ mV s^{-1}. The voltammograms were obtained using one sample to which was gradually added NaOH of varying concentration from 10^{-12} to 10^{-1} M as shown in Table 1. As discussed earlier the sodium coverage in these samples ranges from 5.4×10^{-9}% ([NaOH] = 10^{-12} M) to full coverage ([NaOH] = 10^{-1} M). One of the main features on the voltammograms is the sharp cathodic peak that involves the reduction of oxygen at the metal–solid electrolyte–gas three phase boundaries, tpb, into oxygen anions [11]. The sharp peak may indicate that oxygen adsorption and/or oxygen surface diffusion are slower than charge transfer. The cathodic peak current, i_{pc} and the peak area, A_{pc} are shown in Fig. 1b. As can be seen in this figure an increase in the sodium coverage causes a decrease in the i_{pc}, and in the peak area (i.e. the charge transferred during the oxygen reduction at the tpb). It is postulated that sodium-containing species may

Table 1
Sodium loading and percent coverage of the samples.

[NaOH] added M	Na atom	Na/Pt surface area[a] atom cm^{-2}	%Na coverage
0	Nominally 'clean' sample		
10^{-12}	3×10^{6}*	5.4×10^{4}	5.4×10^{-9}
10^{-8}	3×10^{10}	5.4×10^{8}	5.4×10^{-5}
10^{-4}	3×10^{14}	5.4×10^{12}	0.54
10^{-2}	3×10^{16}	5.4×10^{14}	54.40
10^{-1}	3.3×10^{17}	5.9×10^{15}	590

Na atoms except marked* are cumulative values.

[a] For the platinum surface area and Na coverage calculation it is assumed that the platinum particles are spherical and all the NaOH solution stays on the catalyst surface. This overestimates the sodium coverage as shown in sample [NaOH] = 10^{-1} M for which a % coverage higher than 100 is calculated.
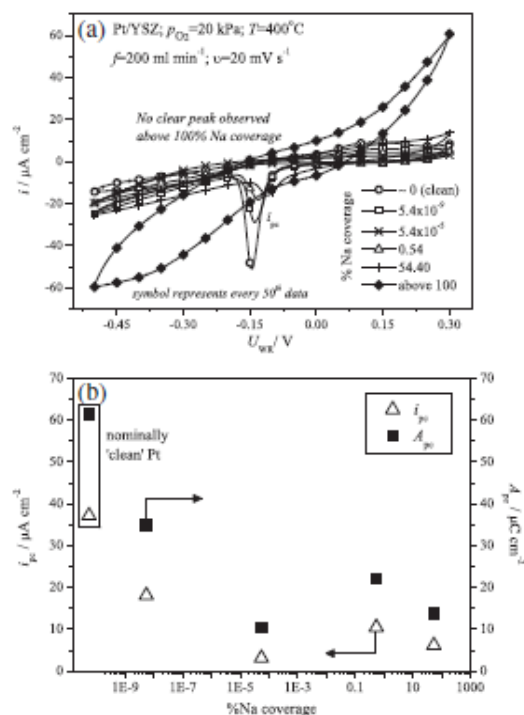
Fig. 1. Effect of sodium addition on the cyclic voltammetry under non-reactive conditions: (a) cyclic voltammograms of 'clean' and sodium-modified platinum catalyst scanned at 20 mV s^{-1} between 0.3 and -0.5 V; $p_{O2} = 20$ kPa O$_2$; Temperature, $T = 400$ °C; Total flow rate, $f = 200$ ml min^{-1}; i_{pc} = cathodic peak height; (b) effect of varying sodium coverage on the cathodic peak height, i_{pc} and the peak area, A_{pc}.

preferentially populate the tpb thus blocking the available sites for oxygen reduction as very low sodium coverages (between 5×10^{-9}% and 0.5%) would not be expected to have an effect on the bulk of the platinum surface but do cause a dramatic change in the charge transfer behaviour of the system. It is interesting to note that at full sodium coverage larger current densities and greater hysteresis in the response are observed possibly indicating that charge transfer is governed by a different mechanism. As the measurements discussed here were performed under non-reactive conditions the role of any sodium present on the catalyst surface (if any) cannot be assessed at this stage.

3.2. Reactive conditions (ethylene oxidation)

A study of the effect of sodium addition on the Pt/YSZ system under reactive conditions was conducted using ethylene oxidation as a probe reaction. First, cyclic voltammograms of 'clean' and sodium-modified platinum catalyst (with 1 μL of 10^{-4} M NaOH or equivalent to 0.54% sodium coverage) were recorded at 5 mV s^{-1} under flow of 3 kPa O$_2$ and 0.5 kPa C$_2$H$_4$ at 350 °C. The OCP of the clean system was -215 mV and that of the sodium-modified sample was -265 mV. The change in the rate of CO$_2$ (area specific rates calculated using $A = 0.88$ cm^2) produced from ethylene oxidation during the cyclic voltammetry experiment is depicted in Fig. 2a as a function of the current density during polarisation. The corresponding current density versus overpotential response is shown
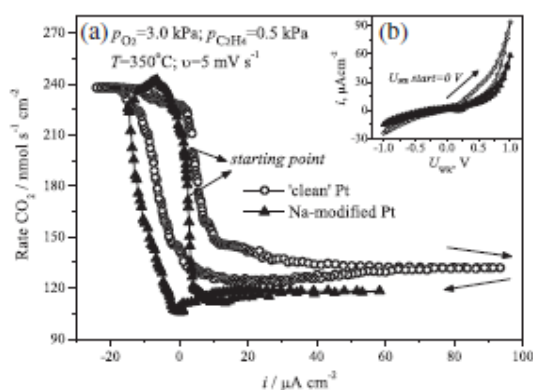
Fig. 2. Effect of sodium addition on the rate of CO₂ production during cyclic voltammetry of platinum catalyst exposed to a gas mixture of 3 kPa O₂ and 0.5 kPa C₂H₄ at 350 °C (reactive conditions): (a) CO₂ production rate for 'clean' and sodium-modified platinum catalyst (with 1 μl of 10^{-4} M NaOH) versus current density, i; (b) current density, i versus U_{WR}. The voltammograms were scanned at 5 mV s⁻¹ between 1 and −1 V, starting from 0 V.

in Fig. 2b. In Fig. 2a we can observe that the rate change in both systems follows a similar pattern, i.e. the CO₂ production rate is decreased for positive current densities and increased for negative values.[1] We can see that the reaction rate of the two systems reaches approximately the same minimum at current densities of the order of $+20\,\mu A\,cm^{-2}$ and the same maximum at a current density of about $-15\,\mu A\,cm^{-2}$. The catalytic rate is clearly influenced by current in a similar way for the two samples. This is consistent with sodium poisoning the tpb while sodium-containing species do not appear to have a significant role (at least at this coverage) on the rest of the surface.

Next, we investigate the rate changes observed for both systems under a constant polarisation (at $\eta=+1$ V and −1 V). Fig. 3 shows a typical plot of the reaction rate (production of CO₂) transient under positive polarisation overpotential, $\eta=+1$ V (Fig. 3a), and under negative polarisation, $\eta=-1$ V (Fig. 3b) using a mixture of 1.5 kPa O₂ and 0.5 kPa C₂H₄ at 350 °C. In both cases we can see that the open circuit rates of the two systems are very similar (around 65 nmol s⁻¹ cm⁻²). This observation supports further our hypothesis that under these conditions the sodium-containing surface species has little influence on the catalytic activity. In Fig. 3a we observe again a decrease in the CO₂ rate upon application of a positive potential. Both the open circuit and the polarised rates of the two systems are very similar. It can be observed that the time constant associated with rate change is longer for the sodium-modified sample consistent with a slower rate of charge transfer for this sample. Negative polarisation, as can be seen in Fig. 3b, has a more pronounced effect on the sodium-modified sample. Under open circuit conditions, the CO₂ production rate of the 'clean' system is 63 nmol s⁻¹ cm⁻² and that of the sodium-modified system is 65 nmol s⁻¹ cm⁻², while for

[1] In previous studies on the EPOC of ethylene oxidation over a platinum catalyst it has been found that positive polarisation generally enhances the rate of ethylene oxidation (i.e. the reaction shows electrophobic behaviour) [S. Bebelis, C.G. Vayenas, Journal of Catalysis, 118 (1989) 125, D. Poulidi, I. Metcalfe, Journal of Applied Electrochemistry, 38 (2008) 1121, M. Stoukides, C.G. Vayenas, Journal of Catalysis, 70 (1981) 137]. However, it has also been found that at temperatures higher than 350 °C (as in the case studied here) negative polarisation may also cause a small rate increase [C. Koutsodontis et al, Topics in Catalysis, 38 (2006) 157]. In addition, depending on the gas phase composition (i.e. the p_{O2}/p_{C2H4} ratio) it is possible to observe a rate enhancement under both positive and negative polarisation [S. Bebelis et al, Solid State Ionics, 129 (2000) 33]. One possible cause for the range of behaviour observed in the different studies (including the work presented here) could be the presence of uncharacterised and unquantified impurities in the different platinum catalysts.
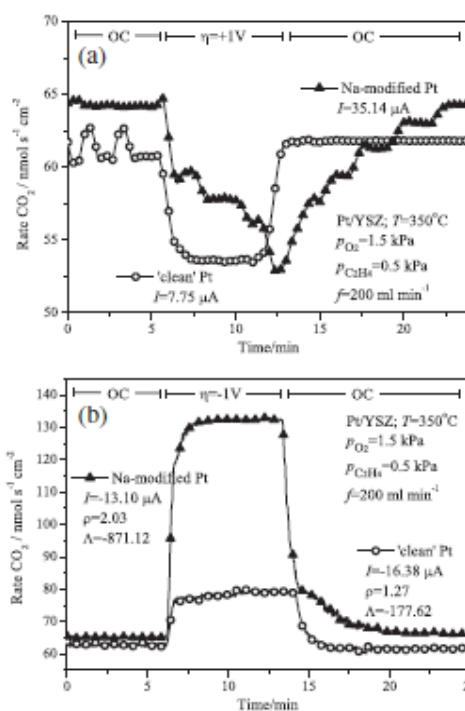

Fig. 3. Effect of sodium addition on CO₂ transients of platinum catalyst (a) CO₂ rate under positive polarisation overpotential, $\eta=+1$ V; (b) CO₂ rate under negative polarisation, $\eta=-1$ V. Sodium added is 1 μl of 10^{-4} M NaOH; gas composition: 1.5 kPa O₂ and 0.5 kPa C₂H₄; Temperature, $T=350$ °C. Total flow rate, $f=200$ ml min⁻¹.

$\eta=-1$ V, the rate increases to 80 nmol s⁻¹ cm⁻² ('clean' system) and 132 nmol s⁻¹ cm⁻² (sodium-modified system).[2] It is clear that sodium modification affects the rate enhancement and the non-faradaicity of the observed promotion in this case. This behaviour could suggest that under negative polarisation, i.e. removal of oxygen from the catalyst surface, activation of the sodium-containing species on the catalyst surface occurs. These species may be in the form of hydroxides and carbonates at low overpotentials that would essentially be spectator species in the experiments described earlier. These species may decompose on application of a large steady negative potential as is the case here generating species that can promote surface reactions. This behaviour is very interesting and warrants further investigation to be fully understood.

The same experiment was also conducted using different gas compositions, where the oxygen flow was varied from 0.5 to 8 kPa and the ethylene flow kept at 0.5 kPa. In this experiment, the open circuit potential, OCP was in the range of −51 to −253 mV. Fig. 4a shows the CO₂ production steady state rate at open circuit and under polarised conditions ($\eta=+1$ V), while Fig. 4b depicts the corresponding rate enhancement ratios. As we can observe and as we discussed earlier on, the difference in the open circuit rate of both systems in Fig. 4a is not very significant in all the conditions studied here. As far as the induced rate modification is concerned Fig. 4b

[2] The rate enhancement ratios, $\rho=r_{oc}/r_{pol}$ and the Faradaic efficiencies, $\Lambda=2$ F $(r_{pol}-r_{oc})/i$ (where, r_{oc} is the open circuit rate, r_{pol} the polarised rate, i is the measured current density at polarisation and F is Faraday's constant) for the two systems are $\rho_{clean}=1.27$ and $\Lambda_{clean}=-177$, and $\rho_{Na}=2.03$, $\Lambda_{Na}=-871$ respectively.
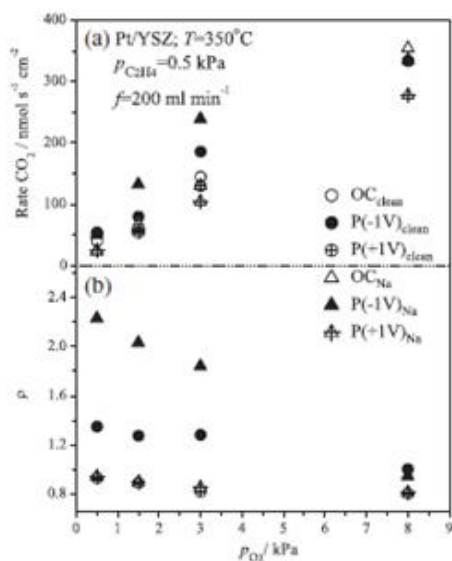
Fig. 4. Comparison of CO₂ production rate during open and closed-circuit conditions for 'clean' and sodium-modified platinum catalyst (with 1 μl of 10⁻⁴ M NaOH); Gas composition: 0.5, 1.5, 3.0 or 8.0 kPa O₂ and 0.5 kPa C₂H₄; Temperature, $T=350$ °C; Total flow rate, $f=200$ ml min⁻¹; OC = Open circuit rate; P = Polarised rate (±1 V).

shows that the ρ values of the sodium-modified system are almost always higher than the 'clean' system, except under oxygen-rich conditions ($p_{O2} = 8$ kPa). In fact, the rate enhancement by sodium modification is most significant when the system is under lean conditions (ρ is highest at a mixture of 0.5/0.5 kPa oxygen/ethylene).

4. Conclusions

From our study, we have shown that addition of sodium to a platinum catalyst surface can affect, to some extent, the characteristics of the oxygen charge transfer reaction and modify the activity of a catalytic reaction. Sodium surface species (which could be in the form of e.g. hydroxides or carbonates) block sites in the *tpb* region and slow down the charge transfer reaction. They may also slightly reduce the open circuit rate of a catalytic reaction (in this case ethylene oxidation) by a surface blocking mechanism. However, on the application of large negative overpotentials these sodium-containing species may decompose leading to the formation of promoting species that cause an increase of reaction rate.

Acknowledgements

References

[1] C.G. Vayenas, S.I. Bebelis, Solid State Ionics 94 (1997) 267–277.
[2] C.G. Vayenas, S. Bebelis, C. Pliangos, S. Brosda, D. Tsiplakides, Electrochemical Activation of Catalysis: Promotion, Electrochemical Promotion, and Metal-Support Interactions, Kluwer Academic/Plenum Publishers, New York, 2001.
[3] A. Katsaounis, J. Appl. Electrochem. 40 (2010) 885–902.
[4] C.G. Vayenas, S. Bebelis, M. Despotopoulou, J. Catal. 128 (1991) 415–435.
[5] S. Bebelis, C.G. Vayenas, J. Catal. 118 (1989) 125–146.
[6] C.G. Vayenas, S. Bebelis, S. Neophytides, J. Phys. Chem. 92 (1988) 5083–5085.
[7] E. Mutoro, B. Luerßen, S. Günther, J. Janek, Solid State Ionics 180 (2009) 1019–1033.
[8] D. Poulidi, I. Metcalfe, J. Appl. Electrochem. 38 (2008) 1121–1126.
[9] W. Schröder, J. Hölzl, Solid State Commun. 24 (1977) 777–780.
[10] J. Cousty, R. Riwan, Surf. Sci. 204 (1988) 45–56.
[11] C.G. Vayenas, A. Ioannides, S. Bebelis, J. Catal. 129 (1991) 67–87.
[12] J. Yi, A. Kaloyannis, C.G. Vayenas, Electrochim. Acta 38 (1993) 2533–2539.